Universitat Autònoma de Barcelona

Departament de Física
Grup de Física Teòrica

Flavor changing neutral decay effects in models with two Higgs boson doublets: Applications to LHC Physics.

Efectes de decaïments amb canvi de sabor neutres
en models amb dos doblets de bosons de Higgs:
Aplicacions a la Física de LHC.

Santi Béjar Latonda

Universitat Autònoma de Barcelona
Grup de Física Teòrica
Institut de Física d'Altes Energies
2005/2006

Memòria presentada per a optar al grau de
Doctor en Ciències Físiques

Director:
Dr. Joan Solà i Peracaula

Vull agrair a en Joan Solà la seva gran dedicació, sense el qual aquest treball no hauria estat possible. Per la seva confiança en el meu saber fer, tant en la feina com en el temps de compilar el resultat final. Ha estat comprensiu i un gran guia en els moments de dubte. La seva visió sobre quins temes eren interessants estudiar de entre tots els camins que hi ha en aquest camp i entre els que ben segur m'hauria perdut.

A en Jaume Guasch, un company infatigable i constant, disposat a resoldre dubtes i a prendre un cafè quan ho necessitava. A més li he d'agrair que m'acollís com a un amic al seu despatx tant de temps sense queixar-se. I per tot el treball que hem fet junts.

Al companys del Grup de Física Teòrica els hi he d'agrair l'entorn que m'ha permés seguir treballant en el camp que m'agrada i no haver perdut l'entusiasme. El treballar dia a dia amb aquests físics ha estat molt enriquidor. Las seves xerrades sobre física, sobre els físics, temes mundans i no tant mundans m'han ajudat a seguir treballant amb illusió a la física.

Al Grup de Física Teòrica per haver-me acollit proporcionat tots els medis necessaris per poder treballar.

A la M^a del Carmen per escoltar i intentar entendre les meves divagacions, les meves explicacions, tot i que la son és més forta de vegades. Espero haver-te transmès una miqueta de la meva passió per la física.

A la família i amics per comprendre que el ser físic teòric no és només una excusa per estar assegut dient que estàs meditant sobre partícules fonamentals, o l'origen de l'univers, en lloc de parar la taula.

This Thesis has been written using Free Software.
The LaTeX2$_\varepsilon$ Typesetting system.
Feynman graphs using `feynMF`.
Plots using Xmgr and Grace plotting tools.
GNU Emacs.
Running in a GNU/Linux system.

Contents

Chapter 1

Introduction

1.1 Summary

In this Thesis we have investigated some effects appearing in top quark and Higgs boson decays with flavor changing neutral currents (FCNC) in the framework of generic Two Higgs Doblet Models (2HDM) and the Minimal Supersymmetric Standard Model (MSSM).

The Standard Model (SM) of Particle Physics interactions has had great success in describing the strong, weak and electromagnetic interactions and its validity has been tested up to the quantum level in past and present accelerators, such as the LEP at CERN or the Tevatron at Fermilab. The last great success of the SM was the discovery in 1994 of its last matter building block, namely the top quark, with a mass of $m_t = 178.0 \pm 2.7 \pm 3.3\,\mathrm{GeV}$. However, the mechanism by which all the SM particles get their masses is still unconfirmed, since no Higgs scalar has been found yet. The fermions couple to the Higgs bosons with a coupling proportional to their mass, so one expects that the large interactions between top quark and Higgs boson particles would give rise to large quantum effects. But the FCNC processes are very suppressed in the SM. So in some cases (specially the ones we are going to deal with in this Ph.D. Thesis) the sole observation of these FCNC processes would be instant evidence of new physics and could greatly help to unravel the type of underlying Higgs model.

We have focused our work on two models: the generic Two Higgs Doblet Models (2HDM) and the Minimal Supersymmetric Standard Model (MSSM). The 2HDM is like the SM with an extra Higgs doblet, so it has more Higgs bosons and in particular some charged. There are two types, I and II, and they differ in the way they give mass to the fermions. The MSSM is an extension of the SM that incorporates Supersymmetry (SUSY). Supersymmetry is an additional transformation that can be added in the action

of Quantum Field Theory, leaving this action unchanged. The main phenomenological consequence is that for any SM particle (p) there should exist a partner for it, which we call *sparticle* ($\tilde{p}$) with different spin but with the same gauge quantum numbers. This extension of the SM provides elegant solutions to some theoretical problems of the SM, such as the *hierarchy problem*.

We have applied these two extensions to the SM to see whether they can produce new FCNC effects. We have computed the following FCNC decays: (1) the branching ratios (B) of the top quark to Higgs bosons and charm quark in the 2HDM; (2) B and number of events at the LHC of the Higgs bosons to top and charm quarks in the 2HDM; (3) B of the Higgs bosons to bottom and strange quarks in the MSSM; (4) cross section and number of events at the LHC of the Higgs bosons to FCNC final states involving the heavy quarks like the top and bottom quark in the MSSM. We also studied the experimental signatures that would allow discover of the nature of these Higgs bosons in the LHC. In this study we have applied the severe restrictions from observed low-energy FCNC processes like $b \to s\gamma$.

Decays of the top quark induced by FCNC are known to be extremely rare events within the SM. This is so not only for the decay modes into gauge bosons, but most notably in the case of the Higgs channels, e.g. $t \to H^{SM}c$, with a branching fraction of 10^{-13} at most. We have found that in the 2HDM the decays of the top quark to Higgs bosons, $t \to (h^0, H^0, A^0)c$, can be the most favored FCNC modes – comparable or even more efficient than the gluon channel $t \to gc$. In both cases the optimal results are obtained for Type II models. However, only the Higgs channels can have rates reaching the detectable level (10^{-5}), with a maximum of order 10^{-4}. Compared with previous results obtained in the Higgs sector of the MSSM, the maximum branching ratios are similar but have different signatures. While in the 2HDM II there is only one Higgs boson that can reach the visible level (h^0 or H^0, but not both), in the MSSM all the channels can be competitive in some region.

Similarly, Higgs boson decays mediated by FCNC are very much suppressed in the Standard Model, at the level of 10^{-15} for Higgs boson masses of a few hundred GeV. We have computed the FCNC decays of Higgs bosons into a top quark, $h \to t\bar{c}$ ($h = h^0, H^0, A^0$), in a general 2HDM. The isolated top quark signature, unbalanced by any other heavy particle, is very clean (without background noise), and should help to identify the potential FCNC events much better than any other final state. We have computed the maximum branching ratios and the number of FCNC Higgs boson decay events at the LHC. The most favorable mode for production and subsequent FCNC decay is the lightest CP-even state (h^0) in the Type II 2HDM, followed by the other CP-even state (H^0) if it is

not very heavy, whereas the CP-odd (A^0) mode can never be sufficiently enhanced. Our calculation shows that the branching ratios of the CP-even states may reach 10^{-5}, and that several hundreds of events could be collected in the highest luminosity runs of the LHC. We also point out some strategies in which to use these FCNC decays as a handle to discriminate between 2HDM and supersymmetric Higgs bosons.

Furthermore, we analyzed the maximum branching ratios for the FCNC decays of the neutral Higgs bosons of the MSSM into bottom quarks, $h \to b\bar{s}$ ($h = h^0, H^0, A^0$), giving the maxima in the $B(h \to b\,\bar{s}) \sim 10^{-4} - 10^{-3}$ range. But this maximum could reach up to $\sim 10^{-2}$ depending on whether or not it is allowed a fine-tunning in the $B(b \to s\gamma)$ restriction, which for naturalness reasons we do not allow. We consider that the bulk of the MSSM contribution to $B(h \to b\,\bar{s})$ should originate from the strong supersymmetric sector, electroweak calculations are in progress. These calculations show that the FCNC modes $h \to b\bar{s}$ can be competitive with other Higgs boson signatures and could play a helpful complementary role in identifying the supersymmetric Higgs bosons, particularly the lightest CP-even state in the critical LHC mass region $m_{h^0} \simeq 90 - 130\,\text{GeV}$.

Finally, we have also analyzed the production and subsequent FCNC decay of the neutral MSSM Higgs bosons to tc and bs in the LHC collider, $pp \to h \to t\bar{c}, b\bar{s}$ and $h \to t\bar{c}, b\bar{s}$ ($h = h^0, H^0, A^0$). Only the strongly-interacting FCNC sector has been computed because it expected to be the most important. We determined the maximum production rates for each of these modes and identified the relevant regions of the MSSM parameter space. The latter are different from those obtained by maximizing only the branching ratio, due to non-trivial correlations between the parameters that maximize/minimize each isolated factor. The production rates for the bs channel can be huge for a FCNC process ($0.1 - 1\,\text{pb}$), but its detection can be problematic. The production rates for the tc channel are more modest ($10^{-3} - 10^{-2}\,\text{pb}$), but its detection should be easier due to the clear-cut top quark signature. A few thousand tc events could be collected in the highest luminosity phase of the LHC, with no counterpart in the SM.

Our general conclusion is that the physics of the processes with flavor changing neutral currents can be very important in seeing the physics beyond the Standard Model and to disentangle the nature of the most adequate model. Experiments at the LHC can be crucial to unravel signs of FCNC physics beyond the SM.

1.2 Motivation

The accepted model for the interactions between elementary particles is the Standard Model (SM) [1–5]. This model is composed of fundamental particles with spin 1/2

(fermions), spin 1 (vector bosons) and one fundamental particle with spin 0, that is the Higgs boson, the only undiscovered particle of the SM. But there are good reasons to think that it is not the final model for the high energy physics. There are different models which try to explain the physics beyond the SM. The simplest model that extends the SM is the 2HDM [6]. The extra pieces of this model are some neutral and charged Higgs bosons. These neutral Higgs boson are those in which we are interested in order to compare with the SM Higgs boson. In this way we can distinguish which model describes better the future experimental results. Another not so simple model is the MSSM [7–10][1], and which has some characteristics of the 2HDM and, as we have said, has more or less twice the number of particles than the SM, as can be seen in chapter 2.

The top quark is the latest-discovered elementary particle of the SM. It almost completes all of the building blocks of the SM. But for theoretical and aesthetic reasons we need to introduce a mechanism to give masses to the particles. One mechanism that allows this is the Higgs mechanism. It is based on introducing a new (undiscovered yet) particle of spin 0. So recently the Higgs boson has become the most wanted particle. The top quark physics is very important in the investigation of the high energy physics. It interacts with Higgs bosons with the highest possible strength (because it is proportional to the mass of the quark) and therefore this property may help to discover the Higgs boson. Moreover, it provides a big phase space, so it can decay in particles that the others cannot.

The flavor changing neutral currents are a kind of processes, especially important to test the SM. They are characterised by one quark changing its flavor in the interaction (effective or not) with neutral particles (currents). Experimentally these processes are very suppressed, especially for the physics of the top quark, as we have seen. In the SM the branching ratios in the top quark case are so tiny that we cannot think of measuring them experimentally. But we could perhaps find models that, even being depressed, can give values nearer to our experimental possibilities.

In the near and middle future, with the upgrades of the Tevatron (Run II, TeV33), the advent of the LHC, and the construction of an e^+e^- Linear Collider (LC, nowadays called International Linear Collider ILC) [13–15], new results on top quark physics [16], and possibly on Higgs physics, will be obtained that may be extremely helpful complementing the precious information already collected at LEP I and II from Z and W physics. Both types of machines, the hadron colliders and the LC will work at high luminosities and produce large amounts of top quarks. In the LHC, for example, the production of top quark pairs will be $\sigma(t\bar{t}) = 800\ pb$ – roughly two orders of magnitude larger than in

[1] For a review see [11, 12]

the Tevatron Run II. In the so-called low-luminosity phase ($10^{33}\,cm^{-2}s^{-1}$) of the LHC, one expects about three $t\bar{t}$-pairs per second (ten million $t\bar{t}$-pairs per year!) [17]. And this number will be augmented by one order of magnitude in the high-luminosity phase ($10^{34}\,cm^{-2}s^{-1}$). As for a future LC running at e.g. $\sqrt{s} = 500\ GeV$, one has a smaller cross-section $\sigma(t\bar{t}) = 650\ fb$ but a higher luminosity factor ranging from $5 \times 10^{33}\,cm^{-2}s^{-1}$ to $5 \times 10^{34}\,cm^{-2}s^{-1}$ and of course a much cleaner environment [18]. With datasets from LHC and LC increasing to several $100\,fb^{-1}$/year in the high-luminosity phase, one should be able to pile up an enormous wealth of statistics on top quark decays. Therefore, not surprisingly, these machines should be very useful to analyze rare decays of the top quark and of the Higgs boson(s), viz. decays whose branching fractions are so small ($\lesssim 10^{-5}$) that they could not be seen unless the number of collected decays is very large.

The reason for the interest in these decays is at least twofold. First, the typical branching ratios for the rare top quark decays predicted within the Standard Model (SM) are so small that the observation of a single event of this kind should be "instant evidence", so to speak, of new physics; and second, due to its large mass ($m_t = 178.0 \pm 2.7 \pm 3.3\,\mathrm{GeV}$ [19]), the top quark could play a momentous role in the search for Higgs physics beyond the SM. While this has been shown to be the case for the top quark decay modes into charged Higgs bosons, both in the Minimal Supersymmetric Standard Model (MSSM) and in a general two-Higgs-doublet model (2HDM) [20, 21][2], we expect that a similar situation would apply for top quark FCNC decays into non-SM neutral Higgs bosons and for Higgs boson FCNC decays.

1.3 Today's situation

The search for physics beyond the Standard Model (SM) is a very relevant, if not the most important, endeavor within the big experimental program scheduled in the forthcoming Large Hadron Collider (LHC) experiment at CERN [13, 14]. There are several favorite searching lines on which to concentrate, but undoubtedly the most relevant one (due to its central role in most extensions of the SM) is the physics of the Higgs boson(s) with all its potential physical manifestations.

As we mention above, experimentally, processes involving Flavor Changing Neutral Current (FCNC) have been shown to have rather low rates [19]. Letting aside the meson-meson oscillations, such as $K^0 - \bar{K}^0$ and $B^0 - \bar{B}^0$, the decay processes mediated by FCNC are also of high interest and are strongly suppressed too. For instance, we have the

[2]For a review of the main features of loop-induced supersymmetric effects on top quark production an decay, see e.g. Ref. [22].

radiative B-meson decays, with a typical branching ratio $B(b \to s\,\gamma) \sim 10^{-4}$. But we also have the FCNC decays with the participation of the top quark as a physical field, which are by far the most suppressed decay modes [23, 24]. Indeed, the top quark decays into gauge bosons ($t \to c\,V$; $V \equiv \gamma, Z, g$) are well known to be extremely rare events in the SM. The branching ratios are, according to Ref. [24]: $\sim 5 \times 10^{-13}$ for the photon, slightly above 1×10^{-13} for the Z-boson, and $\sim 4 \times 10^{-11}$ for the gluon channel, or even smaller according to other estimates [25]. Similarly, the top quark decay into the SM Higgs boson, H^{SM}, is a very unusual decay, typically $B(t \to c\,H^{SM}) \sim 10^{-14}$ [26].

	SM	2HDM	MSSM
$B(t \to c\gamma)$	$\sim 5 \times 10^{-13}$	$\lesssim 1 \times 10^{-7}$	$< 1 \times 10^{-6}$
$B(t \to cZ)$	$\gtrsim 1 \times 10^{-13}$	$< 1 \times 10^{-6}$	$< 1 \times 10^{-7}$
$B(t \to cg)$	$\sim 4 \times 10^{-11}$	$\lesssim 1 \times 10^{-5}$	$\lesssim 1 \times 10^{-5}$
$B(t \to cH)$	$\sim 10^{-13} - 10^{-15}$	$\lesssim 10^{-4}$	$\lesssim 10^{-4}$
$B(H \to t\bar{c})$	$\sim 10^{-13} (m_H < 2m_W)$	$\lesssim 10^{-4}$	$\lesssim 10^{-4}$
	$\lesssim 10^{-15} (m_H > 2m_W)$		
$B(H \to b\bar{s})$	$\lesssim 10^{-7} (m_H < 2M_W)$	$\lesssim 10^{-5}$	$\lesssim 10^{-4}$
	$\lesssim 10^{-10} (m_H > m_t)$		

Table 1.1: Rare FCNC branching ratios of the top quark and the Higgs boson decays.

The reason for this rareness is simple: for FCNC top quark decays in the SM, the loop amplitudes are controlled by down-type quarks, mainly by the bottom quark. Therefore, the scale of the loop amplitudes is set by m_b^2 and the partial widths are of order

$$\Gamma(t \to V\,c) \sim \left(\frac{|V_{tb}^* V_{bc}|}{16\pi^2}\right)^2 \alpha\, G_F^2\, m_t\, m_b^4\, F \sim \left(\frac{|V_{bc}|}{16\pi^2}\right)^2 \alpha_{em}^2 \alpha\, m_t \left(\frac{m_b}{M_W}\right)^4 F, \qquad (1.1)$$

and similarly for the FCNC Higgs boson decays

$$\Gamma(H^{SM} \to t\,\bar{c}) \sim \left(\frac{|V_{tb}^* V_{bc}|}{16\pi^2}\right)^2 \alpha_W^3\; m_H \left(\lambda_b^{SM}\right)^4 \sim \left(\frac{|V_{bc}|}{16\pi^2}\right)^2 \alpha_W\; G_F^2\, m_H\, m_b^4\,, \tag{1.2}$$

$$B(H^{SM} \to t\,\bar{c}) \sim \left(\frac{|V_{bc}|}{16\pi^2}\right)^2 \alpha_W\; G_F\, m_b^2 \sim 10^{-13} \quad (\text{for } m_H < 2m_W)\,, \tag{1.3}$$

$$B(H^{SM} \to t\,\bar{c}) \sim \left(\frac{|V_{bc}|}{16\pi^2}\right)^2 \alpha_W\; G_F\, \frac{m_b^4}{m_H^2} \lesssim 10^{-15} \quad (\text{for } m_H > 2m_W)\,, \tag{1.4}$$

$$B(H^{SM} \to b\,\bar{s}) \sim \left(\frac{|V_{ts}|}{16\pi^2}\right)^2 \alpha_W\; G_F\, \left(\frac{m_H^4}{m_b^2}\right) \lesssim 10^{-7} \quad (\text{for } m_H < 2\,M_W)\,, \tag{1.5}$$

$$B(H^{SM} \to b\,\bar{s}) \sim \left(\frac{|V_{ts}|}{16\pi^2}\right)^2 \alpha_W\; G_F\, \left(\frac{m_t^4}{m_H^2}\right) \lesssim 10^{-10} \quad (\text{for } m_H > m_t)\,, \tag{1.6}$$

where α is α_{em} for $V = \gamma, Z$ and α_s for $V = g$, G_F is Fermi's constant, $\alpha_W = g^2/4\pi$ and g being the $SU(2)_L$ weak gauge coupling. Notice the presence of $\lambda_b^{SM} \sim m_b/M_W$, which is the SM Yukawa coupling of the bottom quark in units of g. The factor $F \sim (1 - m_V^2/m_t^2)^2$ results, upon neglecting m_c, from phase space and polarization sums. Notice that the dimensionless fourth power mass ratio, in parenthesis in eq. (1.1), and the fourth power of λ_b^{SM} stems from the GIM mechanism and is responsible for the ultra-large suppression beyond naive expectations based on pure dimensional analysis, power counting and CKM matrix elements.

The GIM mechanism [27] is related to the unitarity of the mixing matrices between quarks. The Minimal Standard Model (SM) embeds the GIM mechanism naturally, due to the presence of only one Higgs doublet giving mass simultaneously to the down-type and the up-type quarks, and as a result no tree-level FCNCs interactions appear. FCNCs are radiatively induced, and are therefore automatically small. However, when considering physics beyond the SM, new horizons of possibilities open up which may radically change the pessimistic prospects for FCNC decays involving a Higgs boson and the top quark. Because of the loop-induced FCNCs effects, the SM and non-SM loops enter the FCNC observables at the same order of perturbation theory, and new physics competes on the same footing with SM physics to generate a non-vanishing value for these rare processes. It may well be that the non-SM effects are dominant and become manifest. Conversely, it may happen that they become highly constrained.

The addition of further Higgs doublets to the SM in the most general way introduces potentially large tree-level FCNC interactions, which would predict significant FCNC rates in contradiction with observation. However, by introducing an *ad-hoc* discrete symmetry these interactions are forbidden. This gives rise to two classes of Two-Higgs-Doublet Models (2HDM) which avoid FCNCs at the tree-level, known conventionally as type I

and type II 2HDMs [6]. In Type I 2HDM (also denoted 2HDM I) one Higgs doublet, Φ_1, does not couple to fermions at all and the other Higgs doublet, Φ_2, couples to fermions in the same manner as in the SM. For more details see chapter 2. In contrast, in Type II 2HDM (also denoted 2HDM II) one Higgs doublet, Φ_1, couples to down quarks (but not to up quarks) while Φ_2 does the other way around. Such a coupling pattern is automatically realized in the framework of supersymmetry (SUSY), in particular in the MSSM, but it can also be arranged in non-supersymmetric extensions if we impose a discrete symmetry, e.g. $\Phi_1 \to -\Phi_1$ and $\Phi_2 \to +\Phi_2$ (or vice versa) plus a suitable transformation for the right-handed quark fields, this symmetry is only violated by soft terms of dimension two.

Supersymmetry (SUSY) is certainly related to Higgs boson physics, and at the same time it may convey plenty of additional phenomenology. Ever since its inception, SUSY has been one of the most cherished candidates for physics beyond the SM, and as such it will be scrutinized in great detail at the LHC. It is no exaggeration to affirm that the LHC will either prove or disprove the existence of SUSY, at least in its most beloved low-energy realization, namely the one which is needed to solve the longstanding naturalness problem in the Higgs sector of the SM [8]. On the other hand, SUSY provides an appealing extension of the SM, which unifies the fermionic and bosonic degrees of freedom of the fundamental particles and provides a natural solution to the hierarchy problem. The search for SUSY particles has been one of the main programs of the past experiments in high energy physics (LEP, SLD, Tevatron) and continues to play a central role in the present accelerator experiments (Tevatron II) and in the planning of future experimental facilities like the LHC and the LC. The Minimal Supersymmetric Standard Model (MSSM) is the simplest extension of the SM which includes SUSY, and for this reason its testing will be one of the most prominent aims of these powerful experiments. If SUSY is realized around the TeV scale, the LHC experiments shall be able to directly produce the SUSY particles for masses smaller than a few TeV [28, 29]. On the other hand, the presence of SUSY may also be tested indirectly through the quantum effects of the supersymmetric particles. For one thing, it has been known since long ago that SUSY particles may produce large virtual effects on Higgs boson observables [3].

In Ref. [42] it was shown that the vector boson modes can be highly enhanced within the context of the MSSM. This fact was also dealt with in great detail in Ref. [43] where a dedicated study was presented of the FCNC top quark decays into the various Higgs bosons of the MSSM (see also [44]) showing that these can be the most favored FCNC top quark decays – above the expectations on the gluon mode $t \to c\,g$. For the 2HDM it was proven that while the maximum rates for $t \to c\,g$ were one order of magnitude more

[3] See e.g. [20, 30–41] and references therein. For a review see e.g. [11].

favorable in the MSSM than in the 2HDM, the corresponding rates for $t \to c\,h^0$ were comparable both for the MSSM and the general 2HDM, namely up to the 10^{-4} level and should therefore be visible both at the LHC and the LC [25].

As in the 2HDM, in MSSM one has to impose some restrictions to avoid tree-level FCNCs among the extra predicted particles, which would induce one-loop FCNC interactions among the SM particles. But, in fact, MSSM *requires* their existence, because of the $SU(2)_L$ gauge symmetry. Of course, low energy measurements constrain the FCNC couplings (the most stringent being the $B(b \to s\gamma)$). A potentially relevant FCNC interaction is the gluino with the squarks, not very much constrained experimentally.

Concerning the FCNC interactions of Higgs bosons with third generation quarks, it was demonstrated long ago [43] that the leading term corresponds to a *single particle insertion approximation*. This produces a flavor change in the internal squark loop propagator, since in this case the chirality change can already take place at the squark-squark-Higgs boson interaction vertex. Adding this to the fact that the Higgs bosons (in contrast to gauge bosons) have a privileged coupling to third generation quarks, one might expect that the FCNC interactions of the type quark-quark-Higgs bosons in the MSSM become highly strengthened with respect to the SM prediction. This was already proven in the rare decay channels $\Gamma(t \to ch)$ [43] (h being any of the neutral Higgs bosons of the MSSM $h \equiv h^0, H^0, A^0$) where the maximum rate of the SUSY-QCD induced branching ratio was found to be $B(t \to ch) \simeq 10^{-5}$, eight orders of magnitude above the SM expectations $B(t \to cH^{SM}) \simeq 10^{-13}$. Similar enhancement factors have been found in the (top,bottom)-quark-Higgs boson interactions in other extensions of the SM, both in the MSSM (see chapters 6-7 and Refs. [43, 45–50]) and in the general two-Higgs-doublet model (2HDM) (see chapters 4- 5 and Ref. [51]), and also in other extensions of the SM– see [25] for a review.

The power of FCNC observables can be gauged e.g. by the implications of the bottom-quark rare decay $b \to s\gamma$: the experimentally measured allowed range $B(b \to s\gamma) = (3.3 \pm 0.4) \times 10^{-4}$ [52–58] may impose tight constraints on extensions of the SM. For example, it implies a lower bound on the charged Higgs boson mass $m_{H^\pm} \gtrsim 350\,\text{GeV}$ in general type II 2HDMs [59–62].

After this panoramic view of the FCNC processes in the SM and beyond, the work presented in this Thesis is as follows: in chapter 2 (resp. 3) we give the basic notations of the 2HDM (resp. MSSM); in chapter 4 we compute the FCNC top quark decay in the 2HDM $B(t \to ch)$; in chapter 5 we compute the Higgs boson production and FCNC decay in the 2HDM $\sigma(pp \to h \to t\bar{c})$ at the LHC and $B(h \to t\bar{c})$; in chapter 6 we compute the FCNC Higgs boson decay in the MSSM $B(h \to b\bar{s})$; and in chapter 7 the Higgs boson

production and decay in the MSSM $\sigma(pp \to h \to t\bar{c}, b\bar{s})$ and $B(h \to t\bar{c}, b\bar{s})$. This PhD. work is based on the following articles [63–69].

In chapter 4 we show that within the simplest extension of the SM, namely the general two-Higgs-doublet model, the FCNC top quark decays into Higgs bosons, $t \to (h^0, H^0, A^0)c$, can be the most favored FCNC modes – comparable or even more efficient than the gluon channel $t \to gc$. In both cases the optimal results are obtained for Type II models. However, only the Higgs channels can have rates reaching the detectable level 10^{-5}, with a maximum of order 10^{-4} which is compatible with the charged Higgs bounds from radiative B-meson decays. We compare with the previous results obtained in the Higgs sector of the MSSM.

In chapter 5 we consider the FCNC decays of Higgs bosons into a top quark in a general two-Higgs-doublet model (2HDM). The isolated top quark signature, unbalanced by any other heavy particle, should help to identify the potential FCNC events much more than any other final state. We compute the maximum branching ratios and the number of FCNC Higgs boson decay events at the LHC collider at CERN. The most favorable mode for production and subsequent FCNC decay is the lightest CP-even state in the Type II 2HDM, followed by the other CP-even state, if it is not very heavy, whereas the CP-odd mode can never be sufficiently enhanced. Our calculation shows that the branching ratios of the CP-even states may reach 10^{-5}, and that several hundred events could be collected in the highest luminosity runs of the LHC. We also point out some strategies to use these FCNC decays as a handle to discriminate between 2HDM and supersymmetric Higgs bosons.

In chapter 6 we analyze the maximum branching ratios for the FCNC decays of the neutral Higgs bosons of the MSSM into bottom and charm quarks, $h \to b\bar{s}$ $(h = h^0, H^0, A^0)$. We consistently correlate these decays with the radiative B-meson decays $(b \to s\gamma)$. A full-fledged combined numerical analysis is performed of these high-energy and low-energy FCNC decay modes in the MSSM parameter space. Our calculation shows that the available data on $B(b \to s\gamma)$ severely restricts the allowed values of $B(h \to b\,\bar{s})$. While the latter could reach a few percent level in fine-tuned scenarios, the requirement of naturalness reduces these FCNC rates into the modest range $B(h \to b\,\bar{s}) \sim 10^{-4} - 10^{-3}$. We expect that the bulk of the MSSM contribution to $B(h \to b\,\bar{s})$ should originate from the strong supersymmetric sector. Our results are encouraging because they show that the FCNC modes $h \to b\bar{s}$ can be competitive with other Higgs boson signatures and could play a helpful complementary role to identify the supersymmetric Higgs bosons, particularly the lightest CP-even state in the critical LHC mass region $m_{h^0} \simeq 90 - 130\,\text{GeV}$.

In chapter 7 we analyze the production and subsequent decay of the neutral MSSM

Higgs bosons ($h \equiv h^0,\ H^0,\ A^0$) mediated by FCNC in the LHC collider. We have computed the h-production cross-section times the FCNC branching ratio, $\sigma(pp \to h \to qq') \equiv \sigma(pp \to h) \times B(h \to qq')$, in the LHC focusing on the strongly-interacting FCNC sector. Here qq' is an electrically neutral pair of quarks of different flavors, the dominant modes being those containing a heavy quark: tc or bs. We determine the maximum production rates for each of these modes and identify the relevant regions of the MSSM parameter space, after taking into account the severe restrictions imposed by low energy FCNC processes. The analyses of $\sigma(pp \to h \to qq')$ singles out regions of the MSSM parameter space different from those obtained by maximizing only the branching ratio, due to non-trivial correlations between the parameters that maximize/minimize each isolated factor. The production rates for the bs channel can be huge for a FCNC process ($0.1 - 1\,\text{pb}$), but its detection can be problematic. The production rates for the tc channel are more modest ($10^{-3} - 10^{-2}\,\text{pb}$), but its detection should be easier due to the clear-cut top quark signature. A few thousand tc events could be collected in the highest luminosity phase of the LHC, with no counterpart in the SM.

Chapter 2

Two Higgs Doublet Models (2HDM)

2.1 Introduction

The 2HDM are models that extend minimally the Higgs sector of the SM. They introduce one more doublet of complex scalar fields with hypercharge $Y = +1$. The most general Lagrangian with the SM gauge symmetry $SU(2)_L \times U(1)_Y$ that contains these Higgs bosons can be divided in three terms: a kinetic term $\mathcal{L}_{kin}$, the Yukawa couplings term (Higgs-fermions interactions) $\mathcal{L}_Y$ and the potential for the two Higgs doublets $\mathcal{V}(\phi_1, \phi_2)$:

$$\mathcal{L}_{Higgs} = \mathcal{L}_{kin} + \mathcal{L}_Y - \mathcal{V}(\phi_1, \phi_2)\,, \tag{2.1}$$

$$\mathcal{L}_{kin} = \sum_{i=1,2} \left(D_\mu \phi_i\right)^\dagger \left(D^\mu \phi_i\right), \tag{2.2}$$

$$D_\mu = \partial_\mu - ig\frac{\overrightarrow{\sigma}}{2}\overrightarrow{W}_\mu - ig'\frac{Y}{2}B_\mu\,, \tag{2.3}$$

where D_μ is the covariant derivative of $SU(2)_L \otimes U(1)_Y$, and σ_i are the Pauli matrices[1].

The Higgs potential that spontaneously breaks the symmetry $SU(2)_L \otimes U(1)_Y$ to $U(1)_{EM}$ is [6, 70]:

$$\begin{aligned}
\mathcal{V}(\phi_1, \phi_2) =& \lambda_1(\phi_1^\dagger\phi_1 - v_1^2)^2 + \lambda_2(\phi_2^\dagger\phi_2 - v_2^2)^2 + \\
&+ \lambda_3\left[(\phi_1^\dagger\phi_1 - v_1^2) + (\phi_2^\dagger\phi_2 - v_2^2)\right]^2 + \\
&+ \lambda_4\left[(\phi_1^\dagger\phi_1)(\phi_2^\dagger\phi_2) - (\phi_1^\dagger\phi_2)(\phi_2^\dagger\phi_1)\right] + \\
&+ \lambda_5\left[\mathrm{Re}(\phi_1^\dagger\phi_2) - v_1 v_2\cos\xi\right]^2 + \\
&+ \lambda_6\left[\mathrm{Im}(\phi_1^\dagger\phi_2) - v_1 v_2\sin\xi\right]^2,
\end{aligned} \tag{2.4}$$

[1] $tr(\sigma_i\sigma_j) = 2\delta_{ij}$

where all the λ_i are real parameters, because the Lagrangian must be hermitic. This is the most general Lagrangian compatible with the gauge symmetry and the discrete symmetry $\phi_1 \to -\phi_1$ [6, 70], this symmetry is only violated by soft terms of dimension two. We impose this last symmetry to forbid the FCNC at tree level. Moreover, this potential must be bounded from below, so the λ_i must be non-negative. But in fact, the allowed range for the parameters λ_i corresponding to this minimum is a range in the parameter space such that the square Higgs boson masses are positive and that $V(0,0) > 0$.

In this context the minimum of the potential is:

$$\langle \phi_1 \rangle \equiv \begin{pmatrix} 0 \\ v_1 \end{pmatrix} , \tag{2.5}$$

$$\langle \phi_2 \rangle \equiv \begin{pmatrix} 0 \\ v_2 e^{i\xi} \end{pmatrix} , \tag{2.6}$$

which breaks the gauge symmetry giving $U(1)_{EM}$.

We need two physical parameters in order to know their value, which are usually taken to be:

$$M_W^2 = \frac{1}{2} g^2 (v_1^2 + v_2^2) \equiv g^2 \frac{v^2}{2} \quad , \quad \tan\beta = \frac{v_2}{v_1} \ , \quad 0 < \beta < \frac{\pi}{2}. \tag{2.7}$$

If we impose $\lambda_5 = \lambda_6$ (like in sypersymmetry) we can write the last two terms of eq. (2.4) as:

$$\left| \phi_1^\dagger \phi_2 - v_1 v_2 e^{i\xi} \right|^2 . \tag{2.8}$$

The phase ξ can disappear with a redefinition of the fields without affecting the others terms of the potential (this phase will appear in other terms of the total Lagrangian). Then, the Higgs potential is CP conserving.

At last, the final Higgs potential is:

$$\begin{aligned} \mathcal{V}(\phi_1, \phi_2) =& \lambda_1 (\phi_1^\dagger \phi_1 - v_1^2)^2 + \lambda_2 (\phi_2^\dagger \phi_2 - v_2^2)^2 + \\ &+ \lambda_3 \left[(\phi_1^\dagger \phi_1 - v_1^2) + (\phi_2^\dagger \phi_2 - v_2^2) \right]^2 + \\ &+ \lambda_4 \left[(\phi_1^\dagger \phi_1)(\phi_2^\dagger \phi_2) - (\phi_1^\dagger \phi_2)(\phi_2^\dagger \phi_1) \right] + \\ &+ \lambda_5 |\phi_1^\dagger \phi_2 - v_1 v_2|^2 . \end{aligned} \tag{2.9}$$

There are different forms for the Yukawa terms of the Lagrangian to satisfy the Glashow and Weinberg [71] theorem. The Glashow and Weinberg theorem says that for a general $SU(2) \times U(1)$ gauge theory where we demand that the neutral-current interactions conserve all quark flavor naturally the necessary and sufficient conditions are: All quarks of fixed charge and helicity must (1) transform according to the same irreducible

representations of weak $SU(2)$, (2) correspond to the same eigenvalue of weak T_3, and (3) receive their contributions in the quark mass matrix form a single source (either from the vacuum expectations value of a single neutral Higgs boson or from a unique gauge-invariant bare mass term). In practice this implies that all fermions of a given electric charge couple to no more than one Higgs doublet.

From the Lagrangian (2.4) with the potential (2.9) and the Yukawa terms we can obtain the full 2HDM spectrum, as well as the interactions, which contain the usual SM gauge interactions, the fermion-Higgs interactions, and the pure 2HDM interactions. A detailed treatment of this Lagrangian, and the process of derivation of the forthcoming results can be found in [72].

2.1.1 2HDM I

In this model one of the Higgs doublets (ϕ_2) couple to all the fermions. The couplings with the quarks is of the form:

$$\mathcal{L}_Y^{(I)} = -\sum_{i,j=1}^{3} \left[D_{ij}^q \left(\bar{q}_L^{(i)} \phi_2 \right) q_{dR}^{(j)} + U_{ij}^q \left(\bar{q}_L^{(i)} \tilde{\phi}_2 \right) q_{uR}^{(j)} + \text{h.c.} \right] + \text{leptons}\,, \tag{2.10}$$

where

$$\tilde{\phi} = i\sigma_2 \phi^*\,, \tag{2.11}$$

$$q^{(i)} = \begin{pmatrix} q_u^{(i)} \\ q_d^{(i)} \end{pmatrix}\,, \tag{2.12}$$

$$q^{(1)} = \begin{pmatrix} u \\ d \end{pmatrix}\,, \quad q^{(2)} = \begin{pmatrix} c \\ s \end{pmatrix}\,, \quad q^{(3)} = \begin{pmatrix} t \\ b \end{pmatrix}\,, \tag{2.13}$$

and similarly for the leptonic doublets $l^{(i)}$ that contain the neutrinos and the leptons.

This model is very related with the minimal model (SM), being the only difference a smaller VEV $v_2 < v_{SM}$ ($v \sim 174\,GeV$) and bigger Yukawa couplings.

2.1.2 2HDM II

Now one doublet (ϕ_1) couples to the right-handed (RH) down fermions (q_{dR}, l_{dR}) and is responsible of the down masses; the other doublet (ϕ_2) couples to the RH up fermions (q_{uR}, l_{uR}) and is responsible of their masses. Taking any flavor base, i.e. one in which $f_L^{(i)}$ are isospin doublets the Lagrangian is:

$$\mathcal{L}_Y^{(II)} = -\sum_{i,j=1}^{3} \left[D_{ij}^q \left(\bar{q}_L^{(i)} \phi_1 \right) q_{dR}^{(j)} + U_{ij}^q \left(\bar{q}_L^{(i)} \tilde{\phi}_2 \right) q_{uR}^{(j)} + \text{h.c.} \right] + \text{leptons}\,. \tag{2.14}$$

The mass matrix will be proportional to the VEV of the Higgs as:

$$M_u^{(q,l)} = v_2 U^{(q,l)}\,, \tag{2.15}$$

$$M_d^{(q,l)} = v_1 D^{(q,l)}\,, \tag{2.16}$$

This is basically the Higgs sector required in the MSSM.

2.1.3 2HDM III

This is the most general 2HDM without FCNC at tree level, being the other two important particular cases. The Yukawa interactions in this case, using any flavor base, is:

$$\mathcal{L}_Y^{(III)} = -\sum_{i,j=1}^{3}\Big[D^q_{1,ij}\big(\bar{q}_L^{(i)}\phi_1\big)q_{dR}^{(j)} + D^q_{2,ij}\big(\bar{q}_L^{(i)}\phi_2\big)q_{dR}^{(j)} + \tag{2.17}$$

$$+ U^q_{1,ij}\big(\bar{q}_L^{(i)}\tilde{\phi}_1\big)q_{uR}^{(j)} + U^q_{2,ij}\big(\bar{q}_L^{(i)}\tilde{\phi}_2\big)q_{uR}^{(j)} + \text{h.c.}\Big] + \tag{2.18}$$

$$+ [\bar{l}Hl \quad \text{terms}]\,, \tag{2.19}$$

where the 3×3 matrices D_1, D_2, U_1, U_2 are such that diagonalize simultaneously with the quark mass matrix.

2.2 2HDM spectrum

2.2.1 Higgs sector

We will use this structure for the doublets:

$$\phi_i = \begin{pmatrix} \phi_i^+ \\ \operatorname{Re}\phi_i^0 + i\operatorname{Im}\phi_i^0 \end{pmatrix} \qquad i = 1, 2\,. \tag{2.20}$$

These fields are not physical fields, they do not have a well defined mass, as there are bilinear terms within the scalar fields with different fields. The next thing is to diagonalize the mass matrix. It can be seen that the mass matrix is a diagonal matrix in boxes for the fields a) ϕ_1^+, ϕ_2^+, b) $\operatorname{Re}\phi_1^0, \operatorname{Re}\phi_2^0$ and c) $\operatorname{Im}\phi_1^0, \operatorname{Im}\phi_2^0$ (the real and imaginary part can be treated separately by CP invariance). So we have to separately diagonalize the different boxes. If we define the rotation angle as:

$$R(\omega) = \begin{pmatrix} \cos\omega & \sin\omega \\ -\sin\omega & \cos\omega \end{pmatrix}\,, \tag{2.21}$$

the rotations (transformations) of the fields are:

$$\begin{pmatrix} G^{\pm} \\ H^{\pm} \end{pmatrix} = R(\beta) \begin{pmatrix} \phi_1^{\pm} \\ \phi_2^{\pm} \end{pmatrix} , \tag{2.22}$$

$$\begin{pmatrix} H^0 \\ h^0 \end{pmatrix} = \sqrt{2} R(\alpha) \begin{pmatrix} \mathrm{Re}\,\phi_1^0 - v_1 \\ \mathrm{Re}\,\phi_2^0 - v_2 \end{pmatrix} , \tag{2.23}$$

$$\begin{pmatrix} G^0 \\ A^0 \end{pmatrix} = \sqrt{2} R(\beta) \begin{pmatrix} \mathrm{Im}\,\phi_1^0 \\ \mathrm{Im}\,\phi_2^0 \end{pmatrix} , \tag{2.24}$$

with their masses:

$$m_{H^{\pm}}^2 = \lambda_4 (v_1^2 + v_2^2) , \tag{2.25}$$

$$m_{A^0}^2 = \lambda_5 (v_1^2 + v_2^2) , \tag{2.26}$$

$$m_{H^0,h^0}^2 = \frac{1}{2} \left[M_{11} + M_{22} \pm \sqrt{(M_{11} - M_{22})^2 + 4M_{12}^2} \right] , \tag{2.27}$$

where M_{ij} are defined from the CP-even mass matrix

$$M = \begin{pmatrix} 4v_1^2(\lambda_1 + \lambda_3) + v_2^2 \lambda_5 & (4\lambda_3 + \lambda_5) v_1 v_2 \\ (4\lambda_3 + \lambda_5) v_1 v_2 & 4v_2^2(\lambda_2 + \lambda_3) + v_1^2 \lambda_5 \end{pmatrix} . \tag{2.28}$$

The mixing angles β and α are:

$$\tan\beta = \frac{v_2}{v_1} , \tag{2.29}$$

$$\sin 2\alpha = \frac{2M_{12}}{\sqrt{(M_{11} - M_{22})^2 + 4M_{12}^2}} ,$$

$$\cos 2\alpha = \frac{M_{11} - M_{22}}{\sqrt{(M_{11} - M_{22})^2 + 4M_{12}^2}} . \tag{2.30}$$

Now we can redefine the parameters of the theory as:

$$4 \text{ masses} : m_{h^0}, m_{H^0}, m_{A^0}, m_{H^{\pm}} \tag{2.31}$$

$$2 \text{ mixing angles} : \alpha, \beta \tag{2.32}$$

At tree level we get:

$$\frac{G_F}{\sqrt{2}} = \frac{g^2}{8M_W^2} , \tag{2.33}$$

where we find the value of v

$$v = \sqrt{v_1^2 + v_2^2} = 2^{-3/4} G_F^{-1/2} \sim 174\, GeV. \tag{2.34}$$

To obtain the magnitudes as functions of the physical magnitudes one has to invert the mass equations (2.25) and (2.30):

$$\lambda_1 = \frac{\cos^2\alpha\, m_{H^0}^2 + \sin^2\alpha\, m_{h^0}^2}{4\, v_1^2} - \frac{v_2^2}{4\, v_1^2}\,\lambda_5 - \lambda_3\,, \tag{2.35}$$

$$\lambda_2 = \frac{\sin^2\alpha\, m_{H^0}^2 + \cos^2\alpha\, m_{h^0}^2}{4\, v_2^2} - \frac{v_1^2}{4\, v_2^2}\lambda_5 - \lambda_3\,, \tag{2.36}$$

$$\lambda_3 = \cos\alpha\,\sin\alpha\,\frac{m_{H^0}^2 - m_{h^0}^2}{4\, v_1 v_2} - \frac{\lambda_5}{4}\,, \tag{2.37}$$

$$\lambda_4 = \frac{m_{H^\pm}^2}{v^2}\,, \tag{2.38}$$

$$\lambda_5 = \frac{m_{A^0}^2}{v^2}\,. \tag{2.39}$$

2.3 Interactions in the mass-eigenstate basis

We need to convert the interaction Lagrangian to a Lagrangian in the mass-eigenstate basis, which is the one used in the computation of the physical quantities. We quote only the interactions that we will need in our studies.

- W–Higgs: this interaction is obtained from the kinetic term of the Lagrangian:

$$\begin{aligned}
\mathcal{L}_{WHH} &= \frac{ig}{2} W_\mu^+ \begin{pmatrix} G_1^+ \\ H_2^+ \end{pmatrix}^\dagger \overleftrightarrow{\partial_\mu} \left[R(\beta-\alpha) \begin{pmatrix} H^0 \\ h^0 \end{pmatrix} + i \begin{pmatrix} G^0 \\ A^0 \end{pmatrix} \right] + \text{h. c.} \\
\mathcal{L}_{WWH} &= g M_W W^2 \begin{pmatrix} \cos(\beta-\alpha) & \sin(\beta-\alpha) \end{pmatrix} \begin{pmatrix} H^0 \\ h^0 \end{pmatrix}.
\end{aligned} \tag{2.40}$$

- quarks–Higgs: they follow after replacing in (2.10) and (2.14) the mass-eigenstates Higgs fields (2.22):

$$\begin{Bmatrix} \mathcal{L}_{Htb}^I \\ \mathcal{L}_{Htb}^{II} \end{Bmatrix} = \frac{g V_{tb}}{\sqrt{2}\, M_W}\, H^- \overline{b} \left[m_t \cot\beta\, P_R + m_b \begin{Bmatrix} -\cot\beta \\ \tan\beta \end{Bmatrix} P_L \right] t + \text{h.c.} \tag{2.41}$$

$$\begin{aligned}
\begin{Bmatrix} \mathcal{L}_{hqq}^I \\ \mathcal{L}_{hqq}^{II} \end{Bmatrix} &= \frac{-g\, m_b}{2\, M_W \begin{Bmatrix} \sin\beta \\ \cos\beta \end{Bmatrix}} \overline{b} \left[h^0 \begin{Bmatrix} \cos\alpha \\ -\sin\alpha \end{Bmatrix} + H^0 \begin{Bmatrix} \sin\alpha \\ \cos\alpha \end{Bmatrix} \right] b \\
&+ \frac{i\, g\, m_b}{2\, M_W} \begin{Bmatrix} -\cot\beta \\ \tan\beta \end{Bmatrix} \overline{b}\, \gamma_5\, b\, A^0 + \frac{i\, g\, m_t}{2\, M_W \tan\beta}\, \overline{t}\, \gamma_5\, t\, A^0 \\
&+ \frac{-g\, m_t}{2\, M_W\, \sin\beta}\, \overline{t} \left[h^0\, \cos\alpha + H^0\, \sin\alpha \right] t\,.
\end{aligned} \tag{2.42}$$

$H^{\pm}H^{\mp}H^0$	$-\frac{g}{M_W \sin 2\beta}\left[(m^2_{H^\pm} - m^2_{A^0} + \frac{1}{2}m^2_{H^0})\sin 2\beta\cos(\beta-\alpha) + \right.$ $\left. +(m^2_{A^0} - m^2_{H^0})\cos 2\beta \sin(\beta-\alpha)\right]$
$H^{\pm}H^{\mp}h^0$	$-\frac{g}{M_W \sin 2\beta}\left[(m^2_{H^\pm} - m^2_{A^0} + \frac{1}{2}m^2_{h^0})\sin 2\beta\sin(\beta-\alpha) + \right.$ $\left. +(m^2_{h^0} - m^2_{A^0})\ \cos 2\beta\ \cos(\beta-\alpha)\right]$
$h^0h^0H^0$	$-\frac{g\cos(\beta-\alpha)}{2\,M_W\ \sin 2\beta}\ \left[(2\,m^2_{h^0} + m^2_{H^0})\ \sin 2\alpha - \right.$ $\left. -m^2_{A^0}\,(3\sin 2\alpha - \sin 2\beta)\right]$
$A^0A^0H^0$	$-\frac{g}{2\,M_W \sin 2\beta}\ \left[m^2_{H^0}\ \sin 2\beta\cos(\beta-\alpha) + \right.$ $\left. +2(m^2_{H^0} - m^2_{A^0})\ \cos 2\beta\ \sin(\beta-\alpha)\right]$
$A^0A^0h^0$	$-\frac{g}{2\,M_W \sin 2\beta}\ \left[m^2_{h^0}\ \sin 2\beta\sin(\beta-\alpha) + \right.$ $\left. +2(m^2_{h^0} - m^2_{A^0})\ \cos 2\beta\ \cos(\beta-\alpha)\right]$
$H^{\pm} - H^{\mp} - A^0$	0
$H^{\pm} - G^{\mp} - H^0$	$(-ig)(m^2_{H^\pm} - m^2_{H^0})\dfrac{\sin(\beta-\alpha)}{2M_W}$
$H^{\pm} - G^{\mp} - h^0$	$ig(m^2_{H^\pm} - m^2_{h^0})\dfrac{\cos(\beta-\alpha)}{2M_W}$
$H^{\pm} - G^{\mp} - A^0$	$\pm g\,\dfrac{(m^2_{H^\pm} - m^2_{A^0})}{2M_W}$
$G^{\pm} - G^{\mp} - H^0$	$(-ig)\dfrac{m^2_{H^0}\cos(\beta-\alpha)}{2M_W}$
$G^{\pm} - G^{\mp} - h^0$	$(-ig)\dfrac{m^2_{h^0}\sin(\beta-\alpha)}{2M_W}$
$G^{\pm} - G^{\mp} - A^0$	0

Table 2.1: Feynman rules for the trilinear couplings involving the Higgs self-interactions and the Higgs and Goldstone boson vertices in the Feynman gauge, with all momenta pointing inward. These rules are common to both Type I and Type II 2HDM under the conditions explained in the text. We have singled out some null entries associated to CP violation.

where we have used the third quark family, the V_{tb} is the corresponding element of the CKM matrix and $P_{L,R} = (1/2)(1 \mp \gamma_5)$ are the chiral projectors.

- Trilinear Higgs couplings: they are summarized in 2.1, and are valid for Type I and Type II models. Had we not imposed the restriction $\lambda_5 = \lambda_6$, then the trilinear rules would be explicitly dependent on the λ_5 parameter.

2.4 Constraints

There are multiple constraints that must be imposed, obviously one of such constraints is that they must reproduce the behaviour of the SM up to energy scales probed so far.

Analysing the perturbativity of the theory one finds that the allowed range for $\tan\beta$ is:

$$0.1 < \tan\beta \lesssim 60\,. \tag{2.43}$$

The custodial symmetry [73, 74] ($SU(2)$) is a good symmetry at tree level, so the quadratic violations of this symmetry must be experimentally fixed. So, the one-loop corrections of the parameter ρ from the 2HDM sector can not be bigger than one per mil of the SM [75]:

$$|\delta\rho^{\mathrm{2HDM}}| \leqslant 0.001\,. \tag{2.44}$$

To be precise, the latter is the extra effect that $\delta\rho$ can accommodate at one standard deviation ($1\,\sigma$) from the 2HDM fields beyond the SM contribution [43]. This is a stringent restriction that affects the possible mass splittings among the Higgs fields of the 2HDM, and its implementation in our codes does severely prevent the possibility from playing with the Higgs boson masses to artificially enhance the FCNC contributions.

Moreover, the charged Higgs bosons have an important indirect restriction from the radiative decays of the B meson, specially the ratio $B(B \to X_s\,\gamma)$ – or $B(b \to s\gamma)$ at the quark level [52–58]:

$$B(b \to s\gamma) = (3.3 \pm 0.4) \times 10^{-4}\,. \tag{2.45}$$

The Higgs contribution to $B(b \to s\gamma)$ (that have been computed at the NLO in QCD [62]) is positive: bigger experimental ratio means that the charged Higgs mass can be smaller. From the different analysis of the literature [59–62] we get:

$$m_{H^\pm} > 350\,\mathrm{GeV} \tag{2.46}$$

for virtually any $\tan\beta \gtrsim 1$. This bound does not apply to Type I models because at large $\tan\beta$ the charged Higgs couplings are severely suppressed, whereas at low $\tan\beta$ we recover the previous unrestricted situation of Type II models.

We can derive lower bounds for the neutral Higgs masses in these models [76, 77]. For example, using the Bjorken process $e^+e^- \to Z + h^0$ and the production of pairs of Higgs boson $e^+e^- \to h^0(H^0) + A^0$ we can get the following restrictions in almost all the parameter space [78, 79]:

$$m_{h^0} + m_{A^0} \begin{cases} \gtrsim 100\,\mathrm{GeV} & \forall\,\tan\beta \\ \gtrsim 150\,\mathrm{GeV} & \tan\beta > 1 \end{cases}. \tag{2.47}$$

In each of these cases there is a small region in the parameter space in the ranges of the CP-even Higgs masses and CP-odd masses around [78, 79]:

$$m_{h,^0A^0} = 20 - 30\,\mathrm{GeV}\,. \tag{2.48}$$

Although, as can be seen in the electroweak precision fits in Ref. [80], in the high $\tan\beta$ range a light Higgs boson h^0 is statistically correlated with a light $H^{\pm}$, so this situation is not favoured by the $b \to s\gamma$ restriction. Moreover, since our interest in Type II models is mainly focused in the large $\tan\beta$ regime, the corner in the light CP-even mass range is a bit contrived. At the end of the day one finds that, even in the worst situation, the strict experimental limits still allow generic 2HDM neutral scalar bosons as light as $70\,GeV$ or so. As we said, most of these limits apply to Type II 2HDM's, but we will conservatively apply them to Type I models as well.

Finally, the unitarity bound can be approximately formulated by imposing that the absolute value of the trilinear coupling of the 2HDM Higgs can not be bigger than the Trilinear coupling of the SM Higgs:

$$|\lambda_{HHH}| \leqslant \left|\lambda^{(SM)}_{HHH}(m_H = 1\,TeV)\right| = \frac{3\,g\,(1\,TeV)^2}{2\,M_W}\ . \tag{2.49}$$

Chapter 3

The Minimal Supersymmetric Standard Model (MSSM)

3.1 Introduction

It goes beyond the scope of this Thesis to study the formal theory of Supersymmetry [81, 82], however we would like, at least, to give a feeling on what is it. Supersymmetry (SUSY) can be introduced in many manners.

Let us consider the symmetries of the scattering matrix S, that is, those transformations that can be reduced to an interchange of asymptotic states. Before the discovery of Supersymmetry the only symmetries know were: the following: (1) the ones corresponding to the Poincare group; (2) the so called internal global symmetries, both of them ruled by a Lie algebra; and (3) discrete symmetries such as parity (P), charge conjugations (C) and the time reversal (T). A 1967 theorem due to Coleman and Mandula establishes rigorously that, under very general conditions, these are the only symmetries allowed for S if we do not want to induce trivial scattering (fixed angles and speeds) in $2 \to 2$ processes.

This theorem may be eluded relaxing some of its hypotheses. The Supersymmetry appears precisely when assuming that the generators of the new symmetry we want to add have a spinorial character instead of a scalar one, therefore transforming under $(\frac{1}{2}, 0)$ and $(0, \frac{1}{2})$ representations of the Lorentz group. Fermionic spinorial generators necessarily have an anti-commutative algebra, generically known as a graded Lie algebra. The algebra is not closed with just the SUSY generators, thus it can not be understood as an internal symmetry, but it rather forms an extension of the space-time symmetries of the Poincare group.

Following this line of thought, one could relax some other hypotheses of the Coleman-

Mandula theorem in order to introduce new theories. SUSY is the only known extension for the S matrix symmetries. Accepting as the only valid extensions of the Coleman-Mandula theorem conditions the presence of a graded Lie algebra, one can show (Haag, Lopuszańki and Sohnius theorem) that spinorial generators different from those of SUSY are forbidden.

Next, we have to define the "superspace", the supersymmetric space of the "superfields". We add to the space-time coordinates x other sets of spinorial coordinates $(\theta, \bar{\theta})$ (as many sets as the dimension of the space-time) that are Grassmann variables, i.e. they anti-commute. In the case of adding just one set it is said that we have a $N = 1$ Supersymmetry and a $N = 1$ superspace:

$$\begin{aligned} \text{space} - \text{time} &\rightarrow N = 1 \text{ Superspace} \\ x^\mu &\rightarrow (x^\mu, \theta^\alpha, \bar{\theta}^{\dot{\alpha}}) \end{aligned} \tag{3.1}$$

where $\alpha = 1, 2$. The supersymmetric transformations have the parameters $(\Lambda, a, \xi, \bar{\xi})$, where Λ is the Lorentz matrix, a is the translation 4-vector, and the Weyl spinors $\xi, \bar{\xi}$. The generators of SUSY transformations consist of are the ones of the Poincare group and the new spinorial generators Q_α and $\bar{Q}_{\dot{\alpha}}$, satisfying the graded Lie algebra. The infinitesimal purely SUSY transformation of a superfield $\Phi(x, \theta, \bar{\theta})$ is:

$$\Phi \rightarrow \Phi + \delta_S \Phi \tag{3.2}$$

$$\delta_S = -i(\xi^\alpha Q_\alpha + \bar{\xi}_{\dot{\alpha}} \bar{Q}^{\dot{\alpha}}) \tag{3.3}$$

The functions defined in the Superspace are polynomial functions of the $(\theta, \bar{\theta})$ variables (since $\theta_\alpha^2 = \bar{\theta}_{\dot{\alpha}}^2 = 0$). Thus we can decompose the functions (superfields) of this Superspace in components of θ^0, θ_α, $\bar{\theta}_{\dot{\alpha}}$, $\theta_\alpha \theta_\beta$, ... each of these components will be a function of the space-time coordinates. Analogously to the space-time, we can define in the Superspace scalar superfields, vector superfields, ... For example in a 4-dimensional space time with $N = 1$ supersymmetry a scalar superfield has 10 components.

We can define fields with specific properties with respect to the θ variables [81, 82]. A scalar *chiral* field in a $4D$ $N = 1$ Superspace has 4 components:

$$\Phi_L = A + \sqrt{2}\theta\psi + \theta\theta F \equiv (A, \psi, F) \tag{3.4}$$

$$\Phi_R = A^* + \sqrt{2}\bar{\theta}\bar{\psi} + \bar{\theta}\bar{\theta} F^* \equiv (A^*, \bar{\psi}, F^*) \tag{3.5}$$

where A is a scalar field, ψ and $\bar{\psi}$ are Weyl spinors (left-handed and right handed Dirac fermions) and F is an auxiliary scalar field. This auxiliary field is not a dynamical field since its equations of motion do not involve time derivatives. To this end we are left

with a superfield, whose components represent an ordinary scalar field and an ordinary chiral spinor. So if nature is described by the dynamics of this field we would find a chiral fermion and a scalar with identical quantum numbers. That is *Supersymmetry relates particles which differ by spin 1/2*. When a SUSY transformation (Q) acts on a superfield it transform spin s particles into spin $s \pm 1/2$ particles.

Thus, for a $N = 1$ SUSY, we find that to any chiral fermion there should be a scalar particle with exactly the same properties. This fact is on the basis of the absence of quadratic divergences in boson mass renormalization, since for any loop diagram involving a scalar particle there should be a fermionic loop diagram, which will cancel quadratic divergences between each other, though logarithmic divergences remain.

Supersymmetric interactions can be introduced by means of generalized gauge transformations, and by means of a generalized potential function, the Superpotential, which give rise to masses, Yukawa-type interactions, and a scalar potential.

As no scalar particles have been found at the electroweak scale we may infer that, if SUSY exists, it is broken. We can allow SUSY to be broken maintaining the property that no quadratic divergences are allowed: this is the so called Soft-SUSY-Breaking mechanism [83]. We can achieve this by only introducing a small set of SUSY-Breaking terms in the Lagrangian, to wit: masses for the components of lowest spin of a supermultiplet and triple scalar interactions. However, other terms like explicit fermion masses for the matter fields would violate the Soft-SUSY-Breaking condition.

The MSSM is the minimal Supersymmetric extension of the Standard Model. It is introduced by means of a $N = 1$ SUSY, with the minimum number of new particles. Thus for each fermion f of the SM there are two scalars related to its chiral components called "sfermions" ($\tilde{f}_{L,R}$), for each gauge vector V there is also a chiral fermion: "gaugino" ($\tilde{v}$), and for each Higgs scalar H another chiral fermion: "higgsino" ($\tilde{h}$). In the MSSM it turns out that, in order to be able of giving masses to up-type and down-type fermions, we must introduce two Higgs doublets with opposite hypercharge, and so the MSSM Higgs sector is of the so called Type II 2HDM (see chapter 2, section 3.4.1 and Ref. [6]).

To build the MSSM Lagrangian we must build a Lagrangian invariant under the gauge group $\mathrm{SU}(3)_C \times \mathrm{SU}(2)_L \times \mathrm{U}(1)_Y$, it must also include the superfields with the particle content of the Table 3.1 and in addition it must contain the terms that breake supersymmetry softly. But this Lagrangian violates the baryonic and leptonic number, so we have to introduce an additional symmetry. In the case of the MSSM this symmetry is the so-called R-symmetry. In its discrete form it relates the spin (S), the baryonic number (B) and the leptonic number (L) in the so-called R-parity:

$$R = (-1)^{2S+L+3B} \tag{3.6}$$

so that is 1 for the SM fields and -1 for its supersymmetric partners. In the way the MSSM is implemented R-parity is conserved, this means that R-odd particles (the superpartners of SM particles) can only be created in pairs, also that in the final product decay of an R-odd particle at least one SUSY particle exists, and that the Lightest Supersymmetric Particle (LSP) is stable.

3.2 Field content

The field content of the MSSM consist of the fields of the SM plus all their supersymmetric partners, and an additional Higgs doublet. The Table 3.1 shows all the correspondences and all the fields. All these fields suffer some mixing, so the physical (mass eigenstates) fields look much different from these ones, as shown in Table 3.2. The gauge fields mix up to give the well known gauge bosons of the SM, $W^{\pm}_{\mu}$, Z^{0}_{μ}, A_{μ}, the gauginos and higgsinos mix up to give the chargino and neutralino fields, and finally the Left- and Right-chiral sfermions mix among themselves in sfermions of indefinite chirality. Letting aside the intergenerational mixing between fermions and sfermions that give rise to the well known Cabibbo-Kobayashi-Maskawa (CKM and superCKM) matrix.

Superfield	SM particle	Sparticle	$SU(3)_C$	$SU(2)_L$	$U(1)_Y$
Matter					
$\hat{L}$	leptons $L = (\nu_l, l)_L$	*sleptons* $\tilde{L} = (\tilde{\nu}_{lL}, \tilde{l}_L)$	1	2	-1
$\hat{R}$	leptons $R = l^-_L$	*sleptons* $\tilde{R} = \tilde{l}^+_R$	1	1	2
$\hat{Q}$	quarks $Q = (u, d)_L$	*squarks* $\tilde{Q} = (\tilde{u}_L, \tilde{d}_L)$	3	2	1/3
$\hat{U}$	quarks $U = u^c_L$	*squarks* $\tilde{U} = \tilde{u}^*_R$	3^*	1	$-4/3$
$\hat{D}$	quarks $D = d^c_L$	*squarks* $\tilde{D} = \tilde{d}^*_R$	3^*	1	2/3
$\hat{H}_1$	Higgs $H_1 = (H^0_1, H^-_1)$	*Higgsinos* $\tilde{H}_1 = (\tilde{H}^0_1, \tilde{H}^-_1)$	1	2	-1
$\hat{H}_2$	Higgs $H_2 = (H^+_2, H^0_2)$	*Higgsinos* $\tilde{H}_2 = (\tilde{H}^+_2, \tilde{H}^0_2)$	1	2	1
Gauge					
$\hat{G}$	gluon g_μ	*gluino* $\tilde{g}$	8	0	0
$\hat{V}$	w (W_1, W_2, W_3)	*wino* $(\tilde{W}_1, \tilde{W}_2, \tilde{W}_3)$	1	3	0
$\hat{V}'$	b B^0	*bino* $(\tilde{B}^0$	1	1	0

Table 3.1: Particle contents of the MSSM superfields

Name	Mass eigenstates	Gauge eigenstates
Higgs bosons	$h^0\ H^0\ A^0\ H^\pm$	$H_1^0\ H_2^0\ H_1^-\ H_2^+$
squarks	$\tilde{t}_1\ \tilde{t}_2\ \tilde{b}_1\ \tilde{b}_2$	$\tilde{t}_L\ \tilde{t}_R\ \tilde{b}_L\ \tilde{b}_R$
sleptons	$\tilde{\tau}_1\ \tilde{\tau}_2\ \tilde{\nu}_\tau$	$\tilde{\tau}_L\ \tilde{\tau}_R\ \tilde{\nu}_\tau$
neutralinos	$\tilde{N}_1\ \tilde{N}_2\ \tilde{N}_3\ \tilde{N}_4$	$\tilde{B}^0\ \tilde{W}^0\ \tilde{H}_1^0\ \tilde{H}_2^0$
charginos	$\tilde{C}_1^\pm\ \tilde{C}_2^\pm$	$\tilde{W}^\pm\ \tilde{H}_1^-\ \tilde{H}_2^+$

Table 3.2: Mass eigenstates of the MSSM particles. For notational simplicity only the third sfermion generation is presented.

3.3 Lagrangian

The MSSM interactions come from three different kinds of sources:

- Superpotential:

$$W = \epsilon_{ij}\left[f\hat{H}_1^i\hat{L}^j\hat{R} + h_d\hat{H}_1^i\hat{Q}^j\hat{D} + h_u\hat{H}_2^j\hat{Q}^i\hat{U} - \mu\hat{H}_1^i\hat{H}_2^j\right] \ . \tag{3.7}$$

  The superpotential contributes to the interaction Lagrangian (3.14) with two different kind of interactions. The first one is the Yukawa interaction, which is obtained from (3.7) just replacing two of the superfields by its fermionic field content, whereas the third superfield is replaced by its scalar field content:

$$\begin{aligned} V_Y \ = \ & \epsilon_{ij}\left[fH_1^iL^jR + h_dH_1^iQ^jD + h_uH_2^jQ^iU - \mu\tilde{H}_1^i\tilde{H}_2^j\right] \\ & +\epsilon_{ij}\left[f\tilde{H}_1^iL^j\tilde{R} + h_d\tilde{H}_1^iQ^j\tilde{D} + h_u\tilde{H}_2^jQ^i\tilde{U}\right] \\ & +\epsilon_{ij}\left[f\tilde{H}_1^i\tilde{L}^jR + h_d\tilde{H}_1^i\tilde{Q}^jD + h_u\tilde{H}_2^j\tilde{Q}^iU\right] \\ & + \text{h.c.} \ . \end{aligned} \tag{3.8}$$

  The second kind of interactions are obtained by means of taking the derivative of the superpotential:

$$V_W = \sum_i \left|\frac{\partial W(\varphi)}{\partial\varphi_i}\right|^2 \ , \tag{3.9}$$

  φ_i being the scalar components of superfields.

- Interactions related to the gauge symmetry, which contain:
  - the usual gauge interactions

– the gaugino interactions:

$$V_{\tilde{G}\psi\tilde{\psi}} = i\sqrt{2}g_a\varphi_k\bar{\lambda}^a\left(T^a\right)_{kl}\bar{\psi}_l + \text{ h.c.} \tag{3.10}$$

where (φ, ψ) are the spin 0 and spin 1/2 components of a chiral superfield respectively, T^a is a generator of the gauge symmetry, λ_a is the gaugino field and g^a its coupling constant.

– and the D-terms, related to the gauge structure of the theory, but that do not contain neither gauge bosons nor gauginos:

$$V_D = \frac{1}{2}\sum D^a D^a \ , \tag{3.11}$$

with

$$D^a = g^a\varphi_i^*\left(T^a\right)_{ij}\varphi_j \ , \tag{3.12}$$

φ_i being the scalar components of the superfields.

- Soft-SUSY-Breaking interaction terms:

$$V_{\text{soft}}^{\text{I}} = \frac{g}{\sqrt{2}M_W\cos\beta}\epsilon_{ij}\left[m_l A_l H_1^i\tilde{L}^j\tilde{R} + m_d A_d H_1^i\tilde{Q}^j\tilde{D} - m_u A_u H_2^i\tilde{Q}\tilde{U}\right] + \text{ h.c.} \quad . \tag{3.13}$$

The trilinear Soft-SUSY-Breaking couplings A_f can play an important role, specially for the third generation interactions and masses, and they are in the source of the large value of the bottom quark mass renormalization effects.

The full MSSM Lagrangian is then:

$$\begin{aligned}
\mathcal{L}_{\text{MSSM}} \;=\; & \mathcal{L}_{\text{Kinetic}} + \mathcal{L}_{\text{Gauge}} - V_{\tilde{G}\psi\tilde{\psi}} - V_D - V_Y - \sum_i\left|\frac{\partial W\left(\varphi\right)}{\partial\varphi_i}\right|^2 \\
& - V_{\text{soft}}^{\text{I}} - m_1^2\, H_1^\dagger H_1 - m_2^2\, H_2^\dagger H_2 - m_{12}^2\left(H_1 H_2 + H_1^\dagger H_2^\dagger\right) \\
& - \frac{1}{2}m_{\tilde{g}}\,\psi_{\tilde{g}}^a\psi_{\tilde{g}}^a - \frac{1}{2}M\,\tilde{w}_i\tilde{w}_i - \frac{1}{2}M'\,\tilde{B}^0\tilde{B}^0 \\
& - m_{\tilde{L}}^2\,\tilde{L}^*\tilde{L} - m_{\tilde{R}}^2\,\tilde{R}^*\tilde{R} - m_{\tilde{Q}}^2\,\tilde{Q}^*\tilde{Q} - m_{\tilde{U}}^2\,\tilde{U}^*\tilde{U} - m_{\tilde{D}}^2\,\tilde{D}^*\tilde{D} \ ,
\end{aligned} \tag{3.14}$$

where we have also included the Soft-SUSY-breaking masses.

From the Lagrangian (3.14) we can obtain the full MSSM spectrum, as well as the interactions, which contain the usual SM gauge interactions, the fermion-Higgs interactions that correspond to a Type II Two-Higgs-Doublet Model [6], and the pure SUSY interactions. A very detailed treatment of this Lagrangian, and the process of derivation of the forthcoming results can be found in [84].

3.4 MSSM spectrum

3.4.1 Higgs boson sector

As seen in 2.1, when a Higgs doublet is added to the SM there exist two possibilities for incorporating it, avoiding Flavour Changing Neutral Currents (FCNC) at tree level [6]. The first possibility is not to allow a coupling between the second doublet and the fermion fields, this is the so called Type I 2HDM. The second possibility is to allow both Higgs doublets to couple with fermions, the first doublet only coupling to the Right-handed down-type fermions, and the second one to Right-handed up-type fermions, this is the so called Type II 2HDM.

The Higgs sector of the MSSM is that of a Type II 2HDM [6], with some SUSY restrictions. After expanding (3.14) the Higgs potential reads

$$\begin{aligned} V &= m_1^2\,|H_1|^2 + m_2^2\,|H_2|^2 - m_{12}^2\,\left(\epsilon_{ij}\,H_1^i\,H_2^j + \text{h.c.}\right) \\ &+ \frac{1}{8}(g^2+g'^2)\,\left(|H_1|^2 - |H_2|^2\right)^2 + \frac{1}{2}\,g^2\,|H_1^\dagger\,H_2|^2\,. \end{aligned} \tag{3.15}$$

This is equivalent to the 2HDM potential (2.9) with the following restrictions:

$$\lambda_1 = \lambda_2 \tag{3.16}$$

$$\lambda_3 = \frac{1}{8}(g^2+g'^2) - \lambda_1 \tag{3.17}$$

$$\lambda_4 = 2\lambda_1 - \frac{1}{2}g^2 \tag{3.18}$$

$$\lambda_5 = \lambda_6 = 2\lambda_1 - \frac{1}{2}(g^2+g'^2). \tag{3.19}$$

The neutral Higgs bosons fields acquire a vacuum expectation value (VEV),

$$\langle H_1\rangle_0 = \begin{pmatrix} v_1 \\ 0 \end{pmatrix} \quad \langle H_2\rangle_0 = \begin{pmatrix} 0 \\ v_2 \end{pmatrix}\ . \tag{3.20}$$

We need two physical parameters in order to know their value, which are usually taken to be M_W and $\tan\beta$:

$$M_W^2 = \frac{1}{2}g^2(v_1^2+v_2^2) \equiv g^2\frac{v^2}{2} \tag{3.21}$$

$$M_Z^2 = \frac{1}{2}(g^2+g'^2)v^2 \equiv M_W^2\cos^2\theta_W \tag{3.22}$$

$$\tan\beta = \frac{v_2}{v_1}\ , \quad 0<\beta<\frac{\pi}{2} \tag{3.23}$$

$$\tan\theta_W = \frac{g'}{g} \tag{3.24}$$

These VEV's make the Higgs fields to mix up. There are five physical Higgs fields: a couple of charged Higgs bosons ($H^{\pm}$); a "pseudoscalar" Higgs ($CP = -1$) A^0; and two scalar Higgs bosons ($CP = 1$) H^0 (the heaviest) and h^0 (the lightest). There are also the Goldstone bosons G^0 and $G^{\pm}$. The relation between the physical Higgs fields and that fields of (3.2) is

$$\begin{pmatrix} -H_1^{\pm} \\ H_2^{\pm} \end{pmatrix} = \begin{pmatrix} \cos\beta & -\sin\beta \\ \sin\beta & \cos\beta \end{pmatrix} \begin{pmatrix} G^{\pm} \\ H^{\pm} \end{pmatrix} , \tag{3.25}$$

$$\begin{aligned} \begin{pmatrix} H_1^0 \\ H_2^0 \end{pmatrix} = \begin{pmatrix} v_1 \\ v_2 \end{pmatrix} + \frac{1}{\sqrt{2}} \begin{pmatrix} \cos\beta & -\sin\beta \\ \sin\beta & \cos\beta \end{pmatrix} \begin{pmatrix} H^0 \\ h^0 \end{pmatrix} \\ + \frac{i}{\sqrt{2}} \begin{pmatrix} -(\cos\beta & -\sin\beta) \\ \sin\beta & \cos\beta \end{pmatrix} \begin{pmatrix} G^0 \\ A^0 \end{pmatrix} \end{aligned} \tag{3.26}$$

where α is given in (3.28) [6].

All the masses of the Higgs sector of the MSSM can be obtained with only two parameters, the first one is $\tan\beta$ (3.24), and the second one is a mass; usually this second parameter is taken to be either the charged Higgs mass $m_{H^{\pm}}$ or the pseudoscalar Higgs mass m_{A^0}. We will take the last option. From (3.15) one can obtain the tree-level mass relations between the different Higgs particles,

$$\begin{aligned} m_{H^{\pm}}^2 &= m_{A^0}^2 + M_W^2 \ , \\ m_{H^0,h^0}^2 &= \frac{1}{2}\left(m_{A^0}^2 + M_Z^2 \pm \sqrt{\left(m_{A^0}^2 + M_Z^2\right)^2 - 4\, m_{A^0}^2\, M_Z^2 \cos^2 2\beta} \right) \ , \end{aligned} \tag{3.27}$$

and the mixing angle between the two scalar Higgs is obtained by means of:

$$\cos 2\alpha = -\cos 2\beta \left(\frac{m_{A^0}^2 - M_Z^2}{m_{H^0}^2 - m_{h^0}^2} \right) \ , \ \sin 2\alpha = -\sin 2\beta \left(\frac{m_{H^0}^2 + m_{h^0}^2}{m_{H^0}^2 - m_{h^0}^2} \right) \ . \tag{3.28}$$

The immediate consequence of such a constrained Higgs sector, is the existence of absolute bounds (at tree level) for the Higgs masses:

$$0 < m_{h^0} < M_Z < m_{H^0}, \quad M_W < m_{H^{\pm}}. \tag{3.29}$$

It must be taken into account, though, that the radiative corrections, mainly due to the top-stop supermultiplet, and also the bottom-sbottom one, are susceptible of relaxing the limits (3.29) in a significant manner.

A good approximation for effective mixing angle α_{eff} including only the leading one-loop contributions of top, stop, bottom and sbottom follows from the diagonalization of

the one-loop Higgs mass matrix [85–88]:

$$\mathcal{M}^2_{\text{Higgs}} = \frac{\sin 2\beta}{2}\begin{pmatrix} \cot\beta\ M_Z^2 + \tan\beta\ m^2_{A^0} + \sigma_t + \omega_b & -M_Z^2 - m^2_{A^0} + \lambda_t + \lambda_b \\ -M_Z^2 - m^2_{A^0} + \lambda_t + \lambda_b & \tan\beta\ M_Z^2 + \cot\beta\ m^2_{A^0} + \omega_t + \lambda_b \end{pmatrix}. \tag{3.30}$$

where

$$\begin{aligned}
\omega_t = \frac{N_C G_F m_t^4}{\sqrt{2}\pi^2 \sin^2\beta} & \left(\log\left(\frac{m_{\tilde{t}_1} m_{\tilde{t}_2}}{m_t^2}\right) + \frac{A_t(A_t - \mu\cot\beta)}{m^2_{\tilde{t}_1} - m^2_{\tilde{t}_2}} \log\frac{m^2_{\tilde{t}_1}}{m^2_{\tilde{t}_2}} \right. \\
& \left. + \frac{A_t^2 (A_t - \mu\cot\beta)^2}{(m^2_{\tilde{t}_1} - m^2_{\tilde{t}_2})^2}\left(1 - \frac{m^2_{\tilde{t}_1} + m^2_{\tilde{t}_2}}{m^2_{\tilde{t}_1} - m^2_{\tilde{t}_2}} \log\frac{m_{\tilde{t}_1}}{m_{\tilde{t}_2}}\right) \right) \\
\lambda_t = -\frac{N_C G_F m_t^4}{\sqrt{2}\pi^2 \sin^2\beta} & \left(\frac{\mu(A_t - \mu\cot\beta)}{m^2_{\tilde{t}_1} - m^2_{\tilde{t}_2}} \log\frac{m^2_{\tilde{t}_1}}{m^2_{\tilde{t}_2}} \right. \\
& \left. + \frac{2\mu A_t (A_t - \mu\cot\beta)^2}{(m^2_{\tilde{t}_1} - m^2_{\tilde{t}_2})^2}\left(1 - \frac{m^2_{\tilde{t}_1} + m^2_{\tilde{t}_2}}{m^2_{\tilde{t}_1} - m^2_{\tilde{t}_2}} \log\frac{m_{\tilde{t}_1}}{m_{\tilde{t}_2}}\right) \right) \\
\sigma_t = \frac{N_C G_F m_t^4}{\sqrt{2}\pi^2 \sin^2\beta} & \frac{\mu^2 (A_t - \mu\cot\beta)^2}{(m^2_{\tilde{t}_1} - m^2_{\tilde{t}_2})^2}\left(1 - \frac{m^2_{\tilde{t}_1} + m^2_{\tilde{t}_2}}{m^2_{\tilde{t}_1} - m^2_{\tilde{t}_2}} \log\frac{m_{\tilde{t}_1}}{m_{\tilde{t}_2}}\right)
\end{aligned} \tag{3.31}$$

with the following substitutions for the bottom/sbottom factors:

$$(\omega_b, \lambda_b, \sigma_b) \leftrightarrow (\omega_t, \lambda_t, \sigma_t) \qquad \text{with} \begin{cases} t & \leftrightarrow b \\ \sin\beta & \leftrightarrow \cos\beta \\ A_t - \mu\cot\beta & \leftrightarrow A_b - \mu\tan\beta \end{cases} \tag{3.32}$$

This approximate effective mixing angle α_{eff} is determined by

$$\tan\alpha_{eff} = \frac{-(m^2_{A^0} + M_Z^2)\ \tan\beta + (\lambda_t + \lambda_b)(1 + \tan^2\beta)/2}{M_Z^2 + m^2_{A^0}\tan^2\beta + (\sigma_t + \omega_b - M^2_{h^0,eff})(1 + \tan^2\beta)}\ , \tag{3.33}$$

where $M_{h^0,eff}$ is the solution for the light Higgs mass:

$$\begin{aligned}
M^2_{H^0,h^0,eff} \ = \ & \frac{m^2_{A^0} + M_Z^2 + \omega_t + \sigma_t + \omega_b + \sigma_b}{2} \pm \left(\frac{(m^2_{A^0} + M_Z^2)^2 + (\omega_t - \sigma_t + \sigma_b - \omega_b)^2}{4} \right. \\
& - m^2_{A^0} M_Z^2 \cos^2 2\beta + \frac{(\omega_t - \sigma_t + \sigma_b - \omega_b)\cos 2\beta}{2}(m^2_{A^0} - M_Z^2) \\
& \left. - \frac{(\lambda_t + \lambda_b \sin 2\beta)}{2}(m^2_{A^0} + M_Z^2) + \frac{(\lambda_t + \lambda_b)^2}{4} \right)^{1/2}.
\end{aligned} \tag{3.34}$$

In the limit where $m_{A^0} \gg M_Z$, $\cos(\beta - \alpha) = \mathcal{O}(M_Z^2/m^2_{A^0})$, which means that the h^0 couplings to Standard Model particles approach values corresponding precisely to the couplings of the SM Higgs boson. There is a significant region of MSSM Higgs sector

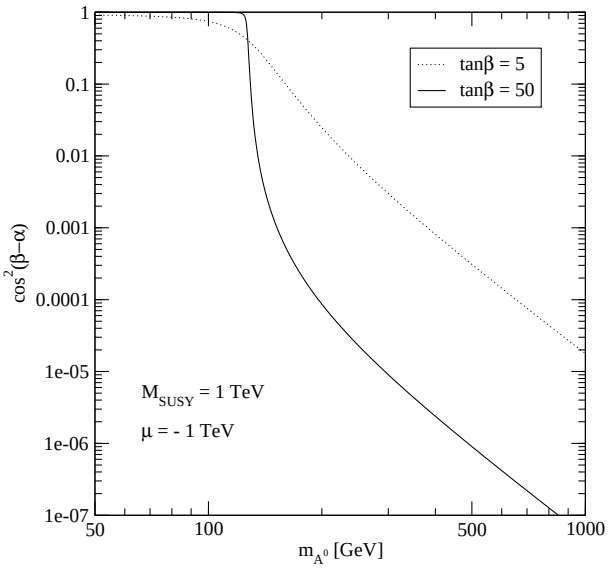

Figure 3.1: The value of $\cos^2(\beta-\alpha)$ is shown as a function of m_{A^0} for two choices of $\tan\beta = 5$ and $\tan\beta = 50$. When radiative-corrections are included, one can define an approximate loop-corrected angle α as a function of m_{A^0}, $\tan\beta$ and the MSSM parameters. In the figures above, we have incorporated radiative corrections, assuming that $M_{\rm SUSY} \equiv m_{\tilde{q}} = m_{\tilde{d}} = m_{\tilde{u}} = 1\,\text{TeV}$. The decoupling effect, in which $\cos^2(\beta-\alpha) \propto M_Z^4/{m_{A^0}}^4$ for $m_{A^0} \gg m_Z$, continues to hold even when radiative corrections are included.

parameter space in which the decoupling limit applies, because $\cos(\beta-\alpha)$ approaches zero quite rapidly once m_{A^0} is larger than about 200 GeV, as shown in Fig. 3.1. As a result, over a significant region of the MSSM parameter space, the search for the lightest CP-even Higgs boson of the MSSM is equivalent to the search for the SM Higgs boson. This result is more general; in many theories of non-minimal Higgs sectors, there is a significant portion of the parameter space that approximates the decoupling limit. Consequently, simulations of the SM Higgs signal are also relevant for exploring the more general Higgs sector.

3.4.2 The SM sector

In this section we give some expressions to obtain some MSSM parameters as a function of the SM parametrization.

As stated above (sec. 3.4.1) the VEV's can be obtained by means of (3.24), and the

Z mass can be obtained at tree-level by the relation:

$$\sin^2\theta_W = 1 - \frac{M_W^2}{M_Z^2} \ .$$

Fermion masses are obtained from the Yukawa potential (3.8) letting the neutral Higgs fields acquire their VEV (3.20). The up-type fermions get their masses from the H_2^0 whereas H_1^0 gives masses to down-type fermions, so

$$m_u = h_u v_2 = \frac{h_u\sqrt{2}M_W \sin\beta}{g} \ , \ m_d = h_d v_1 = \frac{h_d\sqrt{2}M_W \cos\beta}{g} \ ,$$

and the Yukawa coupling can be obtained as

$$\lambda_u = \frac{h_u}{g} = \frac{m_u}{\sqrt{2}M_W \sin\beta} \ , \ \lambda_d = \frac{h_d}{g} = \frac{m_d}{\sqrt{2}M_W \cos\beta} \ . \tag{3.35}$$

3.4.3 Sfermion sector (Flavor-diagonal case)

The sfermion mass terms are obtained from the derivative of the superpotential (3.9), the D-terms (3.11) and the Soft-SUSY-Breaking terms (3.14) letting the neutral Higgs fields get their VEV (3.20), and one obtain the following mass matrices:

$$\mathcal{M}_{\tilde{q}}^2 = \begin{pmatrix} M_{\tilde{q}_L}^2 + m_q^2 + \cos 2\beta (T_3^{q_L} - Q_q s_W^2) M_Z^2 & m_q M_{LR}^q \\ m_q M_{LR}^q & M_{\tilde{q}_R}^2 + m_q^2 + \cos 2\beta \, Q_q \, s_W^2 \, M_Z^2 \end{pmatrix} , \tag{3.36}$$

being Q the corresponding fermion electric charge, $T_3^{q_L}$ the third component of weak isospin, $M_{\tilde{q}_{L,R}}$ the Soft-SUSY-Breaking squark masses [7–10] (by $SU(2)_L$-gauge invariance, we must have $M_{\tilde{t}_L} = M_{\tilde{b}_L}$, whereas $M_{\tilde{t}_R}$, $M_{\tilde{b}_R}$ are in general independent parameters), $s_\theta = \sin\theta_W$, and

$$\begin{aligned} M_{LR}^u &= A_u - \mu \cot\beta \ , \\ M_{LR}^d &= A_d - \mu \tan\beta \ . \end{aligned} \tag{3.37}$$

We define the sfermion mixing matrix as ($\tilde{q'}_a = \{\tilde{q'}_1 \equiv \tilde{q}_L, \ \tilde{q'}_2 \equiv \tilde{q}_R\}$ are the weak-eigenstate squarks, and $\tilde{q}_a = \{\tilde{q}_1, \tilde{q}_2\}$ are the mass-eigenstate squark fields)

$$\begin{aligned} \tilde{q'}_a &= \sum_b R_{ab}^{(q)} \tilde{q}_b, \\ R^{(q)} &= \begin{pmatrix} \cos\theta_q & -\sin\theta_q \\ \sin\theta_q & \cos\theta_q \end{pmatrix} . \end{aligned} \tag{3.38}$$

$$R^{(q)\dagger} \mathcal{M}_{\tilde{q}}^2 R^{(q)} = \mathrm{diag}\{m_{\tilde{q}_2}^2, m_{\tilde{q}_1}^2\} \qquad (m_{\tilde{q}_2} \geq m_{\tilde{q}_1}) \, , \tag{3.39}$$

$$\tan 2\theta_q = \frac{2\, m_q\, M^q_{LR}}{M^2_{\tilde{q}_L} - M^2_{\tilde{q}_R} + \cos 2\beta (T_3^{q_L} - 2Q_q s^2_W) M^2_Z}\,. \tag{3.40}$$

From eq. (3.36) we can see that the sfermion mass is dominated by the Soft-SUSY-Breaking parameters ($M_{\tilde{f}} \gg m_f$ for $f \neq$ top), and that the non-diagonal terms could be neglected, except in the case of the top squark (and bottom squark at large $\tan\beta$), however we will maintain those terms, the reason is that, although the A parameters do not play any role when computing the sfermion masses, they do play a role in the Higgs-sfermion-sfermion coupling, and thus it has an effect on the Higgs self-energies. Moreover these A parameters are constrained by the approximate (necessary) condition of absence of colour-breaking minima,

$$A_q^2 < 3\,(m_{\tilde{t}}^2 + m_{\tilde{b}}^2 + M_H^2 + \mu^2)\,, \tag{3.41}$$

where $m_{\tilde{q}}$ is of the order of the average squark masses for $\tilde{q} = \tilde{t}, \tilde{b}$ [89–92].

All the Soft-SUSY-Breaking parameters are free in the strict MSSM, however some simplifications must be done to be able of making a feasible numerical analysis. As the main subject of study are the third generation squarks we make a separation between them and the rest of sfermions. This separation is justified by the evolution of the squark masses from the (supposed) unification scale down to the electroweak scale [12] (see also section 3.7.1 for a more detailed discussion).

So we will use the following approximations:

- equality of the diagonal elements of eq. (3.36)

$$\mathcal{M}^2_{\tilde{q}D} \equiv \mathcal{M}^2_{\tilde{q}11} = \mathcal{M}^2_{\tilde{q}22}\ , \tag{3.42}$$

  for each charged slepton and each squark of the the first and second generation.

- the first and second generation squarks share the same value of the A parameter (3.37) and the mass parameter (3.42)

- sleptons also share the same value for (3.42) and A parameters (3.37).

3.4.4 Sfermion sector (Non-flavor-diagonal case)

Very important for our FCNC studies is when the squark mass matrix does not diagonalize with the same matrix as the one for the quarks. We introduce then intergenerational mass terms for the squarks, but in order to prevent the number of parameters from being too large, we have allowed (symmetric) mixing mass terms only for the left-handed squarks. This simplification is often used in the MSSM, and is justified by RGE analysis [93].

The flavor mixing terms are introduced through the parameters δ_{ij} defined as

$$(M^2_{LL})_{ij} = m^2_{ij} \equiv \delta_{ij}\, m_i\, m_j \ , \tag{3.43}$$

where m_i is the mass of the left-handed i squark, and m^2_{ij} is the mixing mass matrix element between the generations i and j. Thus we must diagonalize two 6×6 mass matrices in order to obtain the mass-eigenstates squark fields. Generalizing the notation in Sec. 3.4.3 we introduce the 6×6 mixing matrices as follows:

$$\tilde{q}'_\alpha = \sum_\beta R^{(q)}_{\alpha\beta} \tilde{q}_\beta \tag{3.44}$$

$$R^{(q)\dagger} \mathcal{M}^2_{\tilde{q}} R = \mathcal{M}^2_{\tilde{q}D} = \mathrm{diag}\{m^2_{\tilde{q}_1}, \ldots, m^2_{\tilde{q}_6}\} \ , \ q \equiv u,\, d \ , \tag{3.45}$$

where $\mathcal{M}^2_{(\tilde{u},\tilde{d})}$ is the 6×6 square mass matrix for up-type (or down-type) squarks in the EW basis, with indices $\alpha = 1, 2, 3, \ldots, 6 \equiv \tilde{u}_L, \tilde{u}_R, \ldots, \tilde{t}_R$ for up-type squarks, and similarly for down-type squarks. In this study we are only interested in the up-type quarks-squarks system, so we will drop out the (q) super-index in the forthcoming expressions. The rotation matrix R introduces gluino mediated tree-level FCNC between quarks and squarks.

To analyze the contributions from these flavor and chiral mixed squarks we can use the so-called mass insertion approximation. This is based on the fact that the δ_{ij} parameters are small, so instead of diagonalizing the 6×6 squared mass matrix we can treat them as an interaction (see Fig. 3.2):

$$\begin{aligned} \mathcal{L} \ &\ni \begin{pmatrix} \tilde{q}^*_{iL} & \tilde{q}^*_{jL} \end{pmatrix} \begin{pmatrix} p^2 - m^2_i & m^2_{ij} \\ m^2_{ji} & p^2 - m^2_j \end{pmatrix} \begin{pmatrix} \tilde{q}_{iL} \\ \tilde{q}_{jL} \end{pmatrix} \\ &= \begin{pmatrix} \tilde{q}^*_{iL} & \tilde{q}^*_{jL} \end{pmatrix} \begin{pmatrix} p^2 - m^2_i & 0 \\ 0 & p^2 - m^2_j \end{pmatrix} \begin{pmatrix} \tilde{q}_{iL} \\ \tilde{q}_{jL} \end{pmatrix} + \begin{pmatrix} \tilde{q}^*_{iL} & \tilde{q}^*_{jL} \end{pmatrix} \begin{pmatrix} 0 & m^2_{ij} \\ m^2_{ji} & 0 \end{pmatrix} \begin{pmatrix} \tilde{q}_{iL} \\ \tilde{q}_{jL} \end{pmatrix} \end{aligned} \tag{3.46}$$

and similarly for the left-right squark matrix.

3.5 Interactions in the mass-eigenstate basis

We need to convert the MSSM interaction Lagrangian (3.14) to a Lagrangian in the mass-eigenstate basis, which is the one used in the computation of the physical quantities. As the expression for the full interaction Lagrangian in the MSSM is rather lengthy we quote only the interactions that we will need in our studies.

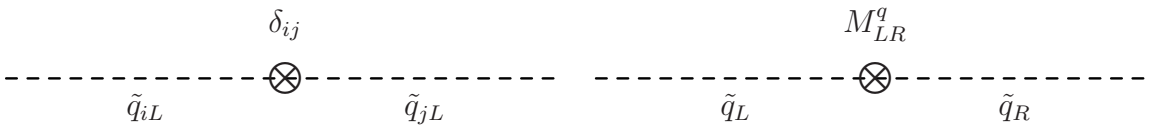

Figure 3.2: Diagrams in the mass insertion approximation

- quark–quark–neutral Higgs: this is the usual Yukawa interaction from Type II 2HDM, in the MSSM it follows after replacing in (3.8) the mass-eigenstate Higgs fields (3.25):

$$\begin{aligned}\mathcal{L}_{Hqq} &= -\frac{g m_d}{2M_W \cos\beta}\left[\left(\cos\alpha\, H^0 - \sin\alpha\, h^0\right)\bar{d}d - i\sin\beta\,\bar{d}\gamma_5 d\, A^0\right] \\ &\quad -\frac{g m_u}{2M_W \sin\beta}\left[\left(\sin\alpha\, H^0 + \cos\alpha\, h^0\right)\bar{u}u - i\cos\beta\,\bar{u}\gamma_5 u\, A^0\right] \ , \quad (3.47)\end{aligned}$$

  where we have replaced the Yukawa couplings h_i in favour of masses and $\tan\beta$.

- quark–gluon interactions: this is the usual QCD Lagrangian

$$\mathcal{L}_{QCD} = \frac{g_s}{2}\, G^c_\mu\, \lambda^c_{ij}\, \bar{q}_i\, \gamma^\mu\, q_j \ . \quad (3.48)$$

- quark–squark–gluino: the supersymmetric version of the strong interaction is obtained from (3.10):

$$\begin{aligned}\mathcal{L}_{\tilde{g}q\tilde{q}} &= -\frac{g_s}{\sqrt{2}}\,\bar{\psi}^{\tilde{g}}_c\left[R^*_{5\alpha}\,P_L - R^*_{6\alpha}\,P_R\right]\tilde{q}^*_{\alpha,i}\,\lambda^c_{ij}\,t_j \\ &- \frac{g_s}{\sqrt{2}}\,\bar{\psi}^{\tilde{g}}_c\left[R^*_{3\alpha}\,P_L - R^*_{4\alpha}\,P_R\right]\tilde{q}^*_{\alpha,i}\,\lambda^c_{ij}\,c_j \\ &- \frac{g_s}{\sqrt{2}}\,\bar{\psi}^{\tilde{g}}_c\left[R^*_{1\alpha}\,P_L - R^*_{2\alpha}\,P_R\right]\tilde{q}^*_{\alpha,i}\,\lambda^c_{ij}\,u_j \ . \quad (3.49)\end{aligned}$$

$$\mathcal{L}_{\tilde{g}q\tilde{q}} = -\frac{g_s}{\sqrt{2}}\tilde{q}^*_{a,i}\,\bar{\psi}^{\tilde{g}}_c\,(\lambda^c)_{ij}\left(R^{(q)*}_{1a}P_L - R^{(q)*}_{2a}P_R\right)q_j + \text{ h.c.} \ , \quad (3.50)$$

  where λ^c are the Gell-Mann matrices.

- squark–squark–neutral Higgs: the origin of this interaction is twofold, on one side the superpotential derivative (3.9), and on the other the Soft-SUSY-Breaking trilinear

interactions. It is convenient to express the results in the $\tilde{q}_L - \tilde{q}_R$ basis, and use the transformation 3.44 or 3.38.

$$\begin{aligned}
\mathcal{L}_{h\tilde{q}\tilde{q}} &= -\frac{gM_Z}{c_\theta}\sum_{i=u,d}\left[(T_3^{iL} - Q_i {s_\theta}^2)\tilde{q}_{iL}^*\tilde{q}_{iL} + Q_i {s_\theta}^2 \tilde{q}_{iR}^*\tilde{q}_{iR}\right] \\
&\qquad \times \left(H^0\cos(\beta+\alpha) - h^0\sin(\beta+\alpha)\right) \\
&- \frac{gm_d^2}{M_W\cos\beta}(\tilde{d}_L^*\tilde{d}_L + \tilde{d}_R^*\tilde{d}_R)(H^0\cos\alpha - h^0\sin\alpha) \\
&- \frac{gm_u^2}{M_W\sin\beta}(\tilde{u}_L^*\tilde{u}_L + \tilde{u}_R^*\tilde{u}_R)(H^0\cos\alpha - h^0\sin\alpha) \\
&- \frac{gm_d}{2M_W\cos\beta}(\tilde{d}_R^*\tilde{d}_L + \tilde{d}_L^*\tilde{d}_R) \\
&\qquad \times \left[(-\mu\sin\alpha + A_d\cos\alpha)H^0 + (-\mu\cos\alpha - A_d\sin\alpha)h^0\right] \\
&- \frac{gm_u}{2M_W\sin\beta}(\tilde{u}_R^*\tilde{u}_L + \tilde{u}_L^*\tilde{u}_R) \\
&\qquad \times \left[(-\mu\cos\alpha + A_u\sin\alpha)H^0 + (+\mu\sin\alpha + A_u\cos\alpha)h^0\right] \\
&- \frac{igm_u}{2M_W}(\mu + A_d\tan\beta)(\tilde{d}_R^*\tilde{d}_L - \tilde{d}_L^*\tilde{d}_R)A^0 \\
&- \frac{igm_u}{2M_W}(\mu + A_u\cot\beta)(\tilde{u}_R^*\tilde{u}_L - \tilde{u}_L^*\tilde{u}_R)A^0
\end{aligned} \tag{3.51}$$

3.6 Flavor changing neutral currents

The most general MSSM includes tree-level FCNCs among the extra predicted particles, which induce one-loop FCNC interactions among the SM particles. Given the observed smallness of these interactions, tree-level SUSY FCNCs are usually avoided by including one of the two following assumptions: either the SUSY particle masses are very large, and their radiative effects are suppressed by the large SUSY mass scale; or the soft SUSY-breaking squark mass matrices are aligned with the SM quark mass matrix, so that both mass matrices are simultaneously diagonal. However, if one looks closely, one soon realizes that the MSSM does not only include the possibility of tree-level FCNCs, but it actually *requires* their existence [93]. Indeed, the requirement of $SU(2)_L$ gauge invariance means that the up-left-squark mass matrix can not be simultaneously diagonal to the down-left-squark mass matrix, and therefore these two matrices can not be simultaneously diagonal with the up-quark and the down-quark mass matrices, that is, unless both of them are proportional to the identity matrix. But even then we could not take such a possibility too seriously, for the radiative corrections would produce non-zero elements in the non-diagonal part of the mass matrix (i.e. induced by $H^\pm$ and $\chi^\pm$, see Fig. 3.3). All in all, we naturally expect tree-level FCNC interactions mediated by the SUSY partners of the

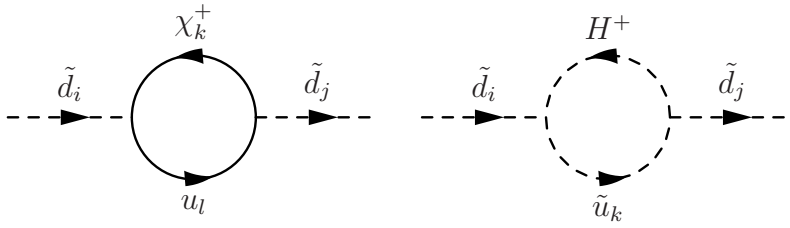

Figure 3.3: Feynman graphs contributing to the squark mixing.

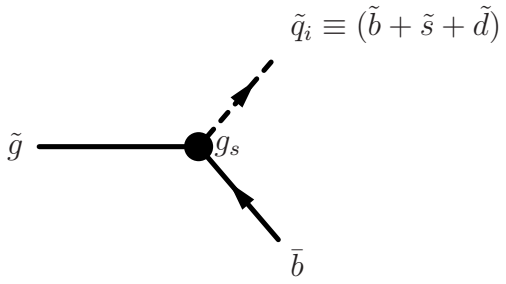

Figure 3.4: Tree level FCNC strong interactions.

SM particles. As an example in the MSSM that one can not set the FCNC Higgs bosons interactions to zero without being inconsistent notice that $\Gamma(\tilde{t} \to c\chi^0)$ is UV divergent in the absent of these couplings [94]. The potentially largest FCNC interactions are those originating from the strong supersymmetric (SUSY-QCD) sector of the model (viz. those interactions involving the squark-quark-gluino couplings, see Fig. 3.4), and in chapters 6 and 7 we mainly concentrate on those. These couplings induce FCNC loop effects on more conventional fermion-fermion interactions, like the gauge boson-quark vertices Vqq'.

Of course, low energy meson physics puts tight constraints on the possible value of the FCNC couplings, especially for the first and second generation squarks which are sensitive to the data on $K^0 - \bar{K}^0$ (see Fig. 3.5) and $D^0 - \bar{D}^0$ [95, 96]. The third generation system is, in principle, very loosely constrained since present data on $B^0 - \bar{B}^0$ mixing still leaves much room for FCNCs and the most stringent constraints are given by the $B(b \to s\gamma)$ measurement [52–58]. Therefore, the relevant FCNC gluino coupling δ_{23} [95, 96] is not severely bound at present. The lack of tight FCNC constraints in the top-bottom quark doublet enables the aforementioned lower bound on the charged Higgs boson mass in the MSSM to be easily avoided, to wit: by arranging that the SUSY-electroweak (SUSY-EW) contribution to $B(b \to s\gamma)$ from the top-squark/chargino loops screens partially

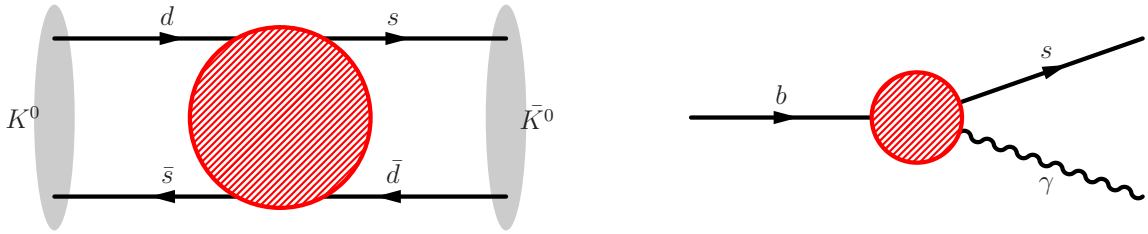

Figure 3.5: Diagram of the processes $K^0 - \bar{K}^0$ and $B \to X_s\,\gamma$ at quark level

the charged Higgs boson contribution. This situation can be naturally fulfilled if the higgsino mass parameter (μ) and the soft SUSY-breaking top-squark trilinear coupling (A_t) satisfy the relation $\mu\, A_t < 0$ [97–101]. The relevant Wilson operator in the effective theory involves a chirality flip:

$$O_7 = \frac{e}{16\pi^2}\; m_b\; (\bar{s}_L\; \sigma^{\mu\nu}\; b_R)\; F_{\mu\nu}. \tag{3.52}$$

In Fig. 3.6 one can see the leading contributions to this operator. The most important contribution is expected to be SUSY-QCD one. Roughly speaking its amplitude goes like:

$$A^{SUSY-QCD}(b \to s\gamma) \sim \delta_{23} \frac{m_b(A_b - \mu \tan\beta)}{M^2_{\rm SUSY}} \times \frac{1}{m_{\tilde{g}}}. \tag{3.53}$$

This amplitude can be as large as minus twice the SM contribution, so the total MSSM amplitude can respect the experimental $b \to s\gamma$ restriction. We would regard this choice as a fine-tuning of the parameters, hence unnatural, but in fact it is excluded experimentally [102].

On the other hand, if we assume that the squark mass matrices are diagonal at a certain energy scale (Λ) and write the Renormalization Group Equations [93], then non-diagonal terms are generated in the left-left sector, because λ_u and λ_d are not simultaneously diagonal.

$$\begin{aligned}
(M^d_{RR})^2 &= \mu_0(\tilde{d}_R)\mathbb{1} + \mu_1(\tilde{d}_R)\lambda_d^\dagger\lambda_d \\
(M^u_{RR})^2 &= \mu_0(\tilde{u}_R)\mathbb{1} + \mu_1(\tilde{u}_R)\lambda_u^\dagger\lambda_u \\
(M^d_{LL})^2 &= \mu_0(\tilde{d}_L)\mathbb{1} + \mu_1(\tilde{d}_L)\lambda_d\lambda_d^\dagger + \mu_2(\tilde{d}_L)\lambda_u\lambda_u^\dagger \\
(M^u_{LL})^2 &= \mu_0(\tilde{u}_L)\mathbb{1} + \mu_1(\tilde{u}_L)\lambda_u\lambda_u^\dagger + \mu_2(\tilde{u}_L)\lambda_d\lambda_d^\dagger
\end{aligned}$$

And then the FCNC terms are communicated from the up to the down sector by the

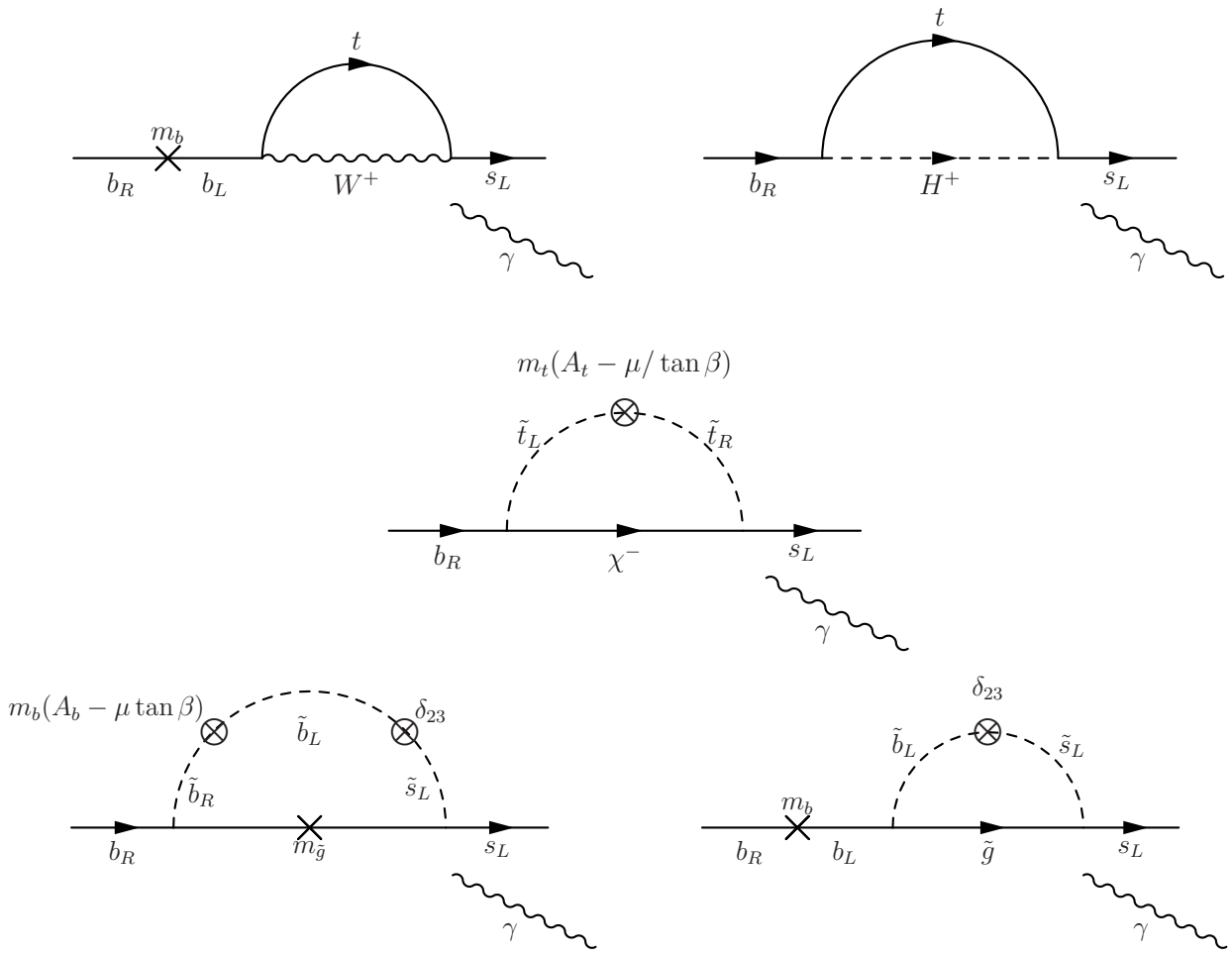

Figure 3.6: Leading contributions to the $b \to s\gamma$ Wilson operator O_7.

CKM matrix, due to the $SU(2)$ gauge invariant:

$$(M^d_{LL})^2 = V^\dagger_{CKM} \times (M^u_{LL})^2 \times V_{CKM} \tag{3.54}$$

The FCNC gluino interactions also induce large contributions to $B(b \to s\gamma)$, see Fig. 3.6. It should be noted however that the leading contributions to the Vqq' FCNC interactions from the third quark generation correspond to a *double insertion* term, in which the squarks propagating in the loop suffer a double mutation: a flavor conversion and a chirality transition. This fact has been demonstrated in the $B(b \to s\gamma)$ observable itself [103], as well as in the FCNC rare decay width $\Gamma(t \to cg)$ [43]. As a consequence, the loose limits on the third generation FCNC interactions derived under the assumption that the leading terms contributing to $b \to s\gamma$ correspond to the *single particle insertion approximation* [95, 96] are not valid and more complex expressions must be taken into account [104].

The FCNC effects in the $K^0 - \bar{K^0}$ system can be described with an effective Lagrangian with a mass matrix as:

$$\begin{pmatrix} m_K^2 & A \\ A & m_K^2 \end{pmatrix} \Rightarrow \text{diagonalize} \Rightarrow m^2_{K_{1,2}} = m_K^2 \pm A \tag{3.55}$$

so the signal of FCNC can determined by the mass difference of the eigenstates:

$$\Delta m_K \equiv |m_{K_1} - m_{K_2}| \tag{3.56}$$

In contrast the experimental signal for $b \to s\gamma$ is directly its branching ratio. The experimental measurements are [19, 53–55, 57]:

$$B(b \to s\gamma) = (3.3 \pm 0.4) \times 10^{-4} \tag{3.57}$$

$$\Delta m_K = (3.483 \pm 0.006) \times 10^{-12}\,\text{MeV} \qquad (d\bar{s} \leftrightarrow \bar{d}s) \tag{3.58}$$

$$m_K = 497.648 \pm 0.022\,\text{MeV}$$

$$\Delta m_D < 4.6 \times 10^{-11}\,\text{MeV} \qquad (c\bar{u} \leftrightarrow \bar{c}u) \tag{3.59}$$

$$m_D = 1864.6 \pm 0.5\,\text{MeV}$$

$$\Delta m_B = (3.304 \pm 0.046) \times 10^{-10}\,\text{MeV} \qquad (b\bar{d} \leftrightarrow \bar{b}d) \tag{3.60}$$

$$m_B = 5279.4 \pm 0.5\,\text{MeV}$$

that translated to δ_{ij} restrictions they read:

$$\begin{aligned} \delta_{12} &\lesssim .1\,\sqrt{m_{\tilde{u}}\, m_{\tilde{c}}}/500\,\text{GeV} \\ \delta_{13} &\lesssim .098\,\sqrt{m_{\tilde{u}}\, m_{\tilde{t}}}/500\,\text{GeV} \\ \delta_{23} &\lesssim 8.2\, m_{\tilde{c}}\, m_{\tilde{t}}/(500\,\text{GeV})^2 \end{aligned} \tag{3.61}$$

3.7 MSSM parametrization

3.7.1 MSSM parameters

Since SUSY is a broken symmetry we have to deal with a plethora of Soft-SUSY-Breaking parameters, namely

- $\tan\beta$,
- masses for Left- and Right-chiral sfermions,
- a mass for the Higgs sector,
- gaugino masses,
- triple scalar couplings for squarks and Higgs.

This set of parameters is often simplified to allow a comprehensive study. Most of these simplifications are based on some universality assumption at the unification scale. In minimal supergravity (mSUGRA) all the parameters of the MSSM are computed from a restricted set of parameters at the Unification scale, to wit: $\tan\beta$; a common scalar mass m_0; a common fermion mass for gauginos $m_{1/2}$; a common trilinear coupling for all sfermions A_0; and the higgsino mass parameter μ. Then one computes the running of each one of these parameters down to the EW scale, using the Renormalization Group Equations (RGE), and the full spectrum of the MSSM is found.

We will not restrict ourselves to a such simplified model. As stated in the introduction we treat the MSSM as an effective Lagrangian, to be embedded in a more general framework that we don't know about. This means that essentially all the parameters quoted above are free. However for the kind of studies we have performed there is an implicit asymmetry of the different particle generations. We are mostly interested in the phenomenology of the third generation, thus we will treat top and bottom supermultiplet as distinguished from the rest. This approach is well justified by the great difference of the Yukawa couplings of top and bottom with respect to the rest of fermions. We are mainly interested on effects on the Higgs sector, so the smallness of the Yukawa couplings of the first two generations will result on small effects in our final result. We include them, though, in the numerical analysis and the numerical dependence is tested. On the other hand, if we suppose that there is unification at some large scale, at which all sfermions have the same mass, and then evolve these masses to the EW scale, then the RGE have great differences [12]. Slepton RGE are dominated by EW gauge interactions, 1st and 2nd generation squarks RGE are dominated by QCD, and for the 3rd generation squarks there

is an interplay between QCD and Yukawa couplings. Also, as a general rule, the gauge contribution to the RGE equations of left- and right-handed squark masses are similar, so when Yukawa couplings are not important they should be similar at the EW scale.

With the statement above in mind we can simplify the MSSM spectrum by taking an unified parametrization for 1st and 2nd generation squarks (same for sleptons). As we have seen in Sect. 3.4.3 we will use: a common mass[1] for $\tilde{u}_L$ and $\tilde{q}_R$ ($m_{\tilde{u}}$); an unified trilinear coupling A_u for 1st and 2nd generation; a common mass for all $\tilde{\nu}_L$ and $\tilde{l}_R$ ($m_{\tilde{\tau}}$); and a common trilinear coupling A_τ.

For the third generation we will use different trilinear couplings A_t and A_b, as these can play an important role in the kind of processes we are studying (see chapter 6 and 7). Stop masses can present a large gap (due to its Yukawa couplings), being the right-handed stop the lightest one. We will use a common mass for both chiral sbottoms, which we parametrize with the lightest sbottom mass ($m_{\tilde{b}}$), and the lightest stop quark mass ($m_{\tilde{t}}$), as the rest of mass inputs in this sector. This parametrization is useful in processes where squarks only appear as internal particles in the loops (such as the ones studied in chapters 6 and 7), as one-loop corrections to these parameters would appear as two-loop effects in the process subject of study. Gluino mass ($m_{\tilde{g}}$), on the other hand, is let free.

For the Higgs sector two choices are available, we can use the pseudoscalar mass m_{A^0}, or the charged Higgs mass $m_{H^\pm}$. Both choices are on equal footing. As the neutral Higgs particles are the main element for most of our studies we shall use its mass as input parameter in most of our work.

Standard model parameters are well known, we will use present determinations of EW observables [19]

$$\begin{aligned} M_Z &= 91.1899 \pm 0.0021\,\text{GeV} \\ M_W &= 80.418 \pm 0.054\,\text{GeV} \\ G_F &= (1.16639 \pm 0.00001) \times 10^{-5}\,\text{GeV}^{-2} \\ \alpha_{em}^{-1}(M_Z) &= 128.896 \pm 0.090 \end{aligned} \tag{3.62}$$

QCD related observables are not so precise. On the other hand as the main results are not affected by specific value of these observables we will use the following ones

$$\begin{aligned} m_t &= 175\,\text{GeV} \\ m_b &= 5\,\text{GeV} \\ \alpha_s(M_Z) &= 0.11 \end{aligned} \tag{3.63}$$

[1] Note that after diagonalization of the squark mass matrix the physical masses will differ slightly.

3.7.2 Constraints

The MSSM reproduces the behaviour of the SM up to energy scales probed so far [105]. Obviously this is not for every point of the full parameter space!

There exists direct limits on sparticle masses based on direct searches at the high energy colliders (LEP II, SLC, Tevatron). Although hadron colliders can achieve larger center of mass energies than e^+e^- ones, their samples contain large backgrounds that make the analysis more difficult. This drawback can be avoided if the ratio signal-to-background is improved, in fact they can be used for precision measurements of "known" observables (see e.g. [17]). e^+e^- colliders samples are more clean, and they allow to put absolute limits on particle masses in a model independent way.

No significant evidence for a Higgs signal has been detected at LEP [106]. As a result, one can obtain bounds on the possible MSSM Higgs parameters. These limits are often displayed in the m_{A^0}–$\tan\beta$ plane, see Fig. 3.7, although there is additional dependence on various MSSM parameters that effect the radiative corrections to the Higgs masses as discussed above. In representative scans of the MSSM parameters, the LEP Higgs Working Group [106] finds that $m_{h^0} > 91.0$ GeV and $m_{A^0} > 91.9$ GeV at 95% CL. These limits actually correspond to the large $\tan\beta$ region in which Zh^0 production is suppressed, as shown in Fig. 3.7. In this case, the quoted Higgs limits arise as a result of the non-observation of h^0A^0 and H^0A^0 production. As $\tan\beta$ is lowered, the limits on m_{h^0} and m_{A^0} become more stringent. In this regime, the h^0A^0 production is suppressed while the Zh^0 production rate approaches its SM value. Thus, in this case, the SM Higgs limit applies ($m_{h^0} \gtrsim 114\,\text{GeV}$ [19]) as shown in Fig. 3.7(a). The precise region of MSSM Higgs parameter space that is excluded depends on the values of the MSSM parameters that control the Higgs mass radiative corrections. For example, a conservative exclusion limit is obtained in the maximal mixing scenario, since in this case the predicted value of m_{h^0} as a function of m_{A^0} and $\tan\beta$ is maximal (with respect to changes in the other MSSM parameters). The excluded regions of the MSSM Higgs parameter space based on the maximal mixing benchmark scenario of Ref. [107], are shown in Fig. 3.7, and correspond to the exclusion of the range $0.5 < \tan\beta < 2.4$ at the 95% CL. However, the $\tan\beta$ exclusion region can still be significantly reduced (even to the point of allowing all $\tan\beta$ values) by, *e.g.*, taking $M_{\text{SUSY}} = 2$ TeV and $m_t = 180$ GeV, see Fig 3.8 (which still lies within the error bars of the experimentally measured value), and allowing for the theoretical uncertainty in the prediction of $m_{h^0}{}^{\text{max}}$ [108].

Similarly, no evidence for the charged Higgs boson has yet been found. The LEP Higgs Working Group quotes a limit of $m_{H^\pm} > 78.6$ GeV at 95% CL [109], which holds for a more general non-supersymmetric two-Higgs doublet model and assumes only that

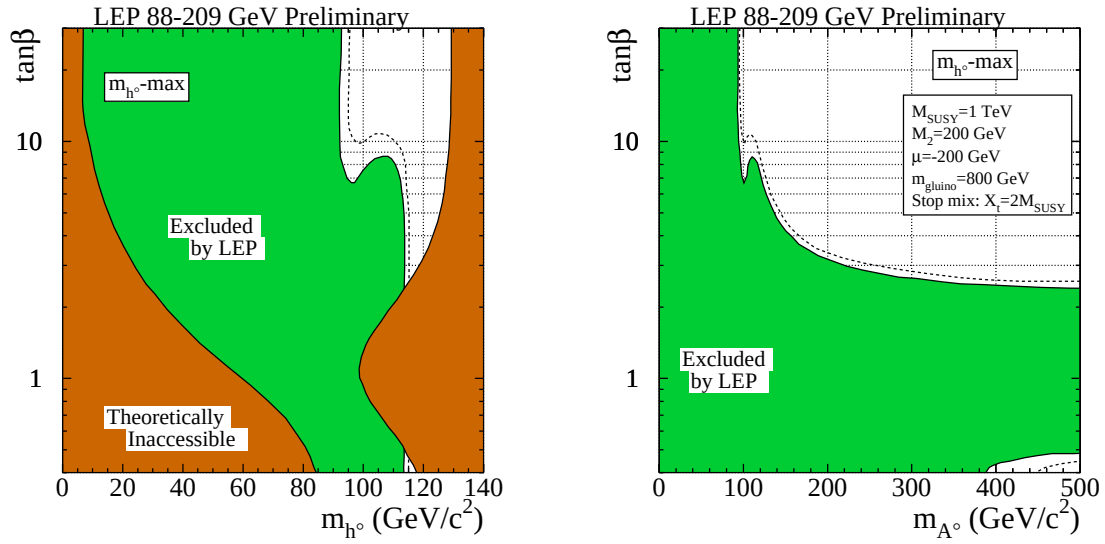

Figure 3.7: LEP2 contours of the 95% CL exclusion limits for MSSM Higgs sector parameters as a function of $\tan\beta$ and (a) m_{h^0} and (b) m_{A^0} (in GeV), taken from Ref. [106]. The contours shown have been obtained for MSSM Higgs parameters chosen according to the maximal mixing benchmark of Ref. [107].

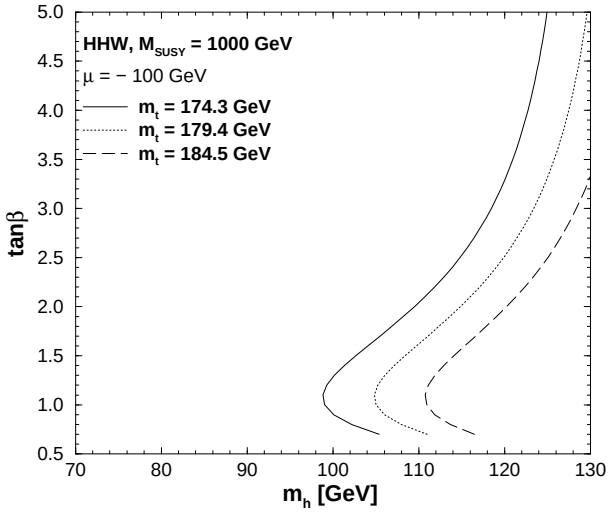

Figure 3.8: Theoretically exclusion limits as in Fig. 3.7 for three different values of the top-quark mass, $m_t = 174.3, 179.4, 184.5\,\text{GeV}$. Taken from Ref. [108]

the H^+ decays dominantly into $\tau^+\nu_\tau$ and/or $c\bar{s}$. Although the MSSM tree-level bound $m_{H^\pm} \geq M_W$ can be relaxed somewhat by radiative corrections, the LEP bound quoted above provides no useful additional constraints on the MSSM Higgs sector. Actual fits to the MSSM parameter space project a preferred value for the charged Higgs mass of $m_{H^\pm} \simeq 120\,\mathrm{GeV}$ [110].

Hadron colliders bounds are not so restrictive as those from e^+e^- machines. Most bounds on squark and gluino masses are obtained by supposing squark mass unification in simple models, such as mSUGRA. At present approximately the limits, with certain conditions, on squarks (1st and 2nd generation) and gluino masses are [19]

$$m_{\tilde{q}} > 250\,\mathrm{GeV}\ ,\ m_{\tilde{g}} > 195\,\mathrm{GeV}\ . \tag{3.64}$$

From the top quark events at the Tevatron a limit on the branching ratio $B(t \to H^+ b)$ can be extracted, and thus a limit on the $\tan\beta - m_{H^\pm}$ relation [20, 32].

Finally indirect limits on sparticle masses are obtained from the EW precision data. We apply these limits through all our computations by computing the contribution of sparticles to these observables and requiring that they satisfy the bounds from EW measurements. We require new contributions to the ρ parameter to be smaller than present experimental error on it, namely

$$|\delta\rho_{\mathrm{new}}| < 0.003\ \ (3\sigma)\,. \tag{3.65}$$

We notice that as $\delta\rho_{\mathrm{new}}$ is also the main contribution from sparticle contributions to Δr [111], new contributions to this parameter are also below experimental constrains. Also the corrections in the α- and G_F-on-shell renormalization schemes will not differ significantly [112].

We recall that at the moment the MSSM may escape the indirect bound from $b \to s\,\gamma$ because the positive charged Higgs virtual contributions can be compensated for by negative stop and chargino loops, if they are not too heavy. Therefore, in the MSSM the charged Higgs can stay relatively light, $m_{H^\pm} \gtrsim 120\,GeV$, just to comply with the aforementioned LEP 200 bounds on m_{A^0} [113].

There exist also theoretical constrains to the parameters of the MSSM. As a matter of fact the MSSM has a definite prediction: there should exist a light neutral scalar Higgs boson h^0. Tree-level analysis put this bound to the Z mass, however the existence of large radiative corrections to the Higgs bosons mass relations grow this limit up to $\sim 130\,\mathrm{GeV}$ [87, 88]. More recently the two-loop radiative corrections to Higgs mass relations in the MSSM have been performed [114–118], and the present upper limit on m_{h^0} is

$$m_{h^0} \leq 130 - 135\,\mathrm{GeV}\ . \tag{3.66}$$

Of course if the MSSM is extended in some way this limit can be evaded, though not to values larger of $\sim 200\,\text{GeV}$ [119, 120].

Another theoretical constraint is the necessary condition (3.41) on squark trilinear coupling (A) to avoid colour-breaking minima. This constraint is easily implemented when the A parameters are taken as inputs, but if we choose a different set of inputs (such as the mixing angle $\theta_{\tilde{q}}$) then it constrains the parameter space in a non-trivial way.

Whatever the spectrum of the MSSM is, it should comply with the benefits that SUSY introduces into the SM which apply if the following condition is fulfilled:

$$M_{\text{SUSY}} \lesssim \mathcal{O}(1\text{ TeV})\ . \tag{3.67}$$

If supersymmetric particles have masses heavier than the TeV scale then problems with GUT's appear. This statement does not mean that SUSY would not exist, but that then the SM would not gain practical benefit from the inclusion of SUSY.

A similar upper bound is obtained when making cosmological analyses, in these type of analyses one supposes the neutralino to be part of the cold dark matter of the universe, and requires its annihilation rate to be sufficiently small to account for the maximum of cold dark matter allowed for cosmological models, while at the same time sufficiently large so that its presence does not becomes overwhelming. Astronomical observations also restrict the parameters of SUSY models, usually in the lower range of the mass parameters (see e.g. [121–123]).

For the various RGE analyses to hold the couplings of the MSSM should be perturbative all the way from the unification scale down to the EW scale. This implies, among other restrictions, that top and bottom quark Yukawa couplings should be below certain limits ($h_{t,b}^2/4\pi < 1$). In terms of $\tan\beta$ this amounts it to be confined in the approximate interval

$$1 < \tan\beta \lesssim 70\ . \tag{3.68}$$

There are additional phenomenological restrictions that bring the lower bound on $\tan\beta$ to roughly 2.4 for the so-called maximal m_h^0 scenario, and 10.5 for the so-called no mixing scenario [113], the upper bound being the same [11].

In the MSSM case we use the more restrictive limits (3.68), see Fig. 3.7, whereas in the 2HDM model the lower limit can be smaller as shown in (2.43). Any deviation from this framework of restrictions will only be for demonstrational purpouses, and will be explicitly quoted in the text.

Chapter 4

Loop Induced FCNC Decays of the Top Quark in a General 2HDM

4.1 Introduction

As we have said in the introduction, in the LHC the production of top quark pairs will be $\sigma(t\bar{t}) = 860\ pb$ – roughly two orders of magnitude larger than in the Tevatron Run II. In the so-called low-luminosity phase ($10^{33}\, cm^{-2}s^{-1}$) of the LHC one expects about three $t\,\bar{t}$-pair per second (ten million $t\,\bar{t}$-pairs per year!) [17]. And this number will be augmented by one order of magnitude in the high-luminosity phase ($10^{34}\, cm^{-2}s^{-1}$). As for a future LC running at e.g. $\sqrt{s} = 500\ GeV$, one has a smaller cross-section $\sigma(t\bar{t}) = 650\ fb$ but a higher luminosity factor ranging from $5 \times 10^{33}\, cm^{-2}s^{-1}$ to $5 \times 10^{34}\, cm^{-2}s^{-1}$ and of course a much cleaner environment [18]. With datasets from LHC and LC increasing to several $100\, fb^{-1}$/year in the high-luminosity phase, one should be able to pile up an enormous wealth of statistics on top quark decays. Therefore, not surprisingly, these machines should be very useful to analyze rare decays of the top quark, viz. decays whose branching fractions are so small ($\lesssim 10^{-5}$) that they could not be seen unless the number of collected top decays is very large.

The situation is dramatic with the top quark decay into the SM Higgs boson, $B(t \to c\, H_{SM}) \sim 10^{-13} - 10^{-15}$ ($m_t = 175\, GeV;\ M_Z \leq M_H \leq 2\ M_W$) [26]. This extremely tiny rate is far out of the range to be covered by any presently conceivable high luminosity machine. On the other hand, the highest FCNC top quark rate in the SM, namely that of the gluon channel $t \to c\, g$, is still 6 orders of magnitude below the feasible experimental possibilities at the LHC. All in all the detection of FCNC decays of the top quark at visible levels (viz. $B(t \to c\, X) > 10^{-5}$) by the high luminosity colliders round the corner

(especially LHC and LC) seems doomed to failure in the absence of new physics. Thus the possibility of large enhancements of some FCNC channels up to the visible threshold, particularly within the context of the general 2HDM and the MSSM, should be very welcome. Unfortunately, although the FCNC decay modes into electroweak gauge bosons $V_{ew} = W, Z$ may be enhanced a few orders of magnitude, it proves to be insufficient to raise the meager SM rates mentioned before up to detectable limits, and this is true both in the 2HDM – where $B(t \to V_{ew}\, c) < 10^{-6}$ [24] – and in the MSSM – where $B(t \to V_{ew}\, c) < 10^{-7}$ except in highly unlikely regions of the MSSM parameter space [124][1]. In this respect it is a lucky fact that these bad news need not to apply to the gluon channel, which could be barely visible ($B(t \to g\, c) \lesssim 10^{-5}$) both in the MSSM [42, 43] and in the general 2HDM [24]. But, most significant of all, they may not apply to the non-SM Higgs boson channels $t \to (h^0, H^0, A^0) + c$ either. As we shall show in the sequel, these Higgs decay channels of the top quark could lie above the visible threshold for a parameter choice made in perfectly sound regions of parameter space!

While a systematic discussion of these "gifted" Higgs channels was made in Ref. [43] for the MSSM case and in other models[2], to the best of our knowledge there is no similar study in the general 2HDM. And we believe that this study is necessary, not only to assess what are the chances to see traces of new (renormalizable) physics in the new colliders round the corner but also to clear up the nature of the virtual effects; in particular to disentangle whether the origin of the hypothetically detected FCNC decays of the top quark is ultimately triggered by SUSY or by some alternative, more generic, renormalizable extension of the SM such as the 2HDM or generalizations thereof. Of course the alleged signs of new physics could be searched for directly through particle tagging, if the new particles were not too heavy. However, even if accessible, the corresponding signatures could be far from transparent. In contrast, the indirect approach based on the FCNC processes has the advantage that one deals all the time with the dynamics of the top quark. Thus by studying potentially new features beyond the well-known SM properties of this quark one can hopefully uncover the existence of the underlying new interactions.

[1] Namely, regions in which there are wave-function renormalization thresholds due to (extremely fortuitous!) sharp coincidences between the sum of the sparticle masses involved in the self-energy loops and the top quark mass. See e.g. Ref. [125] for similar situations already in the conventional $t \to W\, b$ decay within the MSSM. In our opinion these narrow regions should not be taken too seriously.

[2] Preliminary SUSY analysis of the Higgs channels are given in [126], but they assume the MSSM Higgs mass relations at the tree-level. Therefore these are particular cases of the general MSSM approach given in [43]. Studies beyond the MSSM (e.g. including R-parity violation) and also in quite different contexts from the present one are available in the literature, see e.g. [127].

4.2 Relevant fields and interactions in the 2HDM

We will mainly focus our interest on the loop induced FCNC decays

$$t \to c\, h \quad (h = h^0, H^0, A^0)\,, \tag{4.1}$$

in which any of the three possible neutral Higgs bosons from a general 2HDM can be in the final state. However, as a reference we shall compare throughout our analysis the Higgs channels with the more conventional gluon channel

$$t \to c\, g\,. \tag{4.2}$$

Although other quarks could participate in the final state of these processes, their contribution is obviously negligible – because it is further CKM-suppressed. The lowest order diagrams entering these decays are one-loop diagrams in which Higgs, quarks, gauge and Goldstone bosons – in the Feynman gauge – circulate around. While the diagrams for the decays (4.1) are depicted in Fig. 4.1, the ones for the decay (4.2) are not shown [24].

We wish to concentrate here on Type I and Type II models of a sufficiently generic nature, to wit, those which are characterized by the following set of free parameters:

$$(m_{h^0}, m_{H^0}, m_{A^0}, m_{H^\pm}, \tan\alpha, \tan\beta)\,, \tag{4.3}$$

$\tan\beta$ is a key parameter in our analysis. The numerical analysis that we perform in the next section does not depend in any essential way on the simplification $\lambda_5 = \lambda_6$,(2.8). In essence we have just traded λ_5 for $m^2_{A^0}$ in these rules and so by varying with respect to m_{A^0} we do explore most of the quantitative potential of the general 2HDM.

Since we shall perform our calculation in the on-shell scheme, we understand that the physical inputs are given by the electromagnetic coupling and the physical masses of all the particles:

$$(e, M_W, M_Z, m_{h^0}, m_{H^0}, m_{A^0}, m_{H^\pm}, m_f)\,. \tag{4.4}$$

The remaining parameters, except the Higgs mixing angles, are understood to be given in terms of the latter, e.g. the $SU(2)$ gauge coupling appearing in the previous formulae and in Table 2.1 is given by $g = e/s_w$, where the sinus of the weak mixing angle is defined through $s^2_w = 1 - M^2_W/M^2_Z$. It should be clear that, as there are no tree-level FCNC decays of the top quark, there is no need to introduce counterterms for the physical inputs in this calculation. In fact, the calculation is carried out in lowest order ("tree level") with respect to the effective tch and tcg couplings and so the sum of all the one-loop diagrams (as well as of certain subsets of them) should be finite in a renormalizable theory, and indeed it is.

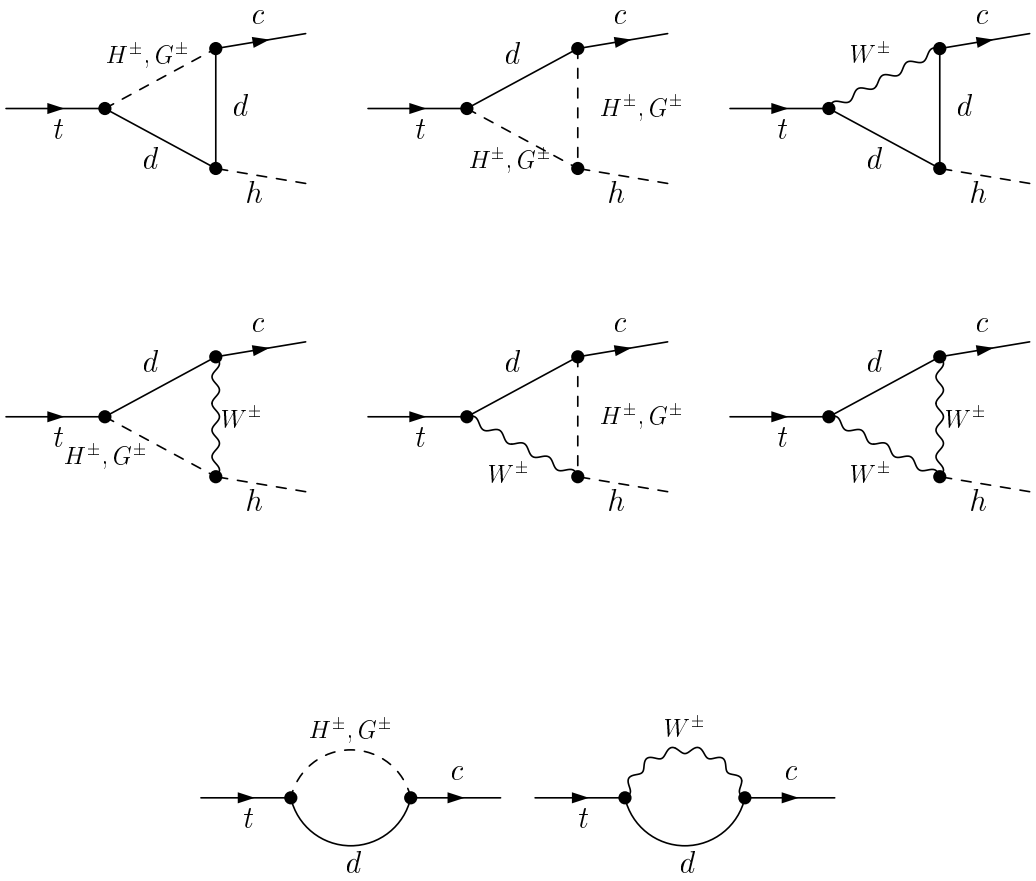

Figure 4.1: One-loop vertex diagrams contributing to the FCNC top quark decays (4.1). Shown are the vertices and mixed self-energies with all possible contributions from the SM fields and the Higgs bosons from the general 2HDM. The Goldstone boson contributions are computed in the Feynman gauge.

4.3 Numerical analysis

From the previous interaction Lagrangians and Feynman rules it is now straightforward to compute the loop induced FCNC rates for the decays (4.1) and (4.2). We shall refrain from listing the lengthy analytical formulae as the computation is similar to the one reported in great detail in Ref. [43]. Therefore, we will limit ourselves to exhibit the final numerical results. The fiducial ratio on which we will apply our numerical computation is the following:

$$B^j(t \to h + c) = \frac{\Gamma^j(t \to h + c)}{\Gamma(t \to W^+ + b) + \Gamma^j(t \to H^+ + b)} \ , \tag{4.5}$$

for each Type $j = I, II$ of 2HDM and for each neutral Higgs boson $h = h^0$, H^0, A^0. While this ratio is not the total branching fraction, it is enough for most practical purposes and it is useful in order to compare with previous results in the literature. Notice that for $m_{H^\pm} > m_t$ (the most probable situation for Type II 2HDM's, see below) the ratio (4.5) reduces to $B^j(t \to h + c) = \Gamma^j(t \to h + c)/\Gamma(t \to W^+ + b)$, which is the one that we used in Ref. [43]. It is understood that $\Gamma^j(t \to h + c)$ above is computed from the one-loop diagrams in Fig. 4.1, with all quark families summed up in the loop. Therefore, consistency in perturbation theory requires to compute $\Gamma(t \to W^+ + b)$ and $\Gamma(t \to H^+ + b)$ in the denominator of (4.5) only at the tree-level (for explicit expressions see e.g. [20]). As mentioned in Sec. 2, we wish to compare our results for the Higgs channels (4.1) with those for the gluon channel (4.2), so that we similarly define

$$B^j(t \to g + c) = \frac{\Gamma^j(t \to g + c)}{\Gamma(t \to W^+ + b) + \Gamma^j(t \to H^+ + b)} \ . \tag{4.6}$$

We have performed a fully-fledged independent analytical and numerical calculation of $\Gamma^j(t \to g + c)$ at one-loop in the context of 2HDM I and II. Where there is overlapping, we have checked the numerical results of Ref. [24], but we point out that they agree with us only if $\Gamma(t \to H^+ + b)$ is included in the denominator of eq. (4.6), in contrast to what is asserted in that reference in which $B(t \to g + c)$ is defined without the charged Higgs channel contribution.

We have performed part of the analytical calculation of the diagrams for both processes (4.1) and (4.2) by hand and we have cross-checked our results with the help of the numeric and algebraic programs FeynArts, FormCalc and LoopTools [128–130], with which we have completed the rest of the calculation. In particular, the cancellation of UV divergences in the total amplitudes was also verified by hand. In addition we have checked explicitly the gauge invariance of the total analytical amplitude for the process (4.2), which is a powerful test. And we have confirmed that our code reproduces the SUSY Higgs contribution of Ref. [43] when we turn on the MSSM Higgs mass relations.

As mentioned above, a highly relevant parameter is $\tan\beta$, which must be restricted to the approximate range (2.43) in perturbation theory[3]. It is to be expected from the various couplings involved in the processes under consideration that the low $\tan\beta$ region could be relevant for both the Type I and Type II 2HDM's. In contrast, the high $\tan\beta$ region is only potentially important for the Type II. However, the eventually relevant

[3]Some authors [131] claim that perturbativity allows $\tan\beta$ to reach values of order 100 and beyond, and these are still used in the literature. We consider it unrealistic and we shall not choose $\tan\beta$ outside the interval (2.43). Plots versus $\tan\beta$, however, will indulge larger values just to exhibit the dramatic enhancements of our FCNC top quark rates.

regions of parameter space are also determined by the value of the mixing angle α, as we shall see below.

Of course there are several restrictions that must be respected by our numerical analysis, see 2.4, as the ρ-parameter restriction, (2.44), and the $b \to s\gamma$ restriction, (2.45). With the charge Higgs boson mass restrictions in section 2.4 [4] in principle the top quark decay $t \to H^+ + b$ is still possible in 2HDM I; but also in 2HDM II, if $m_{H^\pm}$ lies near the lowest end of the previous bound, and in this case that decay can contribute to the denominator of eqs. (4.5)-(4.6).

The combined set of independent conditions turns out to be quite effective in narrowing down the permitted region in the parameter space, as can be seen in Figs. 4.2-4.5 where we plot the fiducial FCNC rates (4.5)-(4.6) versus the parameters (4.3). The cuts in some of these curves just reflect the fact that at least one of these conditions is not fulfilled.

After scanning the parameter space, we see in Figs. 4.2-4.3 that the 2HDM I (resp. 2HDM II) prefers low values (resp. high values) of $\tan\alpha$ and $\tan\beta$ for a given channel, e.g. $t \to h^0\, c$. Therefore, the following choice of mixing angles will be made to optimize the presentation of our numerical results:

$$\begin{aligned} \text{2HDM I}: &\ \tan\alpha = \tan\beta = 1/4\ ; \\ \text{2HDM II}: &\ \tan\alpha = \tan\beta = 50\,. \end{aligned} \tag{4.7}$$

We point out that, for the same values of the masses, one obtains the same maximal FCNC rates for the alternative channel $t \to H^0\, c$ provided one just substitutes $\alpha \to \pi/2 - \alpha$. Equations (4.7) define the eventually relevant regions of parameter space and, as mentioned in section 2.4, depend on the values of the mixing angles α and β, namely $\beta \simeq \alpha \simeq 0$ for Type I and $\beta \simeq \alpha \simeq \pi/2$ for Type II.

Due to the $\alpha \to \pi/2 - \alpha$ symmetry of the maximal rates for the CP-even Higgs channels, it is enough to concentrate the numerical analysis on one of them, but one has to keep in mind that the other channel yields the same rate in another region of parameter space. Whenever a mass has to be fixed, we choose conservatively the following values for both models:

$$m_{h^0} = 100\, GeV\,,\ m_{H^0} = 150\, GeV\,,\ \ m_{A^0} = m_{H^\pm} = 180\, GeV\,. \tag{4.8}$$

Also for definiteness, we take the following values for some relevant SM parameters in our calculation:

$$m_t = 175\, GeV\,,\ m_b = 5\, GeV\,,\ \alpha_s(m_t) = 0.11\,,\ V_{cb} = 0.040\,, \tag{4.9}$$

[4] At the time of this work this restriction was $m_{H^\pm} > (165 - 200)\ GeV$ for virtually any $\tan\beta \gtrsim 1$ [60, 80].

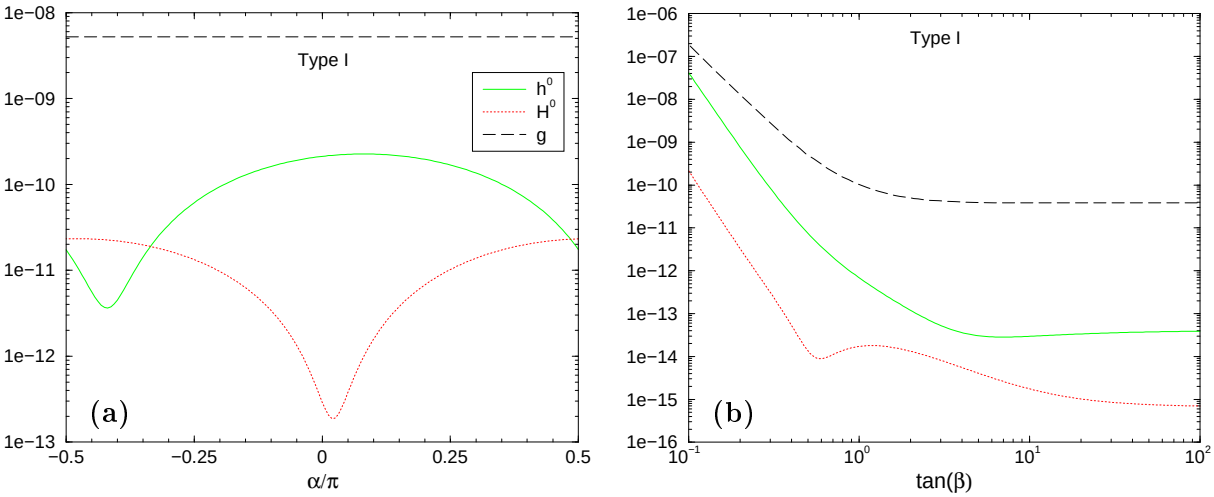

Figure 4.2: Evolution of the FCNC top quark fiducial ratios (4.5)-(4.6) in Type I 2HDM versus: **(a)** the mixing angle α in the CP-even Higgs sector, in units of π; **(b)** $\tan\beta$. The values of the fixed parameters are as in eqs. (4.7) and (4.8).

and the remaining ones are as in [75]. Notice that our choice of m_{A^0} prevents the decay $t \to A^0 c$ from occurring, and this is the reason why it does not appear in Figs. 4.2- 4.3. The variation of the results with respect to the masses is studied in Figs. 4.4-4.5. In particular, in Fig. 4.4 we can see the (scanty) rate of the channel $t \to A^0 c$ when it is kinematically allowed. In general the pseudoscalar channel is the one giving the skimpiest FCNC rate. This is easily understood as it is the only one that does not have trilinear couplings with the other Higgs particles (Cf. Table 2.1). While it does have trilinear couplings involving Goldstone bosons, these are not enhanced. The crucial role played by the trilinear Higgs self-couplings in our analysis cannot be underestimated as they can be enhanced by playing around with both (large or small) $\tan\beta$ *and* also with the mass splittings among Higgses. This feature is particularly clear in Fig. 4.4a where the rate of the channel $t \to h^0 c$ is dramatically increased at large m_{A^0}, for fixed values of the other parameters and preserving our list of constraints. Similarly would happen for $t \to H^0 c$ in the corresponding region $\alpha \to \pi/2 - \alpha$.

From Figs. 4.2a and 4.2b it is pretty clear that the possibility to see FCNC decays of the top quark into Type I Higgs bosons is plainly hopeless even in the most favorable regions of parameter space – the lowest (allowed) $\tan\beta$ end. In fact, the highest rates remain neatly down 10^{-6}, and therefore they are (at least) one order of magnitude below

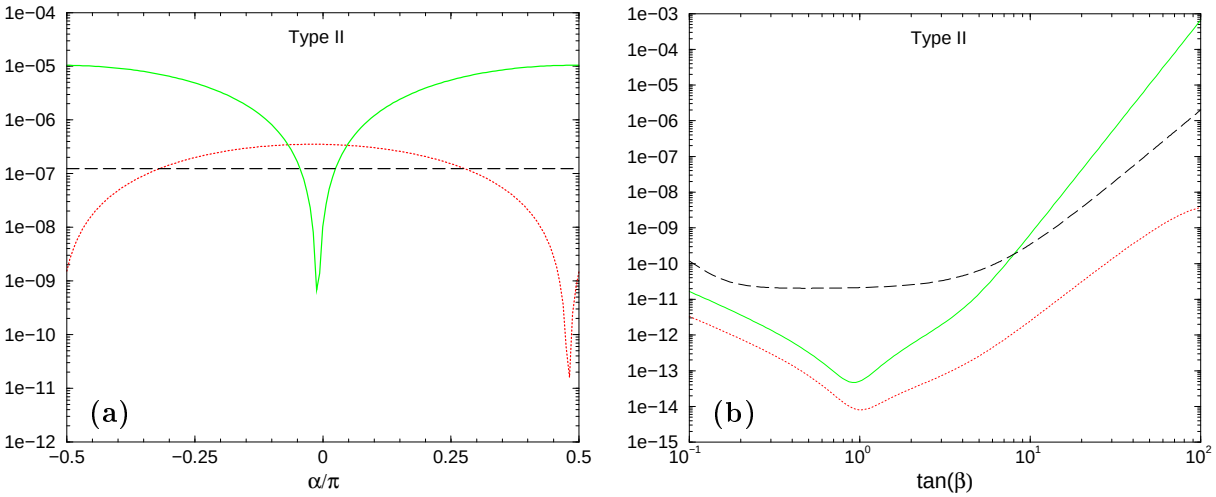

Figure 4.3: As in Fig. 4.2, but for the 2HDM II. The plot in (b) continues above the bound in eq. (2.43) just to better show the general trend.

the threshold sensibility of the best high luminosity top quark factory in the foreseeable future (see Section 4). We remark, in Fig. 4.2, that the rate for the reference decay $t \to g\,c$ in the 2HDM I is also too small but remains always above the Higgs boson rates. Moreover, for large $\tan\beta$ one has, as expected, $B^I\,(\,t \to g\,c) \to B^{SM}\,(\,t \to g\,c) \simeq 4\times 10^{-11}$ because in this limit all of the charged Higgs couplings in the 2HDM I (the only Higgs couplings involved in this decay) drop off. Due to the petty numerical yield from Type I models we refrain from showing the dependence of the FCNC rates on the remaining parameters.

Fortunately, the meager situation just described does not replicate for Type II Higgs bosons. For, as shown in Figs. 4.3a and 4.3b, the highest potential rates are of order 10^{-4}, and so there is hope for being visible. In this case the most favorable region of parameter space is the high $\tan\beta$ end in eq. (2.43). Remarkably, there is no need of risking values over and around 100 (which, as mentioned above, are sometimes still claimed as perturbative!) to obtain the desired rates. But it certainly requires to resort to models whose hallmark is a large value of $\tan\beta$ of order or above $m_t/m_b \gtrsim 35$. As for the dependence of the FCNC rates on the various Higgs boson masses (Cf. Figs. 4.4-4.5) we see that for large m_{A^0} the decay $t \to h^0\,c$ can be greatly enhanced as compared to $t \to g\,c$; and of course, once again, the same happens with $t \to H^0\,c$ in the alternative region $\alpha \to \pi/2 - \alpha$. We also note (from the combined use of Figs. 4.3b, 4.4a and 4.4b) that in the narrow range

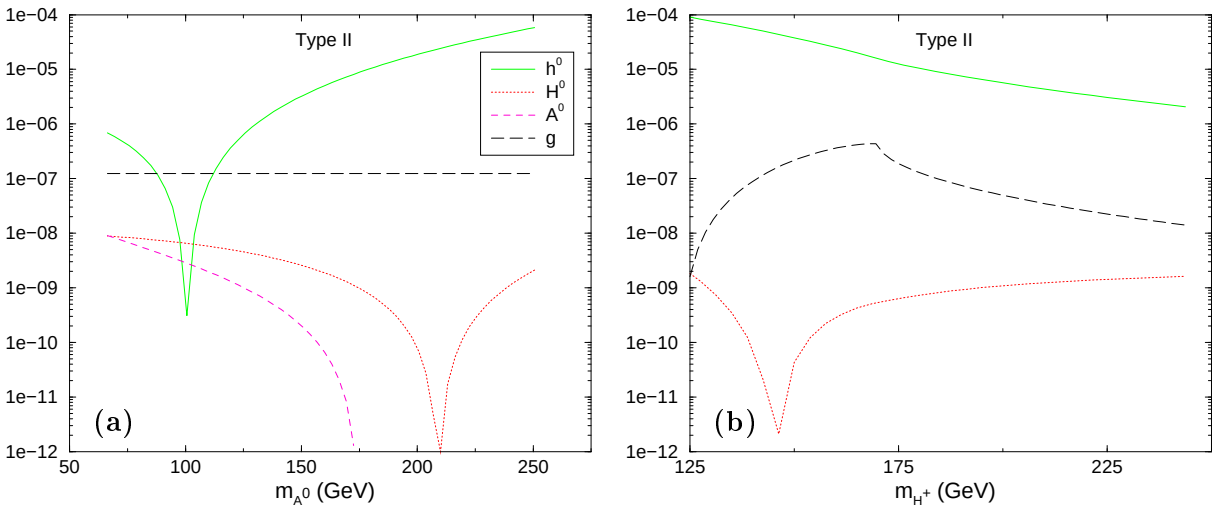

Figure 4.4: Evolution of the FCNC top quark fiducial ratios (4.5)-(4.6) in Type II 2HDM versus: **(a)** the CP-odd Higgs boson mass m_{A^0}; **(b)** the charged Higgs boson mass $m_{H^\pm}$. The values of the fixed parameters are as in eqs. (4.7) and (4.8). The plot in (b) starts below the bound $m_{H^\pm} > 165\,GeV$ mentioned in the text to better show the general trend.

where $t \to H^+ b$ could still be open in the 2HDM II, the rate of $t \to h^0 c$ becomes the more visible the larger and larger is $\tan\beta$ and m_{A^0}. Indeed, in this region one may even overshoot the 10^{-4} level without exceeding the upper bound (2.43) while also keeping under control the remaining constraints, in particular eq. (2.44). Finally, the evolution of the rates (4.5)-(4.6) with respect to the two CP-even Higgs boson masses is shown in Figs. 4.5a and 4.5b. The neutral Higgs bosons themselves do not circulate in the loops (Cf. Fig. 4.1) but do participate in the trilinear couplings (Cf. Table 2.1) and so the evolution shown in some of the curves in Fig. 4.5 is due to both the trilinear couplings and to the phase space exhaustion.

Turning now to the light scalar and pseudoscalar corners in parameter space mentioned above, it so happens that, after all, they prove to be of little practical interest in our case. Ultimately this is due to the quadratic Higgs boson mass differences entering $\delta\rho$ which make very difficult to satisfy the bound (2.44). The reason being that for Type II models the limit $m_{H^\pm} \gtrsim 165\,GeV$ from $b \to s\,\gamma$ implies that the constraint (2.44) cannot be preserved in the presence of light neutral Higgses. In actual fact the analysis shows that if e.g. one fixes $m_{h^0} = 20 - 30\ GeV$, then the minimum m_{A^0} allowed by $\delta\rho$ is $100\,GeV$ and the maximum rate (4.5) is of order 10^{-6}. Conversely, if one chooses $m_{A^0} = 20 - 30\ GeV$,

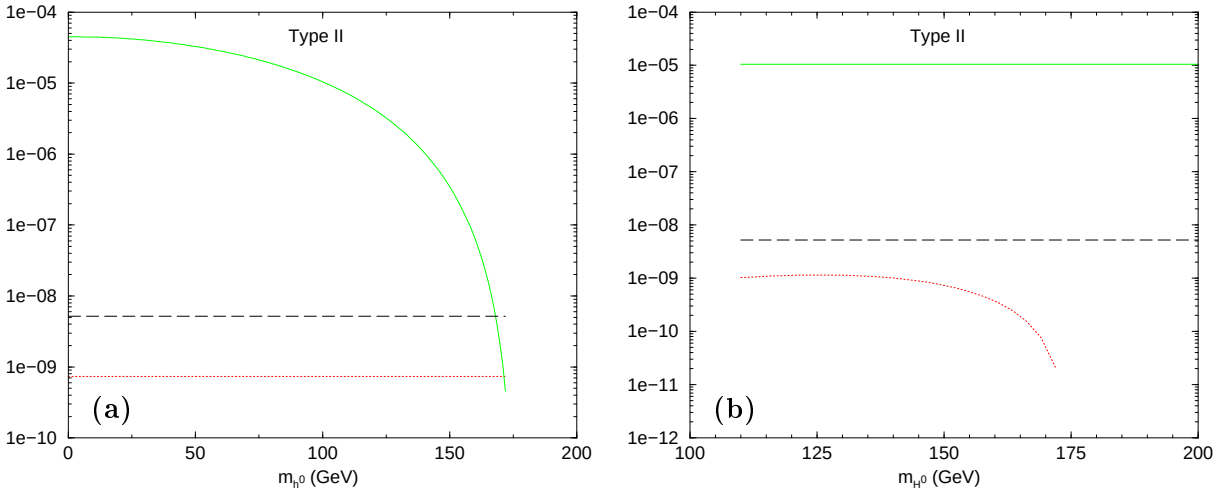

Figure 4.5: As in Fig. 4.4, but plotting versus: **(a)** the lightest CP-even Higgs boson mass m_{h^0}; **(b)** the heaviest CP-even Higgs boson mass m_{H^0}.

then the minimum m_{h^0} allowed by $\delta\rho$ is $120\,GeV$ and the maximum rate (4.5) is near 10^{-4}. Although in the last case the maximum rate is higher than in the first case, it is just of the order of the maximum rate already obtained outside the light mass corners of parameter space. On the other hand, these light mass regions do not help us in Type I models either. Even though for these models we do not have the $b \to s\,\gamma$ bound on the charged Higgs, we still have the direct LEP 200 bound $m_{H^\pm} \gtrsim 78.7\,GeV$ [132] which is of course weaker than the CLEO bound. As a consequence the $\delta\rho$ constraint can be satisfied in the 2HDM I for neutral Higgs bosons lighter than in the corresponding 2HDM II case, and one does get some enhancement of the FCNC rates. Specifically, one may reach up to 10^{-6}. However, the maximal rates (4.5) for the 2HDM I Higgs bosons are so small (see Figs. 4.2a-4.2b) that this order of magnitude enhancement is rendered immaterial. The upshot is that the top quark FCNC processes are not especially sensitive to the potential existence of a very light Higgs boson in either type of 2HDM.

4.4 Discussion and conclusions

The sensitivities to FCNC top quark decays for $100\, fb^{-1}$ of integrated luminosity in the relevant colliders are estimated to be [133]:

$$\begin{aligned} \textbf{LHC}: & B(t \to c\, X) \gtrsim 5 \times 10^{-5}\,, \\ \textbf{LC}: & B(t \to c\, X) \gtrsim 5 \times 10^{-4}\,, \\ \textbf{TEV33}: & B(t \to c\, X) \gtrsim 5 \times 10^{-3}\ . \end{aligned} \tag{4.10}$$

This estimation has been confirmed by a full signal-background analysis for the hadron colliders in Ref. [25]. From these experimental expectations and our numerical results it becomes patent that whilst the Tevatron will remain essentially blind to this kind of physics, the LHC and the LC will have a significant potential to observe FCNC decays of the top quark beyond the SM. Above all there is a possibility to pin down top quark decays into neutral Higgs particles, eq. (4.1), within the framework of the general 2HDM II provided $\tan\beta \gtrsim m_t/m_b \sim 35$. The maximum rates are of order 10^{-4} and correspond to the two CP-even scalars. This conclusion is remarkable from the practical (quantitative) point of view, and also qualitatively because the top quark decay into the SM Higgs particle is, in notorious contradistinction to the 2HDM II case, the less favorable top quark FCNC rate in the SM. On the other hand, we deem practically hopeless to see FCNC decays of the top quark in a general 2HDM I for which the maximum rates are of order 10^{-7}. This order of magnitude cannot be enhanced unless one allows $\tan\beta \ll 0.1$, but the latter possibility is unrealistic because perturbation theory breaks down and therefore one cannot make any prediction within our approach.

We have made a parallel numerical analysis of the gluon channel $t \to c\, g$ in both types of 2HDM's. We confirm that this is another potentially important FCNC mode of the top quark in 2HDM extensions of the SM [24] but, unfortunately, it still falls a bit too short to be detectable. The maximum rates for this channel lie below 10^{-6} in the 2HDM I (for $\tan\beta > 0.1$) and in the 2HDM II (for $\tan\beta < 60$), and so it will be hard to deal with it even at the LHC.

We are thus led to the conclusion that the Higgs channels (4.1), more specifically the CP-even ones, give the highest potential rates for top quark FCNC decays in a general 2HDM II. Most significant of all: they are *the only* FCNC decay modes of the top quark, within the simplest renormalizable extensions of the SM, that have a real chance to be seen in the next generation of high energy, high luminosity, colliders.

The former conclusions are similar to the ones derived in Ref. [43] for the MSSM case, but there are some conspicuous differences on which we wish to elaborate a bit in what

follows [134]. First, in the general 2HDM II the two channels $t \to (h^0, H^0)\, c$ give the same maximum rates, provided we look at different (disjoint) regions of the parameter space. The $t \to A^0\, c$ channel is, as mentioned, negligible with respect to the CP-even modes. Hereafter we will discard this FCNC top quark decay mode from our discussions within the 2HDM context. On the other hand, in the MSSM there is a most distinguished channel, viz. $t \to h^0\, c$, which can be high-powered by the SUSY stuff all over the parameter space. In this framework the mixing angle α becomes stuck once $\tan\beta$ and the rest of the independent parameters are given, and so there is no possibility to reconvert the couplings between h^0 and H^0 as in the 2HDM. Still, we must emphasize that in the MSSM the other two decays $t \to H^0\, c$ and $t \to A^0\, c$ can be competitive with $t \to h^0\, c$ in certain portions of parameter space. For example, $t \to H^0\, c$ becomes competitive when the pseudoscalar mass is in the range $110\, GeV < m_{A^0} \lesssim 170\, GeV$ [43]. The possibility of having more than one FCNC decay (4.1) near the visible level is a feature which is virtually impossible in the 2HDM II. Second, the reason why $t \to h^0\, c$ in the MSSM is so especial is that it is the only FCNC top quark decay (4.1) which is always kinematically open throughout the whole MSSM parameter space, while in the 2HDM all of the decays (4.1) could be, in the worse possible situation, dead closed. Nevertheless, this is not the most likely situation in view of the fact that all hints from high precision electroweak data seem to recommend the existence of (at least) one relatively light Higgs boson [132, 134]. This is certainly an additional motivation for our work, as it leads us to believe that in all possible (renormalizable) frameworks beyond the SM, and not only in SUSY, we should expect that at least one FCNC decay channel (4.1) could be accessible. Third, the main origin of the maximum FCNC rates in the MSSM traces back to the tree-level FCNC couplings of the gluino [43]. These are strong couplings, and moreover they are very weakly restrained by experiment. In the absence of such gluino couplings, or perhaps by further experimental constraining of them in the future, the FCNC rates in the MSSM would boil down to just the electroweak (EW) contributions, to wit, those induced by charginos, squarks and also from SUSY Higgses. The associated SUSY-EW rate is of order 10^{-6} at most, and therefore it is barely visible, most likely hopeless even for the LHC. In contrast, in the general 2HDM the origin of the contributions is purely EW and the maximum rates are two orders of magnitude higher than the full SUSY-EW effects in the MSSM. It means that we could find ourselves in the following situation. Suppose that the FCNC couplings of the gluino get severely restrained in the future and that we come to observe a few FCNC decays of the top quark into Higgs bosons, perhaps at the LHC and/or the LC. Then we would immediately conclude that these Higgs bosons could not be SUSY-MSSM, whilst they could perhaps be CP-even members of a 2HDM II. Fourth,

the gluino effects are basically insensitive to $\tan\beta$, implying that the maximum MSSM rates are achieved equally well for low, intermediate or high values of $\tan\beta$, whereas the maximum 2HDM II rates (comparable to the MSSM ones) are attained only for high $\tan\beta$.

The last point brings about the following question: what could we possibly conclude if the gluino FCNC couplings were not further restricted by experiment and the tagging of certain FCNC decays of the top quark into Higgs bosons would come into effect? Would still be possibly to discern whether the Higgs bosons are supersymmetric or not? The answer is, most likely yes, provided certain additional conditions would be met.

There are many possibilities and corresponding strategies, but we will limit ourselves to point out some of them. For example, let us consider the type of signatures involved in the tagging of the Higgs channels. In the favorite FCNC region (4.7) of the 2HDM II, the combined decay $t \to h\ c \to cb\overline{b}$ is possible only for h^0 or for H^0, but not for both – Cf. Fig. 4.3a – whereas in the MSSM, h^0 together with H^0, are highlighted for $110\,GeV < m_{A^0} < m_t$, with no preferred $\tan\beta$ value. And similarly, $t \to A^0\ c$ is also non-negligible for $m_{A^0} \lesssim 120\,GeV$ [43]. Then the process $t \to h\ c \to cb\overline{b}$ gives rise to high p_T charm-quark jets and a recoiling $b\overline{b}$ pair with large invariant mass. It follows that if more than one distinctive signature of this kind would be observed, the origin of the hypothetical Higgs particles could not probably be traced back to a 2HDM II.

One might worry that in the case of h^0 and H^0 they could also (in principle) decay into electroweak gauge boson pairs $h^0, H^0 \to V_{ew}\overline{V}_{ew}$, which in some cases could be kinematically possible. But this is not so in practice for the 2HDM II if we stick to our favorite scenario, eq. (4.7). In fact, we recall that the decay $h^0 \to V_{ew}\overline{V}_{ew}$ is not depressed with respect to the SM Higgs boson case provided $\beta - \alpha = \pi/2$, and similarly for $H^0 \to V_{ew}\overline{V}_{ew}$ if $\beta - \alpha = 0$. However, neither of these situations is really pinpointed by FCNC physics because we have found $\beta \simeq \pi/2$ in the most favorable region of our numerical analysis, and moreover α was also seen there to be either $\alpha \simeq \pi/2$ (for h^0) or 0 (for H^0), so both decays $h^0, H^0 \to V_{ew}\overline{V}_{ew}$ are suppressed in the regions where the FCNC rates of the parent decays $t \to (h^0, H^0)\ c$ are maximized. Again, at variance with this situation, in the MSSM case $H^0 \to V_{ew}\overline{V}_{ew}$ is perfectly possible – not so $h^0 \to V_{ew}\overline{V}_{ew}$ due to the aforementioned upper bound on m_{h^0} – because $\tan\beta$ has no preferred value in the most favorable MSSM decay region of $t \to H^0\ c$. Therefore, detection of a high p_T charm-quark jet against a $V_{ew}\overline{V}_{ew}$ pair of large invariant mass could only be advantageous in the MSSM, not in the 2HDM. Similarly, for $\tan\beta \gtrsim 1$ the decay $H^0 \to h^0\ h^0$ (with real or virtual h^0) is competitive in the MSSM [135, 136] in a region where the parent FCNC top quark decay is also sizeable. Again this is impossible in the 2HDM II and therefore

it can be used to distinguish the two (SUSY and non-SUSY) Higgs frames.

Finally, even if we place ourselves in the high $\tan\beta$ region both for the MSSM and the 2HDM II, then the two frameworks could still possibly be separated provided that two Higgs masses were known, perhaps one or both of them being determined from the tagged Higgs decays themselves, eq. (4.1). Suppose that $\tan\beta$ is numerically known (from other processes or from some favorable fit to precision data), then the full spectrum of MSSM Higgs bosons would be approximately determined (at the tree level) by only knowing one Higgs mass, a fact that could be used to check whether the other measured Higgs mass becomes correctly predicted. Of course, the radiative corrections to the MSSM Higgs mass relations can be important at high $\tan\beta$ [114], but these could be taken into account from the approximate knowledge of the relevant sparticle masses obtained from the best fits available to the precision measurements within the MSSM. If there were significant departures between the predicted mass for the other Higgs and the measured one, we would probably suspect that the tagged FCNC decays into Higgs bosons should correspond to a non-supersymmetric 2HDM II.

At the end of the day we see that even though the maximum FCNC rates for the MSSM and the 2HDM II are both of order 10^{-4} – and therefore potentially visible – at some point on the road it should be possible to disentangle the nature of the Higgs model behind the FCNC decays of the top quark. Needless to say, if all the fuss at CERN [132] about the possible detection of a Higgs boson would eventually be confirmed, this could still be interpreted as the discovery of one neutral member of an extended Higgs model. Obviously the combined Higgs data from LEP 200 and the possible discovery of FCNC top quark decays into Higgs bosons at the LHC/LC would be an invaluable cross-check of the purportedly new phenomenology.

We emphasize our most essential conclusions in a nutshell: i) Detection of FCNC top quark decay channels into a neutral Higgs boson would be a blazing signal of physics beyond the SM; ii) There is a real chance for seeing rare events of that sort both in generic Type II 2HDM's and in the MSSM. The maximum rates for the leading FCNC processes (4.1) and (4.2) in the 2HDM II (resp. in the MSSM) satisfy the relations

$$B(t \to g\,c) < 10^{-6}(10^{-5}) < B(t \to h\,c) \sim 10^{-4}\,, \tag{4.11}$$

where it is understood that h is h^0 or H^0, but not both, in the 2HDM II; whereas h is most likely h^0, but it could also be H^0 and A^0, in the MSSM ; iii) Detection of more than one Higgs channel would greatly help to unravel the type of underlying Higgs model.

The pathway to seeing new physics through FCNC decays of the top quark is thus potentially open. It is now an experimental challenge to accomplish this program using

the high luminosity super-colliders round the corner.

Chapter 5

Higgs Boson FCNC Decays into Top Quark in a General 2HDM

5.1 Introduction

When considering physics beyond the SM, new horizons of possibilities open up which may radically change the pessimistic prospects for FCNC decays involving a Higgs boson and the top quark. For example, in Ref. [42] it was shown that the vector boson modes can be highly enhanced within the context of the Minimal Supersymmetric Standard Model (MSSM) [7–10]. This fact was also dealt with in great detail in Ref. [43] where in addition a dedicated study was presented of the FCNC top quark decays into the various Higgs bosons of the MSSM (see also [44]), showing that these can be the most favored FCNC top quark decays – above the expectations on the gluon mode $t \to c\,g$. A similar study is performed in the chapter 4 for the FCNC top quark decays into Higgs bosons in a general two-Higgs-doublet model (2HDM).

In the previous chapter analysing the FCNC top quark decays in 2HDM extensions of the SM it was proven that while the maximum rates for $t \to c\,g$ were one order of magnitude more favorable in the MSSM [43] than in the 2HDM, the corresponding rates for $t \to c\,h^0$ were comparable both for the MSSM and the general 2HDM, namely up to the 10^{-4} level and should therefore be visible both at the LHC and the LC [25].

Similarly, one may wonder whether the FCNC decays of the Higgs bosons themselves can be of some relevance. Obviously the situation with the SM Higgs is essentially hopeless, so again we have to move to physics beyond the SM. Some work on these decays, performed in various contexts including the MSSM, shows that these effects can be important [47, 48, 137, 138], as seen in chapter 6. This could be expected, at least for

heavy quarks in the MSSM, from the general SUSY study (including both strong and electroweak supersymmetric effects) of the FCNC vertices $h\,t\,c$ ($h = h^0\,, H^0\,, A^0$) made in Ref. [43]. However, other frameworks could perhaps be equally advantageous. Here we are particularly interested in the FCNC Higgs decay modes into top quark within a general 2HDM, which have not been studied anywhere in the literature to our knowledge. It means we restrict to Higgs bosons heavier than m_t. From the above considerations, and most particularly on the basis of the detailed results obtained in the previous chapter 4 one may expect that some of the decays of the Higgs bosons

$$h \to t\,\bar{c}\,, \qquad h \to \bar{t}\,c \qquad (h = h^0\,, H^0\,, A^0) \tag{5.1}$$

in a general 2HDM can be substantially enhanced and perhaps can be pushed up to the visible level, particularly for h^0 which is the lightest CP-even spinless state in these models [6]. This possibility can be of great relevance on several grounds. On the one hand the severe degree of suppression of the FCNC Higgs decay in the SM obviously implies that any experimental sign of Higgs-like FCNC decay (5.1) would be instant evidence of physics beyond the SM. On the other hand, the presence of an isolated top quark in the final state, unbalanced by any other heavy particle, is an unmistakable carrier of the FCNC signature. Finally, the study of the maximum FCNC rates for the top quark modes (5.1) within the 2HDM, which is the simplest non-trivial extension of the SM, should serve as a fiducial result from which more complicated extensions of the SM can be referred to. Therefore, we believe there are founded reasons to perform a thorough study of the FCNC Higgs decays in minimal extensions of the Higgs sector of the SM and see whether they can be of any help to discover new physics.

The study is organized as follows. In Section 5.2 we summarize the 2HDM interactions most relevant for our study and estimate the expected FCNC rates of the Higgs decays in the SM and the general 2HDM. In Section 5.3 a detailed numerical analysis of the one-loop calculations of the FCNC decay widths and production rates of FCNC Higgs events is presented. Finally, in Section 5.4 we discuss the reach of our results and its phenomenological implications, and deliver our conclusions.

5.2 Expected branching ratios in the SM and the 2HDM

Before presenting the detailed numerical results of our calculation, it may be instructive to estimate the typical expected widths and branching ratios (B) both for the SM decay

$H^{SM} \to t\,\bar{c}$ and the non-standard decays (5.1) in a general 2HDM. This should be especially useful in this kind of rare processes, which in the strict context of the SM are many orders of magnitude out of the accessible range. Therefore, one expects to be able to grossly reproduce the order of magnitude from simple physical considerations based on dimensional analysis, power counting, CKM matrix elements and dynamical features. By the same token it should be possible to guess at the potential enhancement factors in the 2HDM extension of the SM. In fact, guided by the previous criteria the FCNC decay width of the SM Higgs of mass m_H into top quark is expected to be of order

$$\Gamma(H^{SM} \to t\,\bar{c}) \sim \left(\frac{1}{16\pi^2}\right)^2 |V_{tb}^* V_{bc}|^2\, \alpha_W^3\; m_H \left(\lambda_b^{SM}\right)^4 \sim \left(\frac{|V_{bc}|}{16\pi^2}\right)^2 \alpha_W\; G_F^2\, m_H\, m_b^4\,, \quad (5.2)$$

where G_F is Fermi's constant and $\alpha_W = g^2/4\pi$, g being the $SU(2)_L$ weak gauge coupling. We have approximated the loop form factor by just a constant prefactor. Notice the presence of $\lambda_b^{SM} \sim m_b/M_W$, which is the SM Yukawa coupling of the bottom quark in units of g. The fourth power of λ_b^{SM} in (5.2) gives the non-trivial suppression factor reminiscent of the GIM mechanism after summing over flavors. Since we are maximizing our estimation, a missing function related to kinematics and polarization sums, $F(m_t/m_H) \sim (1-m_t^2/m_H^2)^2$, has been approximated to one. To obtain the (maximized!) branching ratio it suffices to divide the previous result by $\Gamma(H^{SM} \to b\,\bar{b}) \sim \alpha_W \left(\lambda_b^{SM}\right)^2 m_H \sim G_F\, m_H\, m_b^2$ to obtain

$$B(H^{SM} \to t\,\bar{c}) \sim \left(\frac{|V_{bc}|}{16\pi^2}\right)^2 \alpha_W\; G_F\, m_b^2 \sim 10^{-13}\,, \quad (5.3)$$

with $V_{bc} = 0.04$, $m_b = 5\,GeV$. In general this B will be even smaller, specially for higher Higgs boson masses ($m_H > 2\,M_W$) for which the vector boson Higgs decay modes $H^{SM} \to W^+\,W^-(Z\,Z)$ can be kinematically available and become dominant. In this case it is easy to see that $B(H^{SM} \to t\,\bar{c})$ will be suppressed by an additional factor of m_b^2/m_H^2, which amounts at the very least to two additional orders of magnitude suppression, bringing it to a level of less than 10^{-15}. Already the optimized branching ratio (5.3) will remain invisible to all foreseeable accelerators in the future! To obtain the corresponding maximized estimation for the 2HDM we use the couplings from (2.42) and the trilinear couplings 2.1.

Let us now first assume large $\tan\beta$ and restrict to Type II models. From the interaction Lagrangians above it is clear that we may replace $\lambda_b^{SM} \to \lambda_b^{SM} \tan\beta$ in the previous formulae for the partial width. Moreover, the leading diagrams in the 2HDM contain the trilinear Higgs couplings $\lambda_{H^+\,H^-\,h}$. Therefore, the maximum B associated to the FCNC

decays (5.1) in a general 2HDM II should be of order[1]

$$B^{II}(h \to t\,\bar{c}) \sim \left(\frac{|V_{bc}|}{16\pi^2}\right)^2 \alpha_W\; G_F\, m_b^2\, \tan^2\beta\; \lambda^2_{H^+\,H^-\,h}\,, \tag{5.4}$$

where $\lambda_{H^+\,H^-\,h}$ is defined here in units of g and dimensionless as compared to Table 2.1. Clearly a big enhancement factor $\tan^2\beta$ appears, but this does not suffice. Fortunately, the trilinear couplings $\lambda_{H^+\,H^-\,h}$ for $h = h^0, H^0$ (but not for $h = A^0$) carry two additional sources of potential enhancement (Cf. Table 2.1) which are absent in the MSSM case. Take e.g. h^0, then we see that under appropriate conditions (for example, large $\tan\alpha$ and large $\tan\beta$) the trilinear coupling behaves as $\lambda_{H^+\,H^-\,h^0} \sim (m^2_{h^0} - m^2_{A^0})\,\tan\beta/(M_W\, m_{H^\pm})$, and in this case

$$B^{II}(h^0 \to t\,\bar{c}) \sim \left(\frac{|V_{bc}|}{16\pi^2}\right)^2 \alpha_W\; G_F\, m_b^2\, \tan^4\beta\, \left(\frac{m^2_{A^0} - m^2_{h^0}}{M_W\, m_{H^\pm}}\right)^2 . \tag{5.5}$$

So finally $B^{II}(h^0 \to t\,\bar{c})$, and of course $B^{II}(h^0 \to \bar{t}\,c)$, can be augmented by a huge factor $\tan^4\beta$ times the square of the relative splitting among the CP-even Higgs decaying boson mass and the CP-odd Higgs mass. Since the neutral Higgs bosons do not participate in the loop form factors (see 4.1), it is clear that various scenarios can be envisaged where these mass splittings can be relevant. In the next section this behaviour will be borne out by explicit calculations showing that $h^0 \to t\,\bar{c}$ can be raised to the visible level in the case of the Type II model. As for the Type I model the Higgs trilinear coupling enhancement is the same, but in the charged Higgs Yukawa coupling all quarks go with a factor $\cot\beta$; hence when considering the leading terms in the loops that contribute one sees that in the corresponding expression (5.4) the term $m_b^2\,\tan^2\beta$ is traded for $m_t\, m_c\,\cot^2\beta$, which is negligible at high $\tan\beta$. Both sources of enhancement are needed, and this feature is only tenable in the 2HDM II. Of course one could resort to the range $\tan\beta \ll 1$ for the Type I models, but this is not theoretically appealing. For example, for $\tan\beta \lesssim 0.1$ the top quark Yukawa coupling $g_t = g\, m_t/(\sqrt{2}\, M_W\, \sin\beta)$, which is present in the interaction Lagrangians above, is pushed into the non-perturbative region $g_t^2/16\pi^2 \gtrsim 1$ and then our calculation would not be justified. And what is worse: for the 2HDM I we would actually need $\tan\beta \leq \mathcal{O}(10^{-2})$ to get significant FCNC rates! In short, we consider that $B^I(h \to t\,\bar{c} + \bar{t}\,c)$ is essentially small (for all h), and that these decays remain always invisible to speak of. Hereafter we abandon the study of the decays (5.1) for the 2HDM I and restrict ourselves to the general 2HDM II.

[1]Here we have normalized the B with respect to the $h \to b\bar{b}$ channel only, because the gauge boson modes will be suppressed in the relevant FCNC region, Cf. Section 3.

5.3 Numerical analysis

Let us now substantiate the previous claims and provide the precise numerical results of the full one-loop calculation of $B^{II}(h \to t\,\bar{c} + \bar{t}\,c)$ [2] as well as of the LHC production rates of these FCNC events. We refer the reader to previous chapters for more details. The diagrams for the decays (5.1) are shown in Fig. 5.1, and the diagrams for the productions can be seen in Fig. 5.2. In what follows we present the final results of our numerical analysis together with a detailed discussion, interpretation and phenomenological application. We have performed the calculations with the help of the numeric and algebraic programs FeynArts, FormCalc and LoopTools [128–130]. The calculation must obviously be finite without renormalization, and indeed the cancellation of UV divergences in the total amplitudes was verified explicitly.

The input set for our numerical analysis is given by the data row

$$(m_{h^0}, m_{H^0}, m_{A^0}, m_{H^\pm}, \tan\alpha, \tan\beta) \tag{5.6}$$

made out of six independent parameters in the general 2HDM. Remaining inputs as in [75]. In practice there are some phenomenological restrictions on the data (5.6) which were already described in the chapter 2, particularly [79]. Again, a key parameter is $\tan\beta$, with the restriction (2.43). In practice, since Type I models are not considered, the effective range for our calculation will be the high $\tan\beta$ end of (2.43).

With these restrictions in mind we have computed the number of FCNC Higgs decay events into top quark at the LHC:

$$pp \to\ h + X \to t\,\bar{c}\,(\bar{t}\,c) + X \qquad (h = h^0, H^0, A^0)\,. \tag{5.7}$$

The necessary cross-sections to compute the production of neutral Higgs bosons at this collider, including all known QCD corrections, have been computed by adapting the codes HIGLU 1.0 and HQQ 1.0 [139] – originally written for the MSSM case [140]– to the general case of the 2HDM[3]. Folding the cross-sections with the one-loop branching ratios of the processes (5.1) we have obtained the number of FCNC Higgs decay events at the LHC. Let us first consider the branching ratios themselves. In Fig. 5.3a,b we show $B^{II}(h^0 \to t\,\bar{c} + \bar{t}\,c)$ for the lightest CP-even state. In particular, Fig. 5.3a shows $B^{II}(h^0 \to t\,\bar{c} + \bar{t}\,c)$ versus the charged Higgs mass $m_{H^\pm}$. In this figure we fix the values of the parameters in (5.6)

[2] Here and throughout we use the notation $B^{II}(h^0 \to t\,\bar{c} + \bar{t}\,c) \equiv B^{II}(h^0 \to t\,\bar{c}) + B^{II}(h^0 \to \bar{t}\,c)$.

[3] We have used the default parton distribution functions and renormalization/factorization scales used in these programs, namely GRV94 with $\mu_R = \mu_F = m_h$ for HIGLU, and CTEQ4L with $\mu_R = \mu_F = \sqrt{\hat{s}} \equiv \sqrt{(p_h + p_Q + p_{\bar{Q}})^2}$ for HQQ.

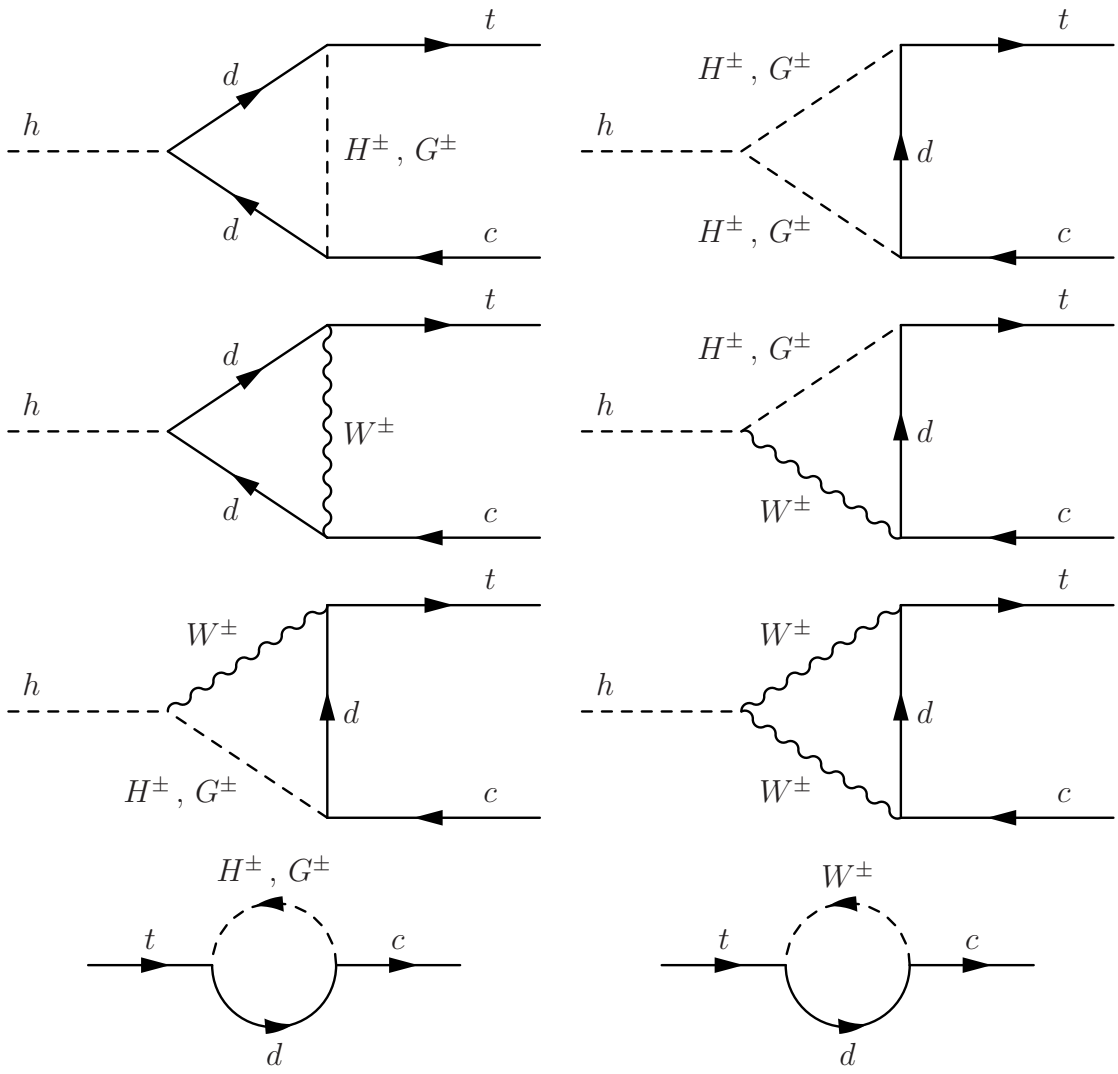

Figure 5.1: One-loop vertex diagrams contributing to the FCNC Higgs decay (5.1). Shown are the vertices and mixed self-energies with all possible contributions from the SM fields and the Higgs bosons from the general 2HDM. The Goldstone boson contributions are computed in the Feynman gauge.

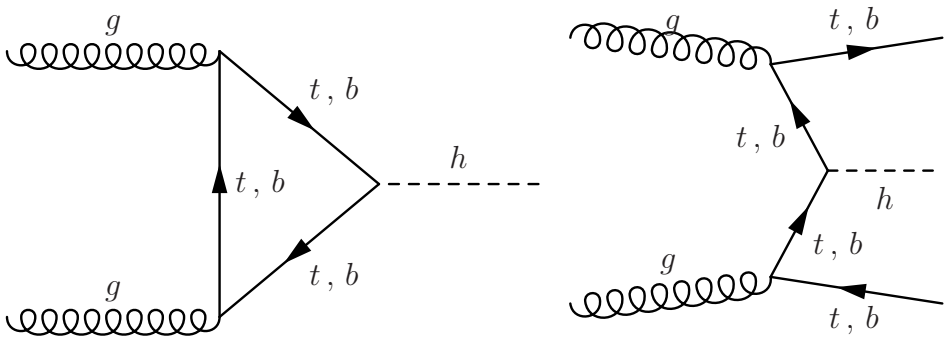

Figure 5.2: Leading order Feynman diagrams for the Higgs boson production at the LHC

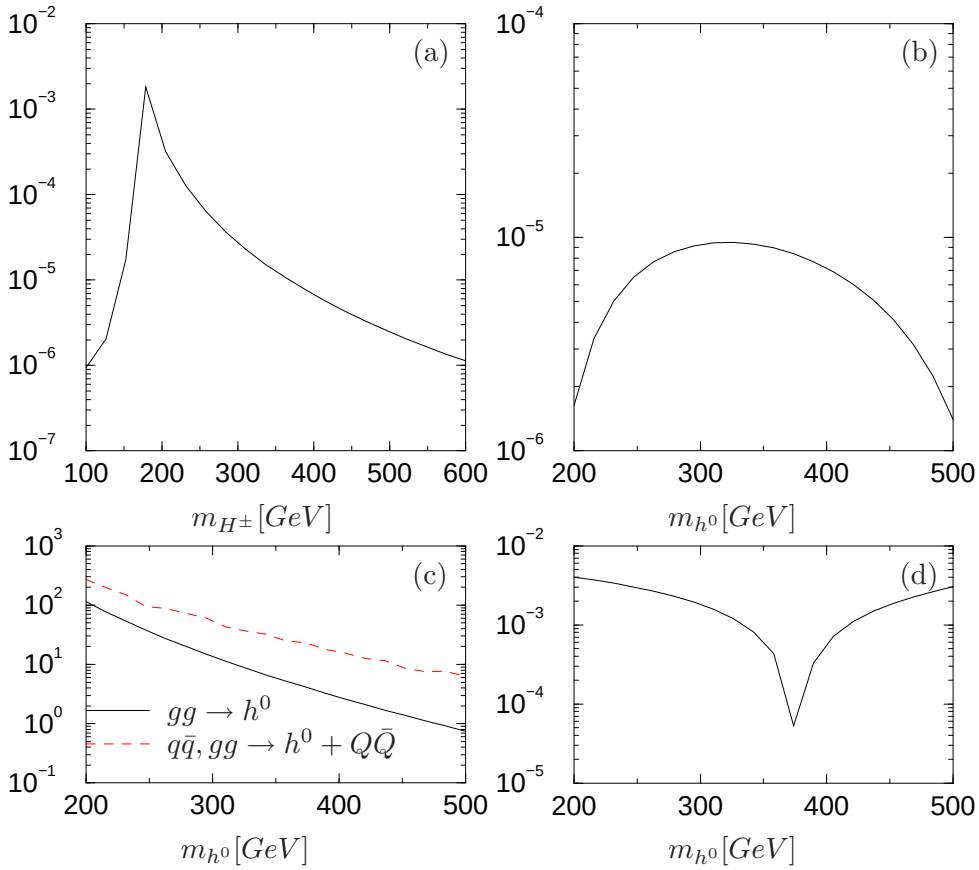

Figure 5.3: **(a)** $B^{II}(h^0 \to t\,\bar{c} + \bar{t}\,c)$ versus $m_{H^\pm}$; **(b)** Idem, versus m_{h^0}; **(c)** The production cross-section (in pb) of h^0 at the LHC versus its mass; **(d)** $\delta\rho^{\rm 2HDM}$ versus m_{h^0}, see the text. In these figures, when a parameter is not varied it is fixed as in eq.(5.8).

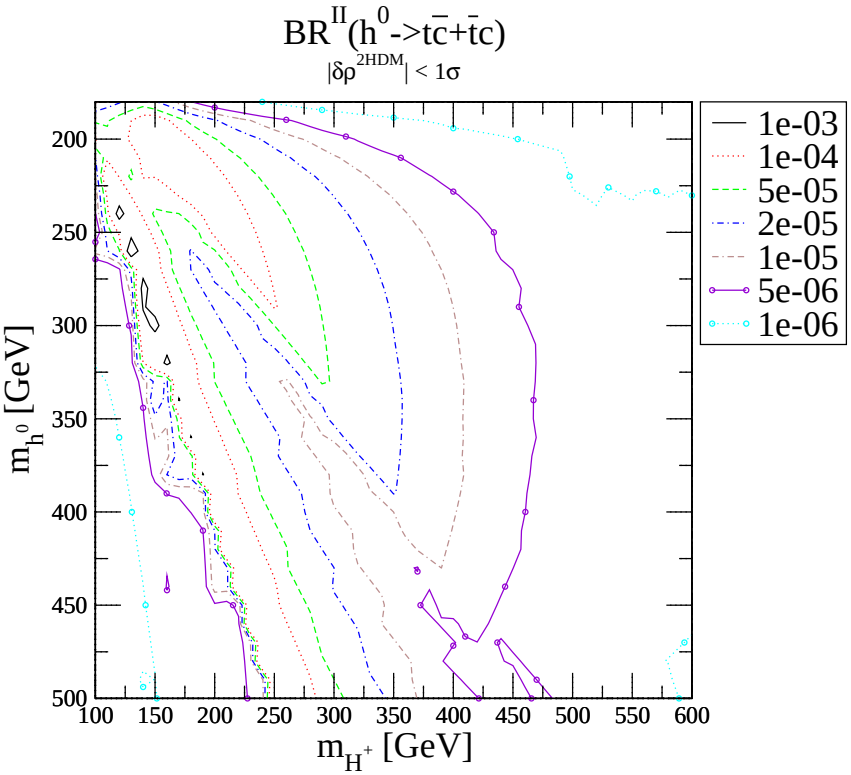

(a)

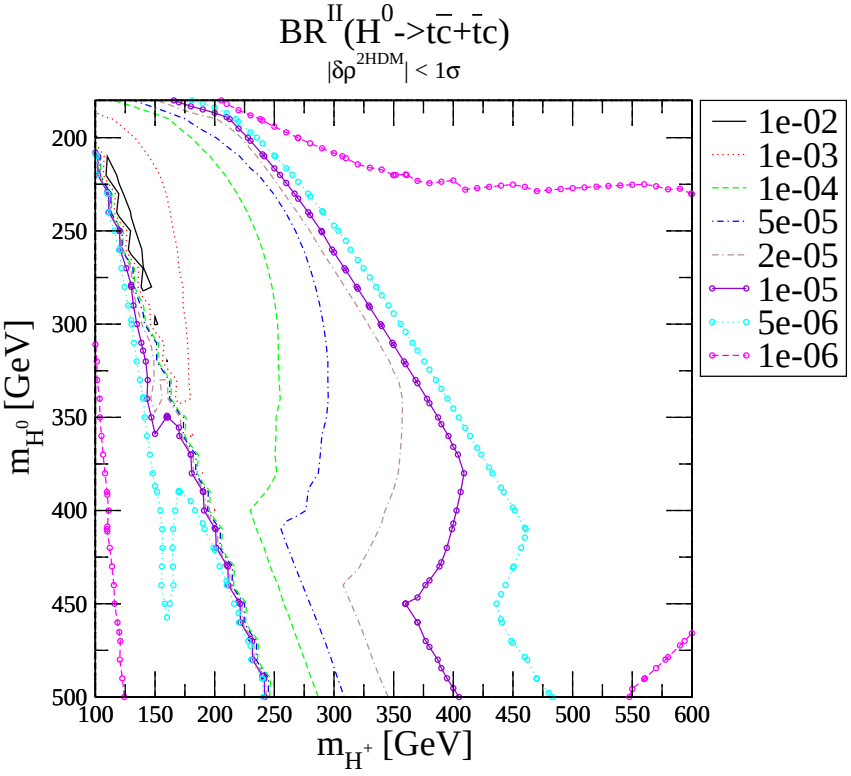

(b)

Figure 5.4: Contour lines in the $(m_{H^\pm}, m_{h^0})$-plane for the branching ratios (2HDM II case) **(a)** $B^{II}(h^0 \to t\,\bar{c} + \bar{t}\,c)$ and **(b)** $B^{II}(H^0 \to t\,\bar{c} + \bar{t}\,c)$ assuming $\delta\rho^{\text{2HDM}}$ at $1\,\sigma$.

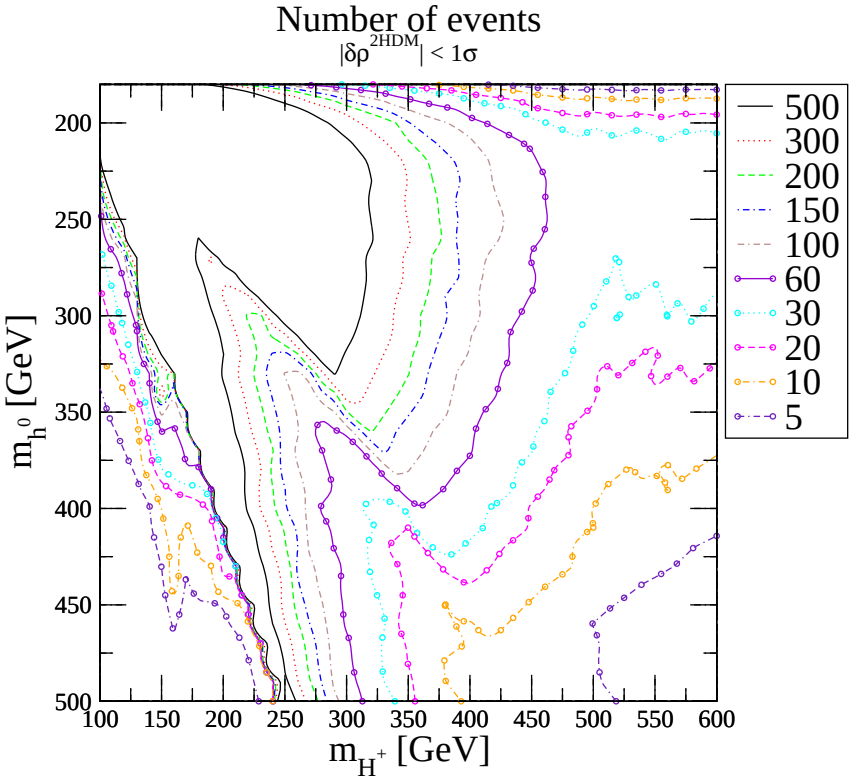

(a)

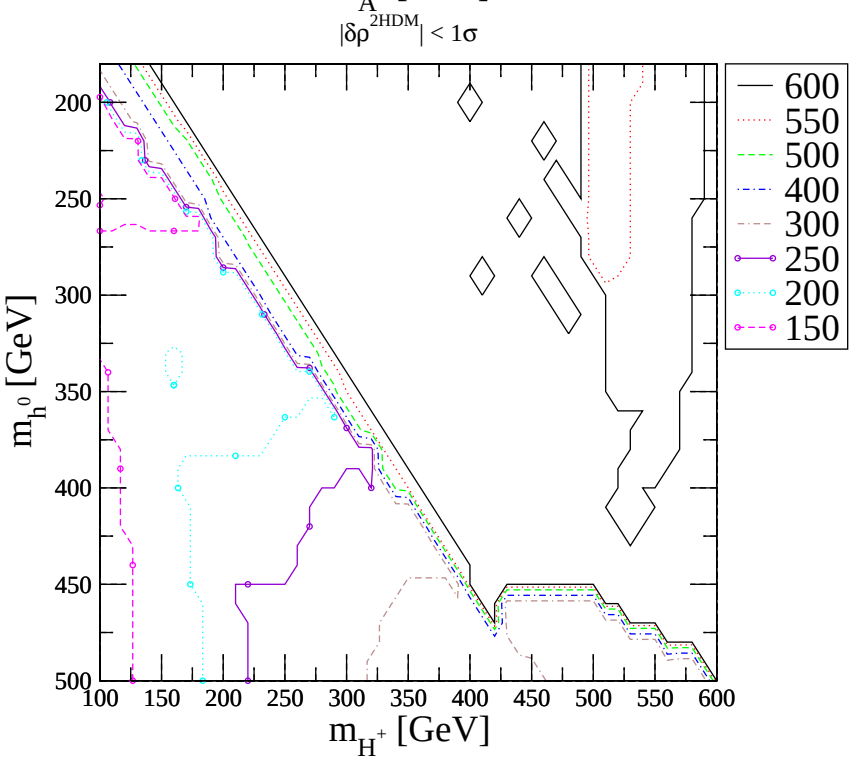

(b)

Figure 5.5: **(a)** Contour lines in the $(m_{H^\pm}, m_{h^0})$-plane for the maximum number of light CP-even Higgs FCNC events $h^0 \to t\,\bar{c} + \bar{t}\,c$ produced at the LHC for $100\,fb^{-1}$ of integrated luminosity within $\delta\rho^{\text{2HDM}}$ at $1\,\sigma$; **(b)** Contour lines showing the value of m_{A^0} that maximizes the number of events.

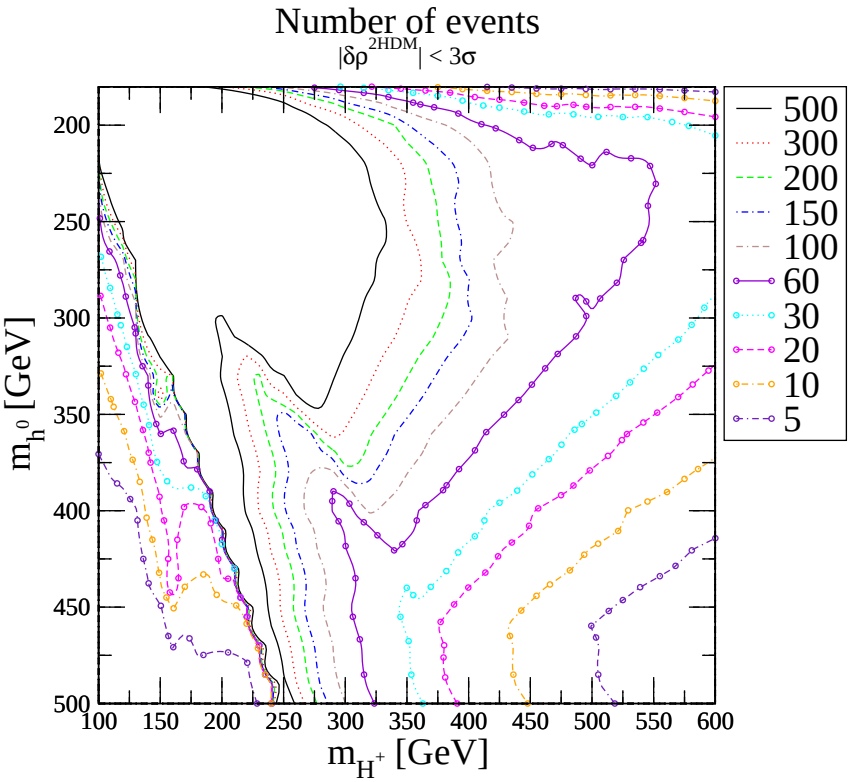

(a)

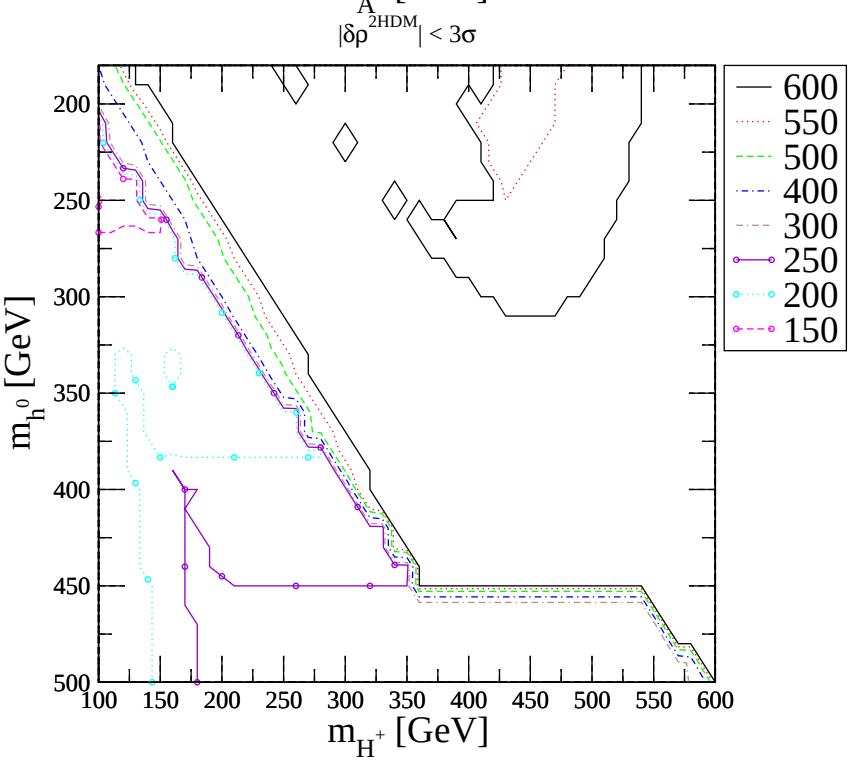

(b)

Figure 5.6: As in Fig. 5.5 but within $\delta\rho^{\rm 2HDM}$ at $3\,\sigma$.

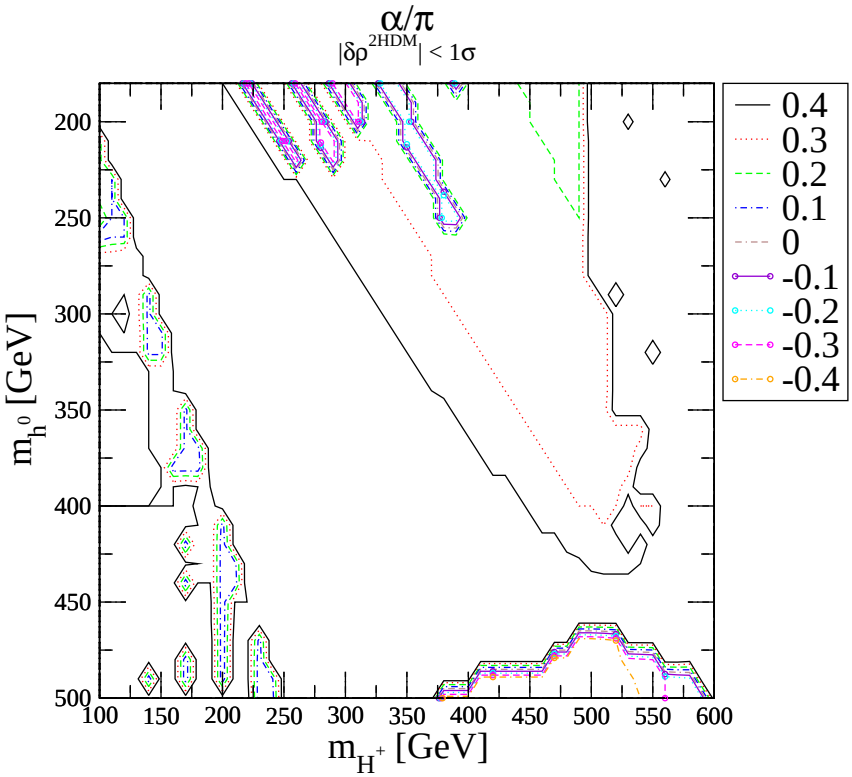

(a)

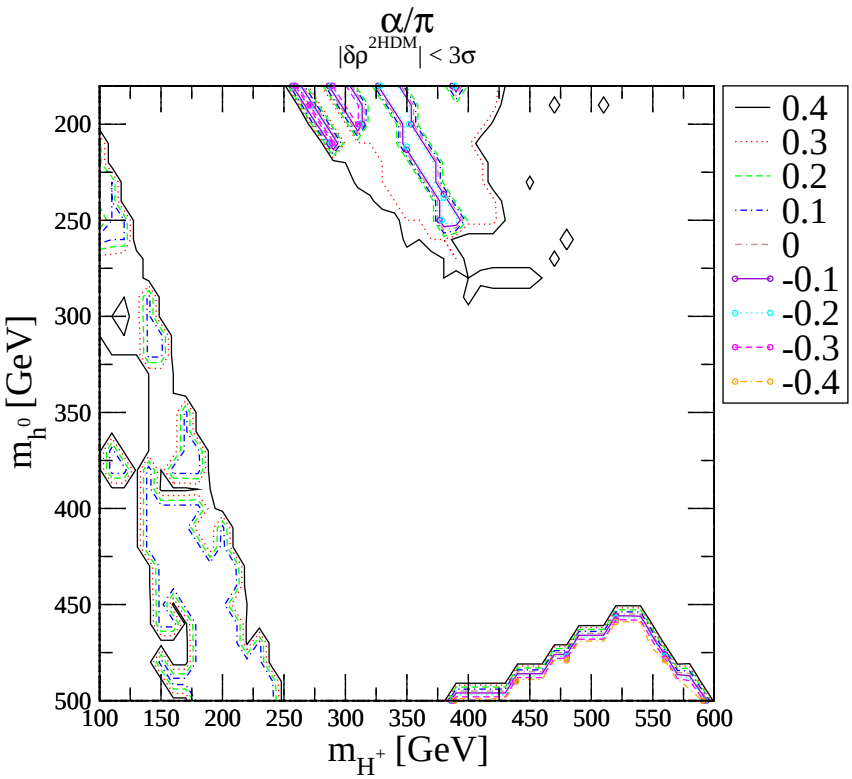

(b)

Figure 5.7: Contour lines $\alpha/\pi = const.$ (α is the mixing angle in the CP-even sector) corresponding to Figs. 5.5-5.6 for $\delta\rho^{\mathrm{2HDM}}$ at **(a)** $1\,\sigma$ and **(b)** $3\,\sigma$.

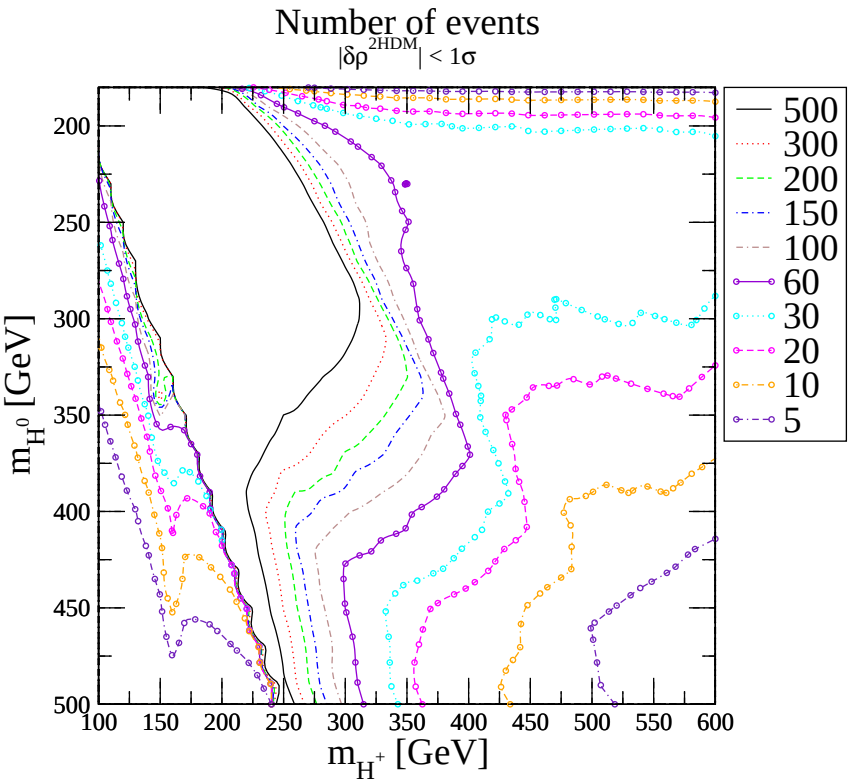

(a)

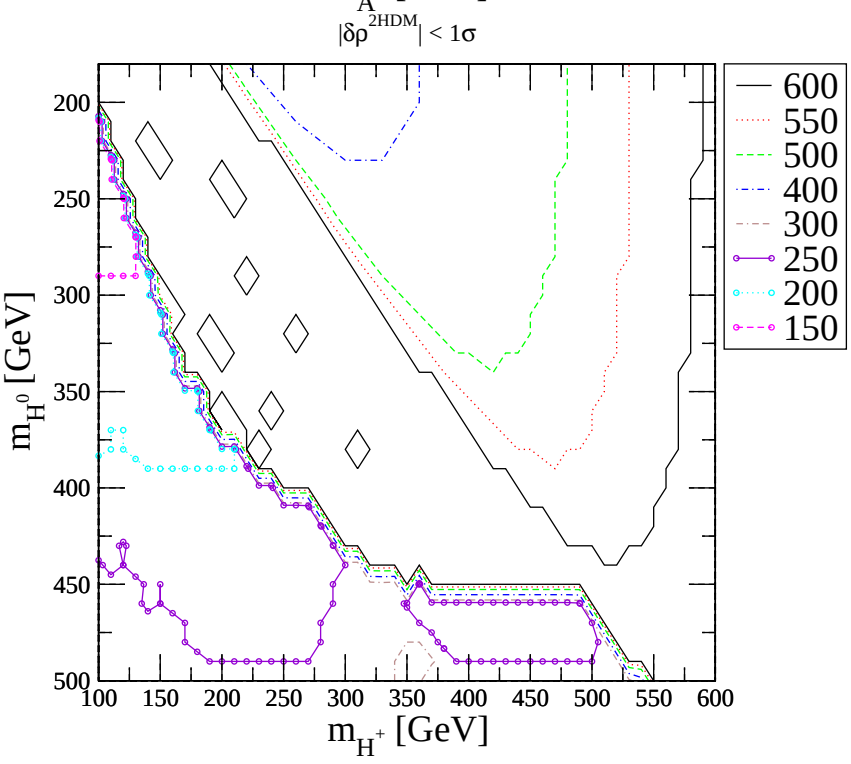

(b)

Figure 5.8: **(a)** Contour lines in the $(m_{H^\pm}, m_{H^0})$-plane for the maximum number of heavy CP-even Higgs FCNC events $H^0 \to t\,\bar{c} + \bar{t}\,c$ (2HDM II case) produced at the LHC for $100\,fb^{-1}$ of integrated luminosity within $\delta\rho^{\mathrm{2HDM}}$ at $1\,\sigma$.

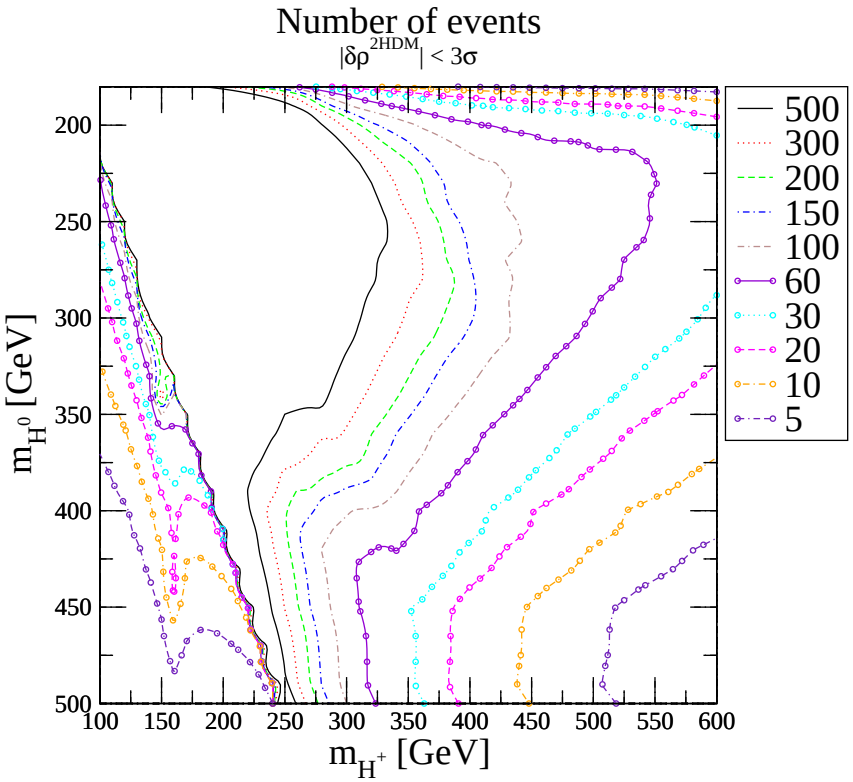

(a)

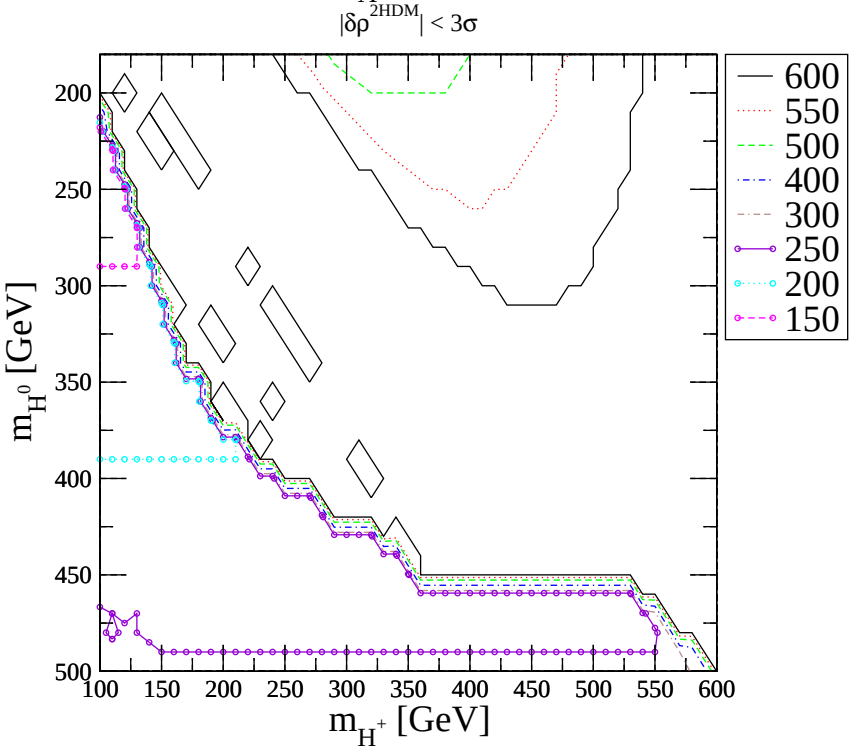

(b)

Figure 5.9: As in Fig. 5.8 but within $\delta\rho^{\rm 2HDM}$ at $3\,\sigma$.

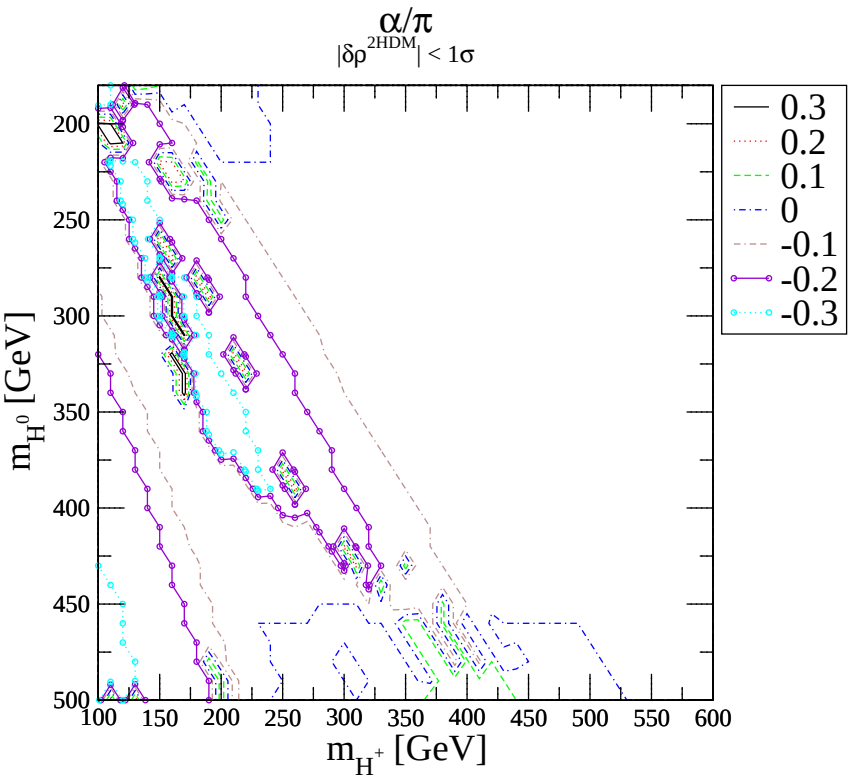

(a)

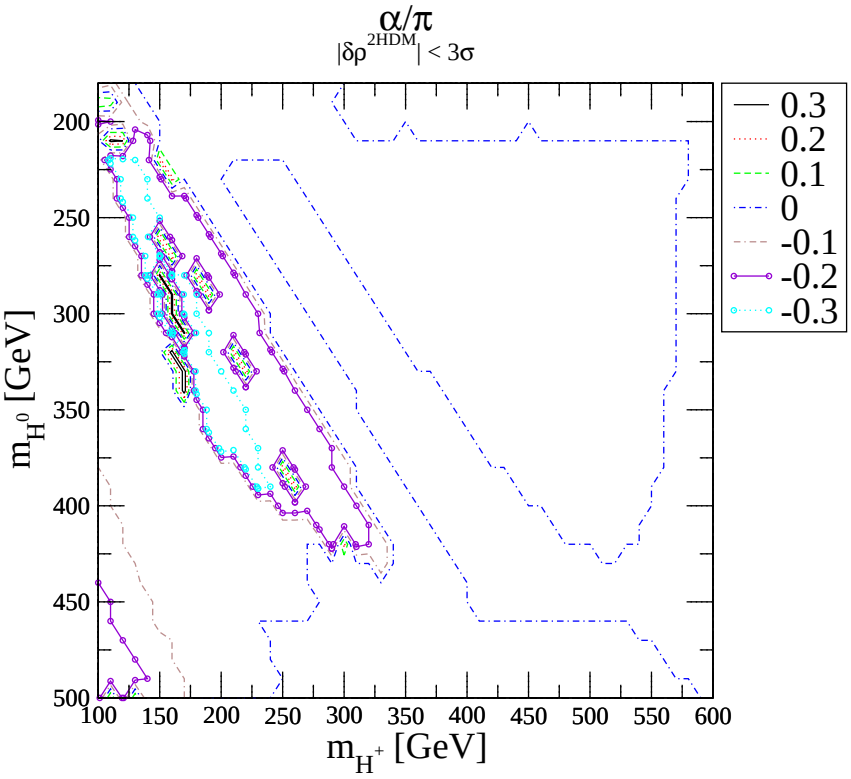

(b)

Figure 5.10: Contour lines $\alpha/\pi = const.$ as in Fig.5.7, but for the heavy CP-even Higgs.

which are not varying as follows:

$$\begin{aligned}&(m_{h^0} = 350\,GeV, m_{H^0} = 600\,GeV, m_{A^0} = 550\,GeV, m_{H^\pm} = 375\,GeV,\\ &\tan\alpha = 30, \tan\beta = 60)\end{aligned} \tag{5.8}$$

After crossing a local maximum (associated to a pseudo-threshold of the one-loop vertex function involving the $h^0\,H^+\,H^-$ coupling) the subsequently falling behavior of the B with $m_{H^\pm}$ clearly shows that the previously discussed bounds on $m_{H^\pm}$ are quite relevant. The branching ratio, however, stays within $10^{-6}-10^{-5}$ for a wide range of heavy charged Higgs masses extending up to $m_{H^\pm} \leq 600\,GeV$ in Fig. 5.3a. Hence, for $m_{H^\pm}$ heavy enough to satisfy the indirect bounds from radiative B-meson decays [62], the maximum B is still sizeable. In Fig. 5.3c the production rate of h^0 bosons at the LHC is shown as a function of m_{h^0}, for fixed parameters (5.6). The production cross-sections for the subprocesses

$$gg \to\ h^0 + X\,, \qquad gg, qq \to\ h^0 + Q\bar{Q}\,, \tag{5.9}$$

contributing to (5.7) in the case of the light CP-even Higgs h^0 are explicitly separated in Fig. 5.3c. The gluon-gluon fusion process proceeds at one-loop and the $h^0 Q\bar{Q}$ associated production proceeds at tree-level [136,141]. Similar subprocesses and results apply for H^0 and A^0 production. At large $\tan\beta$ and the larger the Higgs boson masses the particular associated production mechanism with the bottom quark, $Q = b$, i.e. $h^0\ b\bar{b}$, becomes dominant by far. All other mechanisms for Higgs boson production in Type II models [31, 136, 140, 141], like vector-boson fusion (which contributes also to $h^0 Q\bar{Q}$ when Q are light quarks), vector-boson bremsstrahlung ($q\bar{q} \to h\,V$) and associated $t\,\bar{t}$ production, are subdominant at large $\tan\beta$ and can be neglected for our purposes. Admittedly, some of these mechanisms can be relevant for Higgs boson production in the case of the Type I 2HDM at low $\tan\beta$, but we have already warned that the corresponding FCNC branching ratios are never sufficiently high.

The control over $\delta\rho^{\rm 2HDM}$ is displayed in Fig. 5.3d. Recall that $\delta\rho$ is not sensitive to the mass splitting between m_{h^0} and m_{H^0}, because of CP-conservation in the gauge boson sector, but it does feel all the other mass splittings among Higgs bosons, charged and neutral. A more systematic search of B values in the parameter space is presented in Figs. 5.4a,b corresponding to $B^{II}(h^0 \to t\,\bar{c}+\bar{t}\,c)$ and $B^{II}(H^0 \to t\,\bar{c}+\bar{t}\,c)$ respectively. Here we have scanned independently on the parameters (5.6) while holding the $\delta\rho^{\rm 2HDM}$ bound at $1\,\sigma$. The contour lines in these figures represent the locus of points in the $(m_{H^\pm}, m_{h^0})$-plane giving maximized values of the B in the 2HDM II. Let us remark that the highest value of $\tan\beta$ is always preferred, and therefore all these contour lines correspond to $\tan\beta = 60$.

In practice, to better assess the possibility of detection at the LHC, one has to study the production rates of the FCNC events. These are determined by combining the production cross-sections of neutral 2HDM II Higgs bosons at the LHC and the FCNC branching ratios. If we just adopt the mild LEP bound $m_{H^\pm} \gtrsim 80\,GeV$ and let $m_{H^\pm}$ approach the maximum in Fig. 5.3a then the B can be as large as 10^{-3} and the number of FCNC events can be huge, at the level of ten thousand per $100\,fb^{-1}$ of integrated luminosity. But of course the region near the maximum is too special. Moreover, if we switch on the above mentioned indirect bound from $b \to s\,\gamma$ [62], then the typical B is much smaller (of order 10^{-5}) and the number of events is reduced dramatically, at a level of hundred or less for the same integrated luminosity. On the other hand it may well happen that there are regions of parameter space where $B \sim 10^{-5}$ (see Fig. 5.4) but the production cross-section is too small because the decaying Higgs boson is too heavy. Therefore, it is the product of the two quantities that matters.

The systematic search of the regions of parameter space with the maximum number of FCNC events for the light CP-even Higgs is presented in the form of contour lines in the multiple Figs. 5.5 and 5.6. For instance, each isoline in Figs. 5.5a and 5.6a corresponds to a fixed number of produced FCNC events at the LHC while keeping the value of $\delta\rho^{\rm 2HDM}$ within $1\,\sigma$ or $3\,\sigma$ respectively of its central experimental value. When scanning over the parameter space (5.6) we have found again that $\tan\beta$ is preferred at the highest allowed value ($\tan\beta = 60$) – for Type II models. We have also determined (see Figs. 5.5 b and 5.6 d) the corresponding contour lines for m_{A^0} associated to these events. The m_{A^0}-lines are important because the FCNC processes under consideration are sensitive to the mass splittings between m_{A^0} and the corresponding decaying Higgs boson, see e.g. eq.(5.5) and Table 2.1. The combined figures 5.5 and 5.6 are very useful because they give a panoramic view of the origin of our results in the parameter space. To complete the map of the numerical analysis we provide Fig. 5.7 in which we have projected the contour lines of the CP-even mixing angle α associated to the previous plots. For a given contour line $\alpha/\pi = const.$, the set of inner points have a value of α/π smaller than the one defined by the line itself. In particular, the large domains in Figs. 5.7a,b without contour lines correspond to $\alpha/\pi > 0.4$ and so to relatively large (and positive) $\tan\alpha$. There are a few and small neighborhoods where the FCNC rates for h^0 can be sizeable also for small $\tan\alpha$.

Knowing that high $\tan\alpha$ is generally preferred by $h^0 \to t\,\bar{c} + \bar{t}\,c$, and noting from Figs. 5.5 and 5.6 that large mass splittings between m_{h^0} and m_{A^0} are allowed, we find that the trilinear coupling $\lambda_{H^+\,H^-\,h^0}$ can take the form $\lambda_{H^+\,H^-\,h^0} \sim (m^2_{h^0} - m^2_{A^0})\,\tan\beta/(M_W\,m_{H^\pm})$. Hence it provides a substantial additional enhancement beyond the $\tan\beta$ factor. One can check from the approximate formula (5.5) that the maximum FCNC branching ratios

$B^{II}(h^0 \to t\,\bar{c} + \bar{t}\,c)$ can eventually reach the 10^{-5} level even in regions where the charged Higgs boson mass preserve the stringent indirect bounds from radiative B-meson decays [62]. These expectations are well in agreement with the exact numerical analysis presented in Fig. 5.4, thus showing that eq.(5.5) provides a reasonable estimate, and therefore a plausible explanation for the origin of the maximum contributions. As a matter of fact, we have checked that the single (finite) Feynman diagram giving rise to the estimation (5.5) – the one-loop vertex Feynman diagram with a couple of charged Higgs bosons and a bottom quark in the loop – reproduces the full result with an accuracy better than 10% for $\tan\beta \gtrsim 10-20$. At lower $\tan\beta$ values large deviations are possible but, as warned before, eq. (5.5) is expected to be valid only at large $\tan\beta$. Furthermore, for low values of $\tan\beta \lesssim 20$ the FCNC Bs are too small to be of any phenomenological interest. The exact numerical analysis is of course based on the full expression for the branching ratio

$$B^{II}(h^0 \to t\,\bar{c} + \bar{t}\,c) = \frac{\Gamma(h^0 \to t\,\bar{c} + \bar{t}\,c)}{\Gamma(h^0 \to b\,\bar{b}) + \Gamma(h^0 \to t\,\bar{t}) + \Gamma(h^0 \to V\,V) + \Gamma(h^0 \to H\,H)}\,, \quad (5.10)$$

where all decay widths in the denominator of this formula have been computed at the tree-level in the 2HDM II, since this provides a consistent description of eq. (5.10) at leading order. Here we have defined

$$\Gamma(h^0 \to V\,V) \equiv \Gamma(h^0 \to W^+W^-) + \Gamma(H^0 \to Z\,Z)\,, \quad (5.11)$$

$$\Gamma(h^0 \to H\,H) \equiv \Gamma(h^0 \to A^0\,A^0) + \Gamma(h^0 \to H^+\,H^-)\,. \quad (5.12)$$

We disregard the loop induced decay channels, since they have branching ratios below the percent level all over the parameter space. The τ-lepton decay channel is also neglected, since it is suppressed by a factor of $\mathcal{O}(10^{-2})$ with respect the $b\bar{b}$-channel in the whole 2HDM parameter space. In general the effect of the gauge boson channels $h^0 \to W^+W^-, ZZ$ in the B (5.10) is not so important as in the SM, actually for $\beta = \alpha$ they vanish in the h^0 case because they are proportional to $\sin^2(\beta - \alpha)$. This is approximately the case for large $\tan\alpha$ and large $\tan\beta$, the dominant FCNC region for h^0 decay (Cf. Fig.5.7a and 5.7b). In this region, the mode $h^0 \to t\,\bar{t}$ is, when kinematically allowed, suppressed: $B(h^0 \to t\,\bar{t}) \propto \cos^2\alpha/\sin^2\beta \to 0$ (Cf. Eq. (2.42)). On the other hand there are domains in our plots where the decays $h^0 \to H^+\,H^-$ and $h^0 \to A^0\,A^0$ are kinematically possible and non-(dynamically) suppressed. Indeed, this can be checked from the explicit structure of the trilinear couplings $h^0\,H^+\,H^-$ and $h^0\,A^0\,A^0$ in Table 2.1; in the dominant region for the decays $h^0 \to t\,\bar{c} + \bar{t}\,c$ both of these couplings are $\tan\beta$-enhanced. Nevertheless the decay $h^0 \to A^0\,A^0$ is only possible for $m_{A^0} < m_{h^0}/2$, and since the optimal FCNC regions demand the largest possible values of m_{A^0}, this decay is kinematically blocked

there. On the other hand the mode $h^0 \to H^+ H^-$ is of course allowed if we just take the aforementioned direct limits on the 2HDM Higgs boson masses. But it is never available if we apply the indirect bound from $b \to s\,\gamma$ on the charged Higgs mass mentioned above, unless $m_{h^0} > 2m_{H^\pm} > 700\,GeV$, in which case h^0 is so heavy that its production cross-section is too small for FCNC studies to be further pursued.

The corresponding results for the heavy CP-even Higgs boson are displayed in Figs. 5.8, 5.9 and 5.10. The exact formula for the B in this case reads

$$B^{II}(H^0 \to t\,\bar{c} + \bar{t}\,c) = \frac{\Gamma(H^0 \to t\,\bar{c} + \bar{t}\,c)}{\Gamma(H^0 \to b\,\bar{b}) + \Gamma(H^0 \to t\,\bar{t}) + \Gamma(H^0 \to V\,V) + \Gamma(H^0 \to H\,H)}\,, \tag{5.13}$$

where we have defined

$$\Gamma(H^0 \to V\,V) \equiv \Gamma(H^0 \to W^+W^-) + \Gamma(H^0 \to Z\,Z)\,, \tag{5.14}$$

$$\Gamma(H^0 \to H\,H) \equiv \Gamma(H^0 \to h^0\,h^0) + \Gamma(H^0 \to A^0\,A^0) + \Gamma(H^0 \to H^+\,H^-)\,. \tag{5.15}$$

From the contour lines in Figs. 5.8a and 5.9a it is patent that the number of FCNC top quark events stemming from H^0 decays is comparable to the case of the lightest Higgs boson. However, Fig. 5.10a,b clearly reveals that these events are localized in regions of the parameter space generally different from the h^0 case, namely they prefer $\tan\alpha \simeq 0$. Even so, there are some "islands" of events at large $\tan\alpha$. This situation is complementary to the one observed for h^0 in Fig. 5.7. However, in both cases these isolated regions are mainly concentrated in the segment $m_{H^\pm} < 350\,GeV$. Therefore, if the bound on $m_{H^\pm}$ from $b \to s\,\gamma$ is strictly preserved, it is difficult to find regions of parameter space where the two CP-even states of a general 2HDM II may both undergo a FCNC decay of the type (5.1).

In the dominant regions of the FCNC mode $H^0 \to t\,\bar{c}$ (where $\tan\alpha$ is small and $\tan\beta$ is large), the decay of H^0 into the $t\bar{t}$ final state is suppressed: $B(H \to t\,\bar{t}) \propto \sin^2\alpha/\sin^2\beta \to 0$. In the same regions the gauge boson channels in (5.13) are suppressed too because $\Gamma(H^0 \to W^+W^-, ZZ) \propto \cos^2(\beta - \alpha)$. In principle the heavy CP-even Higgs boson H^0 also could (as h^0) decay into $A^0\,A^0$ and $H^+\,H^-$. But there is a novelty here with respect to the h^0 decays, in that there could be regions where H^0 could decay into the final state $h^0\,h^0$. This contingency has been included explicitly in eq.(5.15). However, in practice, neither one of these three last channels is relevant in the optimal FCNC domains of parameter space. First, the decay $H^0 \to h^0\,h^0$, although it is kinematically possible, is dynamically suppressed in the main FCNC region for H^0. This can be seen from Table 2.1, where the trilinear coupling $H^0\,h^0\,h^0$ becomes vanishingly small at large $\tan\beta$ and small $\tan\alpha$. Second, the coupling $H^0A^0A^0$ in Table 2.1 is non-suppressed in

the present region, but again the mode $H^0 \to A^0\,A^0$ is kinematically forbidden in the optimal FCNC domains because the latter favor large values of the CP-odd mass (see Figs. 5.8b and 5.9b). Third, although in these domains the decay $H^0 \to H^+\,H^-$ is also non-dynamically suppressed (see the corresponding trilinear coupling in Table 2.1), it becomes kinematically shifted to the high mass range $m_{H^0} > 700\,GeV$ if we switch on the indirect bound from $b \to s\,\gamma$. Obviously, in this latter case the H^0 production cross section becomes too small and the FCNC study has no interest. All in all the contributions from (5.11),(5.12),(5.14) and (5.15) are irrelevant for $m_{h^0}, m_{H^0} < 700\,GeV$ as their numerical impact on $B^{II}(h^0, H^0 \to t\,\bar{c} + \bar{t}\,c)$ is negligible. Our formulae (5.10) and (5.13) do contain all the decay channels and we have verified explicitly these features.

As remarked before, in general the most favorable regions of parameter space for the FCNC decays of h^0 and H^0 do not overlap much. The trilinear Higgs boson self-couplings in Table 2.1 (also the fermionic ones) are interchanged when performing the simultaneous substitutions $\alpha \to \pi/2 - \alpha$ and $m_{h^0} \to m_{H^0}$ (see last chapter 4). Furthermore, the LHC production rates of the neutral Higgs bosons fall quite fast with the masses of these particles, as seen e.g. in Fig. 5.3b for the h^0 state. As a consequence that exchange symmetry on the branching ratios does not go over to the final event rates, so in practice the number of FCNC events from H^0 decays are smaller (for the same values of the other parameters) as compared to those for h^0; thus H^0 requires e.g. lighter charged Higgs masses to achieve the same number of FCNC events as h^0. As for the CP-odd state A^0, we have seen that it plays an important indirect dynamical role on the other decays through the trilinear couplings in Table 2.1, but its own FCNC decay rates never get a sufficient degree of enhancement due to the absence of the relevant trilinear couplings, so we may discard it from our analysis.

We notice that this picture is consistent with the decoupling limit in the 2HDM: for $\alpha \to \beta$, the heaviest CP-even Higgs boson (H^0) behaves as the SM Higgs boson, whereas h^0 decouples from the electroweak gauge bosons and may develop enhanced couplings to up and down-like quarks, depending on whether $\tan\beta$ is small or large respectively; in the opposite limit ($\alpha \to \beta - \pi/2$), it is h^0 that behaves as H^{SM}, while H^0 decouples from gauge bosons and may develop the same enhanced couplings to quarks as h^0 did in the previous case. Indeed these are the situations that we find concerning the FCNC decay rates. We recall that the numerical results presented in our figures correspond to an integrated luminosity of $100\,fb^{-1}$. However, the combined ATLAS and CMS detectors might eventually accumulate a few hundred inverse femtobarn [13, 14]. Therefore, hopefully, a few hundred FCNC events (5.1) could eventually be collected in the most optimistic scenario. Actually, the extreme rareness of these events in the SM

suggests that if only a few of them could be clearly disentangled, it should suffice to claim physics beyond the SM.

5.4 Discussion and conclusions

Detection strategies at the CERN-LHC collider for the search of the SM Higgs boson, and also for the three spinless fields of the MSSM Higgs sector, have been described in great detail in many places of the literature [6, 11, 13, 14, 17, 142, 143], but not so well for the corresponding charged and neutral Higgs bosons of the general 2HDM. The result is that the discovery of the SM Higgs boson is guaranteed at the LHC in the whole presumed range $100\,GeV \lesssim m_H \lesssim 1\,TeV$. However, the discovery channels are different in each kinematical region and sometimes the most obvious ones are rendered useless. For example, due to the huge irreducible QCD background from $b\,\bar{b}$ dijets, the decay mode $H^{SM} \to b\,\bar{b}$ is difficult and one has to complement the search with many other channels, particularly $H^{SM} \to \gamma\,\gamma$ [13,14]. We have shown in this work that there are scenarios in the 2HDM parameter space where alternative decays, like the FCNC modes $h^0 \to t\,\bar{c} + \bar{t}\,c$ and $H^0 \to t\,\bar{c} + \bar{t}\,c$, can also be useful. For instance, in the h^0 case, this situation occurs when $\tan\beta$ and $\tan\alpha$ are both large and the CP-odd state is much heavier than the CP-even ones. The potential enhancement is then spectacular and it may reach up to ten billion times the SM value $B(H^{SM} \to t\,\bar{c}) \sim 10^{-15}$, thereby bringing the maximum value of the FCNC branching ratio $B(h^0 \to t\,\bar{c})$ to the level of $\sim 10^{-5}$. As a matter of fact, the enhancement would be much larger were it not because we eventually apply the severe (indirect) lower bound on the charged Higgs mass from $b \to s\,\gamma$ [62]. Although these decays have maximal ratios below $B(h \to \gamma\gamma) \sim 10^{-3}$, they should be essentially free of QCD background [4].

While in the MSSM almost the full $(m_{A^0}, \tan\beta)$-parameter space is covered, with better efficiency at high $\tan\beta$ though, we should insist that within the general 2HDM the tagging strategies are not so well studied and one would like to have further information to disentangle the MSSM scenarios from the 2HDM ones. Here again the study of the FCNC Higgs decays can play a role. Of course the statistics for the FCNC Higgs decays is poor due to the weakness of the couplings and the large masses of the Higgs bosons to be produced. However, in the favorable regions, which are generally characterized by large values of $\tan\beta$ and of $\tan\alpha$, one may collect a few hundred events of the type

[4] Misidentification of b-quarks as c-quarks in tb production might be a source of background to our FCNC events. However, to rate the actual impact of that misidentification one would need a dedicated simulation of the signal versus background, which is beyond the scope of this work.

(5.1)– mainly from h^0 – in the high luminosity phase of the LHC. As we have said, this is basically due to the enormous enhancement that may undergo the FCNC decay rates, but also because in the same regions of parameter space where the Bs are enhanced, also the LHC production rates of the Higgs bosons can be significantly larger (one order of magnitude) in the 2HDM II as compared to the SM.

Interestingly enough, in many cases one can easily distinguish whether the enhanced FCNC events (5.1) stem from the dynamics of a general, unrestricted, 2HDM model, or rather from some supersymmetric mechanisms within the MSSM. This is already obvious from the fact that the ranges of neutral and charged Higgs boson masses in the 2HDM case can be totally incompatible with the corresponding ones in the MSSM. But there are many other ways to discriminate these rare events. For instance, in the 2HDM case the CP-odd modes $A^0 \to t\,\bar{c} + \bar{t}\,c$ are completely hopeless whereas in the MSSM they can be enhanced see chapter 7, [43, 47, 48]. Using this information in combination with the masses of potentially detected Higgs bosons could be extremely useful to pinpoint the supersymmetric or non-supersymmetric nature of them. We may describe a few specific strategies. As it was first shown in Ref. [43], the leading SUSY-FCNC effects associated to the $h\,t\,c$ vertices ($h = h^0\,, H^0\,, A^0$) come from the FCNC gluino interactions which are induced by potentially large misalignments of the quark and squark mass matrices [93,144]. These effects are not particularly sensitive to $\tan\beta$ and they can be very sizeable for both high and moderately low values of this parameter. This sole fact can be another distinguishing feature between FCNC events (5.1) of MSSM or 2HDM origin. If, for example, a few of these events were observed and at the same time the best MSSM fits to the electroweak precision data would favor moderate values of $\tan\beta$, say in the range $10-20$, then it is clear that those events could originate in the FCNC gluino interactions but in no way within the context of the general 2HDM. In this respect it should be mentioned that the FCNC gluino couplings became more restricted from the low-energy meson data [104], and will presumably become further restricted in the near future. The reason being that the same couplings are related, via $SU(2)$ gauge invariance and CKM rotation, to those affecting the down-like quark sector, which will most likely become constrained by the increasingly more precise low-energy meson physics [95,96,104]. In that circumstance the only source of FCNC Higgs decays in the MSSM will stem purely from the electroweak interactions within the super-CKM basis. Then, in the absence of these SUSY-QCD FCNC effects, we could judiciously conclude from the work of Ref. [43] – in which both the SUSY-QCD *and* the SUSY electroweak contributions were computed for the $h\,t\,c$ vertices – that the FCNC rates in the MSSM should diminish dramatically (two to three orders of magnitude). In such case we can imagine the following "provocative" scenario.

Suppose that the LHC finds a light neutral Higgs boson of mass $\lesssim 140\,GeV$ (suggestively enough, in a mass range near the MSSM upper bound for m_{h^0}!) and subsequently, or about simultaneously, a charged Higgs boson and another neutral Higgs boson both with masses around $400\,GeV$ or more. At this point one could naively suspect that a MSSM picture out these findings is getting somehow confirmed. If, however, later on a few FCNC events (5.1) are reported and potentially ascribed to the previously discovered heavy neutral Higgs boson (presumably H^0), then the overall situation could not correspond at all to the MSSM, while it could be perfectly compatible with the 2HDM II. Alternatively, suppose that the FCNC gluino couplings were not yet sufficiently restricted, but (still following the remaining hypotheses of the previous example) a third neutral Higgs boson (presumably A^0) is found, also accompanied with a few FCNC events. Then this situation would be incompatible with the 2HDM II, and in actual fact it would put forward strong (indirect) evidence of the MSSM!!

We should also mention that there are other FCNC Higgs decay modes, as for example $h \to b\,\bar{s} + \bar{b}\,s$, which could be, in principle, competitive with the top quark modes (5.1). In some cases these bottom modes can be highly enhanced in the MSSM case [47, 48]. Actually, a more complete assessment of the FCNC bottom modes in the MSSM case is studied in the chapter 6 – namely one which takes also into account the supersymmetric contributions to the highly restrictive radiative B-meson decays – shows that they are eventually rendered at a similar level of the top modes under study in most of the parameter space.

To summarize, the FCNC decays of the Higgs bosons into top quark final states can be a helpful complementary strategy to search for signals of physics beyond the SM in the LHC. Our comprehensive numerical analysis shows that the FCNC studies are feasible for CP-even Higgs masses up to about $500\,GeV$. While the statistics of these FCNC decays is of course poor, the advantage is that a few tagged and well discriminated events of this sort could not be attributed by any means to the SM, and therefore should call for various kinds of new physics. In this work we have shown that a general 2HDM II is potentially competitive to be ultimately responsible for these FCNC decays, if they are ever found, and we have exemplified how to discriminate this possibility from the more restricted one associated to the MSSM.

Chapter 6

Higgs Boson FCNC Decays into Bottom Quarks in the MSSM

6.1 Introduction

The most general MSSM includes tree-level FCNCs among the extra predicted particles, which induce one-loop FCNC interactions among the SM particles, as discussed in section 3.6.

Concerning the FCNC interactions of Higgs bosons with third generation quarks, it was demonstrated long ago [43] that the leading term corresponds to a *single particle insertion approximation*, which produces a flavor change in the internal squark loop propagator, since in this case the chirality change can already take place at the squark-squark-Higgs boson interaction vertex. Adding this to the fact that the Higgs bosons (in contrast to gauge bosons) have a privileged coupling to third generation quarks, one might expect that the FCNC interactions of the type quark-quark-Higgs bosons in the MSSM become highly strengthened with respect to the SM prediction. This was already proven in the rare decay channels $\Gamma(t \to ch)$ [43] (h being any of the neutral Higgs bosons of the MSSM $h \equiv h^0, H^0, A^0$), where the maximum rate of the SUSY-QCD induced branching ratio was found to be $B(t \to ch) \simeq 10^{-5}$, eight orders of magnitude above the SM expectations $B(t \to cH^{SM}) \simeq 10^{-13}$. Similar enhancement factors have been found in the top-quark-Higgs boson interactions in other extensions of the SM, as seen in chapters 4-7.

From the experience of the previous calculations with the top quark, we expect similar enhancements in the FCNC interactions of the MSSM Higgs bosons with the bottom quark. Indeed, the purpose of this work is to quantify, in a reliable way, the MSSM

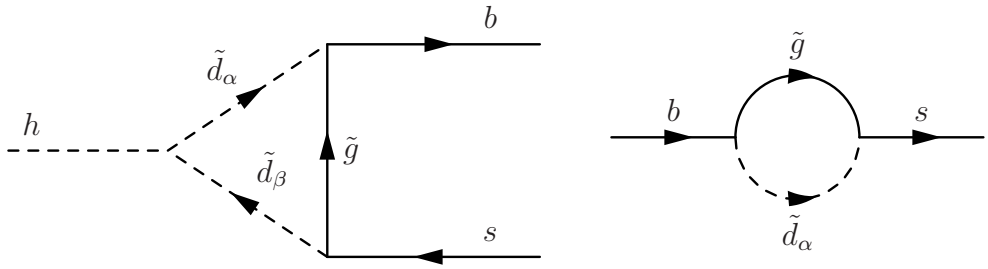

Figure 6.1: One-loop SUSY-QCD vertex diagram contributing to the decay $h \to q\,q'$ and diagrams contributing to mixed $b - s$ self-energy. $\tilde{d}_{\{\alpha,\beta\}}$ represent mass-eigenstate down type squarks of any generation.

expectations on the FCNC Higgs boson decay modes

$$h \to b\,\bar{s}\,, \quad h \to \bar{b}\,s \qquad (h = h^0, H^0, A^0)\,. \tag{6.1}$$

The Feynman diagrams for these decays are depicted in Fig. 6.1. There are other FCNC decay modes involving light quarks. However, only these bottom quark channels are relevant, as the remaining FCNC decays into light quarks are negligible in the MSSM. Moreover, the FCNC decays of Higgs bosons into bottom quarks are specially interesting as they can provide an invaluable tool to discriminate among different extended Higgs boson scenarios in the difficult LHC range $90 < m_h < 130\,\text{GeV}$ [13, 14].

In this work we present what we believe is the first realistic estimate of the SUSY-QCD contributions to the FCNC branching ratios of the MSSM Higgs bosons into bottom quark. Specifically, we compute

$$B(h \to q\,q') = \frac{\Gamma(h \to q\,q')}{\Gamma(h \to X)} \equiv \frac{\Gamma(h \to b\,\bar{s}) + \Gamma(h \to \bar{b}\,s)}{\sum_i \Gamma(h \to X_i)} \tag{6.2}$$

for the three Higgs bosons of the MSSM, $h = h^0, H^0, A^0$, where $\Gamma(h \to X)$ is the – consistently computed – total width in each case. The maximization process of the above branching ratios in the MSSM parameter space is performed on the basis of a simultaneous analysis of the relevant partial decay widths and of the branching ratio of the low-energy FCNC process $b \to s\,\gamma$, whose value is severely restricted by experiment [52–58]. It turns out that the maximum FCNC rates that we find disagree quite significantly with Ref. [47] as they do not impose the restriction of $B(b \to s\gamma)$.[1]

[1] See also Ref. [48] for a combined analysis of flavor-violating and CP-violating MSSM couplings.

The structure of the study is as follows. In Section 6.2 we estimate the expected branching ratios and describe the structure of Eq. (6.2) in the MSSM in more detail; in Section 6.3 we present the numerical analysis, and in Section 6.4 we deliver our conclusions.

6.2 Partial widths and branching ratios

As seen in eqs. (1.5) and (1.6) the branching ratios into bottom quark are much larger than the Higgs boson FCNC branching ratio into top quark in the SM as seen in chapter 5. However, even in the case (1.5) it is still too small to have a chance for detection in the LHC. It is clear that unless new physics comes to play the process $H^{SM} \to b\,\bar{s}$ (and of course $H^{SM} \to \bar{b}\,s$) will remain virtually invisible. Nonetheless the result (1.5) is not too far from being potentially detectable, and one might hope that it should not be too difficult for the new physics to boost it up to the observable level.

Consider how to estimate the potentially augmented rates for the MSSM processes (6.1), if only within a similarly crude approximation as above. Because of the strong FCNC gluino couplings mentioned in Section 6.1 and the $\tan\beta$-enhancement inherent to the MSSM Yukawa couplings (see Ref. [43] for details), we may expect several orders of magnitude increase of the branching ratios (6.2) as compared to the previous SM result. A naive approach might however go too far. For instance, one could look at the general structure of the couplings and venture an enhancement factor typically of order $(\alpha_s/\alpha_W)^2\,\tan^2\beta\,|\delta_{23}/V_{ts}|^2$, which for $\delta_{23} \lesssim 1$ and $\tan\beta > 30$ could easily rocket the SM result some $5-6$ orders of magnitude higher, bringing perhaps one of the MSSM rates (6.2) to the "scandalous" level of 10% or more. But of course only a more elaborated calculation, assisted by a judicious consideration of the various experimental restrictions, can provide a reliable result. As we shall see, a thorough analysis generally disproves the latter overestimate.

The detailed computation of the SUSY-QCD one-loop partial decay widths $\Gamma(h \to q\,q')$ in (6.2) within the MSSM follows closely that of $\Gamma(t \to ch)$ (see Ref. [43]). The rather cumbersome analytical expressions will not be listed here as they are an straightforward adaptation of those presented in the aforementioned references. However, there are a few subtleties that need to be pointed out. One of them is related to the calculation of the total widths $\Gamma(h \to X)$ for the three Higgs bosons $h = h^0, H^0, A^0$ in the MSSM. As long as $\Gamma(h \to q\,q')$ in the numerator of Eq. (6.2) is computed at leading order, the denominator has to be computed also at leading order, otherwise an artificial enhancement of $B(h \to q\,q')$ can be generated. For example, including the next-to-leading (NLO) order QCD corrections to $\Gamma(h \to b\bar{b})$ reduces the decay width by a significant amount [145–149].

Then, to be consistent, the NLO (two-loop) contributions to $\Gamma(h \to q\,q')$ should also be included. Similarly, the one-loop SUSY-QCD corrections to $\Gamma(h \to b\bar{b})$ can be very large and negative [31], which would enhance $B(h \to q\,q')$. At the same time these corrections also contribute to $\Gamma(h \to q\,q')$, such that contributions to the numerator and denominator of Eq. (6.2) compensate (at least partially) each other. Therefore the same order of perturbation theory must be used in both partial decay widths entering the observable $B(h \to q\,q')$ to obtain a consistent result. By the same token, using running masses in the numerator of (6.2) is mandatory, if they are used in the denominator. Last, but not least, consistency with the experimental bounds on related observables should also be taken into account. In this respect an essential role is played by the constraints on the FCNC couplings from the measured value of $B(b \to s\gamma)$. They must be included in this kind of analysis, if we aim at a realistic estimate of the maximal rates expected for the FCNC processes (6.1) in the MSSM. In our calculation we have used the full one-loop MSSM contributions to $B(b \to s\gamma)$ as given in [150] [2].

Let us now summarize the conditions under which we have performed the computation and the approximations and assumptions made in the present analysis:

- We include the full one-loop SUSY-QCD contributions to the partial decay widths $\Gamma(h \to q\,q')$ in (6.2).

- We assume that FCNC mixing terms appear only in the LH-chiral sector of the squark mixing matrix. This is the most natural assumption, and, moreover, it was proven in Ref. [43] that the presence of FCNC terms in the RH-chiral sector enhances the partial widths by a factor two at most – not an order of magnitude.

- The Higgs bosons total decay widths $\Gamma(h \to X)$ are computed at leading order, including all the relevant channels: $\Gamma(h \to f\bar{f}, ZZ, W^+W^-, gg)$. The off-shell decays $\Gamma(h \to ZZ^*, W^\pm W^{\mp *})$ have also been included. The one-loop decay rate $\Gamma(h \to gg)$ has been taken from [151] and the off-shell decay partial widths have been computed explicitly and found perfect agreement with the old literature on the subject [152]. We have verified that some of the aforementioned higher order decays are essential to consistently compute the total decay width of $\Gamma(h^0 \to X)$ in certain regions of the parameter space where the maximization procedure probes domains in which some (usually leading) two-body processes become greatly diminished. We have checked that our implementation of the various Higgs boson decay rates is consistent with

[2] Ref. [150] contains a partial two-loop computation of $B(b \to s\gamma)$, but only the one-loop contributions have been used for the present work.

the results of HDECAY [153]. However, care must be exercised if using the full-fledged result from HDECAY. For example, it would be inconsistent, and numerically significant, to compute the total widths $\Gamma(h \to X)$ with this program and at the same time to compute the SUSY-QCD one-loop partial widths $\Gamma(h \to q\,q')$ without including the leading conventional QCD effects through e.g. the running quark masses.

- The Higgs sector parameters (masses and CP-even mixing angle α) have been treated using the leading m_t and $m_b \tan\beta$ approximation to the one-loop result [85, 154–156]. For comparison, we also perform the analysis using the tree-level approximation.

- We include the constraints on the MSSM parameter space from $B(b \to s\gamma)$. We adopt $B(b \to s\gamma) = (2.1 - 4.5) \times 10^{-4}$ as the experimentally allowed range within three standard deviations [58]. Only the SUSY-QCD contributions induced from tree-level FCNCs are considered in the present work.

Running quark masses ($m_q(Q)$) and strong coupling constants ($\alpha_s(Q)$) are used throughout. More details are given below, as necessary.

6.3 Full one-loop SUSY-QCD calculation: Numerical analysis

Given the setup described in Section 6.2, we have performed a systematic scan of the MSSM parameter space with the following restrictions:

$$\begin{aligned} \delta_{23} &< 10^{-0.09} \simeq 0.81 \\ A_b &= -1500 \cdots 1500\,\text{GeV} \\ \mu &= -1000 \cdots 1000\,\text{GeV} \\ m_{\tilde{q}} &= 150 \cdots 1000\,\text{GeV} \end{aligned} \tag{6.3}$$

and the following fixed parameters:

$$\begin{aligned} \tan\beta &= 50 \\ m_{\tilde{b}_L} &= m_{\tilde{b}_R} = m_{\tilde{t}_R} = m_{\tilde{g}} = m_{\tilde{q}} \\ A_t &= -300\,\text{GeV}\ . \end{aligned} \tag{6.4}$$

Here $m_{\tilde{b}_{L,R}}$ are the left-chiral and right-chiral bottom-squark soft-SUSY-breaking mass parameters, and $m_{\tilde{q}}$ is a common mass for the strange- and down-squark left- and right-chiral soft SUSY-breaking mass parameters. Following the same notation as in [43], the

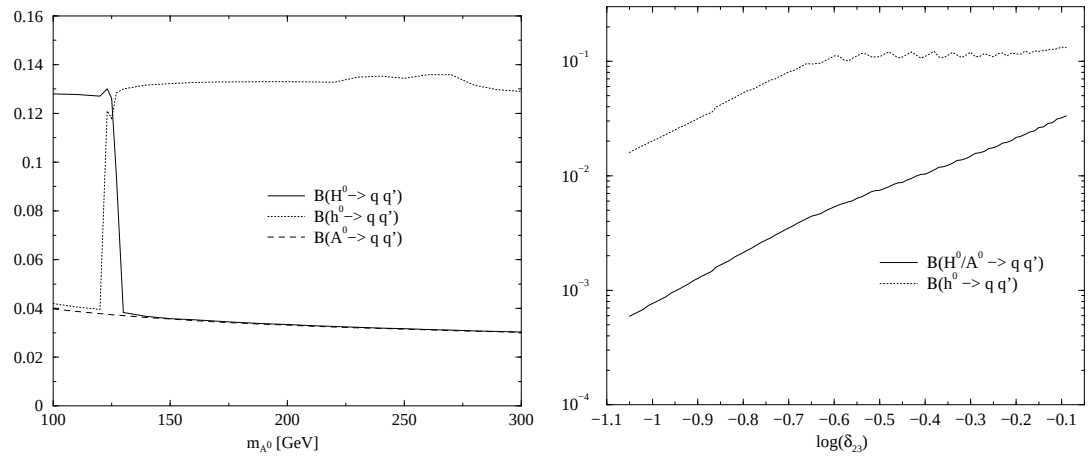

(a) (b)

Figure 6.2: Maximum SUSY-QCD contributions to $B(h \to q\,q')$, Eq. (6.2), as a function of **a)** m_{A^0} and **b)** δ_{23} for $m_{A^0} = 200\,\text{GeV}$.

parameter δ_{23} represents the mixing between the second and third generation squarks. Let us recall its definition:

$$\delta_{23} \equiv \frac{m^2_{\tilde{b}_L \tilde{s}_L}}{m_{\tilde{b}_L} m_{\tilde{s}_L}}\,, \tag{6.5}$$

$m^2_{\tilde{b}_L \tilde{s}_L}$ being the non-diagonal term in the squark mass matrix squared mixing the second and third generation left-chiral squarks. The parameter δ_{23} is a fundamental parameter in our analysis as it determines the strength of the tree-level FCNC interactions induced by the supersymmetric strong interactions, which are then transferred to the loop diagrams of the Higgs boson FCNC decays (6.1).

The result of the scan is depicted in Fig. 6.2. To be specific: Fig. 6.2a shows the maximum value $B^{\max}(h \to q\,q')$ of the FCNC decay rate (6.2) under study as a function of m_{A^0}; Fig. 6.2b displays $B^{\max}(h \to q\,q')$ as a function of the mixing parameter δ_{23} for $m_{A^0} = 200\,\text{GeV}$. Looking at Fig. 6.2 three facts strike the eye immediately : i) the maximum is huge (13%!) for a FCNC rate, actually it is as big as initially guessed from the rough estimates made in Section 6.2; ii) very large values of δ_{23} are allowed; iii) the maximum rate is independent of the pseudo-scalar Higgs boson mass m_{A^0}. We will now analyze facts ii) and iii) in turn, and will establish their incidence on fact i). For further reference, in Table 6.1 we show the numerical values of $B^{\max}(h \to q\,q')$ together with the parameters which maximize the rates for $m_{A^0} = 200\,\text{GeV}$.

One would expect that a large value of δ_{23} should induce a large gluino contribution

Particle	H^0	h^0	A^0
$B(h \to q\,q')$	3.3×10^{-2}	1.3×10^{-1}	3.3×10^{-2}
$\Gamma(h \to X)$	11.0 GeV	1.6×10^{-3} GeV	11.3 GeV
δ_{23}	$10^{-0.09}$	$10^{-0.1}$	$10^{-0.09}$
$m_{\tilde{q}}$	975 GeV	975 GeV	975 GeV
A_b	1500 GeV	730 GeV	1290 GeV
μ	980 GeV	1000 GeV	980 GeV
$B(b \to s\gamma)$	4.42×10^{-4}	4.23×10^{-4}	4.50×10^{-4}

Table 6.1: Maximum values of $B(h \to q\,q')$ and corresponding SUSY parameters for $m_{A^0} = 200\,\text{GeV}$.

Particle	H^0	h^0	A^0
$B(h \to q\,q')$	9.1×10^{-4}	3.1×10^{-3}	9.1×10^{-4}
$\Gamma(h \to X)$	11.2 GeV	1.4×10^{-3} GeV	11.3 GeV
δ_{23}	$10^{-0.43}$	$10^{-0.8}$	$10^{-0.43}$
$m_{\tilde{q}}$	1000 GeV	975 GeV	1000 GeV
A_b	-1500 GeV	-1500 GeV	-1500 GeV
μ	-460 GeV	-1000 GeV	-460 GeV
$B(b \to s\gamma)$	4.49×10^{-4}	4.48×10^{-4}	4.49×10^{-4}

Table 6.2: Maximum values of $B(h \to q\,q')$ and corresponding SUSY parameters for $m_{A^0} = 200\,\text{GeV}$ excluding the *window* region.

to $B(b \to s\gamma)$. In fact it does! However our automatic scanning process picks up the corners of parameter space where the gluino contribution alone is much larger than the SM contribution, but opposite in sign, such that both contributions destroy themselves partially leaving a result in accordance with the experimental constraints. We examine this behaviour in Fig. 6.3, where we show the values of $B(h \to q\,q')$ together with $B(b \to s\gamma)$ as a function of δ_{23} for the parameters which maximize the FCNC rate of the lightest CP-even state h^0 in Table 6.1. We see that, for small values of δ_{23}, the gluino contribution to $B(b \to s\gamma)$ is small, and the total $B(b \to s\gamma)$ prediction is close to the SM expectation. In contrast, as δ_{23} steadily grows, $B(b \to s\gamma)$ decreases fast (meaning a dramatic cancellation between the two contributions) until reaching a point where $B(b \to s\gamma) = 0$. From there on it starts to grow with a large slope, and in its race

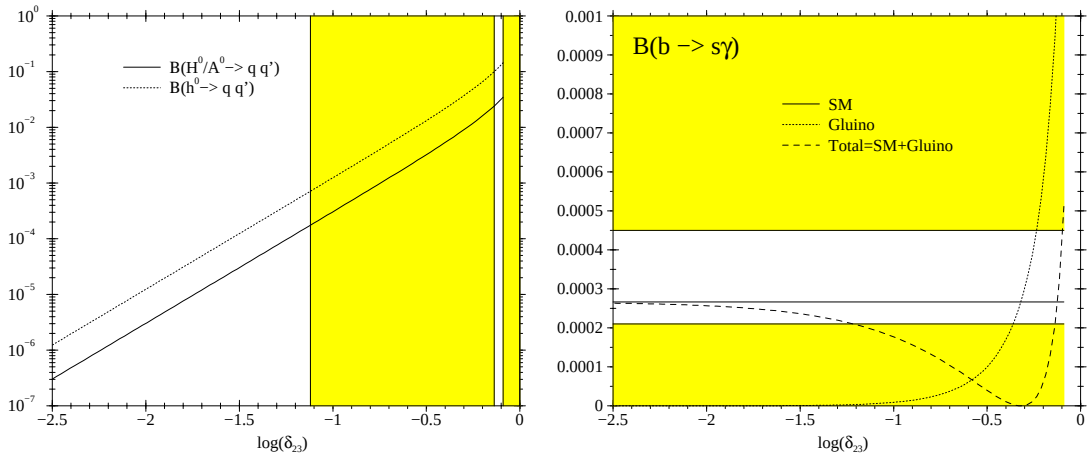

(a) (b)

Figure 6.3: $B(h \to q\,q')$ and $B(b \to s\gamma)$ as a function of δ_{23} for the parameters that maximize $B(h^0 \to q\,q')$ in Table 6.1. The shaded region is excluded experimentally.

eventually crosses the allowed $B(b \to s\gamma)$ region. The crossing is very fast, and so rather ephemeral in the δ_{23} variable, and it leads to the appearance of a narrow allowed *window* at large δ_{23} values, see Fig. 6.3a. We would regard the choice of this window as a fine-tuning of parameters, hence unnatural [3]. For this reason we reexamine the $B(h \to q\,q')$ ratio by performing a new scan of the MSSM parameter space in which we exclude the fine-tuned (or *window*) region. The result for $m_{A^0} = 200\,\text{GeV}$ can be seen in Table 6.2 and Fig. 6.4. This time we see that the maximum values of $B(h \to q\,q')$ are obtained for much lower values of δ_{23}, and the maximum rates have decreased more than one order of magnitude with respect to Table 6.1, reaching the level of few per mil. These FCNC rates can still be regarded as fantastically large. Had we included the SUSY-EW contributions to $B(b \to s\gamma)$, further cancellations might have occurred between the SUSY-EW and the SUSY-QCD amplitudes. Even more: since each contribution depends on a separate set of parameters, one would be able to find a set of parameters in the SUSY-EW sector which creates an amplitude that compensates the SUSY-QCD contributions for almost any point of the SUSY-QCD parameter space. But of course this would be only at the price of performing some fine tuning, which is not the approach we want to follow here.

On the other hand further contributions to $B(b \to s\gamma)$ might exist. In the most general MSSM, flavor-changing interactions for the right-chiral squarks (δ_{23RR}), and mixing left- and right-chiral squarks (δ_{23LR}) can be introduced. The latter can produce significant

[3] At the time of writing this Thesis this fine-tuning is excluded experimentally [102].

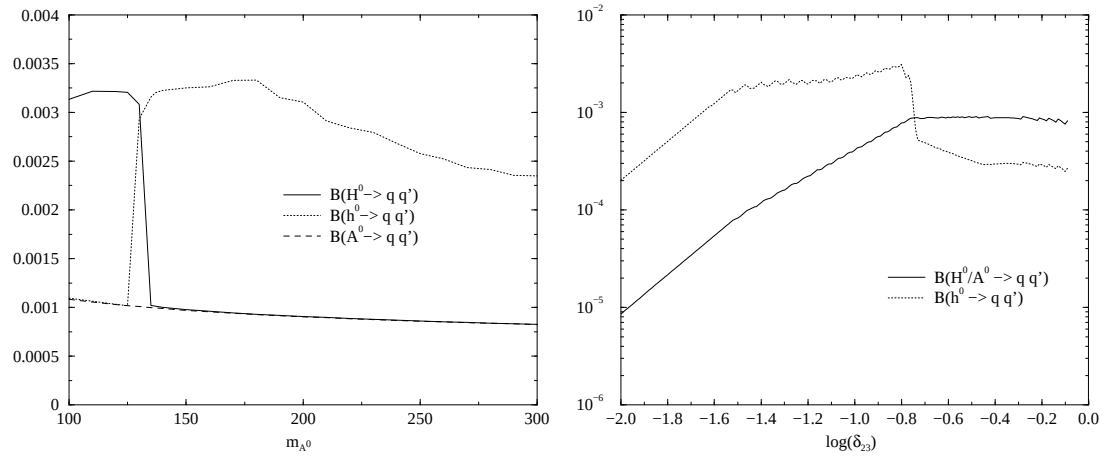

(a) (b)

Figure 6.4: Maximum value of the SUSY-QCD contributions to $B(h \to q\,q')$ as a function of **a)** m_{A^0} and **b)** δ_{23} for $m_{A^0} = 200\,\text{GeV}$, for the scenario excluding the *window* regions.

contributions to $B(b \to s\gamma)$, changing the allowed parameter space. The introduction of δ_{23LR} can produce two possible outcomes: First, in certain regions of the parameter space, the contributions of δ_{23LR} and δ_{23} are of the same sign, enhancing each other. In this situation, the maximum allowed value of δ_{23} is obtained for $\delta_{23LR} = 0$. Second, in other regions of the parameter space the two contributions would compensate each other, producing an overall value of $B(b \to s\gamma)$ in accordance with experimental constraints, even though each contribution would be much larger. Again, we would regard these compensations as unnatural, and would discard that region of the parameter space. In the following we will require that the SUSY-QCD contributions induced by δ_{23} do not compensate the SM ones to give an acceptable value of $B(b \to s\gamma)$; this is equivalent to the condition that the SUSY-QCD amplitude represents a small contribution to the total $B(b \to s\gamma)$ value, and is therefore independent of the inclusion of the other contributions (SUSY-EW, δ_{23LR}).[4]

We turn now our view to the second fact, namely the independence of the maximum rates with respect to m_{A^0}. We will show that it also plays a central role as to the enhancement of $B(h \to q\,q')$. Actually, a good hint is given by the small values of the lightest Higgs boson decay width in Tables 6.1 and 6.2, $\Gamma(h^0 \to X) \sim 2 \times 10^{-3}\,\text{GeV}$. The maximization process of $B(h^0 \to q\,q')$ does not only find the parameters for which

[4]The analysis of Ref. [48] follows the opposite approach, that is: to find the fine-tuning conditions imposed by low energy data that allow for the largest possible value of the FCNC parameters.

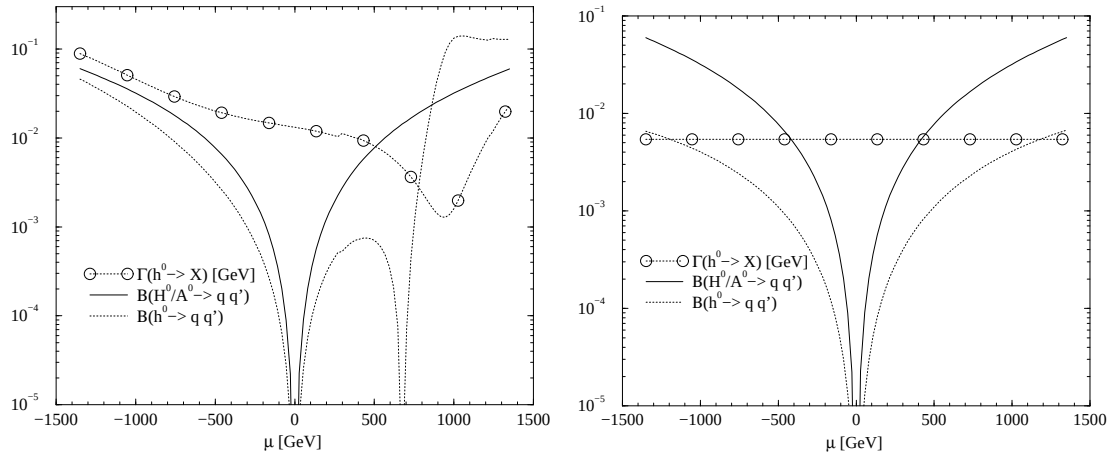

(a) (b)

Figure 6.5: $B(h \to q\,q')$ and $\Gamma(h^0 \to X)$ (in GeV) as a function of μ for **a)** one-loop α angle; **b)** tree-level α angle, and for the parameters that maximize $B(h^0 \to q\,q')$ in Table 6.1. The H^0 and A^0 curves coincide. The $B(b \to s\gamma)$ constraint is not shown.

$\Gamma(h^0 \to q\,q')$ is maximum, but also the parameters for which $\Gamma(h^0 \to X)$ is minimum. Specifically, since $\Gamma(h^0 \to b\bar{b})$ is the dominant decay decay channel of h^0 for large $\tan\beta$, the maximum of $B(h^0 \to q\,q')$ is produced in the parameter range of the so-called *small* α_{eff} *scenario* [157], that is, a parameter range where the radiative corrections make the CP-even Higgs boson mixing angle α vanish (or very small), such that the leading partial decay width $\Gamma(h^0 \to b\bar{b})$ is strongly suppressed. The consequences of this scenario have been extensively studied in Ref. [158]. As advertised in Section 6.2, the possibility that the maximization process explores these regions of the parameter space is the reason why the leading higher order decay channels, and also the leading three-body decay modes have to be taken into account in the computation of the total width.

In Fig. 6.5 we plot the value of the various branching ratios $B(h \to q\,q')$ and of the total width of the lightest CP-even Higgs boson, $\Gamma(h^0 \to X)$, as a function of the higgsino mass parameter μ, the rest of the parameters being those of the third column of Table 6.1, i.e. the ones that maximize the branching ratio $B(h^0 \to q\,q')$. Fig. 6.5a shows that $\Gamma(h^0 \to X)$ has a deep minimum in the range of μ corresponding to the maximum of $B(h^0 \to q\,q')$, which reaches the level of a few percent. If, instead of using the radiatively corrected α value we use the tree-level expression, we obtain the result shown in Fig. 6.5b. Here the total decay width of the Higgs boson is independent of μ, and $B(h \to q\,q')$ does not show any peak. Actually in this case the branching ratio for h^0 becomes smaller than

Particle	H^0	h^0	A^0
$B(h \to q\,q')$	9.0×10^{-4}	1.3×10^{-4}	9.0×10^{-4}
$\Gamma(h \to X)$	11.3 GeV	5.4×10^{-3} GeV	11.3 GeV
δ_{23}	$10^{-0.43}$	$10^{-0.28}$	$10^{-0.43}$
$m_{\tilde{q}}$	1000 GeV	1000 GeV	1000 GeV
A_b	-1500 GeV	-1500 GeV	-1500 GeV
μ	-460 GeV	-310 GeV	-460 GeV
$B(b \to s\gamma)$	4.49×10^{-4}	4.50×10^{-4}	4.49×10^{-4}

Table 6.3: Maximum values of $B(h \to q\,q')$ and corresponding SUSY parameters for $m_{A^0} = 200$ GeV, using the tree-level expressions for the Higgs sector, and excluding the *window* region.

that of H^0 and A^0 for all μ. The maximization procedure in Fig. 6.2 selects for each value of m_{A^0} the MSSM parameters corresponding to the small α_{eff} scenario for that specific value of m_{A^0}. Of course, this discussion regarding the h^0 channels for large values of m_{A^0} has a correspondence with the H^0 channel for low values[5] of m_{A^0}.

As indicated in Section 6.2, we have used a one-loop approximation for the Higgs sector [85, 154–156], instead of the more sophisticated complete two-loop result present in the literature [114, 115]. However, we should stress that the exact MSSM parameters at which the small α_{eff} scenario is realized are not important for the sake of the present analysis. All that matters is that some portion of the parameter space exists, for which $\Gamma(h^0 \to b\bar{b})$ is strongly suppressed, but $\Gamma(h^0 \to q\,q')$ is not.

To compare the maximum value of $B(h^0 \to q\,q')$ obtained with and without the small α_{eff} scenario, we have performed the maximization procedure using the tree-level expressions for the Higgs sector parameters. The result is shown in Table 6.3 and Fig. 6.6. In this case $B(h^0 \to q\,q')$ is reduced by a sizeable factor of $\gtrsim 20$ with respect to Table 6.2, whereby the h^0 rate descends about an order of magnitude below that of the H^0/A^0 channels which remain basically unchanged. Notice also that $\Gamma(h^0 \to X)$ is larger than in previous tables. In spite of the reduction, achieving a FCNC ratio $B(h^0 \to q\,q') \sim 1.3 \times 10^{-4}$ is a remarkable result, three orders of magnitude larger than the maximum SM rate (1.5), and only one order of magnitude below the rare decay $B(h^0 \to \gamma\gamma) \sim 10^{-3}$. Also

[5]Large or low values here means $m_{A^0} > m_{h^0}^{\max}$ or $m_{A^0} < m_{h^0}^{\max}$, i.e. above or below the maximum possible value for the mass of the lightest Higgs boson h^0, respectively.

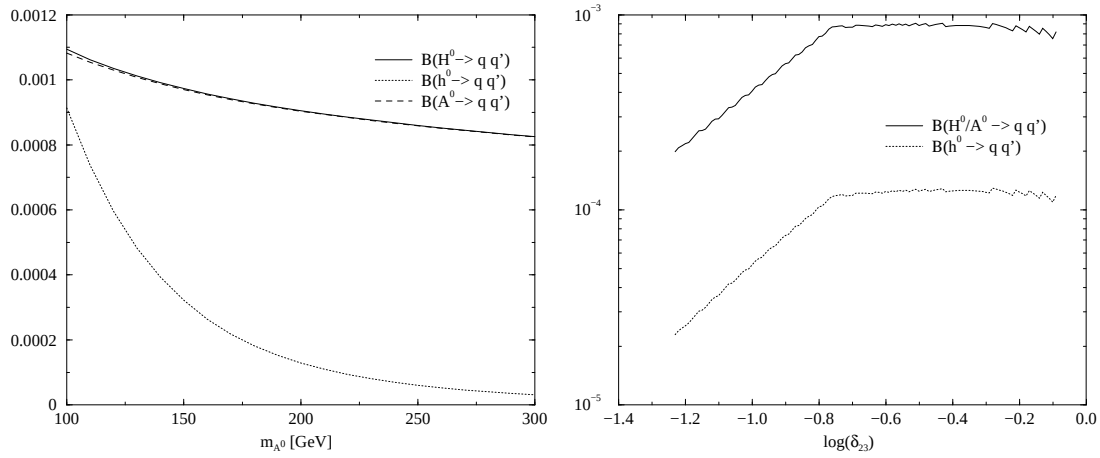

(a) (b)

Figure 6.6: Maximum value of the SUSY-QCD contributions to $B(h \to q\,q')$ as a function of **a)** m_{A^0} and **b)** δ_{23}, for $m_{A^0} = 200\,\text{GeV}$ and for the scenario excluding the *window* region and using the tree-level expressions for the Higgs sector parameters.

worth noticing in Fig. 6.6b (and Fig. 6.4b) is the fact that $B^{\max}(h \to q\,q')$ is essentially flat in δ_{23} in the upper range down to $\delta_{23} \sim 10^{-0.8} \simeq 0.16$. The reason lies in the correlation between $B(h \to q\,q')$ and $B(b \to s\gamma)$. In order to comply with the (non-fine-tuned) value of $B(b \to s\gamma)$ for large δ_{23}, the absolute value of the μ parameter must be small. When δ_{23} decreases, $|\mu|$ can grow to larger values, leaving the overall maximum rates $B^{\max}(h \to q\,q')$ effectively unchanged (see Eq. (6.7) below).

The maximization process selects a squark mass scale in the vicinity of the maximum values used in the scanning procedure. We should point out, however, that the same order of magnitude for $B(h \to q\,q')$ could be obtained with a much lower squark mass scale. In this case the lighter squark masses induce a much larger $B(b \to s\gamma)$ value, and δ_{23} is much more constrained. For example, if we perform a scan in the parameter space (6.3), but fixing the squark mass scale to be $m_{\tilde{q}} < 500\,\text{GeV}$, we obtain the following values for the maximal branching ratios for $m_{A^0} = 200\,\text{GeV}$:

$$B^{\max}(h^0 \to q\,q') = 1.4 \times 10^{-5}\ ,\ B^{\max}(H^0/A^0 \to q\,q') = 9.2 \times 10^{-5}\ , \tag{6.6}$$

with $\delta_{23} \sim 10^{-0.6}$, $\mu \sim -110\,\text{GeV}$, and we have limited ourselves to the scenario avoiding the *window* regions and using the tree-level expression for the Higgs sector parameters. These numbers have to be compared with Table 6.3.

The reason behind this *scale independence* admits an explanation in terms of an ef-

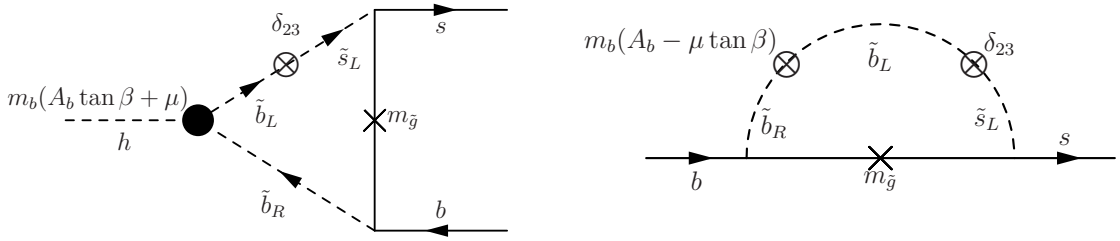

Figure 6.7: One-loop SUSY-QCD vertex diagram contributing to the decay $h \to q\,q'$ and diagrams contributing to mixed $b - s$ self-energy in the mass approximation

fective Lagrangian approach, in which one can estimate the leading effective coupling to behave approximately as 6.7 [48]:

$$g_{hb\bar{s}} \simeq \frac{g m_b}{\sqrt{2} M_W \cos\beta} \frac{2\alpha_s}{3\pi} \delta_{23} \frac{-\mu\, m_{\tilde{g}}}{M^2_{SUSY}} \begin{cases} \sin(\beta-\alpha) & (H^0) \\ \cos(\beta-\alpha) & (h^0) \\ 1 & (A^0) \end{cases} . \tag{6.7}$$

Aside from ensuring (at least) a partial SUSY scale independence of the leading terms, this expression also shows that $B(h \to q\,q')$ has a weak dependence on the soft-SUSY-breaking trilinear coupling A_b. The observed situation is similar to the flavor-conserving $hb\bar{b}$ interactions, where the cancellation of the A_b terms at leading order has been proven [41]. It also shows that the leading non-decoupling SUSY contributions to $\Gamma(h^0 \to q\,q')$ eventually fade out as the decoupling limit of the Higgs sector is approached: $\cos(\beta-\alpha) \to 0$. We have found (using the tree-level expression for α) that the non-leading (SUSY-decoupling) contributions to $\Gamma(h^0 \to q\,q')$ dominate for $m_{A^0} \gtrsim 450\,\text{GeV}$, inducing a value $\Gamma^{\max}(h^0 \to q\,q') \sim 1.2 \times 10^{-5}$, with $\delta_{23} \sim 10^{-1}$, $\mu \sim 1000\,\text{GeV}$.

We further investigate the role of the scale of SUSY masses, and the fine-tuning behaviour in Figs. 6.8 and 6.9. In these figures we give up the equality $m_{\tilde{g}} = m_{\tilde{q}}$ (6.4), the squark masses are fixed at the values stated in Tables 6.2 and 6.1 respectively. Fig. 6.8 shows the values of $B(h \to q\,q')$ for the three Higgs decays and of $B(b \to s\gamma)$ as a function of the gluino mass for the parameters that maximize $B(h^0 \to q\,q')$ when the *window* regions are excluded (third column of Table 6.2). Here we see that, while the gluino contribution to $B(b \to s\gamma)$ decouples *fast* as a function of $m_{\tilde{g}}$, its contribution to $B(h \to q\,q')$ is fairly sustained. Indeed, between $m_{\tilde{g}} = 1\,\text{TeV}$ and $m_{\tilde{g}} = 5\,\text{TeV}$ $B(h^0 \to q\,q')$ decreases only by a factor $\sim 1/4$, while the gluino contribution to $B(b \to s\gamma)$ becomes negligible at $m_{\tilde{g}} = 5\,\text{TeV}$ and we recover the SM prediction. As a consequence, the maximum rates $B(h \to q\,q')$ that we have found are robust, in the sense that further theoretical refine-

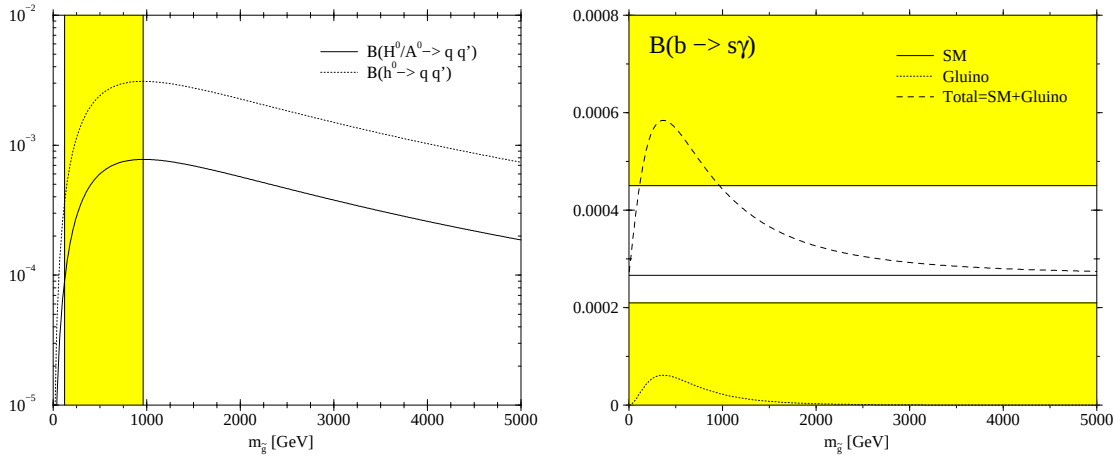

(a) (b)

Figure 6.8: $B(h \to q\,q')$ and $B(b \to s\gamma)$ as a function of $m_{\tilde{g}}$ for the parameters that maximize $B(h^0 \to b\bar{s})$ excluding the window region (see third column of Table 6.2). The shaded region is excluded experimentally.

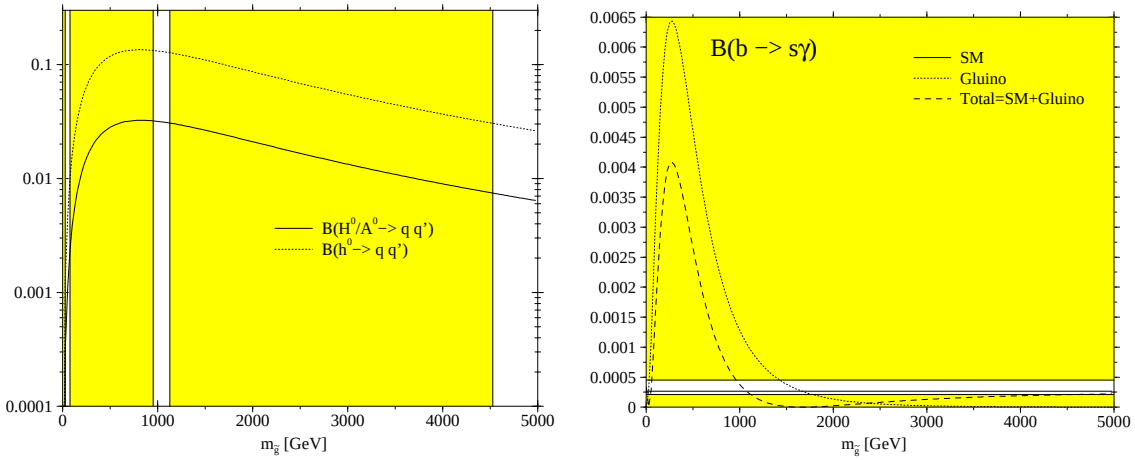

(a) (b)

Figure 6.9: As in Fig. 6.8, but including the window region. The remaining parameters are fixed as in the third column of Table 6.1.

Particle	H^0		h^0		A^0	
	$\Gamma(\,\mathrm{GeV})$	$B(h \to q\,q')$	$\Gamma(\,\mathrm{GeV})$	$B(h \to q\,q')$	$\Gamma(\,\mathrm{GeV})$	$B(h \to q\,q')$
small-α_{eff} *window*	11.0	3.3×10^{-2}	1.6×10^{-3}	1.3×10^{-1}	11.3	3.3×10^{-2}
tree-Higgs *window*	11.3	3.3×10^{-2}	5.4×10^{-3}	4.3×10^{-3}	11.3	3.3×10^{-2}
small-α_{eff} no-*window*	11.2	9.1×10^{-4}	1.4×10^{-3}	3.1×10^{-3}	11.3	9.0×10^{-4}
tree-Higgs no-*window*	11.3	9.1×10^{-4}	5.4×10^{-3}	1.3×10^{-4}	11.3	9.0×10^{-4}
$\tan\beta = 5$	0.11	2.0×10^{-3}	6.0×10^{-3}	1.7×10^{-4}	0.11	2.1×10^{-3}
$\tan\beta = 5$ tree Higgs	0.12	1.9×10^{-3}	4.4×10^{-3}	2.6×10^{-4}	0.11	2.1×10^{-3}
$\tan\beta = 5$ no-*window*	0.15	3.8×10^{-4}	9.7×10^{-3}	1.1×10^{-4}	0.11	5.1×10^{-4}

Table 6.4: Maximum values of $B(h \to q\,q')$ and corresponding $\Gamma(h \to X)$ for the different scenarios studied in this work.

ments and experimental results that change the allowed range of $B(b \to s\gamma)$ can easily be compensated for by a slight increase of the gluino mass ($m_{\tilde{g}}$), which would leave the prediction for $B(h \to q\,q')$ essentially unchanged. We note in Fig. 6.9 the corresponding behaviour of $B(h^0 \to q\,q')$ and $B(b \to s\gamma)$ in the presence of fine-tuning, i.e. as in Table 6.1. In contrast to the previous case, here we observe the presence of two tiny windows in the regions $m_{\tilde{g}} = 25 - 75\,\mathrm{GeV}$ and $m_{\tilde{g}} = 950 - 1125\,\mathrm{GeV}$. In the middle region $m_{\tilde{g}} = 75 - 950\,\mathrm{GeV}$, $B(b \to s\gamma)$ is one order of magnitude larger than the allowed experimental range, and in the region above $m_{\tilde{g}} = 1125\,\mathrm{GeV}$ it only enters the allowed region for $m_{\tilde{g}} > 4500\,\mathrm{GeV}$. In this region $B(h^0 \to q\,q')$ is still large, but at the price of having a gluino five times heavier than the rest of the SUSY spectrum. This is another manifestation of the large fine-tuning that governs this region of the parameter space.

Up to this point we have used the high $\tan\beta$ value quoted in Eq. (6.4). But we have also looked at the impact of varying $\tan\beta$ on $B^{\max}(h \to q\,q')$. Since the latest LEP data restricts $\tan\beta \gtrsim 2.5$, we have used a moderate value of $\tan\beta = 5$. Note that, at low $\tan\beta$, the small α_{eff} scenario does not arise. As a consequence similar results are obtained using either the tree-level or one-loop expressions for the Higgs sector parameters. We

find that the three branching ratios $B^{\max}(h \to q\,q')$ at $\tan\beta = 5$ stay in the same order of magnitude as in the scenarios with $\tan\beta = 50$ (default case) with the tree-level Higgs sector and no-window (Cf. Table 6.2).

6.4 Remarks and conclusions

The main numbers of our analysis are put in a nutshell in Table 6.4, where we show the results presented previously, together with some other scenarios and the low $\tan\beta$ case. The computed maximum values of $B(h \to q\,q')$ must not be taken as exact numbers in practice, but order of magnitude results. The implications that can be derived from Table 6.4 can be synthesized as follows:

1. The SUSY-QCD contributions can enhance the maximum expectation for the FCNC decay rates $B(h \to q\,q')$ enormously. This is seen by comparing the results of Table 6.4 with the maximum value of $B(H^{SM} \to b\bar{s})$ considered in Eq. (1.5). The optimized MSSM branching ratios are at the very least 3 orders of magnitude bigger than the SM result.

2. If no special circumstances apply, that is, if no fine-tuning occurs between the parameters contributing to $B(b \to s\gamma)$ in the MSSM, and if $\Gamma(h^0 \to b\bar{b})$ is not suppressed, the maximum rates are $B^{\max}(h^0 \to q\,q') \simeq 1.3 \times 10^{-4}$, $B^{\max}(H^0/A^0 \to q\,q') \simeq 9 \times 10^{-4}$. This corresponds to the *tree-Higgs/no-window* scenario in Table 6.4.

3. If, however, $\Gamma(h^0 \to b\bar{b})$ is suppressed by the radiative corrections to the CP-even mixing angle α, then $B(h^0 \to q\,q')$ can be an order of magnitude larger: $B^{\max}(h^0 \to q\,q') \sim 3 \times 10^{-3}$. This corresponds to the small α_{eff} scenario, and is indicated by small-α_{eff}/ no-*window* in Table 6.4. The FCNC branching ratio that we find for h^0 in this case should be considered as the largest possible one within the conditions of naturalness (no fine-tuning).

4. On the other hand, if fine-tuning between the gluino and the SM contributions to $B(b \to s\gamma)$ is allowed, but the small-α_{eff} scenario is not realized, then $B^{\max}(h^0 \to q\,q')$ grows one order of magnitude up to $B^{\max}(h^0 \to q\,q') \sim 4 \times 10^{-3}$, whereas $B^{\max}(H^0/A^0 \to q\,q') \sim 3 \times 10^{-2}$. This corresponds to the case labelled *tree-Higgs/window* in Table 6.4.

5. When both special conditions take place simultaneously, viz. fine-tuning in $B(b \to s\gamma)$ (triggered by a very special choice of the δ_{23} parameter in a narrow window

range) and small α_{eff} scenario (independent of assumptions on δ_{23}), we reach an over-optimistic situation where $B^{\max}(h^0 \to q\,q')$ could reach the $\sim 10\%$ level. This is the case referred to as small-α_{eff}/ *window* in Table 6.4.

6. If $\tan\beta$ is low/moderate, then $B^{\max}(h \to q\,q')$ lie in the lower range $\sim 10^{-4}$, which can grow an order or magnitude for $B^{\max}(H^0/A^0 \to q\,q')$ in fine-tuned scenarios (last three rows in Table 6.4).

Although the large FCNC rates mentioned in points 4 and 5 above seem to offer a rather tempting perspective, we will not elaborate on them any further since in our opinion the fine-tuning requirement inherent in them is too contrived. On the other hand, points 2 and 3 offer a moderate, but certainly much more realistic scenario, which in no way frustrates our hopes to potentially detect the FCNC Higgs boson decays (6.1). Indeed, in the case described in point 2, $B(h \to q\,q')$ can be at most of order 10^{-4}. But this is still a fairly respectable FCNC branching ratio (comparable to that of $b \to s\gamma$) and it may lead to a large number of events at a high luminosity collider as seen in chapter 7 for the MSSM and the chapter 4 for the general 2HDM. Moreover, if $\Gamma(h \to X)$ becomes suppressed (e.g. by realizing the small α_{eff} scenario, point 3) then $B(h^0 \to q\,q')$ can be enhanced by an additional order of magnitude.

Our analysis correlates the values of $B(h \to q\,q')$ with that of $B(b \to s\gamma)$, taking into account only the SUSY-QCD contributions due to flavor mixing parameters among the left-chiral squarks. The presence of several other competing contributions to $B(b \to s\gamma)$ alters the borders of the allowed parameter space:

- For the fine-tuned scenarios, the presence and position of the allowed *window* regions in the parameter space depends significantly on all the contributions, and therefore also does the maximum value of $B(h \to q\,q')$. Outside the *window* regions, the computed value of $B(b \to s\gamma)$ can only be made consistent with the experimental range, by means of a large splitting between the squark and gluino masses.

- For the non-fine-tuned scenarios, the inclusion of further contributions to $B(b \to s\gamma)$ also alters the allowed parameter space, but the condition of non-fine-tuning ensures precisely that the change in the allowed range of δ_{23} is smooth, and the corresponding change in $B^{\max}(h \to q\,q')$ is not dramatic.

Of course, the question immediately arises on what will happen if the data from present B-meson factories further constrains the δ_{23} parameter. In that case, we should take into account the (charged-current induced) SUSY-EW contributions to $B(h \to q\,q')$, see [49]). However, we can advance that the SUSY-EW effects on $B^{\max}(h \to q\,q')$ that we find are in

the ballpark of $B^{\max}(h^0 \to q\,q') \sim 3\times10^{-5}$ and $B^{\max}(H^0/A^0 \to q\,q') \sim 1\times10^{-5}$ for a non-fine-tuned scenario, while $B^{\max}(h^0 \to q\,q') \sim 2\times10^{-4}$ and $B^{\max}(H^0/A^0 \to q\,q') \sim 8\times10^{-5}$ for a fine-tuned scenario. From the analysis of the chapter 5 we expect that even with these impoverished MSSM rates the number of FCNC events of that sort should be non-negligible at the LHC.

Even though we have detected the existence of corners of the MSSM parameter space where a Higgs boson FCNC branching ratio can barely reach the 10% level (cf. the narrow windows in Fig. 6.3 and Fig. 6.9), we insist once more that they should be considered rather unlikely as they are associated to fine tuning of the parameters and excluded experimentally [102]. Moreover, in contrast to Ref [47], we find that it is the lightest CP-even state, h^0, the one that could have the largest FCNC branching ratio.

To conclude, we have presented a first realistic estimate of the branching ratios of the Higgs boson FCNC decays (6.1) within the MSSM, assuming that the SUSY-QCD corrections can be as large as permitted by the experimental constraints on $B(b \to s\gamma)$. We have carried out a systematic and self-consistent maximization of the branching ratios (6.2) taking into account this crucial experimental constraint. At the end of the day the results that we obtain, especially for the lightest CP-even Higgs boson of the MSSM, are fairly large: $B^{\max}(h^0 \to q\,q') \sim 10^{-4} - 10^{-3}$. These MSSM rates turn out to be between three to four orders of magnitude larger than the maximum SM rate (1.5), but not five or six orders as naive expectations indicated. Whether this branching ratio is measurable at the LHC [13, 14] or at a high energy e^+e^- Linear Collider [15] can only be established by means of specific experimental analyses. However, on the basis of related studies in the general 2HDM (chapter 5) and from the MSSM (chapter 7), we can foresee that an important number of FCNC events (6.1) can be potentially collected at the LHC. They could play a complementary, if not decisive, role in the identification of low-energy Supersymmetry. In this work we have dealt only with the maximum rates induced by the SUSY-QCD sector of the model.

Chapter 7

Production and FCNC decay of MSSM Higgs bosons into heavy quarks in the LHC

7.1 Introduction

The rareness of the FCNC Higgs boson decay modes, as seen in the previous chapter 6 are an ideal laboratory to look for non-standard interactions superimposed onto the SM ones. Similar considerations apply to the FCNC processes associated to the Hbs vertex, but in this case it is more difficult to pin down the phenomenological signatures. Some work along these lines has already been done, both in the MSSM (see chapter 6 and Refs. [43, 45–50]) and in the general two-Higgs-doublet model (2HDM) (see chapters 4 and 5 and Refs. [51, 64]), and also in other extensions of the SM– see [25] for a review. Up to now, the main effort has been concentrated in computing the FCNC decay modes at one-loop within the new physics, and also in getting a realistic estimate of the maximum branching ratios expected. It is not enough to compute the FCNC branching ratios in, say the MSSM, and then evaluate them in some favorable region of the parameter space, for one has to preserve at the same time the stringent bounds on other observables in which the same physics can be applied, like the aforementioned low-energy $b \to s\gamma$ decay. This kind of correlated study was done very carefully in chapter 6 for the specific Higgs boson FCNC decays into bottom quarks within the MSSM, $h \to b\,s$ ($h = h^0, H^0, A^0$). In this work we extend the latter work by computing also the top quark Higgs boson FCNC decay modes of the heavy MSSM Higgs bosons, $h \to t\,c$ ($h = H^0, A^0$) under the same restrictions (recall that h^0 cannot participate in this decay because $m_{h^0} < m_t$ in the MSSM [11]).

Furthermore, in this work we carry out an additional step absolutely necessary to make contact with experiment, namely we combine the FCNC decay branching ratios of the MSSM Higgs bosons (into both top and bottom quarks) with their MSSM production cross-sections in order to estimate the maximum number of FCNC events expected at LHC energies and luminosities. Only in this way one can assess in a practical way the probability of detecting such processes at the LHC. This computation was done for the general 2HDM in chapter 5, but to the best of our knowledge the corresponding calculation in the MSSM case is not available. In this work we perform this calculation and compare the FCNC results obtained for the MSSM and 2HDM scenarios.

The relevant observable quantity on which we shall focus hereafter is the cross-section for the production of electrically neutral pairs of heavy quarks of different flavors at the LHC, whose origin stems from the FCNC decays of the neutral Higgs bosons of the MSSM, $h = h^0,\, H^0,\, A^0$ [6, 11]. Thus, we aim at the quantity

$$\begin{aligned}\sigma(pp \to h \to q\,q') &\equiv \sigma(pp \to hX) B(h \to q\,q') \equiv \sigma(pp \to hX) \frac{\Gamma(h \to q\,q')}{\Gamma(h \to X)} \\ &\equiv \sigma(pp \to hX) \frac{\Gamma(h \to q\,\bar{q}' + \bar{q}\,q')}{\sum_i \Gamma(h \to X_i)} \quad (qq' \equiv bs \text{ or } tc)\,. \end{aligned} \tag{7.1}$$

Here $\Gamma(h \to X)$ is the – consistently computed – total width in each case. In order to asses the possibility to measure these processes at the LHC, we have performed a scan of the MSSM parameter space to find the maximum possible value of the production rates (7.1) under study. The computation of the combined production rate is necessary, since the correlations among the different factors are important. For example, in chapter 6 it was shown that the maximum branching ratio for the lightest MSSM Higgs boson, $B(h^0 \to b\bar{s})$, is obtained in the regions of the parameter space where the coupling $h^0\,b\,\bar{b}$ is strongly suppressed by quantum effects. On the other hand, the associated production $\sigma(pp \to h^0 b\bar{b})$ is one of the leading processes for the production of the lightest MSSM Higgs boson. It is clear then that, in the regions where $B(h^0 \to b\bar{s})$ is largest, $\sigma(pp \to h^0 b\bar{b})$ will be suppressed. Therefore, the maximum FCNC production rate at the LHC can only be obtained by the combined analysis of the two relevant factors in (7.1) (viz. the branching ratio and the Higgs boson production cross-section). We will see that the effects from each factor are different in different regions of the parameter space. Moreover, the realistic production FCNC rates (7.1) in the MSSM parameter space can be obtained only by including the restrictions imposed by the simultaneous analysis of the branching ratio of the low-energy process $b \to s\,\gamma$, whose range of values is severely limited by experiment [52–58]. As in chapter 6, in this work we limit ourselves to supersymmetric FCNC interactions mediated by the strongly interacting sector of the MSSM, i.e. the SUSY-QCD

flavor-violating interactions induced by the gluinos. The corresponding analysis for the electroweak supersymmetric FCNC effects requires a lengthy separate presentation, and will be reported elsewhere [159].

The work is organized as follows. In Section 7.2 we describe the general setting for our numerical analysis. In Section 7.3 we present the LHC production rates of Higgs boson decaying into bottom quarks through supersymmetric FCNC interactions. In Section 7.4 we present the corresponding FCNC rates for the top quark channel. Finally, in Section 7.5 we compare the MSSM results with the 2HDM results, and deliver our conclusions.

7.2 General setting for the numerical analysis

We have performed the calculations with the help of the numeric programs `HIGLU`, `PPHTT` [136, 139,151,160] and LoopTools [129,161,162]. The calculation must obviously be finite without renormalization, and indeed the cancellation of UV divergences using either dimensional regularization or dimensional reduction – the two methods giving the same results here – in the total amplitudes was verified explicitly. In the following we will detail the approximations used in our computation:

- We include the full one-loop SUSY-QCD contributions to the FCNC partial decay widths $\Gamma(h \to q\,q')$ in the observable (7.1).

- We assume that FCNC mixing terms appear only in the LH-chiral sector of the 6×6 squark mixing matrix. Therefore, this matrix has only non-diagonal blocks in the LH-LH sector. This is the most natural assumption from the theoretical point of view [93], and, moreover, it was proven in Ref. [43] that the presence of FCNC terms in the RH-chiral sector would enhance the partial widths by a factor two at most – not an order of magnitude.

- The Higgs sector parameters (masses and CP-even mixing angle α) have been treated using the leading m_t and $m_b \tan\beta$ approximation to the one-loop result [85, 154–156]. For comparison, we also perform the analysis using the tree-level approximation.

- The Higgs bosons total decay widths $\Gamma(h \to X)$ are computed at leading order, including all the relevant channels: $\Gamma(h \to f\bar{f}, ZZ, W^+W^-, gg)$. The off-shell decays $\Gamma(h \to ZZ^*, W^\pm W^{\mp *})$ have also been included. This is necessary to consistently compute the total decay width of $\Gamma(h^0 \to X)$ in regions of the parameter space where the maximization of the cross-section (7.1) is obtained at the expense of

greatly diminishing the partial decay widths of the two-body process $h^0 \to b\bar{b}$ (due to dramatic quantum effects that may reduce the CP-even mixing angle α to small values [157]). The one-loop decay rate $\Gamma(h \to gg)$ has been taken from [151] and the off-shell decay partial widths have been recomputed explicitly and found perfect agreement with the old literature on the subject [152].

- The MSSM Higgs boson production cross-sections at the LHC have been computed using the programs `HIGLU 2.101` and `PPHTT 1.1` [136, 139, 151, 160]. These programs include the following channels: gluon-gluon fusion $\sigma(pp(gg) \to h)$, associated production with top-quarks $\sigma(pp \to ht\bar{t})$ and associated production with bottom-quarks $\sigma(pp \to hb\bar{b})$. In order to have a consistent description, we have used the leading order approximation for all channels. The corresponding Feynamn diagrams are depicted in 5.2. The QCD renormalization scale is set to the default values for each program, namely $\mu_0 = m_h$ for `HIGLU` and $\mu_0 = (m_h + 2M_Q)/2$ for `PPHTT`. We have used the set of CTEQ4L Parton Distribution Functions [163].

Running quark masses ($m_q(Q)$) and strong coupling constants ($\alpha_s(Q)$) are used throughout, with the renormalization scale set to the decaying Higgs boson mass in the decay processes. More details are given below, as necessary.

Using this setup, we have performed a maximization of the FCNC cross-section, Eq. (7.1), in the MSSM parameter space with the following restrictions on the parameters:

qq'	bs	tc
δ_{23}	$< 10^{-0.09} \simeq 0.81$	
$\tan\beta$	50	5
A_t	$-300\,\text{GeV}$	$\lvert A_t\rvert \leq 3M_{\text{SUSY}}$
A_b	$\lvert A_b\rvert \leq 3M_{\text{SUSY}}$	$300\,\text{GeV}$
μ	$(-1000 \cdots 1000)\,\text{GeV}$	
$m_{\tilde{q}_i}$	$m_{\tilde{d}_\text{L}} = m_{\tilde{d}_\text{R}} = m_{\tilde{u}_\text{R}} = m_{\tilde{g}} \equiv M_{\text{SUSY}}$	
M_{SUSY}	$(150 \cdots 1000)\,\text{GeV}$	
m_{A^0}	$(100 \cdots 1000)\,\text{GeV}$	
$M_{\tilde{q}_i}$	$2\,M_{\tilde{q}_i} > m_{H^0} + 50\,\text{GeV}$	
	$M_{\tilde{q}_i} + M_{\tilde{q}_j} > m_{A^0} + 50\,\text{GeV}$ $(i \neq j)$	

(7.2)

Here $m_{\tilde{q}_i}$ are the LH-chiral and RH-chiral squark soft-SUSY-breaking mass parameters, $m_{\tilde{q}_{L,R}}$, common for the three generations; $M_{\tilde{q}_i}$ are the physical masses of the squarks, and

m_h is the mass of the decaying Higgs boson $h = h^0, H^0, A^0$. These masses are fixed at the tree-level by the values of $(\tan\beta, m_{A^0})$ and the SM gauge boson masses and couplings [6]. Due to the structure of the Yukawa couplings in the MSSM, the value of $\tan\beta$ is fixed at a high (small) value for the bottom (top) quark channel as indicated. The parameter m_{A^0} (the mass of the CP-odd Higgs boson) is assumed to vary in the range indicated in (7.2). At one loop these masses receive corrections from the various SUSY fields, and therefore depend on the values of the remaining parameters in Eq. (7.2). The characteristic SUSY mass scale $M_{\rm SUSY}$ defines the typical mass of the squark and gluino masses [1]. The rest of the parameters of the squark sector are determined by this setup. For instance, by $SU(2)$ gauge invariance we have $m_{\tilde{u}_{\rm L}} = m_{\tilde{d}_{\rm L}}$. Following the same notation as in [43], the parameter δ_{23} represents the mixing between the second and third generation of LH-chiral squarks. Let us recall its definition:

$$\delta_{23} \equiv \frac{m^2_{\tilde{b}_L \tilde{s}_L}}{m_{\tilde{b}_L} m_{\tilde{s}_L}}\,, \tag{7.3}$$

$m^2_{\tilde{b}_L \tilde{s}_L}$ being the non-diagonal term in the squark mass matrix squared mixing the second and third generation of LH-chiral squarks – and an equivalent definition for the up-type quarks.[2] The parameter δ_{23} is a fundamental quantity in our analysis as it determines the strength of the tree-level FCNC interactions induced by the supersymmetric strong interactions, which are then transferred to the loop diagrams of the Higgs boson FCNC decays in Eq. (7.1). The last two restrictions in Eq. (7.2) ensure that the (heavy) Higgs boson decay channels into a pair of squarks are kinematically forbidden. We have checked explicitly for some of the heavy Higgs boson channels (h^0 can never do it in practice) that we obtain the same results if we remove these conditions and include the partial widths $\Gamma(h \to \tilde{q}\tilde{q}^*)$ in the denominator of (7.1). Strictly speaking this condition could be implemented, in the case of the H^0 boson, by just requiring $m_{H^0} < 2\, M_{\tilde{q}_i}$, but we have made it stronger by including an additive term. This term is arbitrary (provided it is not very small) and acts as a buffer, namely it impedes that by an appropriate choice of the squark masses we can approach arbitrarily close the threshold from above, and therefore avoids artificial enhancement effects in our loop calculations (see below). Similarly, for the CP-odd Higgs boson, the condition expressed in (7.2) ensures that we avoid a similar kind of enhancement. In this case, however, the condition is a bit different because the $A^0\, \tilde{q}\tilde{q}^*$

[1] Our programs are able to deal with completely arbitrary masses for each squark, but we are forced to make some simplifications in order to provide a reasonable analysis within a manageable total CPU time, see below.

[2] Recall that the δ_{ij} parameters in the up-sector are related to the corresponding parameters in the down-sector by the Cabibbo-Kobayashi-Maskawa matrix, see e.g. [95, 96].

vertex can only exist with squarks of different chirality types ($A^0\,\tilde{q_L}\tilde{q_R}^*$) or, equivalently, with different mass eigenstates ($A^0\,\tilde{q_i}\tilde{q_j}^*$). We have used fixed values for the soft-SUSY-breaking trilinear couplings A_t and A_b for the bs and tc channels respectively. Our results are essentially independent of these values and their signs.

The task of scanning the MSSM parameter space in order to maximize $\sigma(pp \to h \to q\,q')$ for the various Higgs bosons is quite demanding and highly CPU-time consuming, even under the conditions imposed in Eq. (7.2). As stated in the introduction, our code includes also the restrictions on the MSSM parameter space due to the experimental constraint on $B(b \to s\gamma)$, and therefore contains the full one-loop SUSY-QCD amplitude for $b \to s\gamma$ constructed from the FCNC interactions induced by the gluinos. The scan was carried out with the help of two entirely different methods. In the first method we used a systematic procedure based on dividing the parameter subspace (7.2) into a lattice which we filled with points distributed in a completely homogeneous way. The second is a Monte-Carlo based method, first proposed in [164]. We have adapted the well-known Vegas integration program [165] to generate a sufficient number of "interesting" points in our parameter subspace. The total number of points used in this case was far smaller than in the first method. Obviously the lattice procedure gives more accurate results by increasing arbitrarily the total number of points, but the CPU time becomes prohibitively long for the whole analysis. This is so even after factoring out in a suitable way the phase-space integrals of the Higgs boson production processes, so that these integrals are computed only once for every fixed Higgs boson mass and for all the MSSM points of our scan in the parameter subspace (7.2). The second method is comparatively much faster, but it still involves a quite respectable amount of CPU time for the whole analysis. We found that the partial results obtained by the two methods are compatible at the level of $10-20\%$. For the study of our FCNC processes we consider that this level of accuracy should be acceptable, and for this reason all of the plots that we present in this work have been finally computed with the Vegas-based procedure. This also explains the wiggling appearance observed in the profiles of the curves presented in Sections 3-4. For any given abscissa point in each one of these curves, the corresponding value on the vertical (ordinate) axis is somewhere within a band whose width lies around $10-20\%$ of the central value.

A few words on the effects of the $B(b \to s\gamma)$ constraint in our analysis are now in order. The SUSY-QCD contribution to $B(b \to s\gamma)$ can be quite large, in fact as large as the SM one, and with any sign. This raises the possibility of "fine-tuning" between the two type of contributions in certain (narrow) regions of the parameter space. As a consequence we could highly optimize our FCNC rates in these regions without being in conflict with the

experimentally measured $B(b \to s\gamma)$ band. We have checked that in these regions the number of FCNC events can be artificially augmented by one or two orders of magnitude. Our scanning procedure indeed finds automatically these fine-tuning domains. However, we have systematically avoided them in the presentation of our analysis (for more details see chapter 6). In all of our plots, therefore, we show the results obtained for the non-fine-tuned case only. We adopt $B(b \to s\gamma) = (2.1 - 4.5) \times 10^{-4}$ as the experimentally allowed range within three standard deviations [19].

7.3 Analysis of the bottom-strange channel

The main result of the numerical scan for the bottom channel is shown in Fig. 7.1. To be specific: Fig. 7.1a shows the maximum values of the production cross-sections $\sigma(pp \to h \to q\,q')$ for the three MSSM Higgs bosons $h = h^0, H^0, A^0$ at the LHC, as a function of m_{A^0}; Fig. 7.1b displays the cross-section as a function of $\tan\beta$. In this plot we indicate the value of $\sigma(pp \to h \to q\,q')$ (in pb) in the left-vertical axis, and at the same time we track number of FCNC events (per $100\,\text{fb}^{-1}$ of integrated luminosity) on the right vertical axis. Looking at Fig. 7.1 one can see immediately that at large $\tan\beta$: i) the maximum number of events is remarkably high (10^6 events!) for a FCNC process; ii) there is a sustained region in the h^0 channel, comprising the interval $300\,\text{GeV} \lesssim m_{A^0} \lesssim 900\,\text{GeV}$, with a flat value of 5×10^3 events; iii) the chosen value of $\tan\beta = 50$ is not critical for H^0 and A^0 as long it is larger than 10. In Fig. 7.1b we see that the dependence on $\tan\beta$ is essentially the same for H^0 and A^0, but for h^0 it is quite different: in the region $10 \lesssim \tan\beta \lesssim 30$ the cross-section remains below $10^{-2}\,\text{pb}$, but for $\tan\beta > 30$ it starts climbing fast up to $0.3\,\text{pb}$ at $\tan\beta = 50$. The number of events here reaches a few times 10^4 for all channels (for fixed $m_{A^0} = 200\,\text{GeV}$) [3]. For further reference, in Table 7.1 we show the numerical values of $\sigma(pp \to h \to q\,q')$ together with the parameters which maximize the production for $\tan\beta = 50$ and $m_{A^0} = 200\,\text{GeV}$. We include the value of $B(h \to bs)$ at the maximization point of the FCNC cross-section. We notice that at this point the lightest Higgs boson h^0 is the one having the smallest branching ratio. This is in contrast to the situation when one maximizes the branching ratios independently of the number of events as in chapter 6.

In Fig. 7.2a we show the effect on $\sigma(pp \to h^0 \to b\,s)$, and on the total decay width $\Gamma(h^0 \to X)$, of using the Higgs boson sector at the tree-level or at one-loop in our computation. It is well-known that the h^0 couplings to quarks are particularly sensitive to this issue, and for this reason we focus on the lightest CP-even Higgs boson for these

[3] As already advertised, in reading the plots and tables in this work, one must keep in mind that they are the result of a Monte-Carlo sampling near the region of the maximal values.

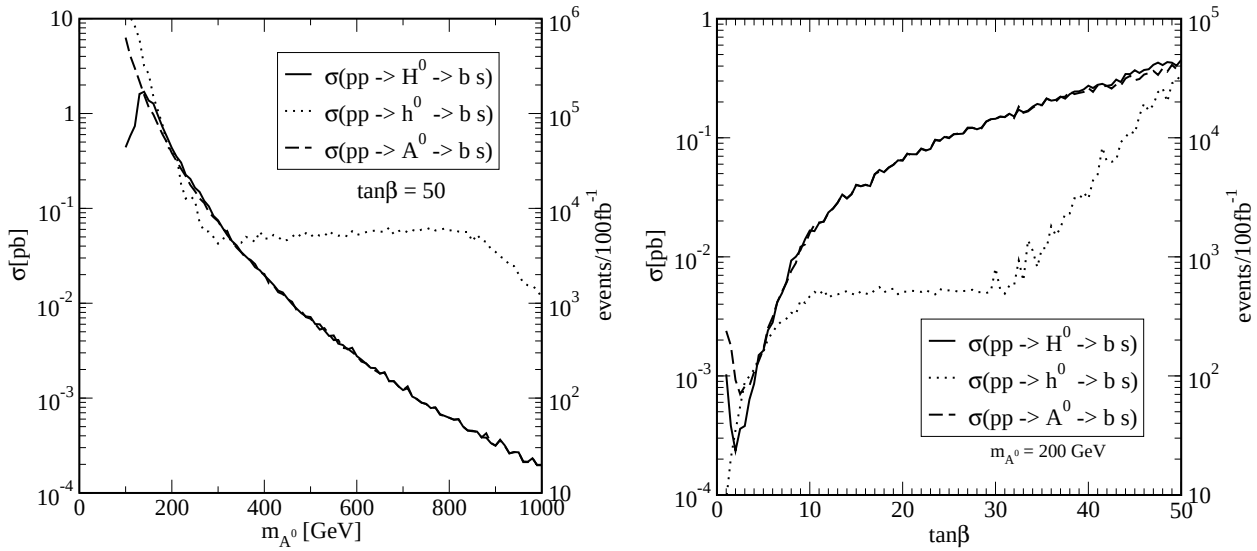

(a) (b)

Figure 7.1: Maximum SUSY-QCD contributions to $\sigma(pp \to h \to b\,s)$, Eq. (7.1), as a function of **(a)** m_{A^0} (at fixed $\tan\beta$) and **(b)** $\tan\beta$ (at fixed m_{A^0}). In each plot the left-vertical axis provides the cross-section in pb and the right-vertical axis tracks the number of events per $100\,\mathrm{fb}^{-1}$ of integrated luminosity.

considerations. We can appreciate the correlations among the different factors that enter the production rate (7.1). The plotted values for $\sigma(pp \to h^0 \to b\,s)$ and $\Gamma(h^0 \to X)$ in Fig. 7.2a correspond precisely to the parameters that maximize (7.1) at the tree-level or at one loop in each case. Fig. 7.2b shows a comparison of the various h^0-production mechanisms for the values that maximize $\sigma(pp \to h^0 \to b\,s)$ at one-loop. Remarkably, the effect of the radiative corrections in the Higgs sector amounts to an enhancement of our maximal FCNC rates of up to three orders of magnitude. As we mentioned in chapter 6 the maximum of $B(h^0 \to b\bar{s})$ is attained under the conditions of the so-called "small α_{eff} scenario" [157, 158], where the two-body decay $h^0 \to b\bar{b}$ is strongly suppressed due to a corresponding suppression of the $h^0\,b\,\bar{b}$ coupling. Since $\Gamma(h^0 \to b\bar{b})$ usually dominates the total width $\Gamma(h^0 \to X)$, the latter also diminishes drastically (at the level of the partial width of a h^0 three-body decay, as mentioned above). In this scenario the production cross-section $\sigma(pp \to h^0 b\bar{b})$ is also suppressed, so the final result is a compromise between the suppression of $\Gamma(h^0 \to b\bar{b})$ and the possible enhancement (or at least sustenance) of $\sigma(pp \to h^0\,X)$ by other mechanisms other than the associated production with bottom quarks (like the mechanism of gluon-gluon fusion, see Fig. 7.2b).

h	H^0	h^0	A^0
$\sigma(pp \to h \to q\,q')$	0.45 pb	0.34 pb	0.37 pb
events/100 fb^{-1}	4.5×10^4	3.4×10^4	3.7×10^4
$B(h \to bs)$	9.3×10^{-4}	2.1×10^{-4}	8.9×10^{-4}
$\Gamma(h \to X)$	10.9 GeV	1.00 GeV	11.3 GeV
δ_{23}	$10^{-0.62}$	$10^{-1.32}$	$10^{-0.44}$
$m_{\tilde{q}}$	990 GeV	670 GeV	990 GeV
A_b	−2750 GeV	−1960 GeV	−2860 GeV
μ	−720 GeV	−990 GeV	−460 GeV
$B(b \to s\gamma)$	4.50×10^{-4}	4.47×10^{-4}	4.39×10^{-4}

Table 7.1: Maximum value of $\sigma(pp \to h \to q\,q')$ (and of the number of bs events per $100\,fb^{-1}$) in the LHC, for $m_{A^0} = 200\,\text{GeV}$ and $\tan\beta = 50$. Shown are also the corresponding values of the relevant branching ratio $B(h \to bs)$ and of the total width of the Higgs bosons, together with the values of the SUSY parameters. The last row includes $B(b \to s\gamma)$.

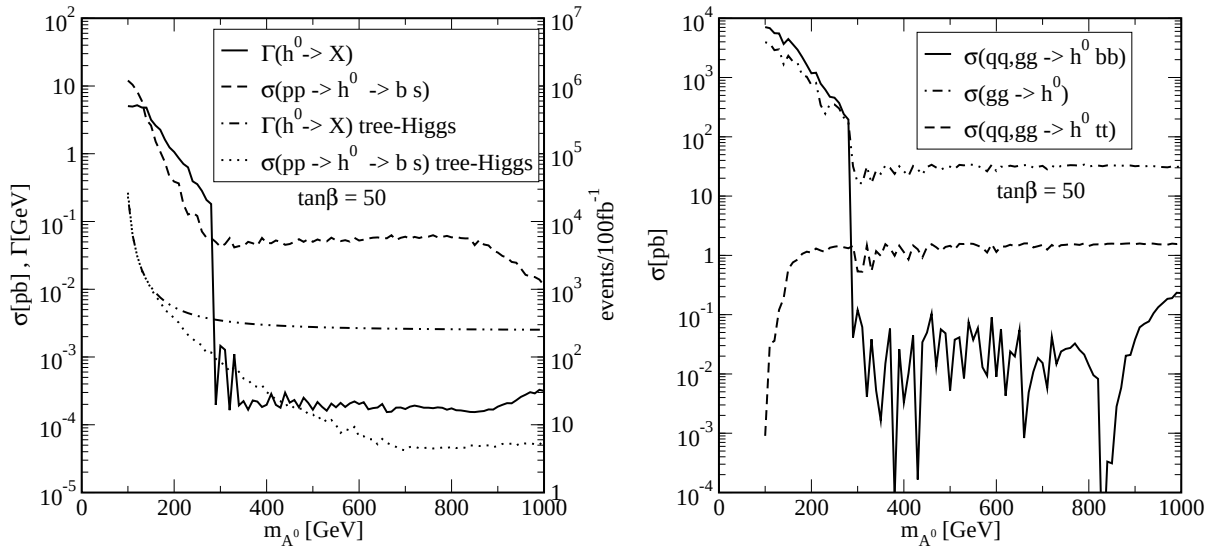

(a) (b)

Figure 7.2: **(a)** h^0 production cross-section and decay width as a function of m_{A^0} with the Higgs mass relations at tree-level and at one-loop. **(b)** Different contributions to the h^0 production cross-section as a function of m_{A^0} corresponding to the maximization of $\sigma(pp \to h^0 \to b\,s)$ using the one-loop Higgs mass relations.

Indeed, for $m_{A^0} \lesssim 300\,\text{GeV}$ we can check in Fig. 7.2b that the most relevant factor for maximizing the FCNC cross-section is the enhancement of the h^0 production channel in association with bottom quarks, $\sigma(pp \to h^0 b\bar{b})$. This channel operates through the $b\bar{b}$-fusion vertex $b\bar{b} \to h^0$ and is highly enhanced at large $\tan\beta$. In the region $m_{A^0} \lesssim 300\,\text{GeV}$ stays as the dominant mechanism for h^0 production, although one can see that the alternate gg-fusion mechanism remains all the way non-negligible. The corresponding effect on our FCNC cross-section (7.1) is nevertheless not obvious because this same parameter choice does also maximize the total width of h^0, mainly through the enhancement of $\Gamma(h^0 \to b\,\bar{b})$. There is a delicate interplay of various factors here. In particular, in the region $m_{A^0} < 300\,\text{GeV}$ the maximized partial width of the FCNC process $h^0 \to bs$ (which is a function of all the parameters in (7.2)) is larger than in the region $m_{A^0} > 300\,\text{GeV}$, but at the same time the total width becomes smaller in the latter region. Overall, the result is that $\sigma(pp \to h^0 \to b\,s)$ is larger in the former m_{A^0} range than in the latter. Furthermore, when we cross ahead the limit $m_{A^0} \simeq 300\,\text{GeV}$ the dominant h^0-production channel changes turn: the associated h^0-production with bottom quarks falls abruptly down (see explanations below) and the gluon-gluon fusion mechanism takes over, so that in this range the h^0-production cross-section becomes completely dominated by $gg \to h^0$. We note that while this mechanism is not so efficient at its maximum as the associated production, it has a virtue: it is non-suppressed in the entire range of m_{A^0}. As a result, in the region above $m_{A^0} \gtrsim 300\,\text{GeV}$ a small value of the $h^0\,b\,\bar{b}$ coupling enhances $B(h^0 \to bs)$ while it does not dramatically suppress the total cross-section $\sigma(pp \to hX)$. For $m_{A^0} > 300\,\text{GeV}$ our sampling procedure finds the maximum by selecting the points in parameter space corresponding to the small α_{eff} scenario, where $B(h^0 \to bs)$ takes the highest values and $\Gamma(h^0 \to X)$ and $\sigma(pp \to h^0 b\bar{b})$ are strongly suppressed – the latter staying below the associated Higgs boson production with top quarks! In this way the net Higgs boson cross-section $\sigma(pp \to h^0)$ is not drastically reduced thanks to the sustenance provided by the gg-fusion channel. Most of the loop contributions to it come from the top quark because the bottom quark contribution is suppressed and the squarks are rather heavy. One can clearly see this sustenance feature in Fig. 7.2 in the form of a long cross-section plateau up to around $m_{A^0} = 1\,\text{TeV}$, beyond which the small α_{eff} scenario cannot be maintained and $\Gamma(h^0 \to X)$ starts increasing and at the same time $\sigma(pp \to h^0 \to b\,s)$ starts decreasing. It is remarkable that this behavior is only feasible thanks to the large radiative corrections in the MSSM Higgs sector. When we, instead, perform the computation using the tree-level relations for the Higgs sector, the small α_{eff} scenario is obviously not possible and the enhancements/suppressions of $\sigma(pp \to h^0 b\bar{b})/\Gamma(h^0 \to X)$ cannot take place. As a result the FCNC rate is some 3 orders of magnitude smaller than in the

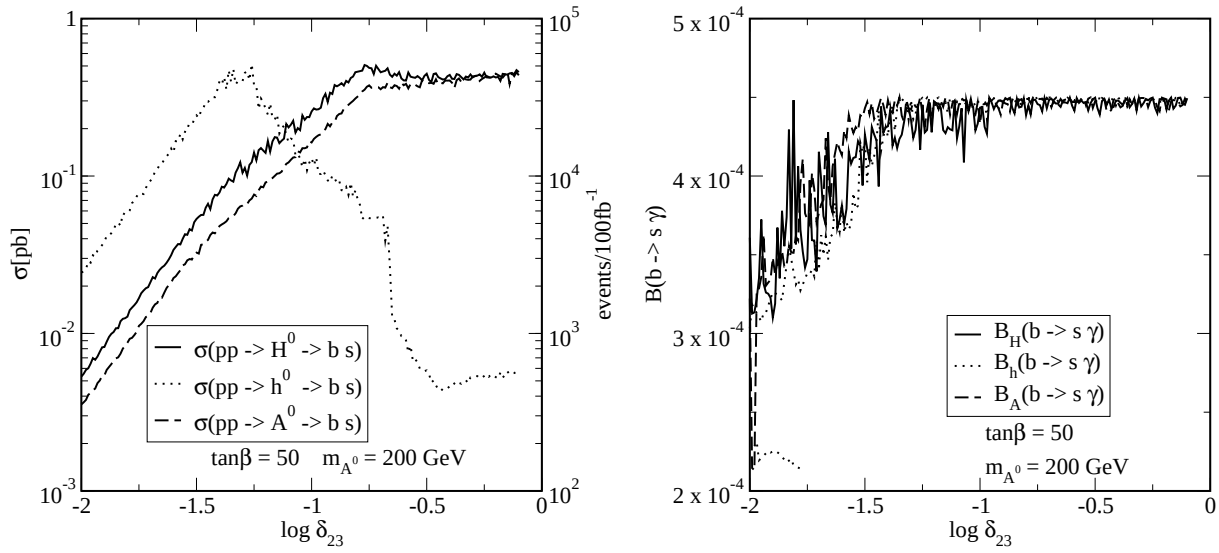

(a) (b)

Figure 7.3: Maximum SUSY-QCD contributions to $\sigma(pp \to h \to b\,s)$, Eq. (7.1), as a function of **(a)** δ_{23} and **(b)** value of $b \to s\gamma$.

previous case.

Next, we turn our attention to the FCNC mixing parameter δ_{23} in Eq. (6.5). The value of δ_{23} at the cross-section maximum is not necessarily the maximum allowed value of δ_{23} in (7.2). This is because it is a conditioned maximum, namely a maximum obtained under the restrictions imposed by $b \to s\gamma$, as illustrated in Fig. 7.3. For further reference in our discussion, and to better grasp some qualitative features of our results, let us write the general form of the SUSY-QCD contribution to $b \to s\gamma$. If we emphasize only the relevant supersymmetric terms under consideration (obviating the powers of the gauge couplings and other factors) we have

$$B(b \to s\gamma) \sim \delta_{23}^2\, m_b^2 (A_t - \mu \tan\beta)^2 / M_{\rm SUSY}^4 \,. \tag{7.4}$$

Fig. 7.3a shows the maximum of $\sigma(pp \to h \to q\,q')$ as a function of δ_{23} for a fixed value of the CP-odd Higgs boson mass $m_{A^0} = 200\,\text{GeV}$, whereas Fig. 7.3b shows the computed value of $B(b \to s\gamma)$ corresponding to the parameter space points where each maximum is attained. At small δ_{23} the SUSY-QCD contribution to $B(b \to s\gamma)$ is negligible, and the experimental restriction $B(b \to s\gamma) = (2.1 - 4.5) \times 10^{-4}$ does not place constraints on the other MSSM parameters (7.2); in other words, in this region the dependence is $\sigma(pp \to h \to q\,q') \propto (\delta_{23})^2$ – the naively expected one. Here $\delta_{23} \lesssim 10^{-1.5} \simeq 0.03$ and

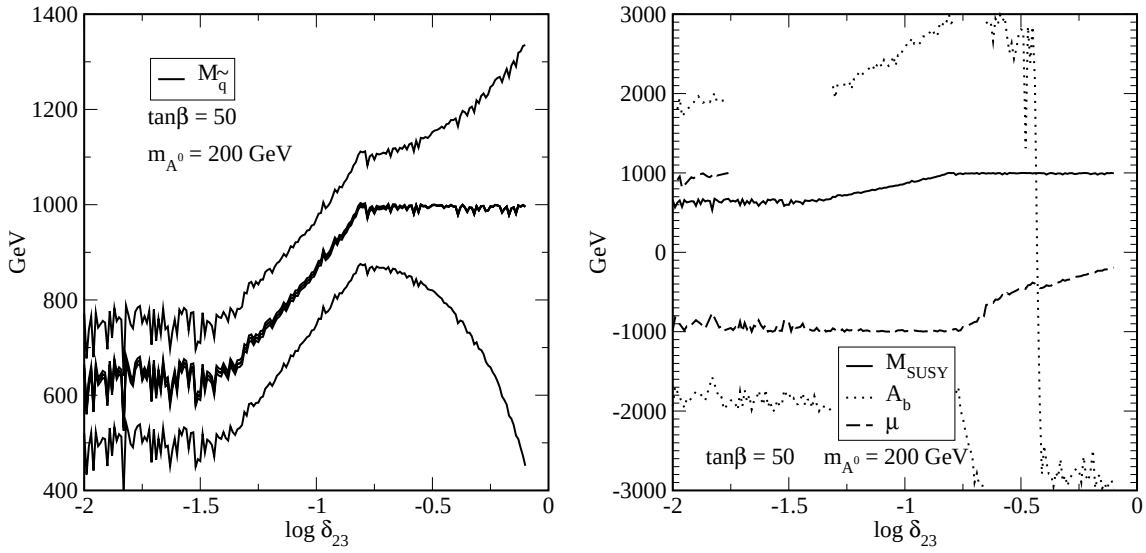

(a) (b)

Figure 7.4: Value of **(a)** down-type squark physical masses ($M_{\tilde{q}}$), four of them are degenerate; **(b)** the parameters (7.2) from the maximization of the h^0 channel in Fig. 7.3a.

the computed $B(b \to s\gamma)$ value lies well within the experimental limit. For larger δ_{23}, $B(b \to s\gamma)$ can be saturated at its uppermost experimentally allowed limit, and the rest of the parameters in (7.2) must change accordingly in order not to cross that limit. This can be appreciated in Fig. 7.4 where we show the range of values taken by the physical down-type squark masses[4] (Fig. 7.4a) and the lagrangian parameters (Fig. 7.4b) from Eq. (7.2) that provide the maximum values of $\sigma(pp \to h^0 \to b\,s)$ in Fig. 7.3. In the small δ_{23} region ($\delta_{23} \lesssim 10^{-1.5} \simeq 0.03$) the parameters and masses that maximize $\sigma(pp \to h \to q\,q')$ are constant – except for the statistical noise unavoidable in a Monte-Carlo procedure. Note also that there are two possible values for the parameters μ and A_b, due to the fact that (the leading contribution of) $\sigma(pp \to h \to q\,q')$ is independent of the sign of these parameters and the Monte-Carlo procedure picks either sign for each point with equal probability. At $\delta_{23} \simeq 10^{-1.5}$ the value of $B(b \to s\gamma)$ becomes saturated and $\sigma(pp \to h^0 \to b\,s)$ reaches its maximum (cf. Fig. 7.3b); however δ_{23} can keep growing, yet without overshooting the $B(b \to s\gamma)$ limits, because the increasing value of δ_{23} is compensated by the growing squark masses (cf. Fig. 7.4a). But this is not all that simple,

[4]There are six different down-type squarks, but four of them are nearly degenerate in mass in our approximation. For the bs-channel, the down squarks are so heavy that the conditions required in the last two rows of (7.2) are automatically satisfied by them in practically all the allowed range for m_{A^0}.

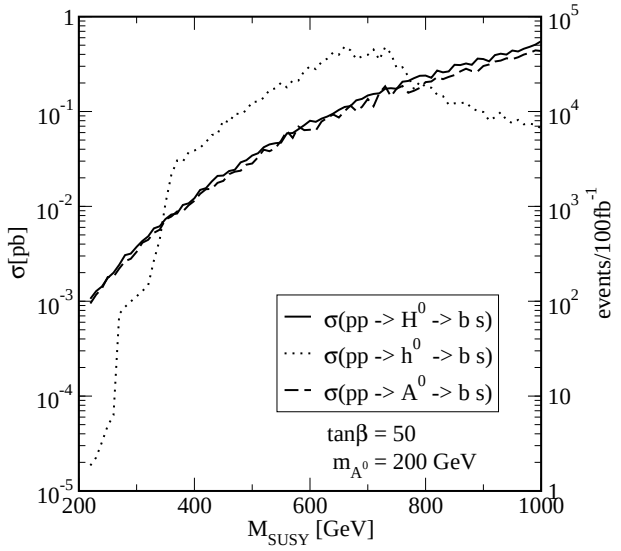

Figure 7.5: Maximum SUSY-QCD contributions to $\sigma(pp \to h \to b\,s)$, Eq. (7.1), as a function of $M_{\rm SUSY}$.

the higher range of δ_{23} can be further divided in two more segments where different dynamical features occur. In the first range, namely $10^{-1.5} \lesssim \delta_{23} \lesssim 10^{-0.75}$, the heavy Higgs boson channels keep on increasing their FCNC rates, but not so the lightest Higgs boson channel $\sigma(pp \to h^0 \to b\,s)$, the reason being that for higher squark masses we reach the region where the small $\alpha_{\rm eff}$ scenario is feasible and hence the h^0 couplings become weakened. The relevant terms of the cross-section can roughly be written as follows (see chapter 6):

$$\sigma(pp \to h^0 \to b\,s) \sim \sigma(pp \to h^0) \times \delta_{23}^2 \cos^2(\beta - \alpha_{\rm eff})\, m_{\tilde g}^2\, \mu^2 / M_{\rm SUSY}^4\,, \qquad (7.5)$$

so that for large $\tan\beta$ and small $\alpha_{\rm eff}$ it becomes reduced. In the second high range of δ_{23}, i.e. for $\delta_{23} \gtrsim 10^{-0.75} \simeq 0.18$, the SUSY mass parameter $M_{\rm SUSY}$ has already reached its allowed maximum value specified in (7.2), therefore other parameters have to change to compensate for the larger δ_{23}. This is confirmed in Fig. 7.4b, where for $\delta_{23} \gtrsim 10^{-0.75}$ the absolute value of μ decreases to preserve the $B(b \to s\gamma)$ upper bound. Correspondingly, in this region $\sigma(pp \to h^0 \to b\,s)$ further falls down, as it is patent in Fig 7.3a. This additional feature can also be understood from the approximate expression of the cross-section given above. At the same time the FCNC rates for $h = H^0, A^0$ keep further growing, but at a much lower pace. This is because their (approximate) contribution goes like (see (6.7):

$$\sigma(pp \to (H^0, A^0) \to bs) \sim \sigma(pp \to H^0, A^0) \times \delta_{23}^2\, (\sin^2(\beta - \alpha_{\rm eff}),\, 1)\, m_{\tilde g}^2\, \mu^2 / M_{\rm SUSY}^4\,, \quad (7.6)$$

similar to the h^0 case but with angular dependences on $\alpha_{\rm eff}$ and β which are non-suppressing in this region (see chapter 6). Again, any further increase of δ_{23} is now partially cancelled by the $b \to s\gamma$ constraint, which demands smaller values of μ. This explains the stabilization of the FCNC rates of the H^0 and A^0 channels in the highest δ_{23} range (cf. Fig. 7.3a). The profile of the squark mass curves in Fig. 7.4a implies a mixing mass matrix with constant diagonal terms (with value $M_{\rm SUSY}$) and growing mixing terms (δ_{23}).

We finish our analysis of $\sigma(pp \to h \to q\,q')$ by looking at its behavior as a function of the SUSY mass scale $M_{\rm SUSY}$, viz. the overall scale for the squark and gluino masses – cf. Eq. (7.2). Fig. 7.5 shows the maximum of $\sigma(pp \to h \to q\,q')$ as a function of $M_{\rm SUSY}$ for fixed $m_{A^0} = 200\,\text{GeV}$ and $\tan\beta = 50$. The interpretation of this figure follows closely the results of the previous ones. At small values of $M_{\rm SUSY}$ the potentially large contribution to $B(b \to s\gamma)$ has to be compensated – see Eq. (7.4) – by small values of δ_{23} and/or $|\mu|$, resulting in a (relatively) small value of $\sigma(pp \to h \to q\,q')$. As $M_{\rm SUSY}$ grows, δ_{23} and $|\mu|$ can take larger values without disturbing the restrictions from $B(b \to s\gamma)$. The leading contribution to our FCNC cross-sections is actually independent of the overall SUSY mass scale $M_{\rm SUSY}$, because for all Higgs boson channels we have found the general behavior (leaving aside other terms mentioned above)

$$\sigma(pp \to h \to q\,q') \sim \sigma(pp \to h) \times \delta_{23}^2\, m_{\tilde{g}}^2\, \mu^2 / M_{\rm SUSY}^4 \quad (h = h^0,\, H^0,\, A^0)\,. \tag{7.7}$$

The last factor effectively behaves as $\delta_{23}^2\,\mu^2/M_{\rm SUSY}^2$, and grows as δ_{23}^2 for increasing $M_{\rm SUSY}$ at fixed ratio $\mu/M_{\rm SUSY}$. Under the same conditions $B(b \to s\gamma)$ causes no problem because it is additionally suppressed by $m_b^2/M_{\rm SUSY}^2$ – cf. Eq. (7.4). Therefore, we are led to a sort of "non-decoupling behavior" of the FCNC rates with increasing $M_{\rm SUSY}$. In other words, we find that for the heavy neutral Higgs bosons (H^0, A^0) the interesting region is (contrary to naive expectations) the high $M_{\rm SUSY}$ range! The lightest Higgs boson (h^0) channel shows a similar overall behavior, but it presents additional features because it is more tied to the evolution of the CP-even mixing angle α. The most interesting region for this channel is (cf. Fig. 7.5) the central squark mass scale $M_{\rm SUSY} \sim 600 - 800\,\text{GeV}$, where the small $\alpha_{\rm eff}$ scenario can take place.

From the combined analysis of Figs. 7.1-7.5 we arrive at the following conclusions concerning the bs final state:

- A significant event rate of FCNC Higgs boson decays $\sigma(pp \to h \to q\,q')$ is expected at the LHC, even after taking into account the limits on $B(b \to s\gamma)$;

- Lightest Higgs boson case, h^0:

  - For $m_{A^0} \lesssim 300\,\text{GeV}$ the rate $\sigma(pp \to h^0 \to b\,s)$ decreases with m_{A^0} but it is the largest in this interval, being produced by the combination of a large production cross-section $\sigma(pp \to h^0 b\bar{b})$ and a moderate $B(h^0 \to b\,s)$. It amounts to a number of events between $\sim 5 \times 10^3$ and $\sim 12 \times 10^5$ for every $100\,\text{fb}^{-1}$ of integrated luminosity at the LHC;
  - For $300\,\text{GeV} \lesssim m_{A^0} \lesssim 850\,\text{GeV}$ we expect a maximum of $\sim 6{\times}10^3$ events/$100\,\text{fb}^{-1}$ in the small α_{eff} scenario, provided by a large $B(h^0 \to b\,s)$ and $\sigma(pp(gg) \to h^0)$ as the dominant production cross-section;
  - For $m_{A^0} > 850\,\text{GeV}$ the number of events starts to decrease slowly;
  - In all cases, this maximum is attained for a large value of $\tan\beta \sim 50$, a moderate value of the SUSY mass scale ($M_{\text{SUSY}} \sim 600 - 800\,\text{GeV}$) and a *low* value of $\delta_{23} \sim 10^{-1.3} \sim 0.05$;

- Heavy Higgs bosons, H^0, A^0:

  - Although not shown in our plots, we have checked that their production rate $\sigma(pp \to H^0\,A^0)$ decreases fast with the Higgs boson mass (due to the decreasing of the production cross-section). We find a maximum FCNC rate of $\sim 5 \times 10^4$ events for $m_{A^0} \simeq 200\,\text{GeV}$, and 20 events for $m_{A^0} \simeq 1\,\text{TeV}$.
  - The maximum is produced at i) large $\tan\beta > 30$, ii) at the highest allowed values of the SUSY mass scale, $M_{\text{SUSY}} \sim 1\,\text{TeV}$, and iii) at a relatively large value of the FCNC mixing parameter, $\delta_{23} \sim 10^{-0.75} \sim 0.18$, but not at the largest allowed value. The small α_{eff} scenario plays no role in the heavy Higgs boson channels.

Altogether one should expect a total maximum of some $120,000$ events/$100\,\text{fb}^{-1}$.

7.4 Analysis of the top-charm channel

The results of the numerical scan for this channel are similar to the *bs* channel, so we will focus mainly on the differences. Fig. 7.6a shows the maximum value of the production cross-section $\sigma(pp \to h \to t\,c)$, Eq. (7.1), under study as a function of m_{A^0}; Fig. 7.6b displays the cross-section as a function of $\tan\beta$. Obviously the lightest Higgs boson (h^0) channel does not appear in these plots, since in the MSSM this boson is always lighter than the top quark. Looking at Fig. 7.6 one can see immediately the following: i) the dominant channel in this case is the heavy scalar Higgs boson, H^0; ii) it varies between 1

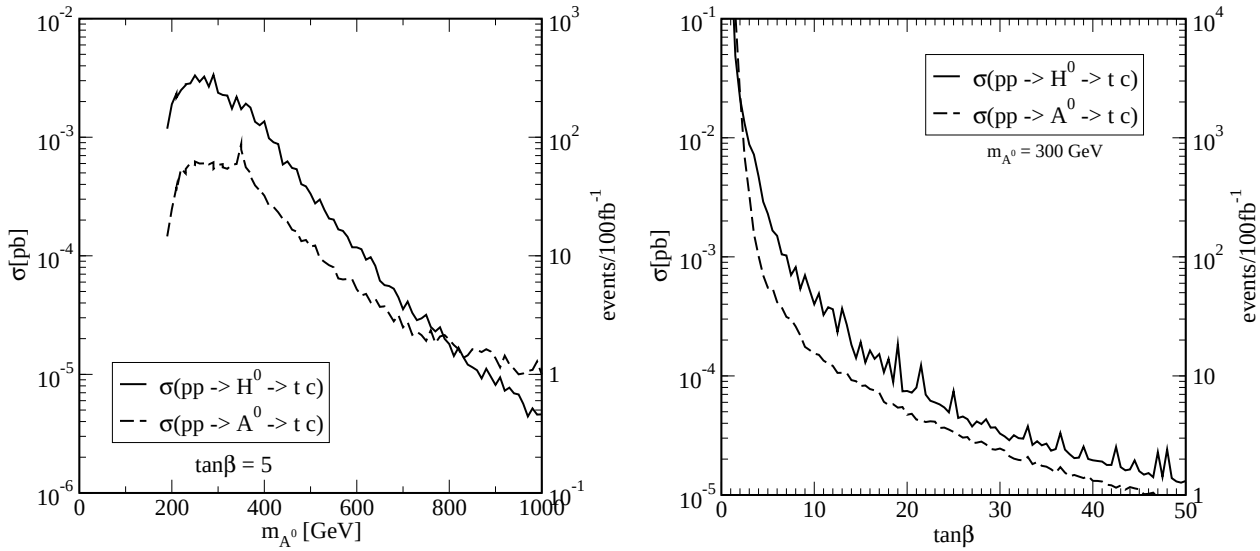

(a) (b)

Figure 7.6: Maximum SUSY-QCD contributions to $\sigma(pp \to h \to t\,c)$, Eq. (7.1), as a function of **(a)** m_{A^0} (at fixed $\tan\beta$) and **(b)** $\tan\beta$ (at fixed m_{A^0}).

and 300 events/100 fb^{-1}; iii) the $\tan\beta$ value is critical with preference for low values. In Table 7.2 we show the numerical values of $\sigma(pp \to h \to t\,c)$ together with the parameters which maximize the production for $\tan\beta = 5$ and $m_{A^0} = 300\,\text{GeV}$. We have included the value of $B(h \to tc)$ at the maximization point of the FCNC cross-section. It is remarkable that for the heavy CP-even Higgs boson one can reach $B(H^0 \to tc) \sim 10^{-3}$ compatible with the $b \to s\gamma$ constraint.

Let us remark that for the heavy Higgs boson channels the features of the small α_{eff} scenario play no significant role because the partial widths into $b\bar{b}$ are proportional either to $\cos^2\alpha_{\text{eff}}$ (in the H^0 case) or to $\sin^2\beta$ (A^0 case). Moreover, in the low $\tan\beta \gtrsim 1$ region (the relevant allowed one for the tc channel) the small α_{eff} scenario does not even have a chance to take place.

We turn now our view to the role of the $B(b \to s\gamma)$ restriction in Figs. 7.7 and 7.8. Fig. 7.7 shows the maximum value of $\sigma(pp \to h \to t\,c)$ as a function of δ_{23} for a fixed value of $m_{A^0} = 300\,\text{GeV}$ together with the corresponding computed value of $B(b \to s\gamma)$, while Fig. 7.8 shows the values of the parameters, Eq. (7.2), that realize this maximum, together with the physical up-type squark masses. In this case the $B(b \to s\gamma)$ restriction is not as critical as in the bs channel, in part due to the fact that the SUSY-QCD contribution to $B(b \to s\gamma)$ is not enhanced at low $\tan\beta$. For $\delta_{23} \lesssim 10^{-1.5}$ the value of $B(b \to s\gamma)$ is well

h	H^0	A^0
$\sigma(pp \to h \to t\,c)$	$2.4 \times 10^{-3}\,\text{pb}$	$5.8 \times 10^{-4}\,\text{pb}$
events/$100\,\text{fb}^{-1}$	240	58
$B(h \to tc)$	1.9×10^{-3}	5.7×10^{-4}
$\Gamma(h \to X)$	0.41 GeV	0.39 GeV
δ_{23}	$10^{-0.10}$	$10^{-0.13}$
$m_{\tilde{q}}$	880 GeV	850 GeV
A_t	−2590 GeV	2410 GeV
μ	−700 GeV	−930 GeV
$B(b \to s\gamma)$	4.13×10^{-4}	4.47×10^{-4}

Table 7.2: Maximum value of $\sigma(pp \to h \to t\,c)$ (and of the number of tc events per $100\,fb^{-1}$) in the LHC, for $m_{A^0} = 300\,\text{GeV}$ and $\tan\beta = 5$. Shown are also the corresponding values of the relevant branching ratio $B(h \to tc)$ and of the total width of the Higgs bosons, together with the values of the SUSY parameters. The last row includes $B(b \to s\gamma)$.

inside the experimental limits (Fig. 7.7b), there is no restriction on the rest parameters (Fig. 7.8b), the squark masses remain constant (Fig. 7.8a), and the maximum value of $\sigma(pp \to h \to t\,c)$ grows here in the naively expected way $(\delta_{23})^2$ (Fig. 7.7a). Above this value ($\delta_{23} \gtrsim 10^{-1.5}$) the parameters have to be adjusted to provide and acceptable range for $B(b \to s\gamma)$ [5]. In this region the SUSY mass M_{SUSY} grows (Fig. 7.8b), and $|\mu|$ decreases, but not so fast as in the bs channel case (Fig. 7.4b). At the same time A_t increases with increasing $\delta_{23} > 10^{-1.5}$. Most of the physical squark masses grow, but one of the up-type squarks (stop squark) can always have the minimum allowed mass – Eq. (7.2). In this region the observables under study grow more slowly, since their original δ_{23}^2 behavior is partially cancelled by the growing of M_{SUSY} with δ_{23}. In Fig. 7.9 we see, again, that $\sigma(pp \to h \to t\,c)$ grows with the SUSY mass scale (although in a way less pronounced than in the bs channel), due to the relaxation of the $b \to s\gamma$ constraint for large M_{SUSY}. While $\sigma(pp \to h \to q\,q')$ is augmented nearly three orders of magnitude in the range $M_{\text{SUSY}} = 200 - 1000\,\text{GeV}$ (Fig. 7.5), the tc channel undergoes only an increase of roughly

[5] The two lines appearing in this region for $B_H(b \to s\gamma)$ mean that the maximum of $\sigma(pp \to H^0 \to t\,c)$ is attained either by the maximum or the minimum allowed value of $B(b \to s\gamma)$, our Monte-Carlo sampling procedure picks either choice with equal probability for each value of δ_{23}.

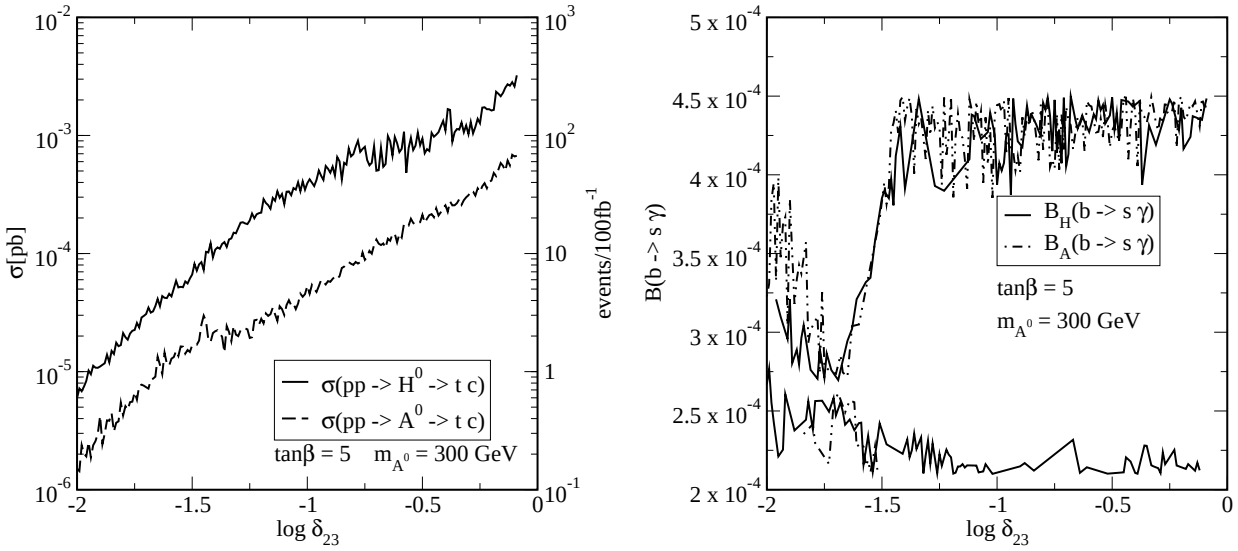

(a) (b)

Figure 7.7: Maximum SUSY-QCD contributions to $\sigma(pp \to h \to t\,c)$, Eq. (7.1), as a function of **(a)** δ_{23} and **(b)** value of $b \to s\gamma$, for fixed $\tan\beta$ and m_{A^0}.

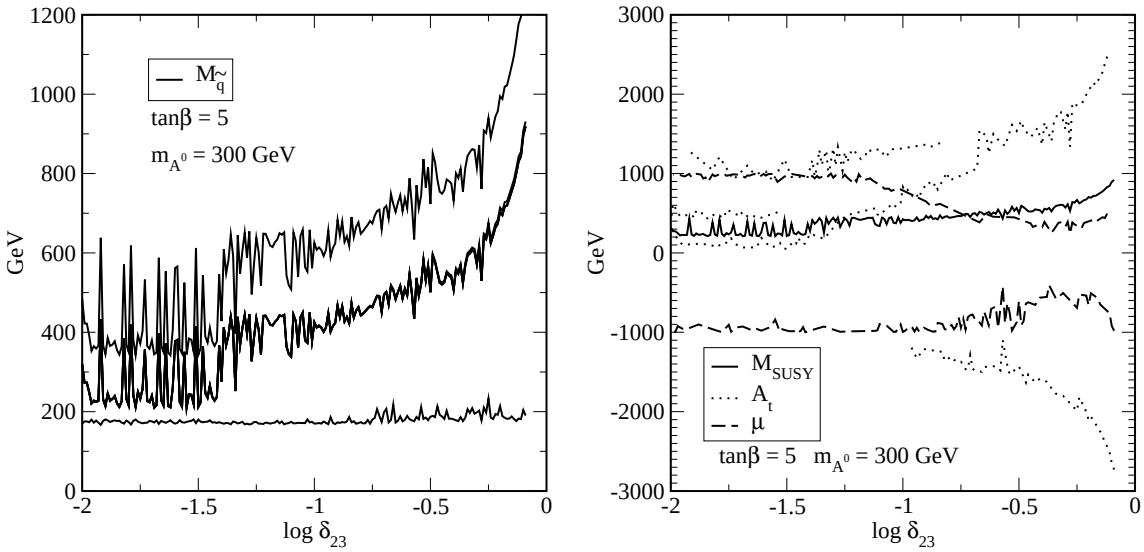

(a) (b)

Figure 7.8: Value of **(a)** up-type squark physical masses ($M_{\tilde{q}}$), four of them are degenerate; **(b)** the parameters (7.2) from the maximization of the H^0 channel in Fig. 7.7a.

a factor 10 in the same parameter range.

How do the two Higgs boson channels H^0 and A^0 compare as sources of tc events? The gg-fusion mechanism is one of the leading processes for Higgs boson production at relatively small values of $\tan\beta \gtrsim 1$ – associated production with $b\bar{b}$ remaining still sizeable. Due to CP conservation, the squark contributions to $gg \to A^0$ cancel out at one-loop and only the quark contributions remain [136]. For large squark masses the production cross-sections for H^0 and A^0 are similar, the latter being slightly larger. We see from Fig. 7.6 that, despite the similarity in production, the H^0 channel gives larger FCNC rates than the A^0 one. The excess of FCNC events from the former can be explained mainly from the constraints that we have imposed from the very beginning on the squarks masses in relation to the Higgs boson masses (see Eq. (7.2)). As we have noted in section 7.2, we can have squarks of the same chirality-type in the $H^0\,\tilde{q}\tilde{q}^*$ vertex, whereas they must necessarily be of opposite chirality-type in the $A^0\tilde{q}\tilde{q}^*$ case. As a result, for small m_{A^0} the squark mass constraints expressed in (7.2) allow the FCNC cross-section maximization process to pick points near the saturation of the mass condition $2\,M_{\tilde{q}_i} > m_{H^0} + 50\,\text{GeV}$, but not of $M_{\tilde{q}_i} + M_{\tilde{q}_j} > m_{A^0} + 50\,\text{GeV}$ for $(i \neq j)$ because only one of the up-squarks can be light (see Fig. 7.8a). This produces an enhancement of the branching ratio of $H^0 \to tc$ and for this reason this FCNC channel dominates in the relatively small m_{A^0} region. However, as soon as m_{A^0} is sufficiently heavy the second mass constraint can also be satisfied and then the two curves in Fig. 7.6 tend to converge.

From the combined analysis of Figs. 7.6-7.9, we conclude that in the case of the H^0 channel we expect a maximum of ~ 300 events/$100\,\text{fb}^{-1}$ decays into top quarks at the LHC. This maximum is achieved for a CP-odd Higgs boson mass of $m_{A^0} \sim 300\,\text{GeV}$, and a moderately low $\tan\beta \sim 5$. This rate can grow one order of magnitude by a lower value of $\tan\beta \sim 2$, but decreases significantly with m_{A^0}. The maximum is obtained at the largest possible value of δ_{23}, and a moderate SUSY mass scale $M_{\text{SUSY}} \sim 600 - 800\,\text{GeV}$, but having one of the squarks light. While the number of events is significantly lower than the bs-channel ones, the tc-channels offers a better opportunity for detection, due to the much lower background.

7.5 Discussion and conclusions

We have carried out a systematic study of the production rate of FCNC processes at the LHC mediated by the decay of neutral Higgs bosons of the MSSM: $\sigma(pp \to h \to q\,q')$ $(h = h^0, H^0, A^0)$ – see Eq. (7.1). Specifically, we have concentrated on the FCNC production of the heavy quark pairs $qq' = bs$ and tc, because they are the only ones that have a chance of

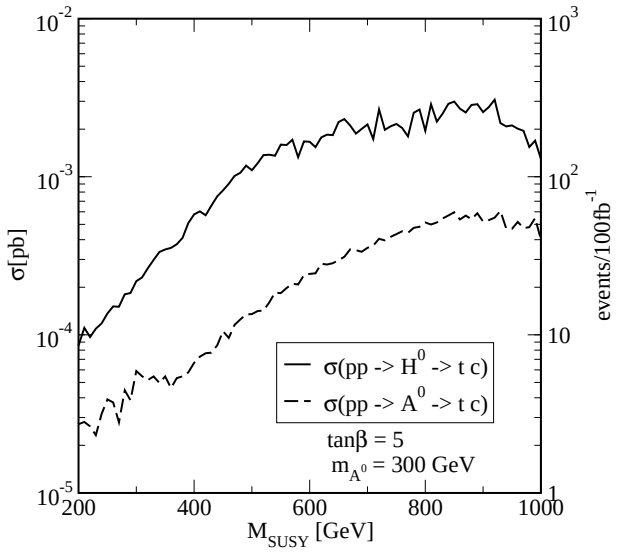

Figure 7.9: Maximum SUSY-QCD contributions to $\sigma(pp \to h \to t\,c)$, Eq. (7.1), as a function of $M_{\rm SUSY}$.

being detected. We have focused on the FCNC supersymmetric effects stemming from the strongly interacting sector of the MSSM, namely from the gluino-mediated flavor-changing interactions. We have performed a maximization of the event rates in the parameter space under a set of conditions that can be considered "irreducible", see Eq. (7.2), i.e. we cannot further shorten this minimal set (e.g. by making additional assumptions on the relations among the parameters) without potentially jeopardizing the conclusions of this study. Even within this restricted parameter subspace the computer analysis has been rather demanding. The numerical scan has been performed using Monte Carlo techniques which we have partially cross-checked with more conventional methods. The maximization of the cross-sections (7.1) has been performed by simultaneously computing the corresponding MSSM quantum effects on the (relatively well-measured) low-energy FCNC decay $b \to s\gamma$ and requiring that the experimental limits on this observable are preserved.

To summarize our results: the total number of FCNC heavy flavor events originating from supersymmetric Higgs boson interactions at the LHC can be large (of order 10^6), but this does not mean that they can be easily disentangled from the underlying background of QCD jets where they are immersed. For example, it is well known that the simple two-body decay $h \to b\,\bar{b}$ is impossible to isolate due to the huge irreducible QCD background from $b\,\bar{b}$ dijets – a result that holds for both the SM and the MSSM [13, 14]. This led a long time ago to complement the search with many other channels, particularly $h \to \gamma\,\gamma$

which has been identified as an excellent signature in the appropriate range. Similarly, the FCNC Higgs boson decay channels may help to complement the general Higgs boson search strategies, mainly because the FCNC processes should be essentially free of QCD background. Notwithstanding other difficulties can appear, such as misidentification of jets. For instance, for the bs final states misidentification of b-quarks as c-quarks in cs-production from charged currents may obscure the possibility that the bs-events can be really attributed to Higgs boson FCNC decays. This also applies to the tc final states, where misidentification of b-quarks as c-quarks in e.g. tb production might be a source of background to the tc events, although in this case the clear-cut top quark signature should be much more helpful (specially after an appropriate study of the distribution of the signal versus the background). However, to rate the actual impact of these disturbing effects one would need an additional study which is beyond the scope of the present work.

An interesting (and counter-intuitive) result of our work is that for all the Higgs boson channels $h = h^0, H^0, A^0$, the FCNC cross-section $\sigma(pp \to h \to q\,q')$ increases with growing SUSY mass scale $M_{\rm SUSY}$. Due to this effective "non-decoupling" behavior (which is more pronounced for the bs channel) the FCNC rates are maximal when the overall squark and gluino mass scale is of order of $M_{\rm SUSY} \lesssim 1\,\text{TeV}$ – with the only proviso that for the tc-channel a single squark should have a low mass ($\gtrsim 150\,\text{GeV}$). Moreover, we find that the two types of FCNC final states (bs and tc) prefer different ranges of $\tan\beta$. The bs-channel is most efficient at high $\tan\beta > 30$, whereas the tc-channel works better in the regime of low $\tan\beta < 10$ (see below). As for the mixing parameter δ_{23} (which is the fundamental supersymmetric FCNC parameter of our analysis, see its definition in (6.5)) we remark that the maximum number of events is not always attained for the largest possible values of it (due to the influence of the $b \to s\gamma$ constraint): in the bs-channel the maximum is achieved for moderate values in the range $0.05 \lesssim \delta_{23} \lesssim 0.2$, whereas the tc-channel prefers the maximum allowed values in our analysis ($\delta_{23} \lesssim 0.8$). We also remark that the naive expectation $\sigma(pp \to h \to q\,q') \sim \delta_{23}^2$ does not always apply.

The number of FCNC events originating from the two channels bs and tc is not alike, and it also depends on the particular Higgs boson. For the bs final states we have found that the optimized value of $\sigma(pp \to h \to q\,q')$ produced by our analysis is $\sim 12\,\text{pb}$. This amounts to $\sim 12\times 10^5$ events per $\int \mathcal{L}dt = 100\,\text{fb}^{-1}$ of data at the LHC. The most favorable Higgs boson channel is the one corresponding to the lightest MSSM Higgs boson, h^0. For this boson there are non-trivial correlations between the two factors in Eq. (7.1), namely between the Higgs boson production cross-section and the FCNC branching ratio. These correlations permit an increase of the total number of FCNC events up to two orders of magnitude in certain cases as compared to the number of events produced by the heavy

Higgs bosons H^0 and A^0, which are essentially free of these correlations. The latter stem from relevant quantum effects on the parameters of the Higgs boson sector at one-loop precisely in the regions of our interest.

On the other hand, the maximum value of $\sigma(pp \to h \to t\,c)$ is more moderate, to wit: $3 \times 10^{-3}\,\text{pb}$, or ~ 300 events/$100\,\text{fb}^{-1}$. For the total integrated luminosity during the operative lifetime of the LHC, which amounts to some $(300 - 400)\,\text{fb}^{-1}$, we estimate that a few thousand tc events could be collected in the most optimistic conditions. This number is of course sensitive to many MSSM parameters, but most particularly to two: m_{A^0} and $\tan\beta$. The mass of the CP-odd Higgs boson should not be heavier than $m_{A^0} \sim (400-500)\,\text{GeV}$ if one does not want to decrease the number of events below a few hundred per $100\,\text{fb}^{-1}$. On the other hand the number of events is very much dependent on the particular range of $\tan\beta$. As we have said above, the lowest possible values are preferred for the tc channel, but the sensitivity in this range is so high that the order of magnitude of $\sigma(pp \to h \to t\,c)$ may change for different (close) choices of $\tan\beta$. Throughout all the analysis of the tc channel we have fixed $\tan\beta$ at an intermediate value, but the maximum number of events per $100\,\text{fb}^{-1}$ would grow from ~ 300 (for our standard choice $\tan\beta = 5$) up to $\sim (500, 900, 2000)$ if we would have chosen $\tan\beta = (4, 3, 2)$ respectively. Such lower values of $\tan\beta$ are usually avoided in some MSSM analyses in the literature, but as a matter of fact there are no fully water-tight experimental bounds on $\tan\beta$ excluding this lower range, apart from the more incontrovertible strict lowest limit $\tan\beta > 1$. We recall that the lower limit on $\tan\beta$ is obtained indirectly from the LEP exclusion data on the light Higgs boson search, and is therefore very sensitive to the inputs used in the computation, specially the top quark mass [108]. Unlike the difficulties in the bs-channel, and in spite of the substantially smaller number of events, we deem more feasible to extract the tc signal at the LHC, due to the presence of the quark top, which carries a highly distinguishable signature.

At this point a comparison with the previous chapter 5 is in order. In that work we have studied in quite some detail the maximum FCNC production rates of Higgs bosons decaying into tc final states within the general two-Higgs-doublet model. It was found that the maximal branching ratio in the 2HDM takes place in the type II 2HDM (or 2HDM II), and reads $B^{II}(h \to tc) \sim 10^{-5}$, whereas in the 2HDM I it is comparatively negligible. After a detailed computation of the event rates (including also the particular restrictions of the $b \to s\gamma$ process, which are different in the 2HDM case as compared to the MSSM) the conclusion was that several hundred tc events could be collected at the LHC under optimal conditions. We clearly identified which are the most relevant Higgs boson modes for this purpose and the domains of the 2HDM II parameter space where these events

could originate from. To make it short, our conclusion in chapter 5 was that the h^0 is the most gifted decay and the ideal situation occurs when $\tan\beta$ and $\tan\alpha$ are both large, and also when the CP-odd state A^0 is much heavier than the CP-even ones (h^0, H^0). Furthermore we found that in the general 2HDM the A^0 state never gives any appreciable FCNC rate into tc. It is easy to see that the mode $A^0 \to bs$ is not favored either (unless $\tan\beta$ is very small and $m_{H^\pm}$ unusually light, both situations rather unappealing).

How it compares with the MSSM case under study? To start with, we note that here the A^0 channel gives essentially the same bs rate as the H^0 one, and that both modes can be quite relevant. At the same time the A^0 rate into tc is, though not dominant, not negligible at all. Some few hundred events of this nature per $100\,\mathrm{fb}^{-1}$ are possible. If this is not enough, in the MSSM the most relevant $\tan\beta$ region for the tc final states is not the highest one (as in the 2HDM II case) but just the opposite: the lowest allowed one. This is an important difference, and one that should help to discriminate between the 2HDM and MSSM models in case that some tc events would be unambiguously tagged at the LHC. After all there are many high precision observables that are highly sensitive to the preferred range of $\tan\beta$, so that the favorite value of $\tan\beta$ could already be fixed from other experiments by the time that some FCNC events could be detected. Apart from the different correlation of the parameters in the non-supersymmetric and supersymmetric model, in the latter case the maximal event rates for the tc mode are typically one order of magnitude higher than the maximal event rates in the former.

The corresponding study for the 2HDM branching ratios into bs final states was performed in [51], although in this work the cross-section and number of events were not computed. However, from the maximum size of the expected branching ratios compatible with $b \to s\gamma$ (viz. $B^{II}(h \to bs) \sim 10^{-6} - 10^{-5}$ in the 2HDM II) it is already pretty obvious that the number of events can never be competitive with the supersymmetric case where $B^{MSSM}(h \to bs) \sim 10^{-4} - 10^{-3}$ as seen in chapter 6. As for the 2HDM I (which is insensitive to the $b \to s\gamma$ bounds) the branching ratios can be at most of order $B^{I}(h \to bs) \sim 10^{-5} - 10^{-3}$ and only so for very small values of $\tan\beta = 0.1 - 0.5$ which are actually excluded in the MSSM.

Summing up and closing: the maximum number of FCNC events in the MSSM case is larger than the highest expected rates both in the 2HDM I and II , the two kind of signatures of physics beyond the SM being perfectly distinguishable because the relevant regions of the parameter space are completely different. If a sample of FCNC events of this kind could be collected, we should be able to ascertain which is its ultimate origin. At the end of the day if one single thing should be emphasized is that the FCNC event rate into bs or tc is so extremely tiny in the SM that if only a dozen events of this kind could be

captured under suitable experimental conditions it would be an undeniable signature of new physics. From what we have seen, the odds should be heavily in favor of attributing it to a supersymmetric origin.

Chapter 8

Conclusions

In this PhD. Thesis we have presented a monographic study of some rare Flavour Changing Neutral Currents (FCNC) induced in the Two-Higgs-Doblet-Models (of both kinds 2HDM I and II) and in the Minimal Supersymmetric Standard Model (MSSM). In particular we have studied the FCNC top quark decay in the 2HDM, $t \to ch$, Higgs boson production and decay in the 2HDM, $pp \to h + X \to t\bar{c}$, $h \to t\bar{c}$, and the Higgs boson production and decay in the MSSM, $pp \to h + X \to t\bar{c}, b\bar{s}$ and $h \to t\bar{c}, b\bar{s}$, in the context of the LHC, where $h = h^0, H^0, A^0$ are the three neutral Higgs bosons in these extended Higgs models.

The main results obtained are the following:

- The non standard effects on the top quark FCNC decay into Higgs boson in the 2HDM II can be very important, at most ten orders of magnitude larger then in the SM, bringing the branching ratios at the level of 10^{-4} or higher in some cases. Thus there is a real chance for seeing rare decays of that sort at the LHC. The effects of the 2HDM I, although sizeable, do not reach the visible level at the LHC.

  It is useful to compare the $t \to hc$ processes with the more conventional rare decay $t \to gc$. The maximum rates for the leading FCNC processes (4.1) and (4.2) in the 2HDM II (resp. in the MSSM) satisfy the relations

  $$B(t \to g\, c) < 10^{-6}(10^{-5}) < B(t \to h\, c) \sim 10^{-4}\,, \tag{8.1}$$

  where it is understood that h is h^0 or H^0, but not both, in the 2HDM II; whereas h is most likely h^0, but it could also be H^0 and A^0, in the MSSM.These decay ratios are compatible with their observation at the LHC if we compare them with the estimations of the sensitivities for 100 fb^{-1} of integrated luminosity in the relevant

colliders [25, 133, 166]:

$$\begin{aligned} \textbf{LHC}: & B(t \to c\,X) \gtrsim 5 \times 10^{-5}\,, \\ \textbf{LC}: & B(t \to c\,X) \gtrsim 5 \times 10^{-4}\,, \\ \textbf{TEV33}: & B(t \to c\,X) \gtrsim 5 \times 10^{-3}\ . \end{aligned} \tag{8.2}$$

The origin of the FCNC effects from the general 2HDM contributions is purely electroweak (namely it stems from enhanced trilinear Higgs boson couplings), in contrast to the MSSM case where they are mainly from the strong (gluino) sector, with the electroweak contributions one-two orders of magnitude below. This can be important because the MSSM strong couplings are very weakly restrained from experiment.

Although the maximum ratio is similar there are different strategies to distinguish between the 2HDM and MSSM FCNC Higgs boson effects in the case that these decays would be detected. A possible strategy would be to look for different signatures for the process $t \to hc \to cb\bar{b}$. In the favorite FCNC region (4.7) of the 2HDM II, the combined decay $t \to h\ \ c \to cb\overline{b}$ is possible only for h^0 or for H^0, but not for both – Cf. Fig. 4.3a – whereas in the MSSM, h^0 together with H^0, are highlighted for $110\,GeV < m_{A^0} < m_t$, with no preferred $\tan\beta$ value. And similarly, $t \to A^0\,c$ is also non-negligible for $m_{A^0} \lesssim 120\,GeV$ [43].

- The potential enhancement of the 2HDM contributions to the Higgs boson decay into top and charm quarks may reach up to ten billion times the SM value $B(H^{SM} \to t\,\bar{c}) \sim 10^{-15}$, thereby bringing the maximum value of the FCNC branching ratio $B(h^0 \to t\,\bar{c})$ to the level of $\sim 10^{-5}$. Adding to this the 2HDM contributions of the Higgs production ($pp \to H + X$) we find that the events $pp \to H + X \to t\bar{c} + X$ could be visible at the LHC, getting a few hundred events for the h^0 and for the H^0, but no for the A^0. Thus, theses events can be very useful to complement the Higgs boson detection strategies, like for example those based on the decay $H^{\rm SM} \to b\bar{b}$ (affected with a huge QCD background) or on the decay $H^{\rm SM} \to \gamma\gamma$ (more promising).

  There are some strategies to distinguish between the 2HDM and the MSSM. An obvious one is the detection of the channel $A^0 \to t\bar{c}$ that is highly suppressed in the 2HDM but it is not so in the MSSM. Another possibility is using the fact that the MSSM contribution to FCNC processes is mainly from the gluino, which is not particularly sensitive to $\tan\beta$, within a range of high and moderately values of this parameter. If, for example, a few of these events were observed and at the same

time the best MSSM fits to the electroweak precision data would favor moderate values of $\tan\beta$, say in the range $10-20$, then it is clear that those events could originate from the FCNC gluino interactions but in no way within the context of the general 2HDM.

- The SUSY-QCD contributions can enhance the maximum expectation for the FCNC decay rates $B(h\to q\,q')$, where $qq'=tc$ or bs, reaching the level of 10^{-3}, in particular $B^{\max}(h^0\to q\,q')\sim 3\times 10^{-3}$ and $B^{\max}(H^0/A^0\to q\,q')\simeq 9\times 10^{-4}$. This corresponds to an scenario where $\Gamma(h^0\to b\bar{b})$ is suppressed by radiative corrections to the CP-even mixing angle α (the so-called small α_{eff} scenario). When it is not the case the maximum ratios give the same result except for the light Higgs boson $B^{\max}(h^0\to q\,q')\simeq 1.3\times 10^{-4}$. So we get branching rations three to nine orders of magnitude higher than in the SM case, depending on the $q\,q'$ channel.

  The total number of FCNC heavy flavor events (tc, bs) originating from supersymmetric Higgs boson interactions at the LHC can be large (of order 10^6 for $b\bar{s}$), but this does not mean that they can be easily disentangled from the underlying background of QCD jets where they are immersed. For the bs final state the maximum number of events is $\sim 12\times 10^5$ for a $100\,fb^{-1}$ of integrated luminosity at the LHC, being the most favorable Higgs boson channel the lightest MSSM Higgs boson, h^0. There are some correlations in this channel that increase the number of events up to two orders of magnitude in certain cases as compared with the other channels H^0, A^0. On the other hand, for the case of tc the maximum number of events is $\sim 300\,\text{events}/100\,\text{fb}^{-1}$ for $\tan\beta=5$, which amounts to few thousand tc events during the lifetime of the LHC. This value is sensitive to the rest of the parameters, in particular m_{A^0} and $\tan\beta$. The mass of the CP-odd Higgs boson should not be heavier than $m_{A^0}\sim(400-500)\,\text{GeV}$ if one does not want to decrease the number of events below a few hundred per $100\,\text{fb}^{-1}$. On the other hand the number of events is very much dependent on the particular range of $\tan\beta$, with a preferred low values, and changing orders of magnitude with tiny changes in $\tan\beta$. For example for the values $\tan\beta=(5,4,3,2)$ we get a number of events $\sim(300,500,900,2000)$. Although such lower values are usually avoided in the literature, they are not strictly excluded experimentally.

  We emphasize the primary differences with the 2HDM. In the MSSM, (1) the A^0 and H^0 channels give essentially the same bs rate, and it can be quite important; (2) the A^0 rate into tc is not negligible; (3) the relevant range in $\tan\beta$ is the lowest allowed one. In general the maximum number of FCNC events in the MSSM case

is larger than the highest expected rates both in the 2HDM I and II, the two kind of signatures of physics beyond the SM being perfectly distinguishable because the relevant regions of the parameter space are completely different.

Although we have shown that the FCNC events considered in this Thesis are in principle visible (namely, we have proven that the branching ratios and production cross section are sizeable enough as compared to other rare, but detected, events), it should be emphasized that the final word can only be said after an appropriate signal versus background experimental study, which is out of the scope of this theoretical investigation. However, we consider highly encouraging that there is no theoretical a priori obstruction for these processes not to be visible in the experimental setup of the LHC collider. In particular the $t\bar{c} + \bar{t}c$ events, with the top quark in the final state, should be very helpful and essentially free from background.

From these positive theoretical results we can assert that the pathway to seeing new physics through FCNC decays of the top quark and Higgs boson is thus potentially open. It is now an experimental challenge to accomplish this program using the high luminosity super-colliders round the corner, in particular the Large Hadron Collider at CERN, which is scheduled to start operating within two years from now, i.e. in 2007.

Appendix A

Vertex functions

In this appendix we briefly collect, for notational convenience, the basic vertex functions frequently referred to in the text. In practice we have performed the calculations using the algebraic and numerical programs FeynArts, FeynCalc and LoopTools [128–130]. The given formulas are exact for arbitrary internal masses and external on-shell momenta. Most of them are an adaptation to the $g_{\mu\nu} = \{+ - - -\}$ metric of the standard formulae of Refs. [167–169]. The basic one-, two- and three-point scalar functions are:

$$A_0(m) = \int d^n\tilde{q}\,\frac{1}{[q^2-m^2]}, \tag{A.1}$$

$$B_0(p,m_1,m_2) = \int d^n\tilde{q}\,\frac{1}{[q^2-m_1^2]\,[(q+p)^2-m_2^2]}\,, \tag{A.2}$$

$$C_0(p,k,m_1,m_2,m_3) = \int d^n\tilde{q}\,\frac{1}{[q^2-m_1^2]\,[(q+p)^2-m_2^2]\,[(q+p+k)^2-m_3^2]}\,; \tag{A.3}$$

using the integration measure

$$d^n\tilde{q} \equiv \mu^{(4-n)}\frac{d^nq}{(2\pi)^n}\,. \tag{A.4}$$

The two and three-point tensor functions needed for our calculation are the following

$$[\tilde{B}_0, B_\mu, B_{\mu\nu}](p,m_1,m_2) = \int d^n\tilde{q}\,\frac{[q^2, q_\mu, q_\mu q_\nu]}{[q^2-m_1^2]\,[(q+p)^2-m_2^2]}\,, \tag{A.5}$$

$$[\tilde{C}_0, C_\mu, C_{\mu\nu}](p,k,m_1,m_2,m_3) = \int d^n\tilde{q}\,\frac{[q^2, q_\mu, q_\mu q_\nu]}{[q^2-m_1^2]\,[(q+p)^2-m_2^2]\,[(q+p+k)^2-m_3^2]}\,. \tag{A.6}$$

By Lorentz covariance, they can be decomposed in terms of the above basic scalar functions and the external momenta:

$$\begin{aligned}
\tilde{B}_0(p,m_1,m_2) &= A_0(m_2) + m_1^2 B_0(p,m_1,m_2)\ , \\
B_\mu(p,m_1,m_2) &= p_\mu B_1(p,m_1,m_2)\ , \\
B_{\mu\nu}(p,m_1,m_2) &= p_\mu p_\nu B_{21}(p,m_1,m_2) + g_{\mu\nu} B_{22}(p,m_1,m_2)\ , \\
\tilde{C}_0(p,k,m_1,m_2,m_3) &= B_0(k,m_2,m_3) + m_1^2 C_0(p,k,m_1,m_2,m_3)\ , \\
C_\mu(p,k,m_1,m_2,m_3) &= p_\mu C_{11} + k_\mu C_{12}\ , \\
C_{\mu\nu}(p,k,m_1,m_2,m_3) &= p_\mu p_\nu C_{21} + k_\mu k_\nu C_{22} + (p_\mu k_\nu + k_\mu p_\nu) C_{23} + g_{\mu\nu} C_{24}\ , \qquad \text{(A.7)}
\end{aligned}$$

where we have defined the Lorentz invariant functions:

$$\begin{aligned}
B_1(p,m_1,m_2) &= \frac{1}{2p^2}[A_0(m_1) - A_0(m_2) - f_1 B_0(p,m_1,m_2)], \qquad \text{(A.8)} \\
B_{21}(p,m_1,m_2) &= \frac{1}{2p^2(n-1)}[(n-2)A_0(m_2) - 2m_1^2 B_0(p,m_1,m_2) \\
&- n f_1 B_1(p,m_1,m_2)], \qquad \text{(A.9)} \\
B_{22}(p,m_1,m_2) &= \frac{1}{2(n-1)}[A_0(m_2) + 2m_1^2 B_0(p,m_1,m_2) + f_1 B_1(p,m_1,m_2)], \qquad \text{(A.10)}
\end{aligned}$$

$$\begin{pmatrix} C_{11} \\ C_{12} \end{pmatrix} = Y \begin{pmatrix} B_0(p+k,m_1,m_3) - B_0(k,m_2,m_3) - f_1 C_0 \\ B_0(p,m_1,m_2) - B_0(p+k,m_1,m_3) - f_2 C_0 \end{pmatrix}, \qquad \text{(A.11)}$$

$$\begin{pmatrix} C_{21} \\ C_{23} \end{pmatrix} = Y \begin{pmatrix} B_1(p+k,m_1,m_3) + B_0(k,m_2,m_3) - f_1 C_{11} - 2C_{24} \\ B_1(p,m_1,m_2) - B_1(p+k,m_1,m_3) - f_2 C_{11} \end{pmatrix}, \qquad \text{(A.12)}$$

$$\begin{aligned}
C_{22} &= \frac{1}{2[p^2k^2 - (pk)^2]}\{-pk[B_1(p+k,m_1,m_3) - B_1(k,m_2,m_3) - f_1 C_{12}] \\
&+ p^2[-B_1(p+k,m_1,m_3) - f_2 C_{12} - 2C_{24}]\}\,, \qquad \text{(A.13)}
\end{aligned}$$

$$C_{24} = \frac{1}{2(n-2)}[B_0(k,m_2,m_3) + 2m_1^2 C_0 + f_1 C_{11} + f_2 C_{12}]\,, \qquad \text{(A.14)}$$

the factors $f_{1,2}$ and the matrix Y,

$$\begin{aligned}
f_1 &= p^2 + m_1^2 - m_2^2, \\
f_2 &= k^2 + 2pk + m_2^2 - m_3^2\,, \\
Y &= \frac{1}{2[p^2k^2 - (pk)^2]} \begin{pmatrix} k^2 & -pk \\ -pk & p^2 \end{pmatrix}. \qquad \text{(A.15)}
\end{aligned}$$

The UV divergences for $n \to 4$ can be parametrized as

$$\begin{aligned}
\epsilon &= n - 4, \\
\Delta &= \frac{2}{\epsilon} + \gamma_E - \ln(4\pi)\,, \qquad \text{(A.16)}
\end{aligned}$$

being γ_E the Euler constant. In the end one is left with the evaluation of the scalar one-loop functions:

$$\begin{aligned} A_0(m) &= \left(\frac{-i}{16\pi^2}\right) m^2(\Delta - 1 + \ln\frac{m^2}{\mu^2})\,, && \text{(A.17)}\\ B_0(p,m_1,m_2) &= \left(\frac{-i}{16\pi^2}\right)\left[\Delta + \ln\frac{p^2}{\mu^2} - 2 + \ln[(x_1-1)(x_2-1)]\right. \\ &\quad \left. + x_1\ln\frac{x_1}{x_1-1} + x_2\ln\frac{x_2}{x_2-1}\right], && \text{(A.18)}\\ C_0(p,k,m_1,m_2,m_3) &= \left(\frac{-i}{16\pi^2}\right)\frac{1}{2}\,\frac{1}{pk+p^2\xi}\Sigma && \text{(A.19)} \end{aligned}$$

with

$$\begin{aligned} x_{1,2} = x_{1,2}(p,m_1,m_2) &= \frac{1}{2} + \frac{m_1^2-m_2^2}{2p^2} \pm \frac{1}{2p^2}\lambda^{1/2}(p^2,m_1^2,m_2^2), && \text{(A.20)}\\ \lambda(x,y,z) &= [x-(\sqrt{y}-\sqrt{z})^2][x-(\sqrt{y}+\sqrt{z})^2]\,, \end{aligned}$$

and where Σ is a bookkeeping device for the following alternate sum of twelve (complex) Spence functions:

$$\begin{aligned} \Sigma &= Sp\left(\frac{y_1}{y_1-z_1^i}\right) - Sp\left(\frac{y_1-1}{y_1-z_1^i}\right) + Sp\left(\frac{y_1}{y_1-z_2^i}\right) - Sp\left(\frac{y_1-1}{y_1-z_2^i}\right)\\ &- Sp\left(\frac{y_2}{y_2-z_1^{ii}}\right) + Sp\left(\frac{y_2-1}{y_2-z_1^{ii}}\right) - Sp\left(\frac{y_2}{y_2-z_2^{ii}}\right) + Sp\left(\frac{y_2-1}{y_2-z_2^{ii}}\right)\\ &+ Sp\left(\frac{y_3}{y_3-z_1^{iii}}\right) - Sp\left(\frac{y_3-1}{y_3-z_1^{iii}}\right) + Sp\left(\frac{y_3}{y_3-z_2^{iii}}\right) - Sp\left(\frac{y_3-1}{y_3-z_2^{iii}}\right). \quad \text{(A.21)} \end{aligned}$$

The Spence function is defined as

$$Sp(z) = -\int_0^1 \frac{\ln(1-zt)}{t}\,dt\,, \qquad \text{(A.22)}$$

and we have set, on one hand:

$$\begin{aligned} z_{1,2}^i &= x_{1,2}(p,m_2,m_1)\,,\\ z_{1,2}^{ii} &= x_{1,2}(p+k,m_3,m_1)\,,\\ z_{1,2}^{iii} &= x_{1,2}(k,m_3,m_2)\,; \qquad \text{(A.23)} \end{aligned}$$

and on the other:

$$y_1 = y_0 + \xi\,, \quad y_2 = \frac{y_0}{1-\xi}\,, \quad y_3 = -\frac{y_0}{\xi}\,, \quad y_0 = -\frac{1}{2}\,\frac{g+h\xi}{pk+p^2\xi}\,, \qquad \text{(A.24)}$$

where

$$g = -k^2 + m_2^2 - m_3^2\,, \qquad h = -p^2 - 2pk - m_2^2 + m_1^2\,, \qquad \text{(A.25)}$$

and ξ is a root (always real for external on-shell momenta) of

$$p^2\xi^2 + 2pk\xi + k^2 = 0\,. \tag{A.26}$$

Derivatives of some 2-point functions are also needed in the calculation of self-energies, and we use the following notation:

$$\frac{\partial}{\partial p^2}B_*(p, m_1, m_2) \equiv B'_*(p, m_1, m_2). \tag{A.27}$$

We can obtain all the derivatives from the basic B'_0:

$$\begin{aligned} B'_0(p, m_1, m_2) &= \left(\frac{-i}{16\pi^2}\right)\left\{\frac{1}{p^2} + \frac{1}{\lambda^{1/2}(p^2, m_1^2, m_2^2)}\right. \\ &\quad \left.\times\left[x_1(x_1-1)\ln\left(\frac{x_1-1}{x_1}\right) - x_2(x_2-1)\ln\left(\frac{x_2-1}{x_2}\right)\right]\right\}, \end{aligned} \tag{A.28}$$

which has a threshold for $|p| = m_1 + m_2$ and a pseudo-threshold for $|p| = |m_1 - m_2|$.

A.1 Limit of heavy internal masses

Next we will present the results when the external moments are much heavier than the internal masses ($p^2 \ll m^2$). The basic equations is:

$$\begin{aligned} \frac{1}{(q+p)^2 - m^2} &= \frac{1}{q^2 - m^2}\left[1 + \frac{p^2 + 2p\cdot q}{q^2 - m^2}\right]^{-1} \\ &= \frac{1}{q^2 - m^2}\left[1 - \frac{p^2 + 2p\cdot q}{q^2 - m^2} + \left(\frac{p^2 + 2p\cdot q}{q^2 - m^2}\right)^2 - \dots\right], \end{aligned} \tag{A.29}$$

which we have to substitute in each of the denominators of the n-point functions. But, all the lineal terms in the expansion become zero under the integrations $\int d^4q$, because of the denominator is a spherically symmetric function. The others terms are integrals of functions of q^2 and $p^2/(q^2 - m^2)^2 \ll 1$, which are negligible in this limit.

Thus the effective substitution is:

$$\frac{1}{(q+p)^2 - m^2} \to \frac{1}{q^2 - m^2}\,, \tag{A.30}$$

in the cases where $p^2 \ll m^2$.

So in this limit the n-point functions do not depend on the moments. It allows us to define, without ambiguities, that the n-point functions without the moments are proportional to the complete n-point functions with the moments equals to zero. As:

$$C_0(0, 0, m_1, m_2, m_3) = \left(\frac{-i}{16\pi^2}\right) C_0(m_1, m_2, m_3)\,, \tag{A.31}$$

with

$$C_0(m_1,m_2,m_3) = \frac{1}{m_1^2-m_2^2}F(m_1,m_2,m_3)\,, \tag{A.32}$$

$$\begin{aligned} F(m_1,m_2,m_3) &= \log\frac{m_1^2}{m_2^2} + \frac{m_3^2}{m_3^2-m_1^2}\log\frac{m_3^2}{m_1^2} - \frac{m_3^2}{m_3^2-m_2^2}\log\frac{m_3^2}{m_2^2} = \\ &= -F(m_2,m_1,m_3)\,. \end{aligned} \tag{A.33}$$

One can see that if, for example, $m_1^2 \gg m_2^2, m_3^2$, then the function (A.31) only depends on this heavy mass as $C_0 \propto \frac{1}{m_1^2}$. The same is true for $m_2^2 \gg m_1^2, m_3^2$ and $m_3^2 \gg m_1^2, m_2^2$.

The function $C_{\mu\nu}(m_1,m_2,m_3)$ is logarithmically divergent and can be easily written as:

$$C_{\mu\nu}(m_1,m_2,m_3) = g_{\mu\nu}\left[\frac{1}{n}B_0(m_2,m_3) + \frac{1}{4}m_1^2 C_0(m_1,m_2,m_3)\right]\,. \tag{A.34}$$

But we can not substitute directly the value of B_0 because is divergent and divided by n.

$$B_0(m_2,m_3) = \Delta - 1 + \log m_3^2 - \frac{m_2^2}{m_2^2-m_1^2}\log\frac{m_3^2}{m_2^2}\,, \tag{A.35}$$

$$\begin{aligned} \lim_{n\to 4}\frac{1}{n}B_0(m_2,m_3) &= \lim_{\epsilon\to 0}\frac{1}{4}\Big(1-\frac{\epsilon}{4}\Big)\Big[\Delta + B_0(m_2,m_3)|_{\text{finite}}\Big] \\ &= \frac{1}{4}\Big[\Delta - \frac{1}{2} + B_0(m_2,m_3)|_{\text{finite}}\Big]\,, \end{aligned} \tag{A.36}$$

where the finite part is defined as the finite part of the (A.35). The final result is:

$$C_{\mu\nu}(m_1,m_2,m_3) = \frac{1}{4}g_{\mu\nu}\Big[\Delta + \hat{C}(m_1,m_2,m_3)\Big]\,, \tag{A.37}$$

where the normalized 3-point function is:

$$\hat{C}(m_1,m_2,m_3) = \Big[-\frac{3}{2} + \log m_3^2 + \hat{E}_0(m_1,m_2,m_3)\Big]\,, \tag{A.38}$$

with

$$\hat{E}_0(m_1,m_2,m_3) = \frac{m_2^2}{m_3^2-m_2^2}\log\frac{m_3^2}{m_2^2} + \frac{m_1^2}{m_1^2-m_2^2}F(m_1,m_2,m_3)\,. \tag{A.39}$$

Some frequent special cases are:

$$\hat{E}_0(M,m,m) = \frac{m^2}{m^2-M^2} - \Big(\frac{M^2}{m^2-M^2}\Big)^2\log\frac{m^2}{M^2}\,, \tag{A.40}$$

$$\hat{E}_0(m,m,M) = \log\frac{m^2}{M^2} + \hat{E}_0(M,m,m)\,. \tag{A.41}$$

The function $\tilde{C}_0(m_1,m_2,m_3)$ is very similar to the previous one, with the result:

$$\tilde{C}_0(m_1,m_2,m_3) = B_0(m_2,m_3) + m_1^2 C_0(m_1,m_2,m_3) = \Delta + \hat{C}(m_1,m_2,m_3) + \frac{1}{2}\,. \tag{A.42}$$

And the last one is $B_1(m_1, m_2)$:

$$B_1(m_1, m_2) = -\frac{1}{2}\Big[\Delta + \log m_2^2 - \frac{1}{2} - \frac{m_1^2}{m_1^2 - m_2^2} - \Big(\frac{m_1^2}{m_1^2 - m_2^2}\Big)^2 \log \frac{m_2^2}{m_1^2}\Big]\,. \tag{A.43}$$

Appendix B

Diagonalizing a squared mass matrix

In this appendix we will show a group of formulas useful to diagonalize a 2×2 squared mass matrix $M^{(2)}$. We will fix our convention for the orthogonal matrixes that diagonalize $M^{(2)}$, showing the analytic expressions for the eigenvalues and the rotations angles, and finally how parametrize the sector in terms of the eigenvalues.

For the mass Lagrangian in the electroweak basis

$$\mathcal{L}_M = \frac{1}{2}\phi'^T M^{(2)} \phi' \tag{B.1}$$

where

$$\phi' \equiv \begin{pmatrix} \phi'_1 \\ \phi'_2 \end{pmatrix} \tag{B.2}$$

are the electroweak eigenstates, and

$$M^{(2)} \equiv \begin{pmatrix} a & c \\ c & b \end{pmatrix} \tag{B.3}$$

is the symmetric squared mass matrix that mix electroweak states. We define R as the orthogonal matrix that diagonalize $M^{(2)}$:

$$R = \begin{pmatrix} \cos\varphi & \sin\phi\varphi \\ -\sin\phi\varphi & \cos\varphi \end{pmatrix} \tag{B.4}$$

$$RM^{(2)}R^T \equiv \text{diag}\{m_1^2, m_2^2\} \tag{B.5}$$

The new mass eigenstates will be:

$$\phi \equiv \begin{pmatrix} \phi_1 \\ \phi_2 \end{pmatrix} = R\phi' \tag{B.6}$$

with the mass eigenstates the Lagrangian can be written as

$$\mathcal{L}_M = \frac{1}{2}m_1^2\phi_1^2 + \frac{1}{2}m_2^2\phi_2^2 \tag{B.7}$$

The mass eigenvalues can be written in terms of the matrix elements as:

$$m_{1,2}^2 = \frac{1}{2}\left[a + b \mp \sqrt{(a-b)^2 + 4c^2}\right] \tag{B.8}$$

where $m_1^2(m_2^2)$ is the lightest (heaviest) particle and in general we can said that is a monotonic decreasing (increasing) function with the mixing term $|c|$. The mixing angle that diagonalize (B.3) can be extracted from the relation:

$$\tan(2\varphi) = \frac{2c}{a-b} \tag{B.9}$$

to know the correct quadrant of φ is more useful this pair of relations:

$$\sin(2\varphi) = \frac{2c}{\sqrt{(a-b)^2+4c^2}}, \qquad \cos(2\varphi) = \frac{a-b}{\sqrt{(a-b)^2+4c^2}}. \tag{B.10}$$

From (B.8) we can extract two relations:

$$m_1^2 + m_2^2 = a + b \tag{B.11}$$

$$-m_1^2 + m_2^2 = \sqrt{(a-b)^2 + 4c^2} \tag{B.12}$$

and from the invariant of the determinant:

$$m_1^2 m_2^2 = ab - c^2. \tag{B.13}$$

These relations can be very useful to reparametrize the mass sector. We have put everything in terms of the three degrees of freedom of the matrix, i.e. a, b, c. We can choose other sets to represent the degrees of freedom and give the rest in terms of these. Next we will present some examples of these reparametrizations.

- Parameters m_1, m_2, φ

$$a = \frac{1}{2}\left[m_1^2(1-\cos 2\varphi) + m_2^2(1+\cos 2\varphi)\right] \tag{B.14}$$

$$b = \frac{1}{2}\left[m_1^2(1+\cos 2\varphi) + m_2^2(1-\cos 2\varphi)\right] \tag{B.15}$$

$$c = -\frac{1}{2}\left[(m_1^2 - m_2^2)\sin 2\varphi\right] \tag{B.16}$$

- Parameters m_1, a, c

$$b = \frac{c^2}{a - m_1^2} + m_1^2 \tag{B.17}$$

$$m_2^2 = \frac{c^2}{a - m_1^2} + a \tag{B.18}$$

$$\tan 2\varphi = \frac{2c}{a - m_1^2 - \frac{c^2}{a - m_1^2}} \tag{B.19}$$

- Parameters m_1, m_2, c

$$a = \frac{1}{2}\left[m_1^2 + m_1^2 \pm \sqrt{(m_1^2 - m_2^2)^2 - 4c^2}\right] \tag{B.20}$$

$$b = \frac{1}{2}\left[m_1^2 + m_1^2 \mp \sqrt{(m_1^2 - m_2^2)^2 - 4c^2}\right] \tag{B.21}$$

$$\tan 2\varphi = \pm\frac{2c}{\sqrt{(m_1^2 - m_2^2)^2 - 4c^2}} \tag{B.22}$$

List of Figures

List of Tables

Bibliography

[1] Steven Weinberg. A model of leptons. *Phys. Rev. Lett.* **19** (1967), 1264-1266.

[2] S. L. Glashow. Partial symmetries of weak interactions. *Nucl. Phys.* **22** (1961), 579-588.

[3] A. Salam. Proc. of the *8th Nobel Symposium*, ed. Svartholm Almqvist and Wicksells, Stockohlm (1968), p. 367.

[4] H. Georgi and S. L. Glashow. Unity of all elementary particle forces. *Phys. Rev. Lett.* **32** (1974), 438-441.

[5] Jogesh C. Pati and Abdus Salam. Lepton number as the fourth color. *Phys. Rev.* **D10** (1974), 275-289.

[6] John F. Gunion, Howard E. Haber, Gordon L. Kane, and Sally Dawson. The Higgs Hunter's Guide. Addison-Wesley, Menlo-Park, 1990. SCIPP-89-13.

[7] H. P. Nilles. Supersymmetry, supergravity and particle physics. *Phys. Rept.* **110** (1984), 1.

[8] Howard E. Haber and G. L. Kane. The search for supersymmetry: probing physics beyond the Standard Model. *Phys. Rept.* **117** (1985), 75.

[9] A. B. Lahanas and D. V. Nanopoulos. The road to no scale supergravity. *Phys. Rept.* **145** (1987), 1.

[10] S. Ferrara, editor. *Supersymmetry*, **1-2**. North Holland/World Scientific, Singapore, 1987.

[11] Marcela Carena and Howard E. Haber. Higgs boson theory and phenomenology. *Prog. Part. Nucl. Phys.* **50** (2003), 63-152. hep-ph/0208209.

[12] Stephen P. Martin. A supersymmetry primer. hep-ph/9709356.

[13] ATLAS Collaboration. Atlas technical proposal for a general-purpose *pp* experiment at the Large Hadron Collider at CERN. Atlas Technical Design Report.

[14] CMS Collaboration. The Compact Muon Solenoid Technical Proposal. CMS Technical Proposal.

[15] J. A. Aguilar-Saavedra et al. ECFA/DESY LC Physics Working Group. TESLA Technical Design Report Part III: Physics at an e+e- Linear Collider. also available at http://tesla.desy.de/tdr. hep-ph/0106315.

[16] M. Beneke et al. Top quark physics. hep-ph/0003033.

[17] F. Gianotti. Precision physics at LHC. Proc. of the *IVth International Symposium on Radiative Corrections (RADCOR 98)*, World Scientific 1999, p. 270, ed. J. Solà.

[18] David J. Miller. Precision studies at a future linear collider. *Proc. of the IVth International Symposium on Radiative Corrections (RADCOR 98)*, World Scientific 1999, p. 289, ed. J. Solà. hep-ex/9901039.

[19] S. Eidelman et al. Particle Data Group. Review of particle physics. *Phys. Lett.* **B592** (2004), 1.

[20] J. A. Coarasa, David Garcia, Jaume Guasch, Ricardo A. Jiménez, and Joan Solà. Quantum effects on $t \to H^+ b$ in the MSSM: A window to *virtual* supersymmetry? *Eur. Phys. J.* **C2** (1998), 373-392. hep-ph/9607485.

[21] J. A. Coarasa, Jaume Guasch, Joan Solà, and Wolfgang Hollik. Top quark decay into charged Higgs boson in a general two- Higgs-doublet model: Implications for the Tevatron data. *Phys. Lett.* **B442** (1998), 326. hep-ph/9808278.

[22] J. Guasch, W. Hollik, J. I. Illana, C. Schappacher, and J. Solà. Top-quark production and decay in the MSSM. hep-ph/0003109.

[23] J. L. Diaz-Cruz, R. Martinez, M. A. Perez, and A. Rosado. Flavor changing radiative decay of thf t quark. *Phys. Rev.* **D41** (1990), 891-894.

[24] G. Eilam, J. L. Hewett, and A. Soni. Rare decays of the top quark in the standard and two Higgs doublet models. *Phys. Rev.* **D44** (1991), 1473-1484. G. Eilam, J.L. Hewett, A. Soni, *Phys. Rev.* **D 59** (1998) 039901, Erratum.

[25] J. A. Aguilar-Saavedra. Top flavour-changing neutral interactions: Theoretical expectations and experimental detection. *Acta Phys. Polon.* **B35** (2004), 2695-2710. hep-ph/0409342.

[26] B. Mele, S. Petrarca, and A. Soddu. A new evaluation of the t $\rightarrow$ c H decay width in the standard model. *Phys. Lett.* **B435** (1998), 401. hep-ph/9805498.

[27] S. L. Glashow, J. Iliopoulos, and L. Maiani. Weak interactions with lepton - hadron symmetry. *Phys. Rev.* **D2** (1970), 1285-1292.

[28] G. Weiglein et al. LHC/LC Study Group. Physics interplay of the LHC and the ILC. hep-ph/0410364.

[29] G. Degrassi et al. SUSY particle physics summary. *Acta Phys. Polon.* **B35** (2004), 2711-2726.

[30] Jaume Guasch, Ricardo A. Jiménez, and Joan Solà. Supersymmetric QCD corrections to the charged Higgs boson decay of the top quark. *Phys. Lett.* **B360** (1995), 47-56. hep-ph/9507461.

[31] J. A. Coarasa, Ricardo A. Jiménez, and Joan Solà. Strong effects on the hadronic widths of the neutral Higgs bosons in the MSSM. *Phys. Lett.* **B389** (1996), 312-320. hep-ph/9511402.

[32] Jaume Guasch and Joan Solà. Implications on the supersymmetric Higgs sector from top quark decays at the Tevatron. *Phys. Lett.* **B416** (1998), 353-360. hep-ph/9707535.

[33] J. A. Coarasa, David Garcia, Jaume Guasch, Ricardo A. Jiménez, and Joan Solà. Heavy charged Higgs boson decaying into top quark in the MSSM. *Phys. Lett.* **B425** (1998), 329-336. hep-ph/9711472.

[34] J. A. Coarasa, Jaume Guasch, and Joan Solà. Radiative corrections to top quark decay into charged Higgs at the Tevatron. hep-ph/9903212.

[35] J. A. Coarasa, Jaume Guasch, and Joan Solà. $\Gamma(H^+ \rightarrow t\bar{b})$ in the MSSM: A handle for SUSY charged Higgs at the Tevatron and the LHC. hep-ph/9903213.

[36] J. A. Coarasa, Jaume Guasch, and Joan Solà. Top quark and charged Higgs at the Tevatron Run II. hep-ph/9909397.

[37] Alexander Belyaev, David Garcia, Jaume Guasch, and Joan Solà. Prospects for supersymmetric charged Higgs boson discovery at the Tevatron and the LHC. *Phys. Rev.* **D65** (2002), 031701. hep-ph/0105053.

[38] Alexander Belyaev, David Garcia, Jaume Guasch, and Joan Solà. Prospects for heavy supersymmetric charged Higgs boson searches at hadron colliders. *JHEP* **06** (2002), 059. hep-ph/0203031.

[39] Alexander Belyaev, Jaume Guasch, and Joan Solà. Supersymmetric effects on heavy charged Higgs boson production in hadron colliders. *Nucl. Phys. Proc. Suppl.* **116** (2003), 296. hep-ph/0210253.

[40] Jaume Guasch, Wolfgang Hollik, and Siannah Peñaranda. Distinguishing Higgs models in $H \to b\bar{b}/H \to \tau^+\tau^-$. *Phys. Lett.* **B515** (2001), 367-374. hep-ph/0106027.

[41] Jaume Guasch, Petra Häfliger, and Michael Spira. MSSM Higgs decays to bottom quark pairs revisited. *Phys. Rev.* **D68** (2003), 115001. hep-ph/0305101.

[42] G. M. de Divitiis, R. Petronzio, and L. Silvestrini. Flavour changing top decays in supersymmetric extensions of the standard model. *Nucl. Phys.* **B504** (1997), 45-60. hep-ph/9704244.

[43] Jaume Guasch and Joan Solà. FCNC top quark decays: A door to SUSY physics in high luminosity colliders? *Nucl. Phys.* **B562** (1999), 3-28. hep-ph/9906268.

[44] J. L. Diaz-Cruz, Hong-Jian He, and C. P. Yuan. Soft SUSY breaking, stop-scharm mixing and Higgs signatures. *Phys. Lett.* **B530** (2002), 179-187. hep-ph/0103178.

[45] Jaume Guasch. FCNC top decays into Higgs bosons in the MSSM. hep-ph/9710267.

[46] Jaume Guasch and Joan Solà. Top quark decays into neutral Higgs bosons and gluon in the MSSM. hep-ph/9909503.

[47] Ana M. Curiel, Maria J. Herrero, and David Temes. Flavour changing neutral Higgs boson decays from squark: Gluino loops. *Phys. Rev.* **D67** (2003), 075008. hep-ph/0210335.

[48] Durmus A. Demir. Higgs boson couplings to quarks with supersymmetric CP and flavor violations. *Phys. Lett.* **B571** (2003), 193-208. hep-ph/0303249.

[49] A. M. Curiel, M. J. Herrero, W. Hollik, F. Merz, and S. Peñaranda. SUSY - electroweak one-loop contributions to flavour- changing Higgs-boson decays. *Phys. Rev.* **D69** (2004), 075009. hep-ph/0312135.

[50] S. Heinemeyer, W. Hollik, F. Merz, and S. Peñaranda. Electroweak precision observables in the MSSM with non- minimal flavor violation. *Eur. Phys. J.* **C37** (2004), 481-493. hep-ph/0403228.

[51] Abdesslam Arhrib. Higgs bosons decay into bottom-strange in two Higgs doublets models. *Phys. Lett.* **B612** (2005), 263-274. hep-ph/0409218.

[52] M. S. Alam et al. CLEO. First measurement of the rate for the inclusive radiative penguin decay $b \to s\gamma$. *Phys. Rev. Lett.* **74** (1995), 2885-2889.

[53] R. Barate et al. ALEPH. A measurement of the inclusive $b \to s\gamma$ branching ratio. *Phys. Lett.* **B429** (1998), 169-187.

[54] S. Ahmed et al. CLEO. b $\to s\gamma$ branching fraction and CP asymmetry. hep-ex/9908022.

[55] K. Abe et al. Belle. A measurement of the branching fraction for the inclusive $B \to X_s\gamma$ decays with Belle. *Phys. Lett.* **B511** (2001), 151-158. hep-ex/0103042.

[56] S. Chen et al. CLEO. Branching fraction and photon energy spectrum for $b \to s\gamma$. *Phys. Rev. Lett.* **87** (2001), 251807. hep-ex/0108032.

[57] B. Aubert et al. BaBar. Determination of the branching fraction for inclusive decays $B \to X_s\gamma$. hep-ex/0207076.

[58] K. Hagiwara et al. Particle Data Group. Review of particle physics. *Phys. Rev.* **D66** (2002), 010001. http://pdg.lbl.gov.

[59] Marco Ciuchini, G. Degrassi, P. Gambino, and G. F. Giudice. Next-to-leading QCD corrections to $B \to X_s\gamma$: Standard model and two-Higgs doublet model. *Nucl. Phys.* **B527** (1998), 21-43. hep-ph/9710335.

[60] Francesca M. Borzumati and Christoph Greub. 2HDMs predictions for $\bar{B} \to X_s\gamma$ in NLO QCD. *Phys. Rev.* **D58** (1998), 074004. hep-ph/9802391.

[61] Francesca M. Borzumati and Christoph Greub. Two Higgs doublet model predictions for $\bar{B} \to X_s\gamma$ in NLO QCD. (Addendum). *Phys. Rev.* **D59** (1999), 057501. hep-ph/9809438.

[62] Paolo Gambino and Mikolaj Misiak. Quark mass effects in $\bar{B} \to X_s\gamma$. *Nucl. Phys.* **B611** (2001), 338-366. hep-ph/0104034.

[63] Santi Béjar, Jaume Guasch, and Joan Solà. Loop induced flavor changing neutral decays of the top quark in a general two-Higgs-doublet model. *Nucl. Phys.* **B600** (2001), 21-38. hep-ph/0011091.

[64] Santi Béjar, Jaume Guasch, and Joan Solà. FCNC top quark decays beyond the standard model. in: Proc. of the 5th International Symposium on Radiative Corrections (RADCOR 2000), Carmel, California, 11-15 Sep 2000. hep-ph/0101294.

[65] Santi Béjar, Jaume Guasch, and Joan Solà. Higgs boson flavor-changing neutral decays into top quark in a general two-Higgs-doublet model. *Nucl. Phys.* **B675** (2003), 270-288. hep-ph/0307144.

[66] Santi Béjar, Francesc Dilmé, Jaume Guasch, and Joan Solà. Higgs boson flavor-changing neutral decays into bottom quarks in supersymmetry. *JHEP* **08** (2004), 018. hep-ph/0402188.

[67] E. W. N. Glover et al. Top quark physics. *Acta Phys. Polon.* **B35** (2004), 2671-2694. hep-ph/0410110.

[68] Santi Béjar, Jaume Guasch, and Joan Solà. Production and FCNC decay of supersymmetric Higgs bosons into heavy quarks in the LHC. *JHEP* **10** (2005), 113. hep-ph/0508043.

[69] Santi Béjar, Jaume Guasch, and Joan Solà. SUSY Higgs boson flavor-changing neutral currents at the LHC. Proc. of the *7th International Symposium on Radiative Corrections (RADCOR05)*, Shonan Village, Japan, October 2-7 2005 (in preparation).

[70] John F. Gunion, Howard E. Haber, Gordon L. Kane, and Sally Dawson. Errata for the Higgs hunter's guide. hep-ph/9302272.

[71] Sheldon L. Glashow and Steven Weinberg. Natural conservation laws for neutral currents. *Phys. Rev.* **D15** (1977), 1958.

[72] Santi Béjar. Decaïments FCNC del quark top en models 2HDM, Master's thesis, Universitat Autònoma de Barcelona, 2001.

[73] M. B. Einhorn, D. R. T. Jones, and M. Veltman. Heavy particles and the rho parameter in the Standard Model. *Nucl. Phys.* **B191** (1981), 146.

[74] M. Veltman. Limit on mass differences in the Weinberg model. *Nucl. Phys.* **B123** (1977), 89.

[75] D. E. Groom et al. (Particle Data Group). Review of particle physics. *Eur. Phys. J.* **C15** (2000), 1.

[76] Maria Krawczyk. Testing 2HDM at muon colliders. hep-ph/9803484.

[77] Maria Krawczyk. Constraints on the Higgs sector from processes involving photons. Workshop on Physics at the First Muon Collider and at the Front End of the Muon Collider, Batavia, IL, 6-9 Nov 1997 [hep-ph/9803484], Workshop on photon interactions and the photon structure, Lund 1998. hep-ph/9812536.

[78] G. Abbiendi et al. (OPAL Collaboration). Two Higgs doublet model and model independent interpretation of neutral Higgs boson searches. hep-ex/0007040.

[79] G. Abbiendi et al. (OPAL Collaboration). Search for Higgs bosons in e+ e- collisions at 183-GeV. *Eur. Phys. J.* **C7** (1999), 407. hep-ex/9811025.

[80] Piotr H. Chankowski, Maria Krawczyk, and Jan Zochowski. Implications of the precision data for very light Higgs boson scenario in 2HDM(II). *Eur. Phys. J.* **C11** (1999), 661. hep-ph/9905436.

[81] J. Wess and J. Bagger. Supersymmetry and supergravity. Princeton, USA: Univ. Pr. (1992) 259 p.

[82] S. J. Gates, Marcus T. Grisaru, M. Rocek, and W. Siegel. Superspace, or one thousand and one lessons in supersymmetry. *Front. Phys.* **58** (1983), 1-548. hep-th/0108200.

[83] L. Girardello and Marcus T. Grisaru. Soft breaking of supersymmetry. *Nucl. Phys.* **B194** (1982), 65.

[84] J. Solà. Correccions radiatives supersimètriques als paràmetres electrofebles, PhD thesis, Universitat Autònoma del Barcelona, 1985.

[85] A. Dabelstein. The One loop renormalization of the MSSM Higgs sector and its application to the neutral scalar Higgs masses. *Z. Phys.* **C67** (1995), 495-512. hep-ph/9409375.

[86] Z. Kunszt and F. Zwirner. Testing the Higgs sector of the minimal supersymmetric standard model at large hadron colliders. *Nucl. Phys.* **B385** (1992), 3-75. hep-ph/9203223.

[87] M. Carena, M. Quiros, and C. E. M. Wagner. Effective potential methods and the Higgs mass spectrum in the MSSM. *Nucl. Phys.* **B461** (1996), 407-436. hep-ph/9508343.

[88] M. Carena, J. R. Espinosa, M. Quiros, and C. E. M. Wagner. Analytical expressions for radiatively corrected Higgs masses and couplings in the MSSM. *Phys. Lett.* **B355** (1995), 209-221. hep-ph/9504316.

[89] J. M. Frere, D. R. T. Jones, and S. Raby. Fermion masses and induction of the weak scale by supergravity. *Nucl. Phys.* **B222** (1983), 11.

[90] Mark Claudson, Lawrence J. Hall, and Ian Hinchliffe. Low-energy supergravity: false vacua and vacuous predictions. *Nucl. Phys.* **B228** (1983), 501.

[91] C. Kounnas, A. B. Lahanas, D. V. Nanopoulos, and M. Quiros. Low-energy behavior of realistic locally supersymmetric Grand Unified Theories. *Nucl. Phys.* **B236** (1984), 438.

[92] J. F. Gunion, H. E. Haber, and M. Sher. Charge / color breaking minima and a-parameter bounds in supersymmetric models. *Nucl. Phys.* **B306** (1988), 1.

[93] M. J. Duncan. Generalized Cabibbo angles in Supersymmetric gauge theories. *Nucl. Phys.* **B221** (1983), 285.

[94] Ken-ichi Hikasa and Makoto Kobayashi. Light scalar top at e+ e- colliders. *Phys. Rev.* **D36** (1987), 724.

[95] F. Gabbiani, E. Gabrielli, A. Masiero, and L. Silvestrini. A Complete analysis of FCNC and CP constraints in general SUSY extensions of the standard model. *Nucl. Phys.* **B477** (1996), 321-352. hep-ph/9604387.

[96] Mikolaj Misiak, Stefan Pokorski, and Janusz Rosiek. Supersymmetry and FCNC effects. in "Heavy Flavours II", eds. A.J. Buras, M. Lindner, Advanced Series on directions in High Energy Physics, World Scientific. hep-ph/9703442.

[97] R. Barbieri and G. F. Giudice. $b \to s\gamma$ decay and supersymmetry. *Phys. Lett.* **B309** (1993), 86-90. hep-ph/9303270.

[98] R. Garisto and J. N. Ng. Supersymmetric $b \to s\gamma$ with large chargino contributions. *Phys. Lett.* **B315** (1993), 372-378. hep-ph/9307301.

[99] Marco Aurelio Diaz. The $b \to s\gamma$ decay in supergravity with radiatively electroweak breaking. *Phys. Lett.* **B322** (1994), 207-212. hep-ph/9311228.

[100] F. M. Borzumati. The Decay $b \to s\gamma$ in the MSSM revisited. *Z. Phys.* **C63** (1994), 291-308. hep-ph/9310212.

[101] Stefano Bertolini and Francesco Vissani. Supersymmetric predictions for the inclusive $b \to s\gamma$ decay. *Z. Phys.* **C67** (1995), 513-524. hep-ph/9403397.

[102] Paolo Gambino, Ulrich Haisch, and Mikolaj Misiak. Determining the sign of the $b \to s\gamma$ amplitude. *Phys. Rev. Lett.* **94** (2005), 061803. hep-ph/0410155.

[103] Francesca Borzumati, Christoph Greub, Tobias Hurth, and Daniel Wyler. Gluino contribution to radiative B decays: Organization of QCD corrections and leading order results. *Phys. Rev.* **D62** (2000), 075005. hep-ph/9911245.

[104] Thomas Besmer, Christoph Greub, and Tobias Hurth. Bounds on flavor violating parameters in supersymmetry. *Nucl. Phys.* **B609** (2001), 359-386. hep-ph/0105292.

[105] W. Hollik. Precison test of the Standard Model and the Minimal Supersymmetric Standard Model. Lecture in Zuoz 2004 Summer School. http://ltpth.web.psi.ch/zuoz2004.

[106] LEP Higgs Working Group. Searches for the neutral Higgs bosons of the MSSM: Preliminary combined results using LEP data collected at energies up to 209-GeV. hep-ex/0107030.

[107] M. Carena, S. Heinemeyer, C. E. M. Wagner, and G. Weiglein. Suggestions for improved benchmark scenarios for Higgs- boson searches at LEP2. hep-ph/9912223.

[108] S. Heinemeyer, W. Hollik, and G. Weiglein. Constraints on tan(beta) in the MSSM from the upper bound on the mass of the lightest Higgs boson. *JHEP* **06** (2000), 009. hep-ph/9909540.

[109] LEP Higgs Working Group for Higgs boson searches. Search for charged Higgs bosons: Preliminary combined results using LEP data collected at energies up to 209- GeV. hep-ex/0107031.

[110] W. Hollik. Electroweak precision observables in the MSSM and global analyses of precision data. hep-ph/9711489.

[111] D. Garcia. Renormalisation of the Z boson width in the Minimal Supersymmetric Standard Model, PhD thesis, Universitat Autònoma de Barcelona, September 1997.

[112] Jaume Inglada Guasch. Supersymmetric radiative corrections to top quark and Higgs boson physics. hep-ph/9906517.

[113] LEP Higgs Working Group. Searches for the neutral Higgs bosons of the MSSM: Preliminary combined results using LEP data collected at energies up to 209-GeV. hep-ex/0107030.

[114] M. Carena, H.E. Haber, S. Heinemeyer, W. Hollik, C.E.M. Wagner, and G. Weiglein. Reconciling the two-loop diagrammatic and effective field theory computations of the mass of the lightest CP-even Higgs boson in the MSSM. *Nucl. Phys.* **B580** (2000), 29-57. hep-ph/0001002.

[115] Jose Ramon Espinosa and Ren-Jie Zhang. Complete two-loop dominant corrections to the mass of the lightest CP-even Higgs boson in the minimal supersymmetric standard model. *Nucl. Phys.* **B586** (2000), 3-38. hep-ph/0003246.

[116] S. Heinemeyer, W. Hollik, and G. Weiglein. QCD corrections to the masses of the neutral CP-even Higgs bosons in the MSSM. *Phys. Rev.* **D58** (1998), 091701. hep-ph/9803277.

[117] Ralf Hempfling and Andre H. Hoang. Two loop radiative corrections to the upper limit of the lightest Higgs boson mass in the minimal supersymmetric model. *Phys. Lett.* **B331** (1994), 99-106. hep-ph/9401219.

[118] H. Haber. Radiative Corrections in the Higgs sector of the MSSM. Proc. of the *IVth International Symposium on Radiative Corrections (RADCOR98)*, Barcelona, 8-12 September 1999. World Scientific, ed. Joan Solà.

[119] M. Masip, R. Munoz-Tapia, and A. Pomarol. Limits on the mass of the lightest Higgs in supersymmetric models. *Phys. Rev.* **D57** (1998), 5340-5344. hep-ph/9801437.

[120] M. Masip. The light Higgs in supersymmetric models with Higgs triplets. *Phys. Lett.* **B444** (1998), 352-357. hep-ph/9810303.

[121] J. A. Grifols, R. N. Mohapatra, and A. Riotto. New astrophysical constraints on the mass of the superlight gravitino. *Phys. Lett.* **B400** (1997), 124-128. hep-ph/9612253.

[122] J.A. Peacock. The need for Cold Dark Matter. Lecture in Zuoz 2004 Summer School. http://ltpth.web.psi.ch/zuoz2004.

[123] F. Pauss. Dark Matter Searches. Lecture in Zuoz 2004 Summer School. http://ltpth.web.psi.ch/zuoz2004.

[124] Jorge L. Lopez, D. V. Nanopoulos, and Raghavan Rangarajan. New supersymmetric contributions to t $\to$ c V. *Phys. Rev.* **D56** (1997), 3100-3106. hep-ph/9702350.

[125] David Garcia, Ricardo A. Jiménez, Joan Solà, and Wolfgang Hollik. Electroweak supersymmetric quantum corrections to the top quark width. *Nucl. Phys.* **B427** (1994), 53-80. hep-ph/9402341.

[126] J. L. Hewett, T. Takeuchi, and S. Thomas. Indirect probes of new physics. SLAC-PUB-7088 hep-ph/9603391.

[127] S. Bar-Shalom, G. Eilam, and A. Soni. The flavor changing top decay t → c sneutrino or sneutrino → t anti-c in the MSSM without R-parity. *Phys. Rev.* **D60** (1999), 035007. hep-ph/9812518.

[128] J. Küblbeck, M. Böhm, and A. Denner. Feyn Arts: computer algebraic generation of Feynman graphs and amplitudes. *Comput. Phys. Commun.* **60** (1990), 165-180.

[129] T. Hahn and M. Pérez-Victoria. Automatized one-loop calculations in four and D dimensions. *Comput. Phys. Commun.* **118** (1999), 153. hep-ph/9807565.

[130] T. Hahn. *FeynArts 2.2*, *FormCalc* and *LoopTools* user's guides, available from `http://www.feynarts.de`.

[131] V. Barger, J. L. Hewett, and R. J. N. Phillips. New constraints on the charged Higgs sector in two Higgs doublet models. *Phys. Rev.* **D41** (1990), 3421.

[132] Tom Junk. (LEP). Searches at LEP. hep-ex/0101015.

[133] Raymond Frey et al. Top quark physics: Future measurements. hep-ph/9704243.

[134] K. Hagiwara. Talk at the *5th International Symposium on Radiative Corrections (RADCOR 2000)*, Carmel, US, September 11-15, 2000, to appear in the (electronic) proceedings of *RADCOR 2000*, ed. H.E. Haber.

[135] Joan Solà. Quantum effects in the minimal supersymmetric standard model. Proceedings, International Workshop, MSSM, Barcelona, Spain, September 9-13, 1997. Singapore, Singapore: World Scientific (1998) 450 p, ed. Joan Solà.

[136] Michael Spira. QCD effects in Higgs physics. *Fortsch. Phys.* **46** (1998), 203-284. and references therein. hep-ph/9705337.

[137] Wei-Shu Hou. Tree level $t \to ch$ or $h \to t\bar{c}$ decays. *Phys. Lett.* **B296** (1992), 179.

[138] Andrea Brignole and Anna Rossi. Lepton flavour violating decays of supersymmetric Higgs bosons. *Phys. Lett.* **B566** (2003), 217-225. hep-ph/0304081.

[139] M. Spira. HIGLU and HQQ packages: `http://people.web.psi.ch/~spira/higlu/`, and `http://people.web.psi.ch/~spira/hqq/`.

[140] Michael Spira. Higgs and SUSY particle production at hadron colliders. hep-ph/0211145.

[141] Michael Spira. MSSM Higgs boson production at the LHC. hep-ph/9711407.

[142] Howard E. Haber. Higgs theory and phenomenology in the standard model and MSSM. hep-ph/0212136.

[143] John F. Gunion. Extended Higgs sectors. hep-ph/0212150.

[144] M. J. Duncan. Flavor changing decays of the Z^0 and supersymmetry. *Phys. Rev.* **D31** (1985), 1139.

[145] E. Braaten and J. P. Leveille. Higgs boson decay and the running mass. *Phys. Rev.* **D22** (1980), 715.

[146] N. Sakai. Perturbative QCD corrections to the hadronic decay width of the Higgs boson. *Phys. Rev.* **D22** (1980), 2220.

[147] Takeo Inami and Takahiro Kubota. Renormalization group estimate of the hadronic decay width of the Higgs boson. *Nucl. Phys.* **B179** (1981), 171.

[148] Manuel Drees and Ken-ichi Hikasa. Heavy quark thresholds in Higgs physics. *Phys. Rev.* **D41** (1990), 1547.

[149] Manuel Drees and Ken-ichi Hikasa. Note on QCD corrections to hadronic Higgs decay. *Phys. Lett.* **B240** (1990), 455. *Erratum, ibid.* **B262**, 497 (1991).

[150] Christoph Bobeth, Mikolaj Misiak, and Joerg Urban. Matching conditions for $b \to s\gamma$ and $b \to sg$ in extensions of the standard model. *Nucl. Phys.* **B567** (2000), 153-185. hep-ph/9904413.

[151] M. Spira, A. Djouadi, D. Graudenz, and P. M. Zerwas. Higgs boson production at the LHC. *Nucl. Phys.* **B453** (1995), 17-82. hep-ph/9504378.

[152] Wai-Yee Keung and William J. Marciano. Higgs scalar decays: $H \to W \pm X$. *Phys. Rev.* **D30** (1984), 248.

[153] A. Djouadi, J. Kalinowski, and M. Spira. HDECAY: A program for Higgs boson decays in the standard model and its supersymmetric extension. *Comput. Phys. Commun.* **108** (1998), 56-74. hep-ph/9704448.

[154] A. Yamada. The Higgs sector of the minimal supersymmetric standard model including radiative corrections. *Z. Phys.* **C61** (1994), 247.

[155] Piotr Chankowski, Stefan Pokorski, and Janusz Rosiek. Complete on-shell renormalization scheme for the minimal supersymmetric Higgs sector. *Nucl. Phys.* **B423** (1994), 437-496. hep-ph/9303309.

[156] A. Dabelstein. Fermionic decays of neutral MSSM Higgs bosons at the one loop level. *Nucl. Phys.* **B456** (1995), 25-56. hep-ph/9503443.

[157] M. Carena, S. Heinemeyer, C. E. M. Wagner, and G. Weiglein. Suggestions for benchmark scenarios for MSSM Higgs boson searches at hadron colliders. *Eur. Phys. J.* **C26** (2003), 601-607. hep-ph/0202167.

[158] M. Carena, S. Mrenna, and C. E. M. Wagner. The complementarity of LEP, the Tevatron and the LHC in the search for a light MSSM Higgs boson. *Phys. Rev.* **D62** (2000), 055008. hep-ph/9907422.

[159] Santi Béjar, Jaume Guasch, and Joan Solà. in preparation.

[160] Michael Spira. HIGLU: A Program for the Calculation of the Total Higgs Production Cross Section at Hadron Colliders via Gluon Fusion including QCD Corrections. hep-ph/9510347.

[161] T. Hahn. *LoopTools* user's guide, available from `http://www.feynarts.de/looptools`.

[162] G. J. van Oldenborgh and J. A. M. Vermaseren. New algorithms for one loop integrals. *Z. Phys.* **C46** (1990), 425-438.

[163] H. L. Lai et al. CTEQ. Improved parton distributions from global analysis of recent deep inelastic scattering and inclusive jet data. *Phys. Rev.* **D55** (1997), 1280-1296. hep-ph/9606399.

[164] Oliver Brein. Adaptive scanning: A proposal how to scan theoretical predictions over a multi-dimensional parameter space efficiently. hep-ph/0407340.

[165] G. Peter Lepage. A new algorithm for adaptive multidimensional integration. *J. Comput. Phys.* **27** (1978), 192.

[166] J. A. Aguilar-Saavedra and G. C. Branco. Probing top flavour-changing neutral scalar couplings at the CERN LHC. *Phys. Lett.* **B495** (2000), 347-356. hep-ph/0004190.

[167] Gerard 't Hooft and M. J. G. Veltman. Scalar one loop integrals. *Nucl. Phys.* **B153** (1979), 365-401.

[168] G. Passarino and M. J. G. Veltman. One loop corrections for e+ e- annihilation into mu+ mu- in the Weinberg model. *Nucl. Phys.* **B160** (1979), 151.

[169] Alan Axelrod. Flavor changing Z0 decay and the top quark. *Nucl. Phys.* **B209** (1982), 349.